ELECTRON RESONANCE SPECTROSCOPY OF U.V. IRRADIATED SUBSTANCES AT LOW TEMPERATURES

Thesis submitted for the Degree of Doctor of Philosophy at the University of Southampton

by

L. KISHORE

1961

Declaration and Acknowledgements

The work described in this thesis was carried out at the Department of Electronics of the University of Southampton, and the Department of Physics of the University College of North Staffordshire, during the period 1958-1961, under the supervision of Professor D.J.E. Ingram. The author is grateful to Professor E.E. Zepler and Professor D.J.E. Ingram for providing the facilities for research in their departments.

The author is especially indebted to Professor D.J.E. Ingram for his supervision, guidance and continual encouragement during the course of study.

Thanks are also due to the members of the teaching and the technical staff of the Department of Electronics, University of Southampton, and the Department of Physics, University College of North Staffordshire, for their advice and assistance, and to Miss S. Lawson and Miss B. Downs for the preparation of the thesis.

It has been a great pleasure to work with the members of the Microwave Research Group. Several discussions with them have been very helpful. Their help and cooperation is gratefully acknowledged.

Finally, thanks are recorded to the Government of India and to the University of Patna for the award of a Scholarship and the study leave.

CONTENTS

CHAPTER I

INTRODUCTION

The production and trapping of free radicals in solids at low temperatures and the properties and behaviour of these frozen free radicals have been the subject of considerable interest in the last few years. The current interest in this field arose to some extent from the possibility of obtaining high performance rocket fuels. Supplementing this have been the practical applications in a wide variety of industries dependent on chemical reactions which are free radical in nature. However, practical considerations apart, the challenge inherent in a study of the behaviour of matter at very low temperatures and its bearing on a wide variety of fields like solid state physics, biology, and astrophysics have largely contributed to the study of frozen free radicals. This study has been made possible in the last decade particularly by the wide availability of low temperature techniques.

1.1. The Characteristic Features of Free Radicals

A free radical has been defined in many ways. One of the most general definitions of a free radical is that it is a molecule, or part of a molecule, in which the normal chemical binding has been modified so that an unpaired electron is left associated with the system. In general, all compounds tend to have as low energy as possible and they do so by forming

saturated chemical bonds which consist of paired electron spins in the outer orbitals. This normal chemical binding is modified in a free radical so as to leave the outer orbitals with an unpaired electron. It follows that a free radical will in general show high chemical reactivity. Also the uncompensated spin motion of the odd electron will endow the free radical with a permanent magnetic moment. Both these characteristic features of free radicals, its high chemical reactivity and magnetism, could be employed for their detection and study.

1.2. Methods of Investigation

1.2.1. Chemical Method

High chemical reactivity has often been employed (e.g. in the mirror technique) to detect the presence of free radicals. The nature of free radicals can sometimes be established by analysing the end products that are formed and quantitative results can be obtained by kinetic studies of the reactions. However, although these methods are applicable to free radicals in the gaseous state, they are not very suitable for low temperature studies, because at low temperatures matter is normally in the solid state and solids do not readily react chemically. However, in many instances it is possible to deduce from the compounds found on warm-up what radicals must have been initially trapped.

1.2.2. Magnetic Methods

In view of the marked limitations inherent in chemical methods of analysis at low temperatures, it was natural that physical methods should be widely exploited to this end. A specific physical property of a free radical is the permanent magnetic moment associated with it. This would endow the free radicals with paramagnetism and, hence, a specimen containing free radicals would tend to move towards regions of high field strength when put into an inhomogeneous magnetic field. This force of attraction can, in effect, be measured accurately in a magnetic susceptibility balance and a precise quantitative estimate of free radical concentration made. Alternatively, the paramagnetic susceptibility may be measured by surrounding the specimen with a coil, the inductance of which is changed by the presence of free radicals. The coil forms part of a resonant circuit tuned at about 1 Mc/s. The change in the resonant frequency is proportional to the susceptibility of the substance introduced and thus gives a quantitative estimate of free radical concentration.

It may be noted that the last one is a non-resonant dynamic method of measuring susceptibility. A resonant method can also be used to study free radicals. This is variously known as Electron Magnetic Resonance (e.m.r.), Electron Paramagnetic Resonance (e.p.r.), Electron Spin Resonance (e.s.r.), or simply as Electron Resonance.

The basic principle of Electron Spin Resonance is as follows.

If a free electron is assumed to be in a d.c. magnetic field of strength H, only two values for the component of the spin angular momentum, and, hence, of the magnetic moment, of the electron along the direction of the magnetic field (taken here as the z-axis) are quantum-theoretically allowed. Corresponding to these two orientations, the changes in the energy of the system are $+|\mu_z|H$ and $-|\mu_z|H$, where $|\mu_z|$ is the absolute value of the component of the magnetic moment along the direction of the magnetic field. Thus the energy difference between the two states of the system corresponding to its two allowed orientations in the magnetic field is $2|\mu_z|H$. It is thus seen that the energy levels diverge linearly with increasing magnetic field. Although this linear divergence has been derived here for the special case of a free electron, it holds in many cases. In such cases, the energy separation between the two (consecutive) levels can be written as

$$\Delta E = g\beta H \qquad \ldots\ldots (1.1)$$

where β is the atomic unit of magnetic moment, called a Bohr Magneton, corresponding to one unit of angular momentum and is equal to $|e|h/4\pi mc$ i.e. to 0.9273×10^{-20} ergs gauss^{-1}, and g is the constant of proportionality; it is called the g-factor or spectroscopic splitting factor and is a measure of the rate

of divergence of the energy levels concerned with increasing magnetic field. For a free electron, $g\beta = 2|\mu_z|$, so that $|\mu_z| = \frac{1}{2}g\beta$.

Now if radiation of frequency, ν, is present such that

$$h\nu = \Delta E \qquad \ldots\ldots (1.2)$$

there will be absorption of energy. This is the phenomenon of Electron Spin Resonance. In most cases, where ΔE is proportional to H, the Bohr frequency condition as given above can be re-written as

$$h\nu = g\beta H \qquad \ldots\ldots (1.3)$$

This is the resonance relation for absorption of radiation due to transition between the successive Zeeman components of the system. The state of affairs is diagramatically shown in Fig. (1.1).

However, the radiation will not only induce absorption but emission as well. But, though the fractional number of systems undergoing induced transitions in either direction per unit time is the same, there will be more of them in the lower energy state than in the upper one when at equilibrium, and thus there will be a net absorption of energy. For most cases where Maxwell-Boltzmann statistics is obeyed, the ratio of populations of the two states at T°K will be given by

$$\frac{n_{\text{upper}}}{n_{\text{lower}}} = \exp(-\Delta E/kT) \qquad \ldots\ldots (1.4)$$

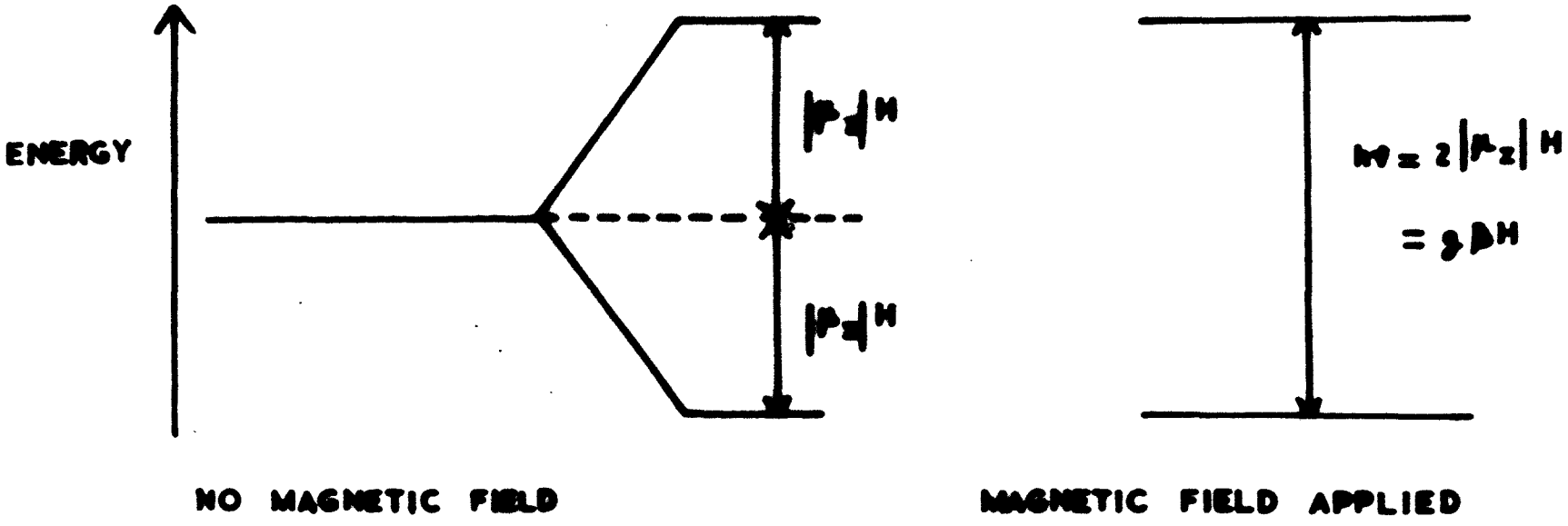

FIG. 1.1 SPLITTING OF LEVELS AND RESONANCE CONDITION.

Two possibilities for increased absorption emerge from this relation. First, ΔE should be kept as large as possible. This implies working at as high a value of the magnetic field as possible. The limit to this is set by the practical design considerations of the magnet. For the ordinarily available laboratory magnets with fields of a few Kilogauss, the radiation frequency falls in the microwave region. By coincidence, this is experimentally a highly developed region of the electromagnetic spectrum. The second requirement is to work at low temperatures, and this is, indeed, done very frequently.

Experimentally, the resonance can be observed by putting the specimen in the path of microwave radiation and noting the change in the transmitted power as the magnetic field is swept through the resonance condition. In principle, either the frequency of the source or the magnetic field can be varied, the other being held constant. In practice, the latter is much easier and is almost always done. This is illustrated in Fig. (1.2).

There is yet another way in which the magnetic properties of the free radicals can be made use of in their detection. The interconversion of ortho and para forms of the hydrogen molecule is very slow under normal conditions of gaseous collision, but, if free radicals are present in the mixture, they will produce very large magnetic perturbations in the hydrogen molecules during collisions with them, and this will

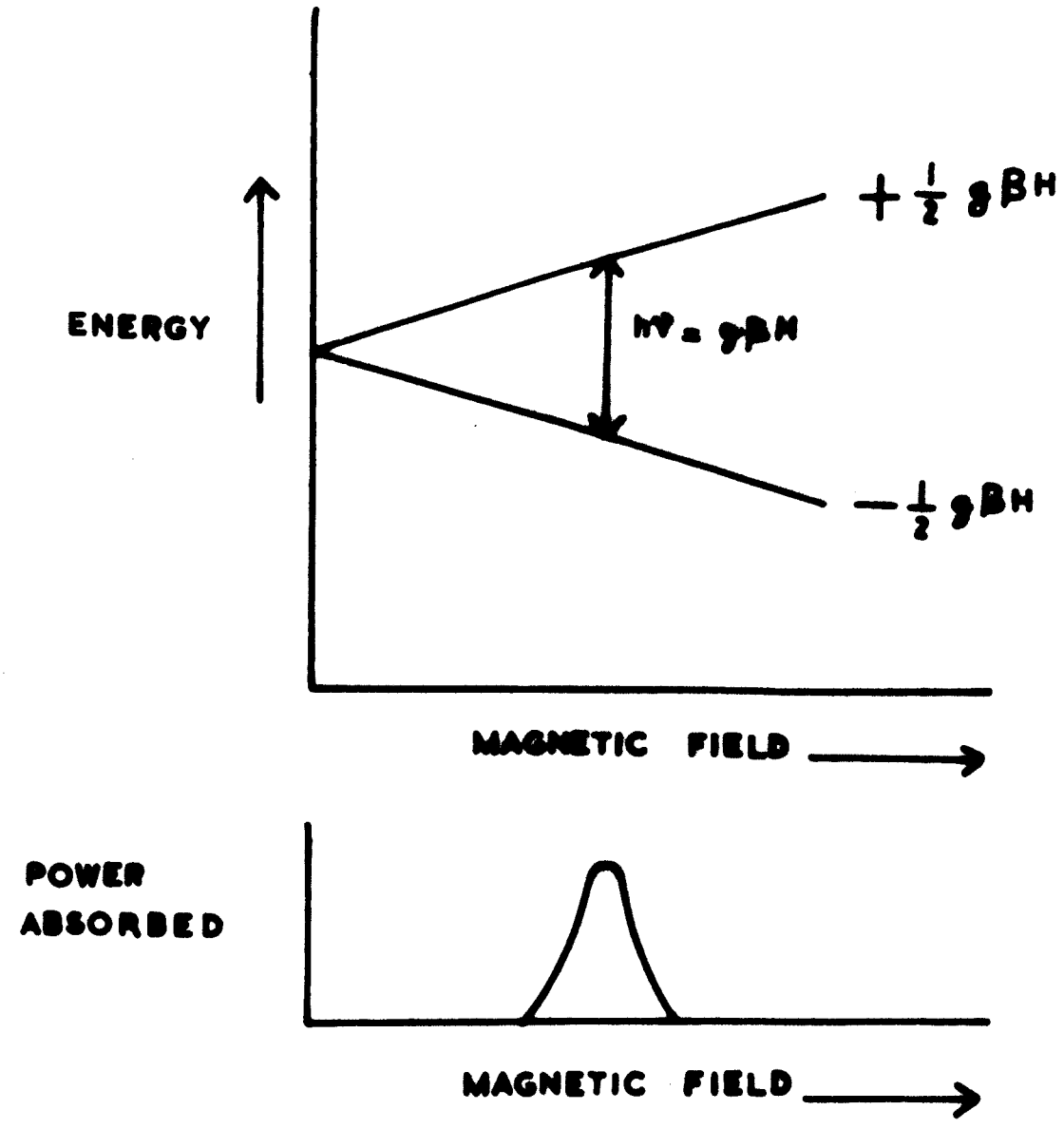

FIG.1.2 ELECTRON RESONANCE AT CONSTANT SOURCE — FREQUENCY.

lead to increased rate of ortho-para interconversion. The catalytic action of free radicals on ortho-para conversion has been used to detect their presence in solid, liquid, and gaseous phases.

1.2.3. Other Physical Methods

Apart from their specific characteristics, i.e. high reactivity and paramagnetism, the free radicals have other general properties like any other chemical species, and there are, accordingly, many physical methods that draw upon these general properties to study free radicals. Mention may be made, among these, of mass spectrometry, and spectroscopy in the visible and ultraviolet, infra-red, and microwave regions, of calorimetry, colorimetry, and x-ray and electron diffraction studies and of the measurements of the dielectric constant, index of refraction, and thermal conductivity.

Of these, the gross methods such as thermal conductivity, index of refraction and calorimetry can be expected to yield quantitative results only if the percentage of radicals present is large. For the same reason, the direct influence of the free radicals on the x-ray diffraction effects is difficult to observe. However, x-ray diffraction methods have been widely used to study the nature of the matrix structure in which the free radicals are trapped. Dielectric constant measurements, too, are of limited applicability; they can be used only if the free radicals have permanent dipole moments.

Of the remaining methods, mass spectrometry and spectroscopy provide the most powerful tools for the study of free radicals. Mass spectrometry, wherever available, yields a complete analysis of the free radicals. The usual method is to introduce the gas containing the free radicals into the ionisation chamber and to subject them to electron bombardment. As the energy of the electrons is increased, the free radicals are ionised and the mass of the ions thus produced is determined. Due to very high resolutions available, the detailed chemical constitution of the species can be unambiguously determined. There is no confusion due to the presence of the stable molecules as these have much higher ionisation potentials. However, the method is limited to free radicals in the gaseous state and only under suitable pressure conditions. This technique has, thus, a limited application.

The optical spectra should, in principle, provide detailed information about free radicals. In most cases where free radicals are short-lived, either their life-time is increased by freezing them at low temperatures or some high speed technique like flash photolysis is used. In the latter, the first flash produces the free radicals photochemically and the second, which follows immediately after, is used to record the absorption spectra of the radicals thus produced. The technique of flash-photolysis is suitable for gaseous state studies. In the solid or liquid phase near room temperatures, the structure is often

wiped out in the visible and ultraviolet range and one gets broad bands. However, at very low temperatures, where molecular motions are greatly diminished, visible and ultraviolet spectroscopy is very useful. Another difficulty in this region of the spectrum is scattering, which, however, is greatly diminished at low temperatures. Emission spectroscopy offers little difficulty so far as scattering is concerned, but it has a limited application since the radicals have first to be excited to higher states. Fluorescence and phosphorescence studies have been very useful in the study of many free radicals.

In the infra-red region, the scattering is a much less serious problem and characteristic lines corresponding to vibrational and rotational structure appear near room temperature. At low temperatures, the number of probable configurations which a complex molecule can take up is considerably reduced and, as a result, the spectra become simpler and sharper. At very low temperatures, however, rotational motion is strongly quenched in many solids. It may be noted that transitions between rotational states will not occur unless the free radical has a permanent electric dipole moment.

The logical extension of infra-red absorption spectroscopy is into the microwave region. In microwave spectroscopy, the analysis is the same as in infra-red spectroscopy, the absorption being, in most cases, associated with rotational motion. The main practical difficulties are (i) introducing the radicals

into the absorption cell and (ii) rapid recombination due to the metal walls of the absorption cell or due to the Stark electrode. Special spectrometers have been designed to reduce these difficulties.

It may be mentioned that electron resonance can be looked upon as a special branch of microwave spectroscopy. Whereas the 'gaseous' microwave spectroscopy is concerned with transitions between 'distinct' energy states of the system, electron resonance deals with transitions between the Zeeman components of a particular energy state (usually the ground state), the Zeeman components being separated due to the perturbations of an external magnetic field.

1.3. Merits of Electron Resonance Spectroscopy

Electron resonance spectroscopy can be used only when the system has a net magnetic moment. However, it is this selective restriction which makes it so useful for the study of free radicals. Electron resonance can thus be used to study the paramagnetic free radical species to the exclusion of the surrounding diamagnetic matrix. Magnetic susceptibility measurements also have this property of specificity, but electron resonance has the added advantage in that it gives extra information which enables one to distinguish between different radical species. This is mainly due to the presence of hyperfine structure in the spectra of most radicals. In principle, the hyperfine structure gives not only the identity of the radical but also its detailed

structure and orbital configuration. In practice, however, the spectra cannot be unambiguously interpreted except in certain cases, and in the absence of any supporting evidence it is not always possible to rely too much on the electron resonance spectra. Nevertheless, the information obtained from electron resonance spectroscopy is very valuable.

1.4. Conclusion

The theoretical advantages of electron resonance spectroscopy are its selectivity towards paramagnetic free radicals to the exclusion of the diamagnetic matrix and the ability to distinguish between different radicals and to give detailed orbital information about the free radicals. The practical advantages are the sensitivity and ease of operation; the free radicals can be introduced into the absorption cavity without much difficulty and observations can be made without disturbing them to any extent. Taking into consideration these advantages, it seems clear that electron resonance spectroscopy is, on the whole, the best and the most convenient way of studying frozen free radicals. The work described in this thesis is concerned with such a study. It describes and discusses e.s.r. spectroscopic investigations of some organic free radicals produced by photodissociation in low temperature glasses.

In the next chapter the general basic theory underlying the principles and analysis of electron resonance is discussed. Chapter III contains a discussion of relaxation effects and line widths. In Chapter IV the principles of an electron resonance spectrograph are given along with the description of the actual spectrometers used and the experimental procedures for measuring the various parameters involved. Chapter V contains the description of experiments and the experimental results. In the sixth and the final chapter the experimental results are discussed in the light of theory and other supporting evidence.

CHAPTER II

BASIC THEORY

2.1. Electron Resonance of an Isolated Electron

2.1.1. Spin and Magnetic Moment of an Electron

In the phenomenon of Electron Resonance, one is concerned with the interaction of the electron with radiation in the presence of a constant magnetic field. Before discussing this interaction, it is worthwhile investigating how an electron behaves in a constant magnetic field when no radiation is present.

Since an electron is a charged particle, its motion in a field of force constitutes a current and hence this motion is, in general, associated with a magnetic moment. However, observations on the fine-structure of optical spectral lines and the anomalous Zeeman effect could not be explained on the basis of the orbital magnetic moment alone. This led Uhlenbeck and Goudsmit to postulate a quantised "spin" motion to the electron. The concept of spin was incorporated into quantum mechanics by Pauli. But whereas his theory explains the effects of spin in quantum-mechanical language, it says nothing about the nature of spin. It was Dirac who gave a really satisfactory theory of the electron spin. The existence of the spin and of the magnetic moment of the electron with their correct values, and rules for spatial quantisation

follow directly from his relativistic quantum mechanics without the necessity of introducing them by an 'ad hoc' hypothesis.

In relativistic considerations, time occurs on the same footing as the spatial coordinates. Hence Dirac assumed a first order wave equation both in space and time (Dirac, 1947). It is now found that, in this representation, it is not the orbital angular momentum $\vec{l}$, but the operator $\vec{j} = \vec{l} + \vec{s}$ which commutes with the Hamiltonian i.e. $\vec{j}$, and not $\vec{l}$, is a constant of motion. Thus relativisitically the electron behaves as though it had a spin angular momentum $\vec{s}$ in the classical sense. The operator $\vec{s}$ is such that in the non-relativistic approximation in the z-representation,

$$s_z^2 = \frac{h^2}{16\pi^2} I$$

where I is a unit matrix. Thus s_z has the eigenvalues $\pm \frac{1}{2} \frac{h}{2\pi}$.

If the electron is in a magnetic field $\vec{H}$, then the vector $\vec{p}$ in the Hamiltonian has to be replaced by $\vec{p} + \frac{|e|}{c}\vec{A}$, where $\vec{A}$ is the vector potential. In the non-relativistic approximation, this gives an extra term

$$+ \frac{|e|}{mc} \vec{S}.\vec{H}$$

in the Hamiltonian. Thus the electron behaves in a magnetic

field as though it had a magnetic moment ($-\frac{|e|}{mc}\vec{S}$) associated with it in the classical sense.

The magnetogyric ratio, γ, for a free electron is thus given by

$$\gamma = -\frac{|e|}{mc}$$

This equation is usually written

$$\gamma = -g\frac{|e|}{2mc}$$

where g, the spectroscopic splitting factor, is 2 for a free electron.

However, with high accuracies attainable in microwave spectroscopy, it became clear that the value, 2, for the g-factor of the free electron was in small error. The necessary correction was also introduced by Dirac. The error was due to the neglect of the interaction of the electron with radiation field (Weisskopf, 1949). To take into account this interaction, it is necessary to quantise the electromagnetic field. The quantisation of the electromagnetic field is equivalent to that of a set of harmonic oscillators, and even in the lowest energy set, there is a net zero point electromagnetic vibration. Now the magnetic moment of the Dirac electron can be considered as due to circular currents of radius h/mc. The zero point oscillations of the electromagnetic field influence these currents to a certain extent and this interaction causes a slight change of the

magnetic moment. The g-factor, after correcting for interaction with the radiation field, is given by

$$g = 2 + \frac{e^2}{\pi hc} \qquad \ldots\ldots \quad (2.1.)$$

$$\text{i.e. } g = 2.0023$$

2.1.2. Quantum-Mechanical Description of E.S.R.

In an electron resonance experiment, the electron is essentially subjected to a magnetic field $H \equiv (2H_1 \cos \omega t, 0, H_0)$. In the absence of the r.f. field, the Hamiltonian would be

$$\mathcal{H}_0 = g\beta S_z H_0 \qquad \ldots\ldots \quad (2.2.)$$

The r.f. field, $2H_1 \cos\omega t$ which is perpendicular to the constant field H_0, may be considered to be a perturbation on the system provided that $H_1 \ll H_0$. The perturbation Hamiltonian is, therefore,

$$\mathcal{H}' = g\beta S_x H_x = g\beta S_x H_1 (\exp i\omega t + \exp - i\omega t) \qquad \ldots\ldots \quad (2.3.)$$

The effect of the perturbation can be investigated by Dirac's theory of variation of constants.

The state function at a time, t, can be written as

$$\Psi = a_1(t)\psi_1^0 \exp(-2\pi i W_1 t/h) + a_2(t)\psi_2^0 \exp(-2\pi i W_2 t/h) \qquad (2.4.)$$

where ψ_1^0 and ψ_2^0 are unperturbed time-independent state functions corresponding to the two possible spin orientations $-\frac{1}{2}$ and $+\frac{1}{2}$ respectively and W_1 and W_2 are the corresponding energy values. The a's are functions of t alone and can be obtained from the equations (2.3.) and (2.4.) together with the perturbed

time-dependent Schrödinger equation

$$(\mathcal{H}_0 + \mathcal{H}')\Psi = \frac{ih}{2\pi}\frac{\partial \Psi}{\partial t} \quad \ldots\ldots \quad (2.5.)$$

If the system is assumed to be in the state Ψ_1^0 at $t = 0$, the probability of finding it in the state Ψ_2^0 at $t > 0$ will be

$$P_{-\frac{1}{2}\rightarrow+\frac{1}{2}} = |a_2(t)|^2$$

$$= 4g^2\beta^2 H_1^2 \left(\tfrac{1}{2}\middle|S_x\middle|-\tfrac{1}{2}\right)^2 \frac{[\sin^2\pi(\nu_{21} - \nu)t]}{(\nu_{21} - \nu)^2}$$

where $\nu_{21} = (W_2 - W_1)/h$ and $\nu = \omega/2\pi$. A plot of the function in the square brackets is shown in Fig. 2.1. It is seen that, for times not too short, the function has an appreciable value only when $W_2 - W_1 \approx h\nu$. Thus there is a large probability for the electron to be found in the state $|+\tfrac{1}{2}\rangle$ if the frequency, ν, of the incident radiation is equal to or very close to ν_{21}. This is the quantum-mechanical description of electron resonance.

It is seen that the probability of a transition depends upon the transition moment $g\beta(\tfrac{1}{2}|S_x|-\tfrac{1}{2})$ as well. For the general case of spin, S, the transition moment is $g\beta(M'|S_x|M)$. Since $(M'|S_x|M) = 0$ unless $M = M' \pm 1$, transitions are allowed only when $\Delta M = \pm 1$. Because of the Hermitian character of S_x,

$$P_{M+1\rightarrow M} = P_{M\rightarrow M+1}$$

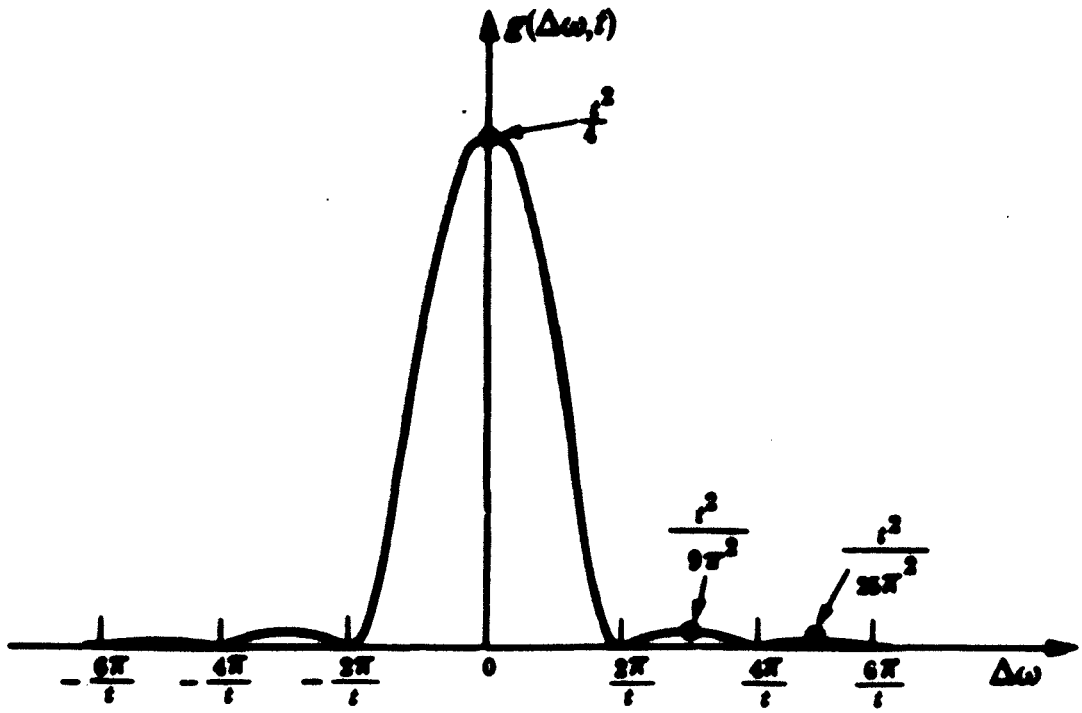

FIG. 2.1. THE FUNCTION $g(\Delta\omega,t) = \frac{\sin^2(\frac{1}{2}t\,\Delta\omega)}{(\Delta\omega)^2}$

i.e. the probability of induced absorption is equal to that of induced emission.

It may be noted that only the first-order perturbation has been considered above. Higher-order perturbation calculations allow some other types of transitions as well (e.g. double quantum transitions, $\Delta M = \pm 2$ transitions etc.) under suitable conditions.

2.1.3. Classical description.

Although electron resonance is essentially a quantum-mechanical process, it is interesting to see that it can be described classically at least in an elementary way. The classical description leads to results that are in agreement with those found quantum-mechanically and is very useful in bringing out certain essential points about the phenomenon in a simple way.

Let us consider a system having a magnetic moment $\vec{\mu}$ and an angular momentum $\vec{M}$ related by the equation

$$\vec{\mu} = \gamma \vec{M} \qquad \ldots\ldots \qquad (2.7.)$$

where γ is the magnetogyric ratio. In a fixed frame of reference A, the equation of motion is

$$\frac{d\vec{M}}{dt} = \vec{\mu} \times \vec{H} \qquad \ldots\ldots \qquad (2.8.)$$

where $\vec{H}$ is the magnetic field as observed in frame A. If $(d\vec{M}/dt)_F$ denotes the time rate of change of angular momentum

as observed from a second frame of reference A' rotating with an angular velocity $\vec{\omega}$ relative to A, then

$$(d\vec{M}/dt)_r = (d\vec{M}/dt) + \vec{\omega} \times \vec{M} \quad \ldots\ldots \quad (2.9.)$$

From equations (2.7.), (2.8.), and (2.9.), one gets

$$(d\vec{M}/dt)_r = \vec{\mu} \times (\vec{H} + \vec{\omega}/\gamma) \quad \ldots\ldots \quad (2.10.)$$

Thus the effective magnetic field observed from the rotating frame A' is

$$\vec{H}_e = \vec{H} + \vec{\omega}/\gamma \quad \ldots\ldots \quad (2.11.)$$

In particular, if $\vec{H}$ has the constant value $\vec{H}_o$ and $\vec{\omega} = -\gamma\vec{H}_o$, the effective field $\vec{H}_e$ vanishes. In this case, therefore, the magnetic moment $\vec{\mu}$ would remain fixed or constant with respect to the rotating frame A'. Hence as observed from A, it will precess about $\vec{H}_o$ with a precessional velocity

$$\vec{\omega}_o = -\gamma\vec{H}_o \quad \ldots\ldots \quad (2.12.)$$

This is the Larmor precession. For an electron, of course, $\gamma = -g\frac{|e|}{2mc}$. Therefore

$$\vec{\omega}_o = g\frac{|e|}{2mc}\vec{H}_o \quad \ldots\ldots \quad (2.13.)$$

Thus $\vec{\omega}_o$ is always along $\vec{H}_o$ irrespective of the direction and sense of $\vec{M}$.

The following physical picture is helpful in understanding the Larmor precession of the electrons in a magnetic field. We consider a free electron spinning about its axis in the classical

sense. The spinning charge would endow the electron with a magnetic moment, whereas the spinning mass would give rise to an angular momentum. The electron can thus be treated like a flywheel with a bar magnet along its axis. If this system is now placed in a steady magnetic field, with the magnet inclined at some angle to the field, the magnet would experience a torque tending to turn it into alignment with the magnetic field. The bar magnet would, however, not turn in this way because of the spinning angular momentum as represented by the flywheel. It will therefore react to the torque by precessing about the field direction like a spinning top in a gravitational field.

We next assume that the applied magnetic field consists of two parts, (i) a constant d.c. field H_0 along the z-axis, and (ii) an a.c. field of magnitude $H_1 \ll H_0$ rotating in the xy plane with an angular velocity $\vec{\omega}$ along the z-axis. The effective field in a frame A' rotating with its x'-axis along H_1 will be

$$H_{z'e} = H_0 + \omega/\gamma$$
$$H_{x'e} = H_1 \qquad \ldots\ldots \quad (2.14.)$$

The field in the rotating frame A' is thus constant; it has a magnitude

$$[(H_0 + \omega/\gamma)2 + H_1 2]^{\frac{1}{2}} \qquad \ldots\ldots \quad (2.15.)$$

and makes an angle θ with the z-direction such that

$$\tan\theta = \frac{H_1}{H_0 + \omega/\gamma} \qquad \ldots\ldots \quad (2.16.)$$

If one now considers another frame A'' rotating about the direction of $\vec{H_e}$ in the frame A' such that

$$\vec{H_e} + \vec{\Omega}/\gamma = 0$$

there would be no torque on the magnetic moment in this new frame A'' and hence it will maintain its initial orientation relative to this frame. Thus the magnetic moment will precess about $\vec{H_e}$ in the frame A' with the precessional velocity $\vec{\Omega} = -\gamma\vec{H_e}$. However, since $H_1 \ll H_0$, the angle θ occurring in the equation (2.16.) will be very small and hence the magnetic moment will always be above the xy-plane. But if ω is very close to $-\gamma H_0 (=\omega_0)$, θ would be large and the magnetic moment would spend a considerable fraction of its time below the xy-plane. This corresponds to the large quantum-mechanical probability of the electron being found in the spin-state $|\frac{1}{2}>$. In particular, when $\omega = \omega_0$, $\vec{H_e}$ becomes identical with $\vec{H_1}$ and the magnetic moment spends half its time above, and half below, the xy-plane. Thus the probability of transition is maximum in this case. This is the phenomenon of spin resonance, and is illustrated in Figs. 2.2(a) and 2.2(b). It may be noted that in the laboratory frame, at resonance, the magnetic moment will precess about both $\vec{H_0}$ and $\vec{H_1}$, the first precession being much faster than the second. The resultant motion will be helical.

The reason why appreciable tipping occurs only at resonance can be seen as follows. In a frame rotating about z-axis with

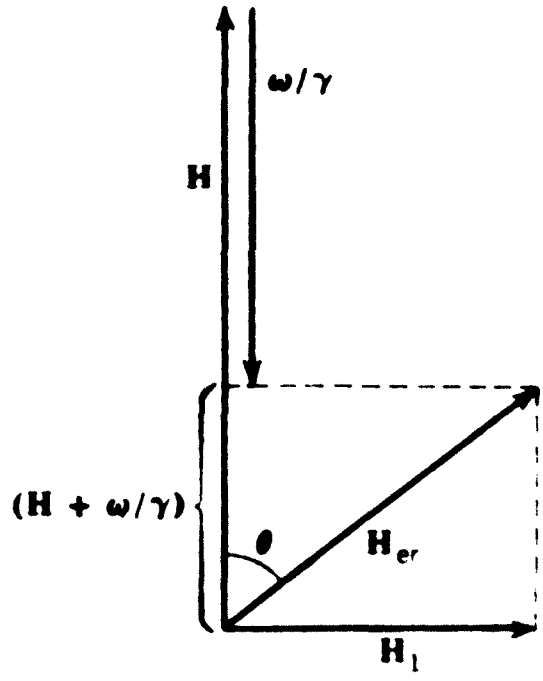

FIG. 2.2(a). EFFECTIVE FIELD IN A ROTATING FRAME NEAR RESONANCE.

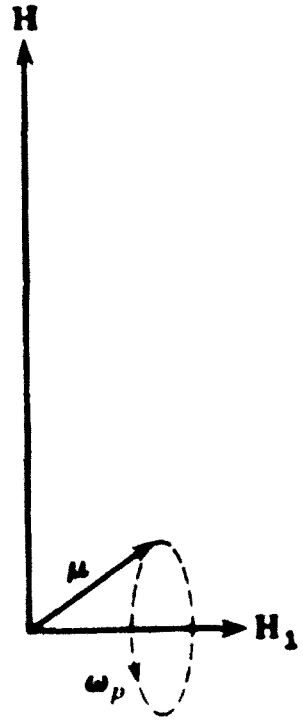

FIG. 2.2(b). Spin resonance in a rotating frame.

angular velocity ω_0, the magnetic moment will not 'see' the field $\overrightarrow{H_0}$. The only torque it would experience in this frame would be that due to $\overrightarrow{H_1}$. If the angular velocity, ω, of $\overrightarrow{H_1}$ is different from ω_0, $\overrightarrow{H_1}$ will also be rotating in this frame and the torque it would exert on the magnetic moment will vary in magnitude and direction. The resulting effect would be a slight wobbling of the steady precessional motion in the laboratory frame. But if $\omega = \omega_0$, the rotating field will be stationary in the rotating frame and will exert a constant torque, thus causing large oscillations in the angle between $\overrightarrow{\mu}$ and $\overrightarrow{H_0}$.

As seen earlier, the angle between μ and H_0 depends on the probabilities of the electron being in the spin-states $|-\frac{1}{2}>$ and $|+\frac{1}{2}>$. The probability of transition can thus be calculated from the geometry of the frames A' and A''. The probability of transition so calculated agrees with that derived quantum-mechanically by Rabi (1937). Thus if a particle of spin $\frac{1}{2}$ is in a steady magnetic field $\overrightarrow{H_0}$ with another perpendicular magnetic field $\overrightarrow{H_1}$ rotating about $\overrightarrow{H_0}$ with angular velocity ω and if it is in the state $|-\frac{1}{2}>$ at a time $t = o$, then it is found that the probability of its being in the state $|+\frac{1}{2}>$ at some later time t is

$$\frac{\theta^2}{(1 - \omega_0/\omega)^2 + (\omega_0/\omega)\,\theta^2} \operatorname{Sin}^2 \left\{ \frac{\omega t}{2} \left[\left(1 - \frac{\omega_0}{\omega}\right)^2 + \frac{\omega_0}{\omega}\,\theta^2 \right]^{\frac{1}{2}} \right\} \quad \ldots\ldots \quad (2.17.)$$

where ω_0 is the Larmor precession angular frequency and θ is

$\tan^{-1} \frac{H_1}{H_0}$ and has been assumed small.

Finally it may be mentioned that it is not necessary to have a truly rotating r.f. field for the resonance to take place. An oscillating r.f. field, $2H_1 \cos\omega t$, which is equivalent to two oppositely rotating fields of magnitude H_1 can be used instead. The component rotating in a direction opposite to that of Larmor precession does not contribute appreciably towards resonance. In fact, Bloch and Siegert (1940) have shown that use of an oscillating field alters the resonance condition from $\omega = -\gamma H_0$ to

$$\omega = -\gamma H \left[1 + \frac{1}{4} \frac{H_1^2}{H_0^2}\right] \qquad \ldots\ldots \quad (2.18.)$$

to a first order.

2.2. Free atom (or ion).

The electrons constituting a free ion will, in general, have orbital angular momenta and hence would have magnetic moments associated with their orbital motion. The resultant orbital angular momentum and the magnetic moment of the whole ion would be the vectorial sum of those of the individual electrons, and the latter may or may not add up to zero. The case where they have non-zero values is considered now.

If one neglects the nuclear magnetism, the magnetic moment of the free atom may be written as $\vec{\mu} = \vec{\mu_S} + \vec{\mu_L}$. $\vec{\mu_L}$ and $\vec{\mu_S}$ are given by the following relations:

$$\vec{\mu_S} = -2\beta\vec{S} \qquad \ldots\ldots \quad (2.19.)$$

$$\vec{\mu_L} = -\beta\vec{L} \qquad \ldots\ldots \quad (2.20.)$$

When Russell-Saunders coupling holds, $\vec{S}$ and $\vec{L}$ are coupled to form a resultant angular momentum $\vec{J}$ i.e.

$$\vec{J} = \vec{L} + \vec{S} \qquad \ldots\ldots \quad (2.21.)$$

The absolute magnitudes of $\vec{S}$ and $\vec{L}$ are constant, and they may be considered as precessing uniformly around $\vec{J}$.

According to equations (2.19.), (2.20.) and (2.21.), the magnetic moment $\vec{\mu}$ is not generally parallel to the total angular momentum $\vec{J}$. Writing $\vec{\mu} = \vec{\mu_{\parallel}} + \vec{\mu_{\perp}}$ where $\vec{\mu_{\parallel}}$ and $\vec{\mu_{\perp}}$ are components respectively parallel and perpendicular to $\vec{J}$, one gets, as shown in Fig. (2.3.),

$$\vec{\mu_{\parallel}} = \vec{\mu_L}\,\mathrm{Cos}\,(\vec{L},\vec{J}) + \vec{\mu_S}\,\mathrm{Cos}\,(\vec{S},\vec{J}) = -g_J\beta\vec{J} \qquad \ldots\ldots \quad (2.22.)$$

$$\text{where } g_J = 1+\frac{\vec{S}.\vec{J}}{J^2} = \frac{3}{2} + \frac{S(S+1)-L(L+1)}{2J(J+1)} \qquad \ldots\ldots \quad (2.23.)$$

g_J is called the Lande g-factor. For L = o, g_J = 2 and for S = o, g_J = 1. However, it may be noted that g_J need not lie between these values. For example, for a $^2P_{\frac{1}{2}}$ state g = 2/3 and for a $^4P_{\frac{1}{2}}$ state g = 8/3.

As a consequence of the uniform precessional motion of $\vec{\mu}$ about $\vec{J}$, the time average of $\vec{\mu_{\perp}}$ vanishes so that the time average

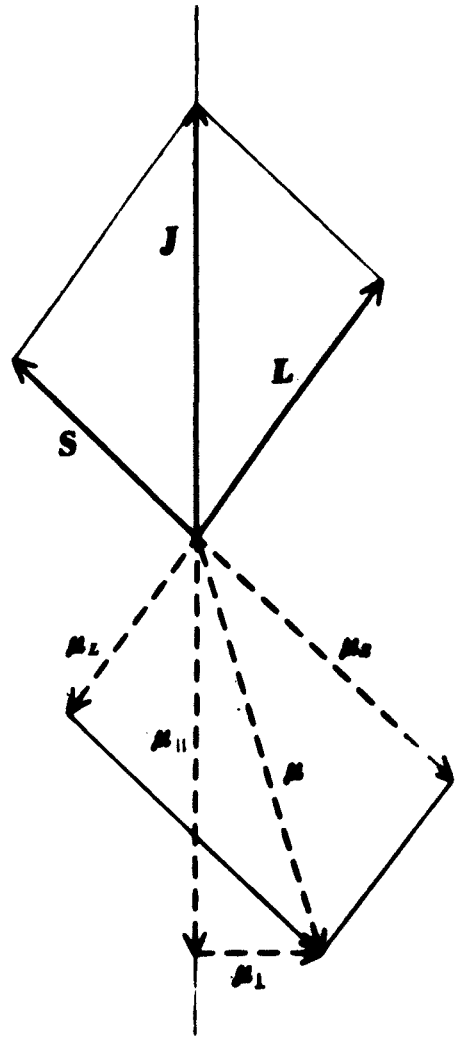

FIG. 2.3. COUPLING OF SPIN AND ORBITAL ANGULAR MOMENTA IN A FREE ATOM OR ION.

of $\vec{\mu}$ is given by $\vec{\mu}_{||}$. The perpendicular part $\vec{\mu}_{\perp}$ is not completely ineffective, however. In the quantum-mechanical description, $\vec{\mu}_{||}$ is constant with respect to time and corresponds to [redacted] diagonal part in the matrix representation of $\vec{\mu}$ in the scheme in which $\vec{J}^2$ is [redacted] diagonal. In the first order perturbation, the level (S,L,J) gains an additional energy $-\mu_{||z}H(=g_J\beta M_J H)$ in the magnetic field H when the latter is applied along the z-axis. $\mu_{\perp}$ corresponds to the off [redacted] diagonal part (connecting states with different J) and in the second order perturbation gives a term proportional to β^2H^2. However, this second order correction is small and is neglected here. The splitting of a level of a given J in a magnetic field is shown in Fig. (2.4.). No electric dipole transitions between these Zeeman levels is possible because of the parity restrictions. However, magnetic dipole transition is allowed as $\langle J,M_J|g\beta S_x H_x|J,M'_J\rangle$ is non-vanishing if $(M_J - M'_J) = 1$. The frequency of the transitions $\Delta M_J = \pm 1$ is thus given by

$$h\nu = g_J\beta\left\{M_J - (M_J-1)\right\}H = g_J\beta H \qquad \ldots\ldots \quad (2.24.)$$

It may be noted that in this case the spectroscopic splitting factor as defined by equation (1.1.) is the same as Lande' g-factor as defined by equation (2.23.).

2.3. Paramagnetic ion in a Crystal Lattice

Besides free atoms studied in the gaseous state , some frozen atomic free radicals show e.s.r. spectra closely approximating those of free atoms. However, in most paramagnetic

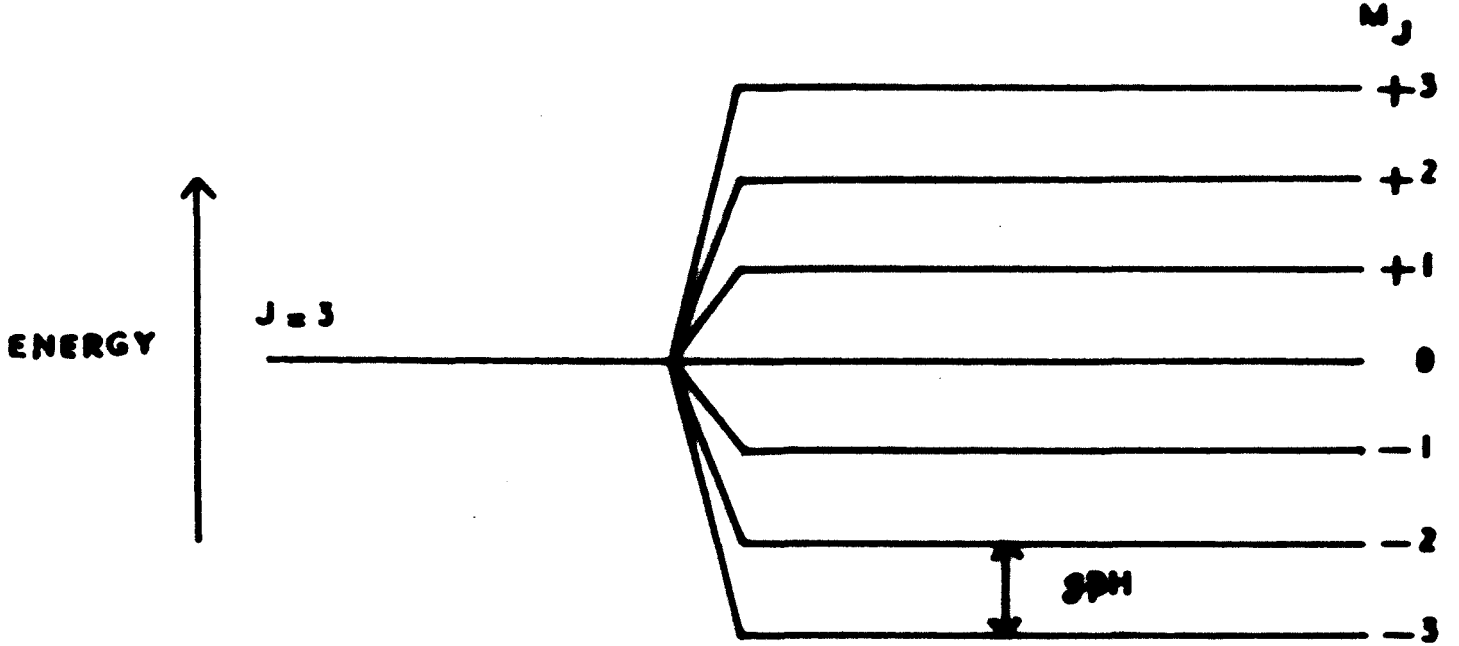

FIG. 2.4 ZEEMAN SPLITTING OF A LEVEL IN A FREE ATOM.

salts in the solid state, the ion is bonded to the surrounding ligands in some way or another and these have profound effect on the energy states of the paramagnetic ion. One method of taking the effect of the ligands into account is to replace them by point charges or point dipoles and regard their interaction with the paramagnetic ion as arising from the electrostatic field of these charges or dipoles. The method is variously known as Crystal Field Theory, Static Field Theory or Electrostatic Theory.

The effect of the crystal field is similar to that of a Stark field in atomic spectroscopy. The actual behaviour of the ion will depend upon the strength of the crystalline field interactions relative to the strength of the electronic coupling within the paramagnetic ion. It is convenient to make the following classification on this basis:

(1) Weak field: In this case the crystalline interactions are much less than the spin-orbit interactions and thus are not sufficiently strong to uncouple $\vec{L}$ and $\vec{S}$. Thus J is a good quantum number and the effect of the crystalline field is to lift the J degeneracy either wholly or partly. The rare earths, with well shielded 4f paramagnetic sub-shell, are good examples of this.

(2) Moderate field: In the intermediate field, the internal crystalline interactions are sufficiently strong to uncouple $\vec{L}$

and $\vec{S}$, but are not sufficient to prevent the individual $\vec{l}$ and $\vec{s}$ vectors from forming $\vec{L}$ and $\vec{S}$ respectively. The ions can therefore be treated as free ions subjected to strong perturbing forces. This situation is exemplified in the ionically bound elements of the iron group.

(3) Strong field: Here the internal fields are sufficiently strong to prevent the formation of $\vec{L}$ and $\vec{S}$. It is no longer possible to treat the ion as a free ion perturbed by the crystal field since its spectroscopic ground state is altered completely by the crystal field interactions. The palladium group and the covalently bonded complexes of the iron group are representative of this case.

The elements of the iron group were the first to be studied by electron resonance and they have been most extensively investigated, both theoretically and experimentally. Since the concepts used to describe their spectra are general and are applicable for the description of other systems as well, they are considered here in some detail.

2.3.1. <u>The Crystal Field</u>.

Assuming that the potential of the crystal field satisfies Laplace's equation, it can be expressed in spherical harmonics. Thus

$$V = \sum_{n,m} A_n^m r^n Y_n^m \quad (\theta, \phi)$$

where Y's are the spherical harmonics and A's are their coefficients. The crystal field is treated as a perturbation. For d electrons, all the terms in the crystal field potential for which n>4 can be omitted while calculating the matrix elements occurring in the secular determinant. This is because the wave functions of the electrons can also be expanded in spherical harmonics $Y_l^i(\theta,\phi)$ and for d electrons l = 2. Thus $\int Y_l^i Y_n^m Y_l^{i'} d\tau$ necessarily vanishes if n>4. Further, matrix elements of terms with odd values of n must vanish because they would change sign on inversion. Also the term with n = o, which is a constant and shifts all the levels of a configuration by the same amount need not be considered. Thus the only terms in the expansion of the crystal field potential which are of significance are those with n = 2 and n = 4. The symmetries of some of the spherical harmonics are mentioned here. $Y_n^o(\theta,\phi)$ shows no dependence on ϕ and has axial symmetry. Spherical harmonics having m = $\pm$ 4, $\pm$ 3 and $\pm$ 2 have tetragonal, trigonal and rhombic symmetry respectively. The combination $Y_4^o(\theta,\phi) + (5/14)^{\frac{1}{2}}\{Y_4^4(\theta,\phi) + \bar{Y}_4^4(\theta,\phi)\}$ has a cubic, or octahedral symmetry where the z-axis of the octahedron lies along the polar axis.

As an example, the effect of a cubic crystal field on the d wave functions is considered below. The matrix elements $\langle l,m_l'|Y_n^m(\theta,\phi)|l,m_l\rangle$ [redacted] vanishes unless $m_l' = m + m_l$. Since the cubic field is described by terms having m = 0 or $\pm$ 4 only, the state $|2,0\rangle$ will have non-zero matrix elements only to states with m = 0 or $\pm$ 4. Since no d wave functions have n = $\pm$ 4 the state $|2,0\rangle$ has a matrix element only with itself i.e. it is an eigenstate. Similary $|2,1\rangle$ and $|2,-1\rangle$ are eigenstates but

the same is not true of $|2,\pm2\rangle$. For these, two mutually orthogonal linear combinations, $\frac{1}{\sqrt{2}}(|2,+2\rangle-|2,-2\rangle)$ and $\frac{1}{\sqrt{2}}(|2,+2\rangle+|2,-2\rangle)$, must be taken. A perturbation calculation shows that $|2,+1\rangle, |2,-1\rangle$ and $\frac{1}{\sqrt{2}}(|2,+2\rangle+|2,-2\rangle)$ are degenerate and so are $|2,0\rangle$ and $\frac{1}{\sqrt{2}}(|2,+2\rangle - |2,-2\rangle)$. The first group is referred to as $d\epsilon$ and the second as $d\gamma$.

The situation can be understood in a simple way as follows. If a d electron is in an octahedral crystal field with pairs of negative charges or dipoles along x,y, and z,axes, then it can be seen from Fig. (2.5.), that d_{xy}, d_{yz}, d_{xz}, orbitals have their maximum lobes pointing in between the ligands, whereas $d_{x^2-y^2}$ and $d_{3z^2-r^2}$ have their maximum lobes pointing towards them. Thus an electron will experience greater repulsion in the latter orbitals than in the former ones and the $d\epsilon$ triplet (d_{xy}, d_{yz}, d_{zx}) will have lower energy than the $d\gamma$ doublet ($d_{x^2-y^2}$, $d_{3z^2-r^2}$).

The splitting of the d orbitals into $d\gamma$ and $d\epsilon$ groups with different energies results in the 'quenching of the orbital angular momentum'. Though the expectation value of $\vec{L}^2$ in the $d\epsilon$ orbitals is 2(2+1), the expectation value of L_z in the three $d\epsilon$ orbitals is +1,0, and -1. Since the expectation value of L_z in the $d\gamma$ orbitals is zero, the d electron in the octahedral crystal field can never exhibit its full angular momentum. This is what is meant by 'quenching of orbital angular momentum.'

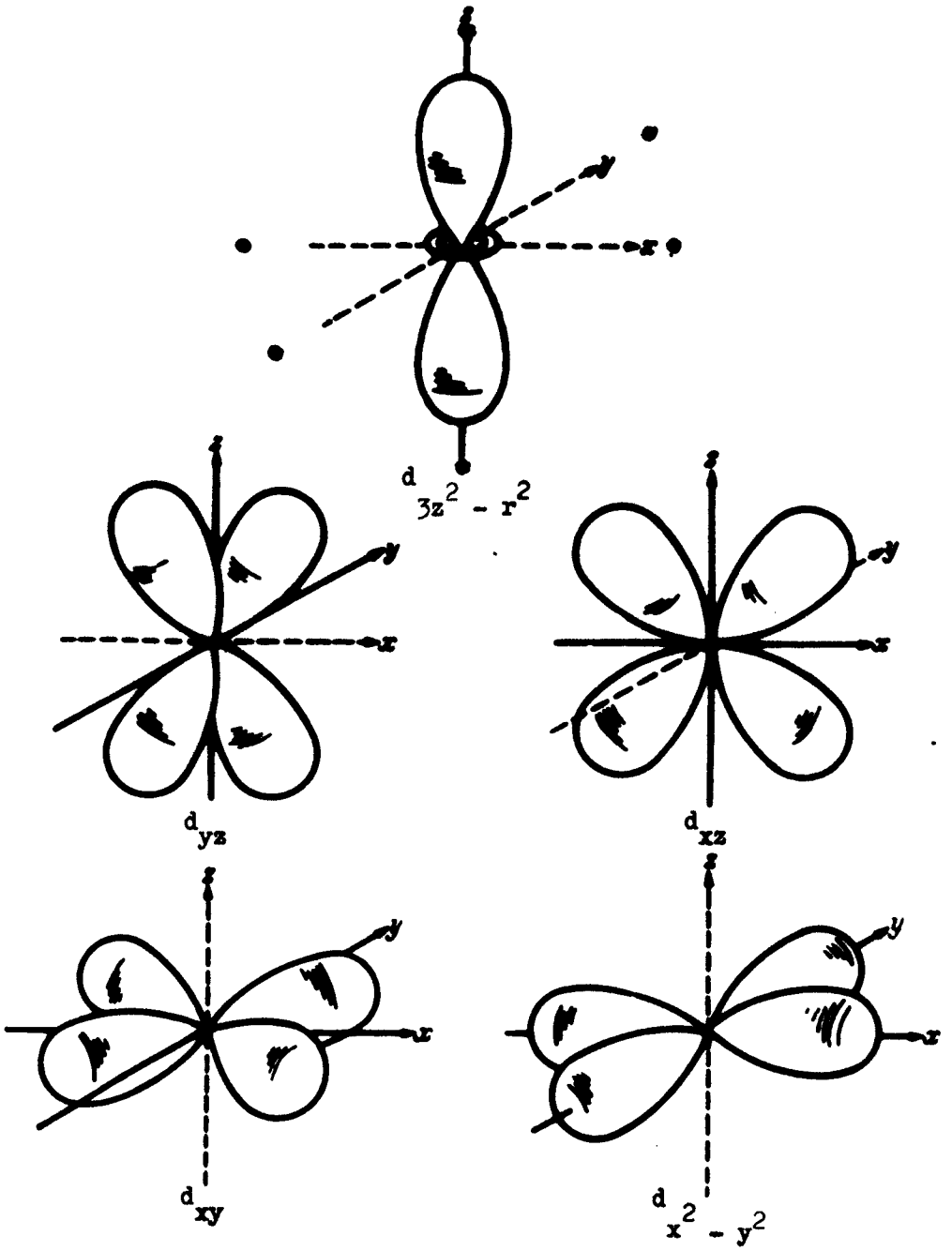

FIG. 2.5. CHARGE CLOUDS ASSOCIATED WITH d-ORBITALS.

(The dots represent negative ions of the octahedral complex).

The $d\epsilon$ electron behaves as if it had an orbital angular momentum of one unit. Alternatively, the orbital degeneracy of the level may be put equal to $2l' + 1$ where l' gives the effective orbital angular momentum. In the case of a $d\epsilon$ electron in an octahedral field, the orbital degeneracy is three and, hence, the effective orbital angular momentum is of one unit.

As another example of the quenching of orbital angular momentum, the $(d\epsilon)^3$ configuration may be considered. In accordance with Hund's rule, one electron will go to each of the $d\epsilon$ orbitals. Because the three $d\epsilon$ orbitals are symmetrical about the origin, the orbital moments of the three electrons will balance to zero. Thus the effective L' will equal to zero, in contrast to the free d^3 ion for which L equals three.

In fact, it can be shown that a $d\epsilon$ electron behaves like a p-electron with a positive charge (Kotani, 1960). Thus the magnetic properties of $(d\epsilon)^n$ configuration can be discussed analogously to p^n, if the magnetogyric ratio $-\frac{|e|}{2mc}$ is replaced by $+\frac{|e|}{2mc}$. The corresponding coupling scheme for angular momenta and magnetic moments is illustrated in Fig. (2.6.).

Small components of the crystal field that are of lower symmetry, and spin-orbit interaction, will further lift the degeneracy of a d orbital. Two general theorems are very helpful in determining the degeneracy of the ground state of the ion.

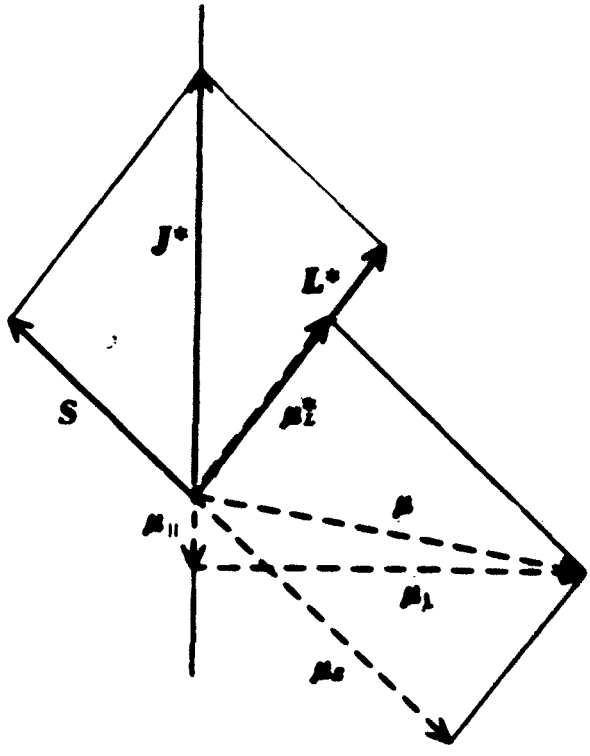

FIG. 2.6. COUPLING OF SPIN AND EFFECTIVE ORBITAL ANGULAR MOMENTUM IN d_ε ORBITALS.

(1) Kramer's Theorem. This theorem states that in a system containing an odd number of electrons, an electric field, of any kind of symmetry whatsoever, cannot completely lift the degeneeracy of the system, but will leave each level with an even degeneracy.

Kramer's degeneracy is related to the invariance of the system under time reversal. In the absence of an external magnetic field, the Hamiltonian of the system remains unchanged when t is replaced by -t. If K represents the operator of time reversal and ψ represents some eigen-state of the system with eigen-value E, then

$$\mathcal{H}K\psi = K\mathcal{H}\psi = KE\psi = EK\psi$$

so that $K\psi$ is also an eigen-solution of the Schrödinger equation with the same eigenvalue E. It can be shown (Low, 1960) that for n electrons, the operator of time reversal is

$$K = i^n s_{y_1} \ldots . S_{y_n} \; C$$

where C is the operator which replaces the function by its complex conjugate and s_y's are y-components of spin functions.

$$s_y = \begin{pmatrix} 0 & -i \\ i & 0 \end{pmatrix}$$

If the two wave functions ψ and $K\psi$ are linearly dependent i.e. if $K\psi = a\psi$ where a is a complex number, then

$$K^2\psi = K(K\psi) = K(a\psi) = a^* K\psi = |a|^2\psi$$

But $$K^2 = (i^n s_{y_1} \ldots s_{y_n})^2 = (-1)^n . 1$$

so that $$|a|^2 = (-1)^n$$

This can be true, however, only for even n. Hence for odd n, $K\psi$ and ψ are necessarily linearly independent and the energy state is degenerate.

However in the presence of an external magnetic field, the time inversion as such is not a symmetry element and hence it does not commute with the Hamiltonian. Hence the energy states are non-degenerate. An external magnetic field would, thus, lift Kramer s degeneracy, if any.

(2) Jahn-Teller Theorem. The theorem of Jahn and Teller states that a non-linear molecule or complex which has a degenerate ground state will spontaneously distort so as to produce an asymmetry sufficient to remove the degeneracy.

The energy-distortion curves for the degenerate states may cross or touch or coincide (Fig. 2.7.). In the first case, as the levels split, one of them would have lower energy and one higher than the centre of gravity which would remain the same as before distortion. Since any system tends to a state having the minimum possible energy, it would distort so as to remove the degeneracy and go over to the lower state.

According to Jahn and Teller, the second case is not possible for real systems. The third case is that of Kramer s degeneracy. Thus a Jahn-Teller distortion cannot remove

FIG. 2.7. JAHN-TELLER EFFECT IN RELATION TO ENERGY DISTORTION CURVES.

The curves (a) cross (b) touch or(c) coincide.

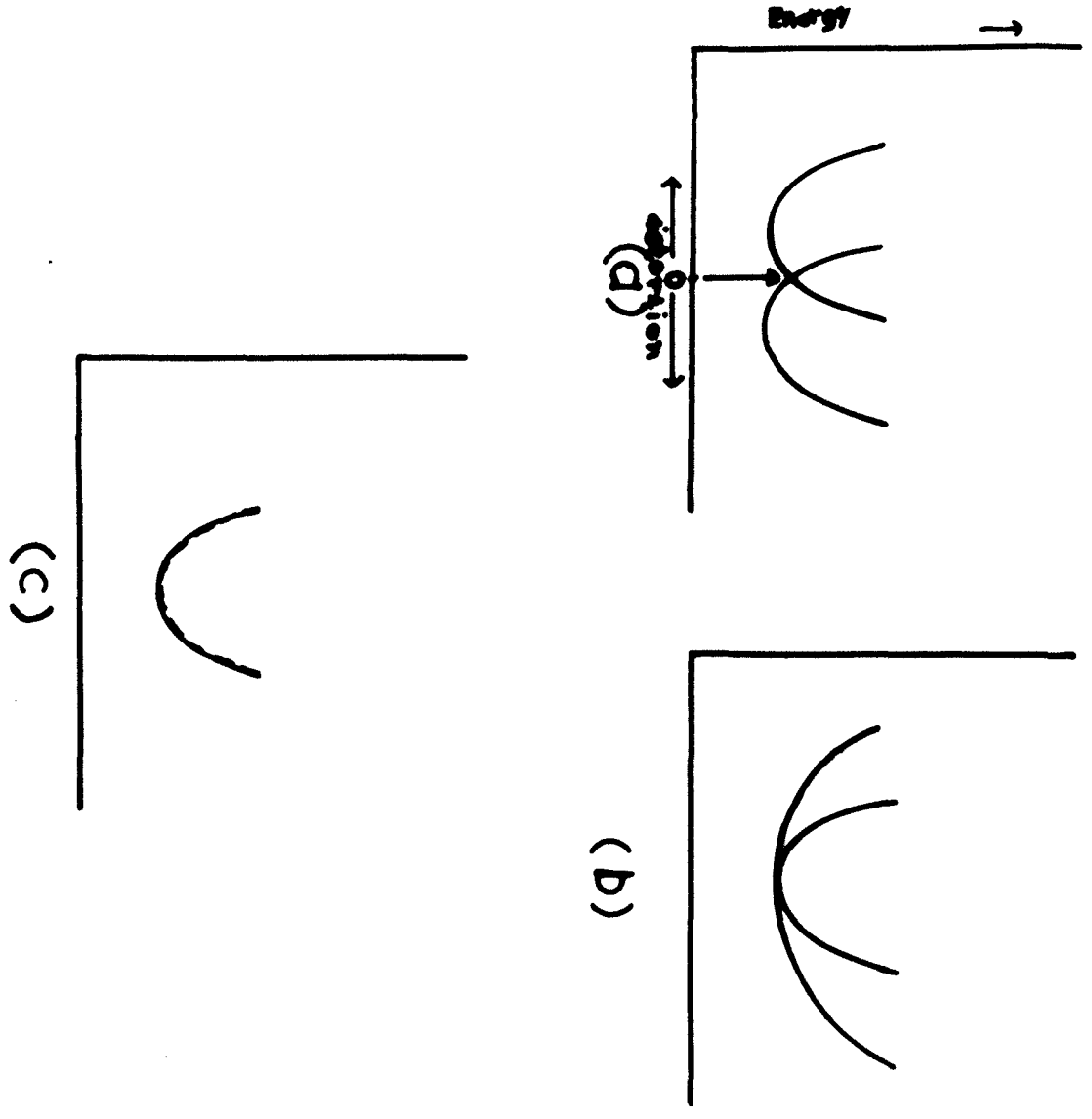

Kramer s degeneracy.

2.3.2. The Theoretical Hamiltonian

The various terms in the Hamiltonian of the free ion (neglecting nuclear hyperfine interactions) are listed below in decreasing order of magnitude. They are:

(a) The Coulomb interaction of the electrons with the nucleus (assumed fixed) and with each other. In the non-relativistic approximation, this is given by

$$\sum_k \left(\frac{\vec{p}_k^2}{2m} - \frac{Ze^2}{r_k} \right) + \sum_{k>j=1}^{N} e^2/r_{kj}$$

Here $\vec{p}_k$ is the linear momentum of the kth electron and $\vec{r}_k$ is the radius vector extending from the nucleus to the electron. The whole expression is summed over all N electrons; k and j refer to the electron in the ion.

This expression is treated by the self-consistent field method in which the electrons move independently of each other within the restrictions of the exclusion principle. Account is next taken of the correlations between the electrons. This gives rise to the correlation energy terms

$$\sum_{kj} (a_{kj} \vec{l}_k . \vec{l}_j + b_{kj} \vec{s}_k . \vec{s}_j)$$

which may be thought of as arising from very large but fictitious magnetic interactions between the corresponding vectors.

(b) The magnetic interactions between spins and orbits given by

$$\sum_{kj} \vec{cl}_k \cdot \vec{s}_j$$

For states of definite L and S of the same configuration, the spin-orbit interaction can be written as

$$\lambda \vec{L} \cdot \vec{S}$$

where λ is the spin-orbit coupling constant.

(c) The magnetic dipolar interaction between the spins given by

$$\sum_{kj} \left(\frac{\vec{s}_k \cdot \vec{s}_j}{r^3_{Kj}} - \frac{3(\vec{r}_{kj} \cdot \vec{s}_k)(\vec{r}_{kj} \cdot \vec{s}_j)}{r^5_{kj}} \right)$$

(d) Interaction with an external magnetic field given by

$$\sum_k \frac{eh}{4\pi mc} (\vec{l} + 2\vec{s})_k \cdot \vec{H} + \frac{e^2H^2}{8mc^2} \sum_k (x^2+y^2)_k$$

The second term in this expression gives rise to diamagnetism and would not be considered further.

The order of magnitude of these terms are 10^5 cm^{-1} for the Coulomb interactions, 10^2-10^3 cm^{-1} for the spin-orbit coupling and 1 cm^{-1} for the magnetic spin-spin coupling. The interaction with the external magnetic field depends upon the strength of the latter and in usual electron resonance experiments it is of the order of 1 cm^{-1}.

For ions in a crystal lattice, there will be an extra term, V, due to the interaction of the electrons with the crystal

field. In the iron group hydrated salts, it is less than the Coulomb interactions but larger than the spin-orbit interactions. For states of a given L and S, the total perturbation Hamiltonian reduces to the form

$$V + (\lambda - \tfrac{1}{2}\rho)(\vec{L}.\vec{S}) - \rho(\vec{L}.\vec{S})^2 + \beta\vec{H}.(\vec{L} + 2\vec{S}) \qquad (2.25.)$$

in which certain constant terms, like $-\frac{1}{3}\rho L(L+1)S(S+1)$, which shift all levels equally have been omitted.

2.3.3. Spin Hamiltonian

The theoretical Hamiltonian can be thrown into a parametric form using the method of Pryce (1950). The method is only applicable when the lowest orbital state is a singlet, and consists of a perturbation treatment in which the spin operators are treated as non-commuting algebraic quantities.

A simple Hamiltonian of the form

$$\mathcal{H} = \beta\vec{H}.(\vec{L} + 2\vec{S}) + \lambda\vec{L}.\vec{S} \qquad (2.26.)$$

can be used to illustrate this. Denoting the unperturbed ground state as $|o\rangle$ and the excited states as $|n\rangle$, and applying first order perturbation theory, one gets

$$\langle 0|\mathcal{H}'|0\rangle = \langle 0|2\beta\vec{H}.\vec{S}|0\rangle + \langle 0|\beta\vec{H}.\vec{L} + \lambda\vec{L}.\vec{S}|0\rangle$$

$$= 2\beta\vec{H}.\vec{S}\langle 0|0\rangle + \langle 0|(\beta H_x + \lambda S_x)L_x + (\beta H_y + \lambda S_y)L_y + (\beta H_z + \lambda S_z)L_z|0\rangle$$

$$= 2\beta\vec{H}.\vec{S} + (\beta H_x + \lambda S_x)\langle 0|L_x|0\rangle + (\beta H_y + \lambda S_y)\langle 0|L_y|0\rangle$$

$$+ (\beta H_z + \lambda S_z)\langle 0|L_z|0\rangle .$$

$$= 2\beta\vec{H}.\vec{S} \qquad (2.27.)$$

since for a singlet orbital state

$$\langle 0|L_x|0\rangle = \langle 0|L_y|0\rangle = \langle 0|L_z|0\rangle = 0$$

Considering the second order perturbation, one gets,

$$-\sum_{n\neq 0} \frac{|\langle 0|\beta\vec{H}.\vec{L} + 2\beta\vec{H}.\vec{S} + \lambda\vec{L}.\vec{S}|n\rangle|^2}{E(n) - E(0)} \qquad (2.28.)$$

It may be noted that, on evaluation of the matrix elements $\langle 0|L_x|n\rangle$ etc., the final expression would be quadratic in the components of $\vec{H}$ and $\vec{S}$ and will take the form

$$-\beta^2 \Lambda_{ij} H_i H_j - \beta f_{ij} H_i S_j + d_{ij} S_i S_j$$

where i, j = x,y,z and Λ_{ij}, f_{ij} and d_{ij} are factors. Thus, for the lowest orbital singlet one gets

$$\mathcal{H}'_s = \beta(2\delta_{ij} - f_{ij})\, H_i S_i - \beta^2 \Lambda_{ij} H_i H_j + d_{ij} S_i S_j \qquad (2.29.)$$

which can also be written in the form

$$\mathcal{H}'_s = \vec{S}.D.\vec{S} + \beta\vec{H}.g.\vec{S} - \beta^2\vec{H}.\Lambda.\vec{H}$$

where $g = 2\delta - f$, Λ and D are tensors. The Hamiltonian so expressed in terms of spin operators only is called the Spin Hamiltonian. Though the expression (2.30) was derived for a simple theoretical Hamiltonian, it is sufficiently general and holds for the Hamiltonian (2.25.) as well.

The spin-Hamiltonian may, alternatively, be considered as a phenomenological description of the system, the parameters g, D, and Λ being determined by the experimental results. Suitable theoretical models have then to be developed to account for the observed values of these constants.

The spin-Hamiltonian can be used even in cases where the lowest level is orbitally degenerate. If transitions between $2S' + 1$ levels are observed experimentally, S' is defined as 'effective' or 'fictitious' spin and is used in the spin Hamiltonian. For an orbital singlet lowest state, the splitting of the spin degeneracy is usually fairly small and the effective spin is equal to the actual spin. For an orbitally degenerate state, however, components of crystal field of lower symmetry and spin-orbit interaction usually produce a splitting of order 100 cm^{-1}, and in accordance with Kramer s and Jahn-Teller theorems, no resonance would be expected if the number of electrons is even and effective spin would be $\frac{1}{2}$ if the number of electrons is odd.

A sufficiently general spin Hamiltonian can be written in the component form as

$$\mathcal{H} = \beta(g_z H_z S_z + g_x H_x S_x + g_y H_y S_y) + D\left\{S_z^2 - 1/3\ S(S+1)\right\} + E(S_x^2 - S_y^2) \quad \ldots\ldots \quad (2.31.)$$

in which the principal axes x, y, and z are assumed to be the same in all terms. The first term in the parentheses represents the splitting of the $(2S + 1)$ multiplets by the applied magnetic

field. In this term g_x, g_y, g_z are the values of the spectroscopic splitting factor g along the principal axes. The term $D\left\{S_z^2 - 1/3\ S(S+1)\right\}$ represents the initial splitting (i.e. with zero magnetic field) of the spin multiplet by an axially symmetric (trigonal or tetragonal) component of the crystalline field. The term $E(S_x^2 - S_y^2)$ represents possible initial splitting by the crystalline field components of still lower symmetry (rhombic).

For an axially symmetric field, the spin Hamiltonian takes the simple form

$$\mathcal{H} = \beta\left\{g_{\parallel}H_zS_z + g_{\perp}(H_xS_x + H_yS_y)\right\} + D\left\{S_z^2 - 1/3\ S(S+1)\right\} \quad \ldots\ldots \quad (2.32.)$$

where the axis of symmetry is taken as the z-axis, and $g_{\parallel} = g_z$ and $g_x = g_y = g_{\perp}$.

Fig. (2.8.) shows, as an example, the splitting of the energy levels by crystal and external magnetic fields in the case of Cr^{3+} ion. It is seen that the 'fine structure' of the transition arises from the 'zero field splitting' of the lowest orbital singlet.

2.3.4. g-factor

It is seen from the terms in $\vec{H}$ and $\vec{S}$ in equation (2.31.) that the spin is no longer completely free. Either it can be regarded as having an anisotropic magnetic moment $\left\{g_xS_x, g_yS_y, g_zS_z\right\}$ or as freely precessing about the field $\left\{g_xH_x, g_yH_y, g_zH_z\right\}$. For an arbitrary orientation of $\vec{H}$ with

FIG. 2.8. ENERGY LEVEL DIAGRAM OF Cr^{3+} IN AN AXIAL FIELD.

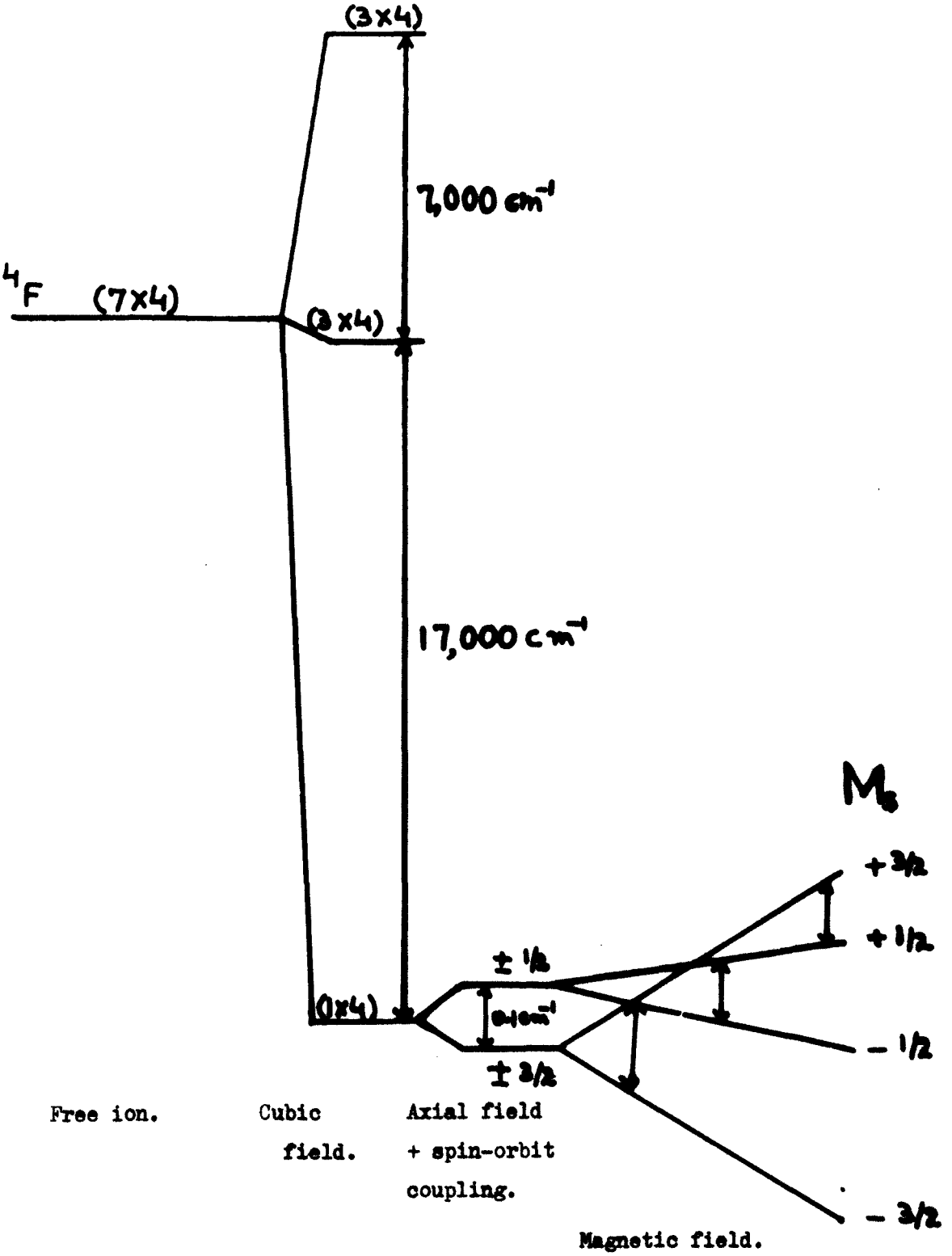

direction cosines (l, m, n) with respect to the coordinate system of the crystal field, the effective magnetic field about which the spin may be supposed to precess freely would be $(g_x^2 l^2 + g_y^2 m^2 + g_z^2 n^2)^{\frac{1}{2}} H$. This may be written as gH, so that

$$g^2 = (g_x^2 l^2 + g_y^2 m^2 + g_z^2 n^2) \qquad \ldots\ldots \qquad (2.33.)$$

If θ and ϕ are the polar and azimuthal angles of $\vec{H}$ in the crystal field coordinate system, equation (2.33.) can be written in the alternative form

$$g^2 = g_{\parallel}^2 \cos^2\theta + g_{\perp}^2 \sin^2\theta \qquad \ldots\ldots \qquad (2.34.)$$

where $g_{\perp}^2 = g_x^2 \cos^2\phi + g_y^2 \sin^2\phi$

and $g_{\parallel} = g_z$

The direction of the effective field, $\vec{gH}$, is given by

$$\cos\psi = \frac{g_{\perp}}{g} \cos\theta \qquad \ldots\ldots \qquad (2.35.)$$

where ψ is the angle between the direction of $\vec{gH}$ and the z-axis. This is illustrated in Fig. (2.9.).

If the term $\beta(g_z H_z S_z + g_x H_x S_x + g_y H_y S_y)$ of the spin Hamiltonian is transformed to a coordinate system having the z' axis along the direction of the effective field, $\vec{gH}$, then it takes a simple form $g\beta S'_z.H$ where g is given by equation (2.33.) (Low, 1960). In the strong magnetic field case, this can be written as $g\beta M'_s H$, so that the resonant frequency for $\Delta M'_s = \pm 1$ transitions would be given by the relation

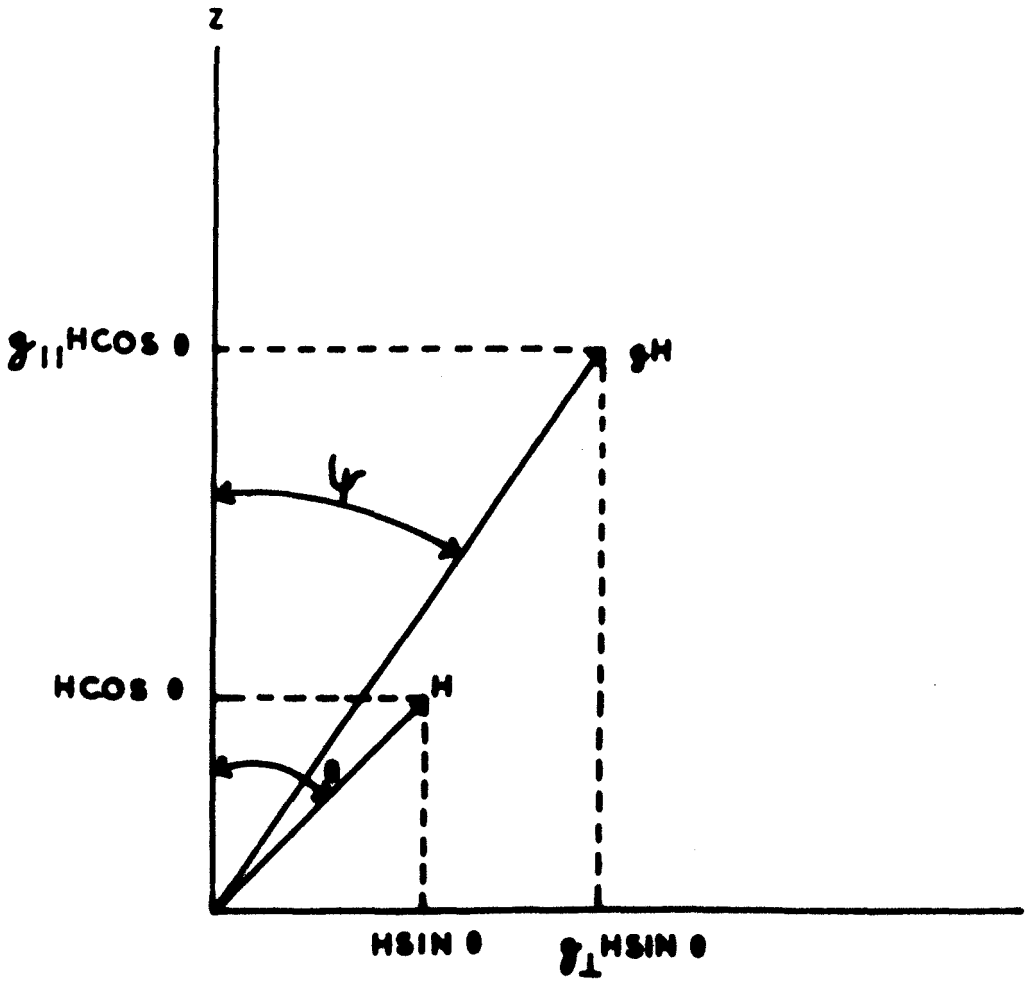

FIG. 2.9 ORIENTATION OF THE EFFECTIVE MAGNETIC FIELD WITH RESPECT TO THE Z-AXIS.

$$h\nu = g\beta H.$$

It is thus seen that the usage of the symbol g in the spin Hamiltonian is consistent with the definition of g-factor given in Chapter I. It is an experimentally defined quantity and measures the splitting between the $2S' + 1$ levels in an external magnetic field, H, applied at any angle with respect to the crystal field axes.

2.3.5. Covalent bonding

So far the effects of the ligands on the metal ion have been taken account of by replacing the ligands with point charges or point dipoles. Thus the interactions have necessarily been assumed to be electrostatic in nature. In covalently bonded complexes this no longer applies. However, the electrostatic theory can still be applied (Van Vleck, 1935). The principal features of the orbital energy-level diagram for d electrons calculated from electrostatic theory agree with those obtained on the basis of the molecular orbital theory. In the latter, the metal and ligand orbitals are combined to give complete molecular orbitals. Since only those orbitals which transform as the same representation of the molecular point group can combine together to give molecular orbitals, the ligand orbitals are first combined among themselves to give symmetry orbitals so as to match those on the metal ion.

A more general approach is that of 'Ligand Field Theory'

where the ligand field splittings are the result of a number of more or less independent mechanisms. The total splitting is thought of as the algebraic sum of a number of individual contributions, due to electrostatic effects, σ bonding, π bonding, etc. Even this, however, is not a completely satisfactory theory and a complete theory would be a molecular orbital one in which all the important electrostatic interactions are dealt with in detail.

In covalently bonded complexes, the covalent forces cause much larger splittings of the energy levels. In terms of the electrostatic theory, this corresponds to the strong field case. The energetic considerations compete with the requirements of the Hund's rule, and if the crystal field is sufficiently strong, the coupling between individual $\vec{l}$'s and $\vec{s}$'s is broken down.

Though the mechanisms postulated by the electrostatic and molecular orbital theories for the energy level splittings are inherently different, this does not prevent the use of spin Hamiltonian in the case of covalent bonding. In a phenomenological theory using a spin Hamiltonian, one is concerned with the amount, and not the cause, of the energy level splittings. Thus a spin Hamiltonian can be used to describe formally the behaviour of a covalently bonded complex as well.

2.3.6. Nuclear Hyperfine Interactions

Many nuclei have electric and magnetic moments, which would interact with the electrons. These interations would now be considered.

2.3.6.1. Magnetic Interactions

The magnetic moment of a nucleus is given by $\vec{\mu_N} = g_N\beta_N\vec{I}$, where g_N is the nuclear g-factor, β_N is a unit of magnetic moment, called the nuclear magneton, and is equal to $eh/4\pi Mc$ where M is the nuclear mass, and $\vec{I}$ is the vector representing the total angular momentum of the nucleus, commonly referred to as the nuclear spin.

$\vec{I}$ is made up of the orbital and intrinsic angular momenta of the nucleons and hence the nuclear spin quantum number I is integral for nuclei with an even number of constituents and is half-integral for nuclei with an odd number. In particular, even-even nuclei have I = 0 in the ground state.

The spin and orbital motions of the unpaired electrons produce a magnetic field at the nucleus. These give rise to the following interactions:

(i) Dipolar interaction between the electron and the nuclear spins. The field due to the electron spin, treated as a dipole, at the nucleus is

$$\vec{H_N} = -g_e\beta_e\sum_k\left[\frac{\vec{s_k}}{r_k^3} - \frac{3(\vec{r_k}.\vec{s_k})\,\vec{r_k}}{r_k^5}\right] \quad \ldots\ldots \quad (2.36.)$$

and hence the interaction energy of the nucleus, treated as a dipole, in this field is

$$-g_eg_N\beta_e\beta_N\sum_k\left[\frac{\vec{s_k}.\vec{I}}{r_k^3} - \frac{3(\vec{r_k}.\vec{s_k})(\vec{r_k}.\vec{I})}{r_k^5}\right] \ldots\ldots \quad (2.37.)$$

(ii) The interaction of the nucleus with the field, $2\beta_e \vec{l_k}/r_k^3$, produced by the orbital motion of the electron at the nucleus. The interaction energy is

$$2\beta_e g_N \beta_N \sum_k \frac{\vec{l_k}.\vec{I}}{r_k^3} \qquad \ldots\ldots \qquad (2.38.)$$

(iii) The Fermi contact interaction

$$\frac{8\pi}{3} g_e g_N \beta_e \beta_N \sum_k \delta(\vec{r_k}) (\vec{s_k}.\vec{I}) \qquad \ldots\ldots \qquad (2.39.)$$

where $\delta(\vec{r_k})$ is the Dirac's delta-function. It is seen that this interaction vanishes unless the electron has a finite probability density at the nucleus.

Expression (2.39.) was derived by Fermi using Dirac's relativistic theory, but the origin of the contact interaction can be simply illustrated in the case of one electron (Landau and Lifshitz, 1958).

The current density, $\vec{j}$, due to the spin motion of the electron is given by

$$\vec{j} = g_e \beta_e c \; \mathrm{curl} \; (|\psi|^2 \vec{s})$$

The magnetic field due to this current distribution at any point, P, will be given by

$$\vec{H} = \frac{1}{c} \int \nabla \left(\frac{1}{r}\right) \times \vec{j} \, dV$$

where r is the distance of the point, P, from the current element $\vec{j}\, dV$, and the operator ∇ refers to the coordinates of the

point P.

Writing $|\psi|^2 \vec{s}$ as $\vec{F}$, one gets

$$\vec{H} = g_e\beta_e \int \nabla \left(\frac{1}{r}\right) \times \text{curl } \vec{F}\, dV$$

and the integration gives

$$\vec{H} = \frac{8\pi g_e\beta_e}{3} \vec{F}(0) = \frac{8\pi}{3} g_e\beta_e \left|\psi(0)^2\right| \vec{s}$$

where $F(0)$ and $\psi(0)$ refer to these quantities at P. The interaction energy of the nucleus of magnetic moment $g_N\beta_N\vec{I}$ with this field is

$$-\frac{8\pi}{3} g_e\beta_e g_N\beta_N |\psi(0)|^2 \vec{s}.\vec{I} \qquad \ldots\ldots \qquad (2.40.)$$

This shows that the interaction vanishes unless the electron has a finite probability density at the nucleus. It may be noted that although the electron cannot stay permanently trapped in the nucleus, it can pass through it and this is sufficient to give rise to the Fermi interaction.

Apart from these interactions of the nuclear spin with the unpaired electrons, the nuclear magnetic moment would also interact with the external magnetic field. This energy would be given by the expression

$$- g_N\beta_N \vec{H}.\vec{I} \qquad \ldots\ldots \qquad (2.41.)$$

2.3.6.2. Electrostatic Interaction

The electrostatic interaction of the nucleus with the electrons can be taken account of in the following way. The

potential of the field produced by a distribution of charges at an external point is

$$\phi = \sum_A \frac{e_A}{|(\vec{r} - \vec{R}_A)|} \qquad \ldots\ldots \qquad (2.42.)$$

where $(\vec{r} - \vec{R}_A)$ are the radius vectors from the charges e_A to the point P where the potential is to be found. The origin of the coordinate system is chosen here at the electrical 'centre of gravity' of the system of charges. The potential ϕ can be expanded in powers of $\vec{R}_A$ and the expansion written as

$$\phi = \phi^{(1)} + \phi^{(2)} + \phi^{(3)} + \cdots \qquad \ldots\ldots \qquad (2.43.)$$

The first term, $\phi^{(1)}$, gives the potential at the point P when all the charges are assumed to be concentrated at a point. This has already been taken account of in establishing the unperturbed Hamiltonian. The second term $\phi^{(2)}$, which represents the dipole field, vanishes for nuclei in the stationary state. The effect of the third term $\phi^{(3)}$ would be considered here. According to Taylor's theorem it is given by

$$\phi^{(3)} = \tfrac{1}{2} \sum e X_\alpha X_\beta \frac{\partial^2}{\partial x_\alpha \partial x_\beta} \left(\frac{1}{r}\right)$$

where the sum goes over all charges; the index numbering the charges has been dropped here; x_α are the components of the vector $\vec{r}$ and X_α those of $\vec{R}$. Moreover, since the function $\frac{1}{r}$ satisfies the Laplace equation i.e.

$$\delta_{\alpha\beta} \frac{\partial^2}{\partial x_\alpha \partial x_\beta} \left(\frac{1}{r}\right) = 0$$

one gets

$$\phi^{(3)} = \tfrac{1}{2}\sum e\,(X_\alpha X_\beta - \tfrac{1}{3}R^2\delta_{\alpha\beta})\,\frac{\partial^2}{\partial x_\alpha \partial x_\beta}\left(\frac{1}{r}\right) \quad \ldots\ldots \quad (2.44.)$$

$$= \frac{Q_{\alpha\beta}}{2}\,\frac{\partial^2}{\partial x_\alpha \partial x_\beta}\left(\frac{1}{r}\right)$$

where the tensor

$$Q_{\alpha\beta} = \sum e\,(3X_\alpha X_\beta - R^2\delta_{\alpha\beta}) \quad \ldots\ldots \quad (2.45.)$$

is the quadrupole moment tensor of the system. It is a symmetric tensor with five independent components. (together with the condition that it must be traceless).

If the distribution of the charges is due to the protons in the nucleus and if the electron of charge, -e, is assumed to be at the point P, then the mutual potential energy of the system due to the quadrupole moment term is

$$V = -e\,\frac{Q_{\alpha\beta}}{6}\,\frac{\partial^2}{\partial x_\alpha \partial x_\beta}\,\frac{1}{r} = -e\,\frac{Q_{\alpha\beta}}{6}\,\frac{(3x_\alpha x_\beta - \delta_{\alpha\beta}r^2)}{r^5} \quad \ldots\ldots \quad (2.46.)$$

The quantum-mechanical quadrupole moment tensor operator can be obtained from the classical expression by replacing $(3X_\alpha X_\beta - R^2\delta_{\alpha\beta})$ by its operator equivalent. This gives

$$Q_{\alpha\beta} = C\left\{\frac{3}{2}\,(I_\alpha I_\beta + I_\beta I_\alpha) - \delta_{\alpha\beta}\,\vec{I}^2\right\} \quad \ldots\ldots \quad (2.47.)$$

The expectation value of Q_{zz} for the state $I_z = I$ is usually called the 'quadrupole moment' and denoted as Q. Expressing the constant C in terms of Q, one gets

$$Q_{\alpha\beta} = \frac{Q}{I(2I-1)}\left\{\frac{3}{2}(I_\alpha I_\beta + I_\beta I_\alpha) - \delta_{\alpha\beta}\vec{I}^2\right\} \quad \ldots\ldots \quad (2.48.)$$

Thus the interaction energy becomes, from equations (2.46.) and (2.48.),

$$V_Q = -\frac{eQ}{6I(2I-1)}\left\{\frac{3}{2}(I_\alpha I_\beta + I_\beta I_\alpha) - \delta_{\alpha\beta}\vec{I}^2\right\} \times \left\{\frac{3x_\alpha x_\beta - \delta_{\alpha\beta}r^2}{r^5}\right\}$$

$$= \frac{eQ}{2I(2I-1)}\left\{\frac{\vec{I}^2}{r^3} - \frac{3(\vec{r}.\vec{I})^2}{r^5}\right\} \quad \text{(Griffith, 1960)}$$

For many electrons, the interaction energy can be written in its final form as

$$V_Q = \frac{e^2Q}{2I(2I-1)} \sum_j \frac{I(I+1)}{r_j^3} - \frac{3(\vec{r}_j.\vec{I})^2}{r_j^5} \quad \ldots\ldots \quad (2.49.)$$

where Q has been expressed in cm^2.

It may be noted that the expectation value of the quadrupole moment operator, Q_{z^2}, vanishes for states with $I = 0$ and $\pm \frac{1}{2}$. Thus only those nuclei that have a nuclear spin $I > \frac{1}{2}$ can have a finite quadrupole moment.

2.3.6.3. Nuclear Terms in Spin Hamiltonian

The nuclear interaction terms can be incorporated in the spin Hamiltonian by the method of Pryce, treating the nuclear spin operators as non-commuting algebraic quantities. A sufficiently general sub-Hamiltonian giving the contributions of nuclear interactions to the spin Hamiltonian can be written as

$$\mathcal{H}' = \vec{S}.T.\vec{I} + \vec{I}.P.\vec{I} - g_N\beta\vec{H}.\vec{I} \qquad \ldots\ldots \qquad (2.50.)$$

or in the component form as

$$\mathcal{H}' = A_x S_x I_x + A_y S_y I_y + A_z S_z I_z + P_z'\left\{I_z^2 - \frac{1}{3} I(I+1)\right\} + P'(I_x^2 - I_y^2) - g_N\beta_N\vec{H}.\vec{I} \qquad \ldots\ldots \qquad (2.51.)$$

It may be mentioned that magnetic interactions between the nucleus and the electrons are generally of the order of 10^{-2} cm^{-1}, and the nuclear quadrupole interactions and the direct interaction of the nuclear spin with the external magnetic field are both of the order of 10^{-4} cm^{-1}.

2.4. Free Radicals

2.4.1. g-factor

The g-factor can be written as

$$g = g_S + g_L + g_{LS} \qquad \ldots\ldots \qquad (2.52.)$$

Both the corrections to g are now considered.

(a) g_L:- In the diatonic molecules, only the component of $\vec{L}$ along the internuclear axis is conserved. This is because the field of force is cylindrically symmetric. The situation is essentially the same as that of an atom in a strong electric field, which is here the electrostatic field of the two nuclei. The molecule will have a permanent orbital magnetic moment only along the internuclear axis. The perpendicular component will be of the high frequency type.

When the molecule is polyatomic and non-linear, the entire orbital moment of the molecule will be of this high frequency type, unless the molecule has unusual symmetry. This is because the existence of a mean magnetic moment for an atom or molecule in the absence of external fields implies the existence of at least a two-fold degeneracy (Van Vleck, 1932). Even for symmetrical molecules, if a degeneracy exists, it will in general be lifted due to Jahn-Teller distortion. Hence the non-linear polyatomic free radicals will have practically no contribution from orbital magnetic moment and $g_L = 0$.

(b) g_{LS}:- This is given approximately by the relation

$$|g_{LS}| \sim \frac{\lambda}{\Delta} \qquad \ldots\ldots \qquad (2.53.)$$

where λ is the spin-orbit coupling constant and Δ is the energy separation between the electronic ground state and the lower excited orbital state (vide equations 2.28. and 2.29.). In general, λ is small when the environment of the electron departs greatly from spherical symmetry, whereas it is often quite appreciable for atoms with their essentially spherical symmetry. For most organic free radicals, therefore,

$|g - g_S| = g_{LS} < 0.01$.

However, in many free radicals containing sulphur and oxygen, considerable g-value shifts have been noted. This is presumably due to high electron affinity of these two atoms. The unpaired electron is considerably localised on these atoms

and, to that extent, is in atomic orbitals with consequential large spin-orbit coupling.

2.4.1.1. Anisotropy of g-factor

A trapped radical must of necessity have some electrostatic interaction with its trapping medium. The effect of the crystal field on the properties of an embedded radical can be studied by examining the nature of the field immediately surrounding the radical in a manner analogous to the treatment of paramagnetic ions. The crystal field would endow an anisotropy to the g-factor. There would also be a built in anisotropy depending upon the symmetry of the radical itself. g is thus a tensor and its value in any direction is given by equation (2.33.).

Since for a monoradical, the ground state is a Kramer s doublet, the effective spin = $\frac{1}{2}$, and the interaction of the unpaired electron with the external field is given by

$$\mathcal{H}_{H.S} = \vec{H}.g.\vec{S}$$

In any sample, which is not a single crystal, one observes a resonance arising from either a superposition or an average of g values. Providing the anisotropy is small enough, the g-factor can be written as

$$g = l^2 g_x + m^2 g_y + n^2 g_z \qquad \ldots\ldots \quad (2.54.)$$

where g_x, g_y, and g_z are the components along the principal axes of the g-tensor. The average g-value would then be given by

$$\langle g \rangle = \frac{g_x + g_y + g_z}{3} \qquad \ldots\ldots \quad (2.54.)$$

It may be noted that equation (2.54.) differs from the equation (2.33.) in that g in equation (2.54.) represents the effective magnetic field in the same direction as the external field.

2.4.2. Hyperfine Interaction

The Hamiltonian for the hyperfine interaction of the unpaired electron with one 'magnetic' nucleus can be written as

$$\mathcal{H}_{hf} = -\frac{8\pi}{3} g_I g_e \beta^2 \psi^2(0) \vec{I}.\vec{S} + g_I g_e \beta^2 \left\{ \frac{\vec{I}.\vec{S}}{r^3} - 3 \frac{(\vec{I}.\vec{r})(\vec{S}.\vec{r})}{r^5} \right\} - \frac{2 g_N \beta^2}{r^3} \vec{I}.\vec{L} \quad \ldots\ldots \quad (2.56.)$$

where $\psi^2(0)$ is the electronic density at the nucleus and g_I is the nuclear g-factor referred to the Bohr magneton β.

2.4.2.1. Isotropic Hyperfine Interaction

The isotropic Fermi contact interaction

$$-\frac{8\pi}{3} g_I g_e \beta^2 \psi^2(0) \vec{I}.\vec{S}$$

couples $\vec{I}$ and $\vec{S}$ giving the total angular momentum $\vec{F} = \vec{I} + \vec{S}$ and thereby causes a zero-fild splitting of the electronic energy level into two hyperfine energy levels, $F = I \pm \frac{1}{2}$, with an energy separation of

$$\Delta W = -\left[(2I + 1)/2\right] 8\pi/3 \; g_I g_e \beta^2 \psi^2(0)$$

In an external magnetic field, the total spin Hamiltonian is

$$\mathcal{H} = g_I \beta \vec{I}.\vec{H}_o + g_e \beta \vec{S}.\vec{H}_o + \frac{2\Delta W}{2I+1} \vec{I}.\vec{S} \quad \ldots\ldots \quad (2.57.)$$

The solution of equation (2.57.) is given by Breit-Rabi formula (Nafe and Nelson, 1948)

$$W_{I\pm\frac{1}{2}} = -\frac{\Delta W}{2(2I+1)} + g_I\beta M_F H_o \pm \frac{\Delta W}{2}\left(1 + \frac{4M_F x}{2I+1} + x^2\right)^{\frac{1}{2}} \quad \ldots\ldots \quad (2.58.)$$

where M_F is the magnetic quantum number of $\vec{F}$ and $x = (g_e - g_I)\beta H_o/\Delta W$.

There are thus altogether $2(2I + 1)$ states.

In a field when the Zeeman energy is much larger than the h.f. energy i.e. when $x \gg 1$, equation (2.58.) reduces approximately to

$$W_{M_I, M_S} = M_I g_I \beta H_o + M_S g_e \beta H_o + A M_I M_S \quad \ldots\ldots \quad (2.59.)$$

where $A = 2\Delta W/(2I + 1)$.

The selection rules for the limiting case are $\Delta M_I = 0$ and $\Delta M = \pm 1$. There are, therefore $2I + 1$ uniformly spaced lines symmetrically placed around the centre position defined by $h\nu_o = g\beta H_o$. Fig. (2.10.) illustrates a h.f. spectrum of this type for $S = \frac{1}{2}$ and $I = 1$.

The case of more than one 'magnetic' nucleus is an easy extension of the above. The spin Hamiltonian in the strong-field case is

$$\mathcal{H} = g\beta\vec{H}.\vec{S} + \sum_i A_i(\vec{S}.\vec{I_i}) - g_I\beta\sum_i \vec{I_i}.\vec{H}$$

where the effective spin $S = \frac{1}{2}$ as before. The energy eigen-values are

$$E = g\beta H M_S + \sum_i A_i M_S M_{I_i} - g_I\beta\sum_i M_{I_i} H \quad \ldots\ldots \quad (2.60.)$$

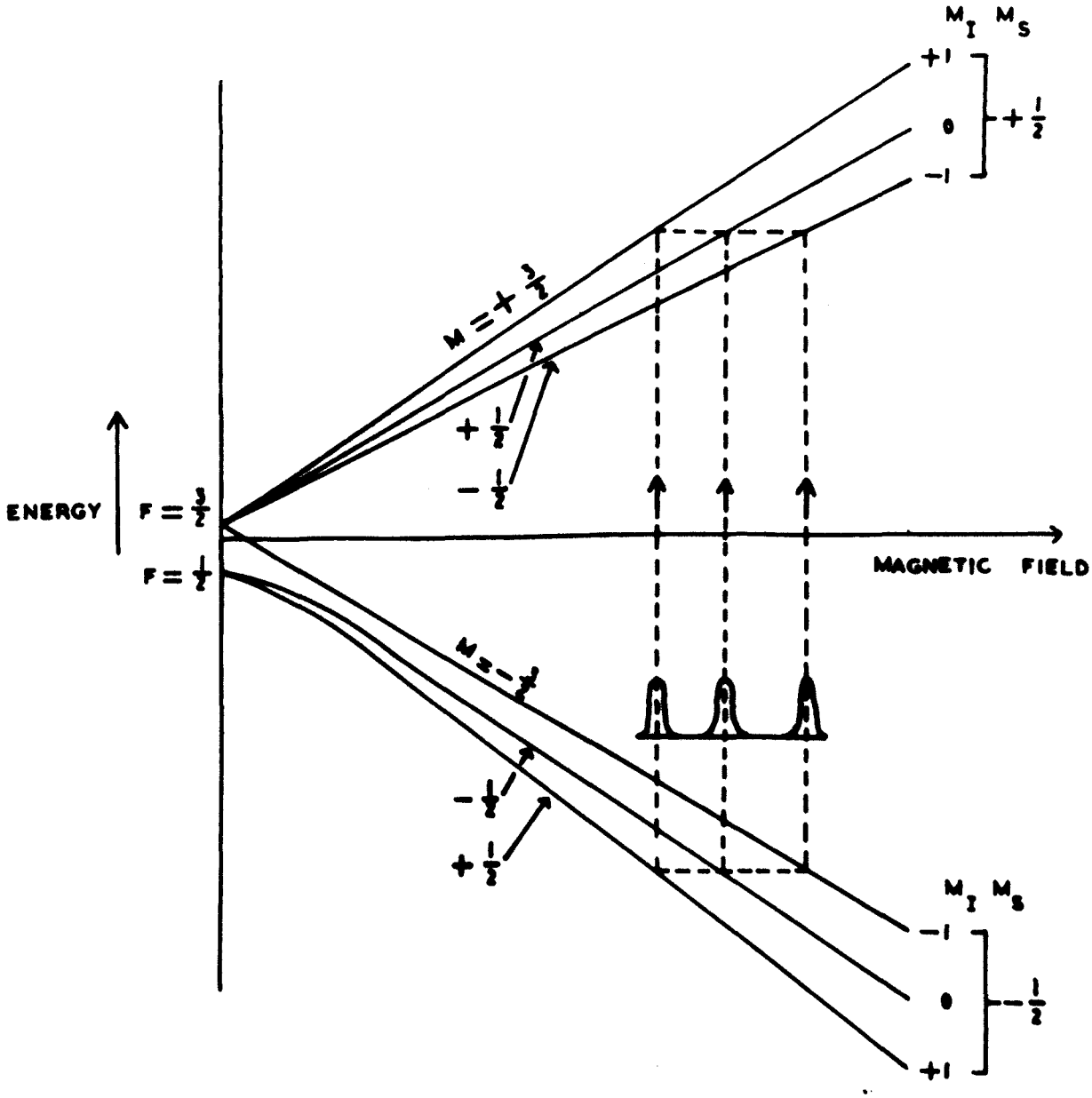

FIG. 2.10 ENERGY LEVEL DIAGRAM FOR $S=\frac{1}{2}$ AND $I=1$ AND THE n.j. SPECTRUM IN STRONG FIELD.

For transitions $\Delta M_I = 0$, $\Delta M_S = \pm 1$, the frequencies are given by

$$h\nu = g\beta H + \sum_i A_i M_{I_i} \qquad \ldots\ldots \quad (2.61.)$$

In general, there will be $\sum_i (2I_i + 1)$ components.

When the coupling constants for all nuclei are the same ($A_i = A$), equation (2.61.) can be written as

$$h\nu = g\beta H + A\sum_i M_i \qquad \ldots\ldots \quad (2.62.)$$

If in addition the spins of the equally coupling nuclei are also equal (i.e. $I_i = I$, $A_i = A$), the total spin $T = \sum_i M_i = nI$, so that

$$h\nu = g\beta H + AM_T = g\beta H + AnI \qquad \ldots\ldots \quad (2.63.)$$

and the hyperfine structure consists of $(2T + 1)$ or $(2nI + 1)$ equally spaced components.

If the equally coupling nuclei are protons ($I = \frac{1}{2}$)

$$h\nu = g\beta H + \frac{An}{2} \qquad \ldots\ldots \quad (2.64.)$$

and there are $(n + 1)$ equally spaced components. Fig. (2.11.) shows, as an illustration, the hyperfine splitting of the energy levels produced by two or three equally coupled protons.

2.4.2.2. Dipolar Hyperfine Structure

The dipolar interaction energy between a nucleus and the unpaired electron spin can be shown to be

$$W_{dip} = -\frac{M_I M_S g_I g_S \beta}{2} \left\langle \frac{3\mathrm{Cos}^2\alpha - 1}{r^3} \right\rangle_{av} (3\mathrm{Cos}^2\theta - 1) \qquad (2.65.)$$

where θ and α are the angles which $\vec{H_o}$ and $\vec{r}$ make respectively

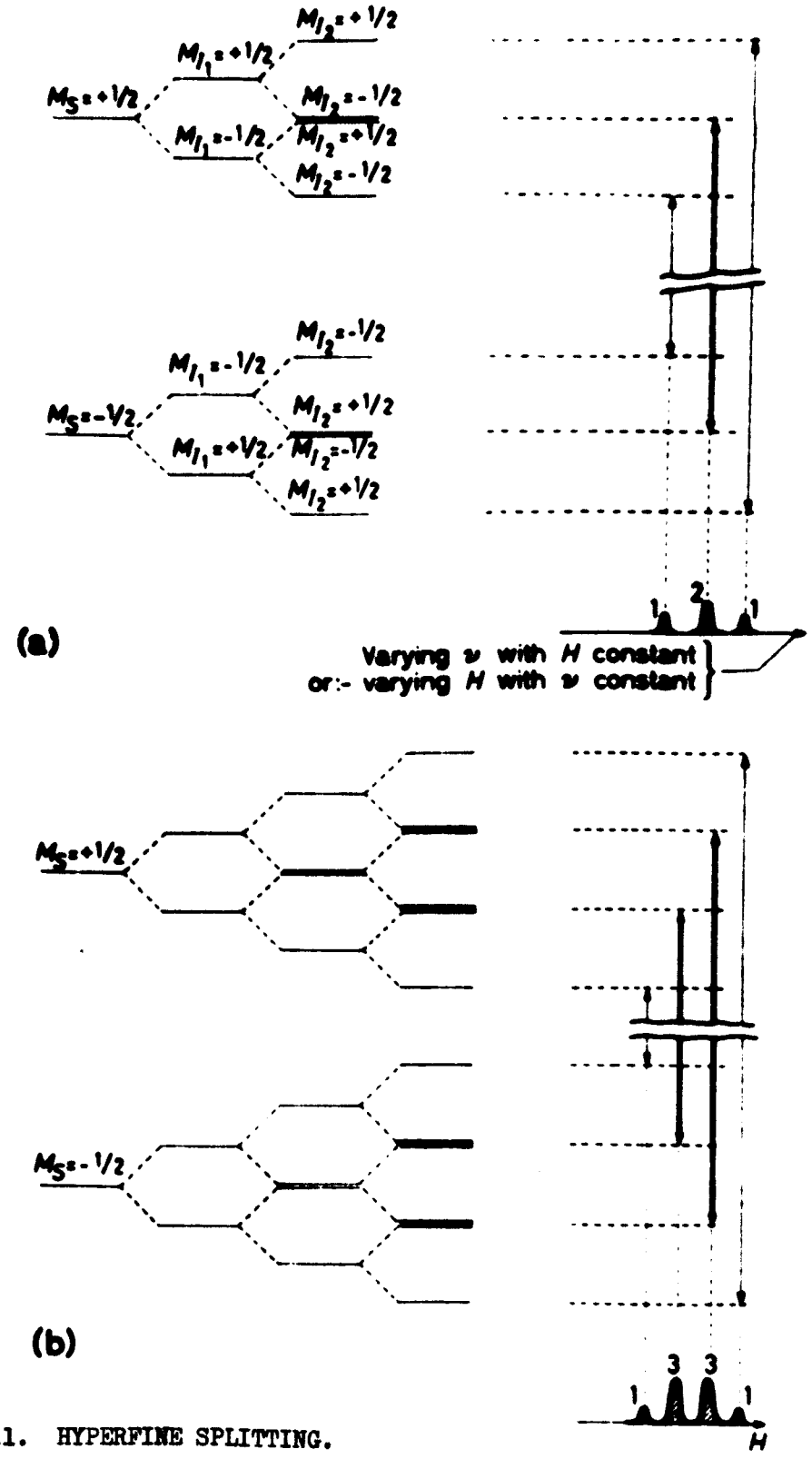

FIG. 2.11. HYPERFINE SPLITTING.

(a) Two equivalent protons. (b) Three equivalent protons.

with a molecular axis of symmetry (Frosch and Foley, 1952).

The term $\left\langle \frac{3\text{Cos}^2\alpha - 1}{r^3} \right\rangle_{av}$ is obtained by averaging over the spatial part of the unpaired electronic wave function. This term vanishes if the electron is in an s-orbital. For a non-s orbital electron, the total energy is

$$W_{M_I,M_S} = M_I g_I \beta H_o + M_S g_e \beta H + M_I M_S A' \quad \ldots\ldots \quad (2.66.)$$

where $A' = \frac{W_{dip}}{M_I M_S}$.

Equation (2.66.) depicts exactly the same type of spectrum as given by equation (2.59.) except that the h.f. separation in this case is a function of the orientation angle.

For an unpaired electron having an admixture of s and non-s character, the coupling constant would be equal to A(s) + A'(non-s).

In the general case when L is not completely quenched and g-value shift and anisotropy are present, the situation can be described phenomenologically by a spin Hamiltonian. Thus for axial symmetry,

$$\mathcal{H} = \beta \left[g_{\parallel} H_z S_z + g_{\perp} (H_x S_x + H_y S_y) \right] + A I_z S_z \qquad (2.67.)$$
$$+ B(I_x S_x + I_y S_y)$$

where z is along the axis of symmetry and the direct nuclear interaction with the external field has been neglected. The solution of equation (2.67.) is in general very complicated, but

in the strong field case, it becomes

$$W = M_s g\beta H_0 + M_I M_S k \quad \ldots\ldots \quad (2.68.)$$

where $g^2 = g_{||}^2 \cos^2\theta + g_{\perp}^2 \sin^2\theta$

and $K^2g^2 = A^2g_{||}^2\cos^2\theta + B^2g_{\perp}^2\sin^2\theta$ (Pryce, 1949) ..... (2.69.)

The quadrupole interactions have not been considered here. This is because they are much weaker than magnetic hyperfine interactions and in most cases the hyperfine structure is due to protons which have no quadrupole moment.

2.4.3. Hyperfine spectral intensities for identical equivalent nuclei

The hyperfine spectral intensities in this case would depend on nuclear statistics. The total wave function $\psi = \psi_e\psi_v\psi_r\psi_n$ (electronic, vibrational, rotation, and nuclear) is symmetric or antisymmetric with respect to a symmetry operation (resulting in the exchange of two identical nuclei) according as the nuclear spin is even or odd. For hydrogen nuclei ($I = \frac{1}{2}$), the total wave function would be antisymmetric. Considering as an example a NH_2 radical, ψ_e for a p_z orbital would change sign with a rotation around the twofold axis whereas ψ_v would not in the zero vibration state. Thus, in the lowest rotational state $J=0$, ψ_n would be symmetric and the intensity ratio of the h.f. components would be 1:1:1 (McConnell, 1958).

If, however, the rotation of NH_2 radical be quenched, the antisymmetric ψ_n would no longer be forbidden and the intensity ratio would be 1:2:1 as shown in Fig. (2.12.).

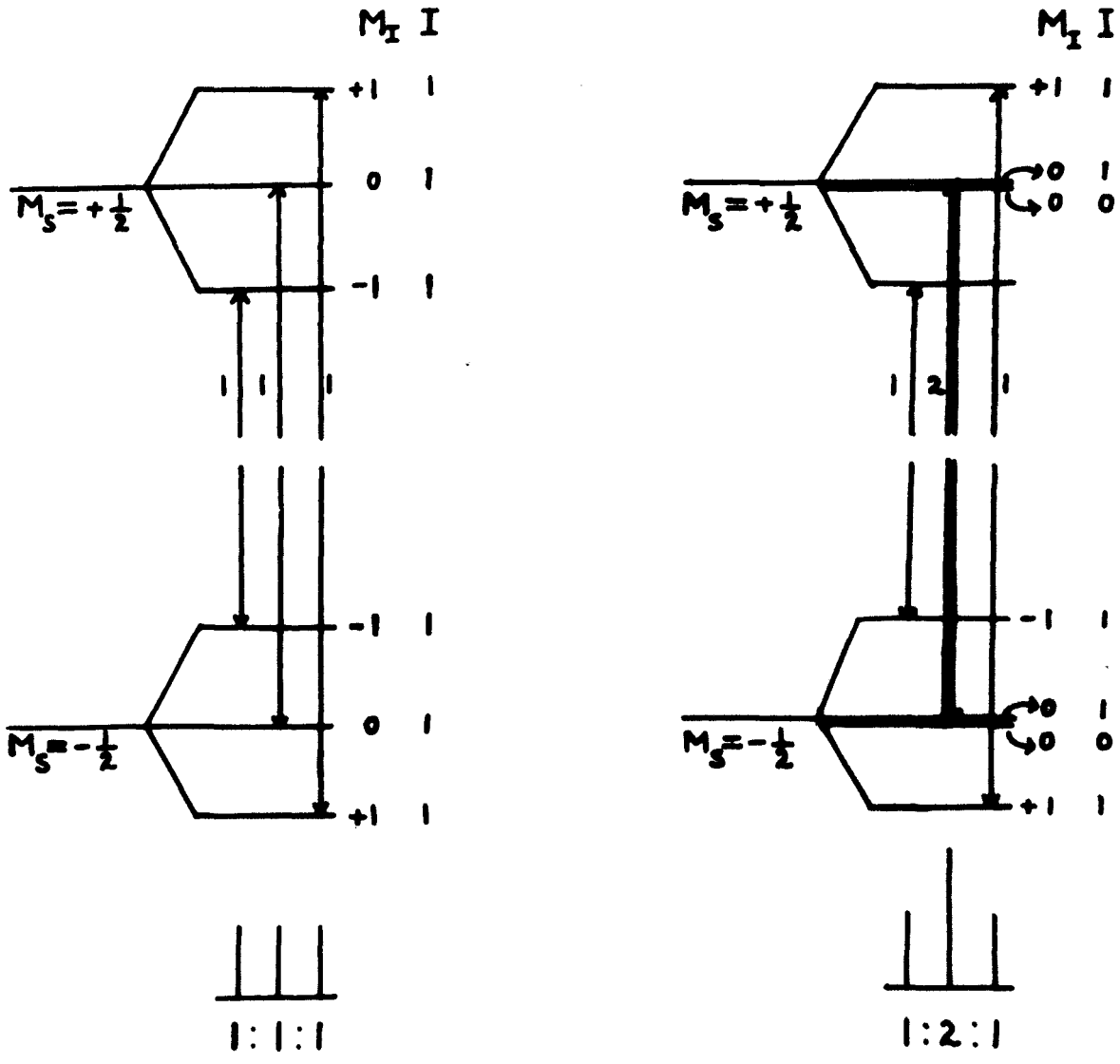

FIG. 2.12. EFFECT OF ROTATION ON HYPERFINE SPECTRAL INTENSITIES.

(NH_2 radical)

In general, when the magnetic nuclei are equivalent in terms of h.f. coupling but non-identical in terms of symmetry, the nuclear spin wave-function of the state (I) in the absence of a magnetic field can be written as

$$(\alpha_1 + \alpha_2 + \alpha_3 + \ \ldots)$$

where α_1, α_2, ... etc. are the nuclear spin wave functions each corresponding to a different value of m_I. If there are n identical nuclei, the total nuclear spin wave function can be written as

$$(\alpha_1 + \alpha_2 + \alpha_3 + \ldots\ldots\ldots)^n$$

Hence the statistical weight of a given h.f. level would be given by the coefficients of the corresponding term in the above polynomial expansion. Thus for hydrogen nuclei ($I = \frac{1}{2}$), the total nuclear spin wave function would be $(\alpha_1 + \alpha_2)^n$ and the statistical weight factors of the h.f. levels, and hence the relative intensities of the h.f. spectral lines would be in the ratio of the binomial coefficients

$$1,\ n,\ \frac{n(n-1)}{2!},\ \ldots \frac{n(n-1)\ldots(n-k+1)}{k!},\ \ldots\ n,\ 1 \qquad (2.70.)$$

CHAPTER III

RELAXATION EFFECTS AND LINE WIDTHS

3.1. Relaxation Mechanisms

3.1.1. Microscopic Theory

3.1.1.1. Spin-Lattice relaxation

The material in which the paramagnetic centres (henceforth referred to in this discussion as 'spins') are embedded is generally referred to as the 'lattice', whether it be solid, liquid or gas. The spins do of necessity interact with the lattice though for most free radicals, the interaction is very weak. The spin-lattice interactions are important in that they are one of the factors determining line widths and line shapes. They are considered in some detail below.

If N_l and N_u are respectively the numbers of spins per c.c. in the lower and the upper magnetic levels of a spin doublet, and $W_\uparrow$ and $W_\downarrow$ the upward and downward transition probabilities per unit time due to spin-lattice relaxation, then the rate of change of the excess number, n, in the lower state due to spin-lattice relaxation is given by

$$\frac{dn}{dt} = 2N_u W_\downarrow - 2N_l W_\uparrow \qquad \ldots\ldots \qquad (3.1.)$$

The factor 2 occurs because each transition changes n by 2.

For thermal equilibrium,

$$n_l W_\uparrow = n_u W_\downarrow$$

so that

$$W_{\downarrow} = W\left(1 + \frac{\mu H_o}{KT}\right)$$

$$W_{\uparrow} = W\left(1 - \frac{\mu H_o}{KT}\right) \quad \ldots\ldots \quad (3.2.)$$

where W = mean of $W_{\downarrow} + W_{\uparrow} = \frac{W_{\downarrow} + W_{\uparrow}}{2}$

μ = maximum measurable component of the magnetic moment of the spin

and T = common temperature of the spin and the lattice when they are in thermal equilibrium $\approx T_L$ (temperature of the lattice) since the heat capacity of the spin system is very small.

Here it has been assumed that $\mu H_o/KT \ll 1$, which is true if it is less than 10,000 gauss and T is greater than 20°K.

From equations (3.1.) and (3.2.), one gets

$$\frac{dn}{dt} = 2W(n_e - n) \quad \ldots\ldots \quad (3.3.)$$

where $n_e = \frac{N\mu H_o}{KT}$ = the value of n under equilibrium, N being the total number, $N_l + N_u$, of the spins per c.c. The solution of equation (3.3.) is

$$(n_e - n) = (n_e - n_i)e^{-2Wt} \quad \ldots\ldots \quad (3.4.)$$

where n_i is the value of n at $t = 0$. Thus the approach to equilibrium is seen to be exponential with characteristic time $T_1 = 1/2W$. Equation (3.4.) can thus be re-written as

$$(n_e - n) = (n_e - n_i)\, e^{-t/T_1} \qquad \ldots\ldots \qquad (3.5.)$$

In the presence of radiation, equation (3.1.) can be written as

$$\frac{dn}{dt} = 2N_u W_{\downarrow} - 2N_{\ell} W_{\uparrow} + 2N_u P - 2N_{\ell} P \qquad \ldots\ldots \qquad (3.6.)$$

Substituting for $W_{\downarrow}$ and $W_{\uparrow}$ from equation (3.2.), one gets

$$\frac{dn}{dt} = 2W(n_e - n) - 2nP \qquad \ldots\ldots \qquad (3.7.)$$

where $n_e = \frac{N\mu H_o}{KT}$ as before. However, the equilibrium value n_e' is given, from equation (3.7.), by

$$\frac{n_e'}{n_e} = \frac{2W}{2W + 2P} = \frac{1}{1 + 2PT_1} \qquad \ldots\ldots \qquad (3.8,)$$

where $T_1 = \frac{1}{2W}$. Denoting the ratio $\frac{n_e'}{n}$ by Z, equation (3.7.) can be re-written as

$$\frac{dn}{dt} = \frac{1}{T_1 Z}(n_e' - n) \qquad \ldots\ldots \qquad (3.9.)$$

The solution of this equation is

$$(n_e' - n) = (n_e' - n_i)\, e^{-t/T_1 Z} \qquad \ldots\ldots \qquad (3.10.)$$

which shows that the approach to the steady state in the presence of radiation is of the same exponential form as that when radiation is absent, but the characteristic time is now $T_1 Z$ instead of just T_1. (The unsteady state can be introduced by suddenly changing the intensity of radiation or the strength of the steady magnetic field.)

Spin Temperature:-

In the absence of radiation, the equilibrium value n_e is given

by

$$n_e = N\mu H_o/KT$$

Here T is the common spin and lattice temperature under thermal equilibrium. When the radiation is present, the spin system can still be described formally by a 'spin temperature', T_s, defined by the relation

$$n_e' = N\mu H_o/KT_s$$

T_s is related to T by the relation

$$T_s/T = n_e/n_e' = 1/\not{Z} \qquad \ldots\ldots \qquad (3.11.)$$

It may be noted, however, that, for spin greater than $\frac{1}{2}$, the concept of spin temperature is less precisely defined; for there will be more than two states, and a unique value of T_s can be obtained only if the ratios of their populations are appropriately related.

Saturation factor:-

From radiation theory, the probability of radiation-induced transitions for $s = \frac{1}{2}$, is

$$P_{\frac{1}{2}\leftrightarrow-\frac{1}{2}} = \frac{1}{4}\gamma^2H_1^2g(\nu) \qquad \ldots\ldots \qquad (3.12.)$$

Substituting for P from this into equation (3.8.), one gets

$$Z = \frac{n_e'}{n_e} = \frac{1}{1+2PT_1} = \frac{1}{1+\frac{1}{2}\gamma^2H_1^2T_1g(\nu)} \qquad \ldots\ldots \qquad (3.13.)$$

At $\nu = \nu_{res.}$, the saturation factor is given by

$$Z_{res} = \frac{1}{1+\frac{1}{2}\gamma^2H_1^2T_1[g(\nu)]_{max}}$$

As shown later,

$$\tfrac{1}{2}[g(\nu)]_{max} = T_2$$

$$\therefore \quad Z_{res} = \frac{1}{1+\gamma^2 H_1^2 T_1 T_2} \qquad \ldots\ldots \qquad (3.14.)$$

It may be noted that the saturation factor $\frac{Z}{Z}$ is defined such that, the larger its value, the smaller is the amount of saturation.

3.1.1.2. Nature of the Spin-Lattice Relaxation Mechanism

According to Kronig (1939), the thermal motion of the lattice alters the crystalline electric field and thus acts on the spin system through spin-orbit coupling. The Fourier spectrum of this fluctuating crystalline field may contain terms which give rise to resonant transitions between the two states involved.

Two mechanisms of this transfer of energy are possible:

(1) Direct process, where a phonon of appropriate frequency is directly absorbed by the spin system, and

(2) Raman process, where energy is exchanged between the phonon and the spin system through inelastic scattering.

Relaxation times for these mechanisms for $s = \frac{1}{2}$ are given by the following expressions:

Direct Process $\qquad T_1 = \dfrac{10^4 . \Delta^4}{\lambda^2 . H^4 . T}$ secs $\qquad \ldots\ldots \qquad (3.15.a)$

Raman Process $$T_1 = \frac{10^4 . \Delta^6}{\lambda^2 . H^6 . T^7} \text{ secs.} \quad \ldots\ldots \quad (3.15.b)$$

where Δ = the height of the next orbital level above the ground state,

λ = the spin-orbit coupling coefficient,

and T = temperature in ^{o}K.

3.1.1.3. Spin-Spin Relaxation

In any assembly of spins, a particular spin would experience not only the external magnet field $\overrightarrow{H_0}$ but also a small local field $\overrightarrow{H}_{local}$ due to the neighbouring spins. The local field would be of the order of $\mu/r3$ where μ is the magnetic dipole moment associated with the neighbouring spin and r is the nearest-neighbour distance. If the spins are identical, the distribution of their Larmor frequency would be over a range $\delta\omega_0$, where $\delta\omega_0 \sim \gamma H_{local}$. If two spins have precession frequencies differing by $\delta\omega_0$ and are initially in phase, then they will be out of phase in a time $T_2 \sim 1/\delta\omega_0$. T_2 thus represents the phase-memory time.

Two identical spins, j and k, will produce magnetic fields at each other oscillating at the Larmor frequency. As a result, they may mutually induce transitions among each other. The energy for the transition of one spin comes from the other; there is, in fact, a mutual exchange of energy in the process. It can be seen that the correct phasing for this 'spin-exchange' process should occur periodically after a time interval of the

order of $1/\delta\omega_o$. The spin-exchange provides another mechanism for spin relaxation. This relaxation mechanism is called spin-spin relaxation.

3.1.2. Macroscopic Theory. The Bloch Formulation

Bloch used a set of macroscopic equations to describe the variation of the components of the total magnetisation per unit volume in resonance experiments. Following him, one can investigate in a phenomenological way the behaviour of the spin system in a magnetic field

$$H_x = H_1 \text{ Cos } \omega t$$
$$H_y = -H_1 \text{ Sin } \omega t \qquad \ldots\ldots \qquad (3.16.)$$
$$H_z = H_o$$

If the magnetic moment $\vec{\mu}$ is regarded as a quantum-mechanical operator, its time derivative would be given by the commutator of the operator and the Hamiltonian $\mathcal{H}$. Since $\mathcal{H} = -\vec{\mu}.\vec{H}$, and $\vec{\mu} = \gamma\vec{I}\ h/2\pi$, the commutator gives, in conjuction with the commutation rules for angular momenta,

$$\frac{d\vec{\mu}_{op}}{dt} = \gamma\vec{\mu}_{op} \times \vec{H} \qquad \ldots\ldots \qquad (3.17.)$$

(Here γ has been taken positive for simplicity; if it is negative the sign of H_y in equation (3.16.) is to be changed.) One can now take the expectation value and sum over all the moments in unit volume. Since the macroscopic magnetisation is defined as

$$\vec{M} = \sum_{\substack{\text{unit} \\ \text{vol}}} \langle \vec{\mu}_{op} \rangle \qquad \ldots\ldots \qquad (3.18.)$$

it follows that

$$\frac{d\vec{M}}{dt} = \gamma \vec{M} \times \vec{H} \qquad \ldots\ldots \qquad (3.19.)$$

Bloch phenomenologically introduced the relaxation times T_1 and T_2 in this equation in the following way.

If M_o represents the equilibrium magnetisation when the transverse rotating field has been withdrawn, the approach to equilibrium for the longitudinal component M_z can be assumed to be given by

$$\frac{dM_z}{dt} = \gamma(\vec{M} \times \vec{H})_z + \frac{1}{T_1}(M_o - M_z) \ldots \qquad (3.20.)$$

where T_1 is the characteristic time for 'longitudinal' relaxation. Similarly the approach to zero for the transverse component of the magnetisation on the withdrawal of the transverse rotating field can be postulated as:-

$$\frac{dM_{x,y}}{dt} = \gamma(\vec{M} \times \vec{H})_{x,y} - \frac{M_{x,y}}{T_2} \ldots\ldots \qquad (3.21.)$$

where T_2 is the characteristic time for 'transverse' relaxation. T_1 and T_2 are thus called the 'longitudinal' and 'tranverse' relaxation times respectively. It may be noted that the law of the longitudinal and transverse relaxations has been introduced phenomenologically as a postulate. The validity of this approach lies in the close agreement of the deductions based on these

postulates with the results of the experiment.

The equations (3.20.) and (3.21.) take a simpler form if transferred to a coordinate system rotating about the z-axis with the r.f. field $\vec{H}_1$. If u and v represent the components of $\vec{M}$ along and perpendicular to the direction of $\vec{H}_1$, so that

$$M_x = u \cos \omega t - v \sin \omega t$$

$$M_y = - u \sin \omega t - v \cos \omega t$$

the equations (3.20.) and (3.21.) become, in the rotating frame,

$$\frac{du}{dt} + \frac{u}{T_2} + (\omega_o - \omega)\, v = 0$$

$$\frac{dv}{dt} + \frac{v}{T_2} + (\omega_o - \omega)\, u + \gamma H_1 M_z = 0 \quad \ldots\ldots \quad (3.22.)$$

$$\frac{dM_z}{dt} + \frac{M_z - M_o}{T_1} - \gamma H_1 v = 0$$

where $\omega_o = \gamma H_o$. The steady state solution of these equations is obtained by putting all the time derivatives equal to zero. Doing this and converting back to fixed axes, one gets

$$M_x = \tfrac{1}{2} M_o \gamma T_2 \left[\frac{T_2(\omega_o - \omega) 2H_1 \cos \omega t + 2H_1 \sin \omega t}{1 + T_2^2 (\omega_o - \omega)^2 + \gamma^2 H_1^2 T_1 T_2} \right]$$

$$M_y = \tfrac{1}{2} M_o \gamma T_2 \left[\frac{2H_1 \cos \omega t - T_2(\omega_o - \omega) 2H_1 \sin \omega t}{1 + T_2^2 (\omega_o - \omega)^2 + \gamma^2 H_1^2 T_1 T_2} \right] \quad \ldots\ldots \quad (3.23.)$$

$$M_z = M_o \left[\frac{1 + T_2^2 (\omega_o - \omega)^2}{1 + T_2^2 (\omega_o - \omega)^2 + \gamma^2 H_1^2 T_1 T_2} \right]$$

These equations represent the effects of the relaxation mechanisms

on the macroscopic magnetisation. As shown in Sec. 3.2., equations (3.23.) predict a Lorentzian line-shape if there is no saturation. In practice, line shapes are not always well approximated by a Lorentz-type curve. This, of course, represents a limitation of the original phenomenological equations.

3.1.2.1. Correlation of the macroscopic and the microscopic descriptions

For simplicity, only the case $s = \frac{1}{2}$ is considered. The longitudinal magnetisation corresponds to the excess of population of the lower state and is given by $M_z = \frac{1}{2} \frac{h}{2\pi} \gamma n$, where n is the excess population in the lower state. Spin-lattice relaxation, which tends to reduce n, thus corresponds to the longitudinal relaxation of the macroscopic theory. In fact, as is seen from equation (3.3.) and the relation $T_1 = \frac{1}{2W}$, the spin-lattice relaxation time is identical with the longitudinal relaxation time defined by Bloch. Since the spin-exchange process does not lead to an over all reduction of the excess population, it does not contribute to the longitudinal relaxation.

The transverse relaxation, on the other hand, arises from spin-spin interaction, which distributes the precession frequencies of the spins over a range of order γH_{loc}. After a time $T \approx \frac{1}{\gamma H_{loc}}$, the phase coherence of these precessions will be destroyed, and any initial transverse magnetisation will have decayed. The transverse relaxation time, thus, corresponds to

the phase-memory time of the microscopic theory.

However, these considerations apply when the magnetic field fluctuations due to lattice or molecular motion are slow. If molecular rotation and diffusion are taking place rapidly so that the local field changes many times during a single rotation of the dipole in its precession, the local field would be averaged out, and the mechanism of decay of all components M_x, M_y, and M_z would become identical.

3.2. Magnetic Susceptibilities

3.2.1. D.C. Susceptibility

For an assembly of identical weakly interacting spins of spin number S in thermal equilibrium at the spin temperature T_s in a steady magnetic field $\vec{H}$, the level $|M_s>$ will have a population of

$$\frac{N_o}{(2S+1)} \exp\left(\frac{M_s g\beta H}{kT_s}\right) \simeq \frac{N_o}{(2S+1)}\left(1 + \frac{M_s g\beta H}{kT_s}\right) \quad \ldots\ldots \quad (3,24.)$$

where N_o is the number of spins per c.c. The above approximation is valid since the energies of normal microwave frequencies correspond to temperatures of about 1^oK. The magnetic moment of all the spins of this level along the direction of $\vec{H}$ will therefore be

$$M_s g\beta(1 + M_s g\beta H/kT_s)\ \frac{N_o}{2S+1}$$

The total magnetic moment along H due to all the levels would be given by

$$\mu_H = \sum_{M_s=-S}^{+S} \frac{N_0 g\beta H}{(2S+1)} \left[\frac{M_s}{H} + \frac{M_s^2 g\beta}{KT_s}\right]$$

$$= \frac{N_0 g^2\beta^2 H}{KT_s} \frac{S(S+1)}{3}$$

so that the static volume susceptibility is

$$\chi_0(T_s) = \frac{1}{3KT_s} N_0 g^2\beta^2 S(S+1) \qquad \ldots\ldots \quad (3.25)$$

3.2.2. High Frequency Susceptibility

3.2.2.1. Macroscopic Theory

A linearly oscillating high frequency magnetic field given by

$$H = 2H_1 \cos \omega t \qquad \ldots\ldots \quad (3.26.)$$

would produce an in-phase magnetisation $2\chi' H_1 \cos \omega t$ and an out-of-phase magnetisation $2\chi'' H_1 \sin \omega t$. The mean rate of absorption of energy by the spin system per c.c. is given by

$$P = \frac{\omega}{2\pi} \int_0^{2\pi/\omega} H \frac{dM}{dt} = 4H_1^2 \frac{\omega^2}{2\pi} \int_0^{2\pi/\omega} (-\chi' \sin\omega t + \chi'' \cos\omega t) \cos\omega t\, dt$$

$$= 2\omega\chi'' H_1^2 = 4\pi\nu\chi'' H_1^2 \qquad \ldots\ldots \quad (3.27.)$$

Expressions for χ' and χ'' can be obtained from Bloch equations (3.23.), which are valid for linearly oscillating field as well, provided the amplitude $2H_1$ is small. Thus if the oscillating field $2H_1 \cos \omega t$ is in the direction of x-axis, the in-phase component of M_x is

$$\tfrac{1}{2} M_0 \gamma T_2 \left[\frac{T_2(\omega_0 - \omega)\, 2H_1 \cos \omega t}{1 + T_2^2(\omega_0 - \omega)^2 + \gamma^2 H_1 T_1 T_2}\right]$$

and the out of phase component is

$$\tfrac{1}{2} M_o \gamma T_2 \left[\frac{2}{1 + T_2^2(\omega_o - \omega)^2 + \gamma^2 H_1 T_1 T_2} \right]$$

χ' and χ'' are therefore given by

$$\chi' = \tfrac{1}{2} \chi_o \omega_o \left[\frac{T_2^2(\omega_o - \omega)}{1 + T_2^2(\omega_o - \omega)^2 + \gamma^2 H_1^2 T_1 T_2} \right] \ldots\ldots \quad (3.28.a.)$$

$$\chi'' = \tfrac{1}{2} \chi_o \omega_o \left[\frac{T_2}{1 + T_2^2(\omega_o - \omega)^2 + \gamma^2 H_1^2 T_1 T_2} \right] \ldots\ldots \quad (3.28.b.)$$

where $\chi_o \left(= \frac{M_o}{H_o} \right)$ is the d.c. susceptibility. Fig. (3.1.) shows a plot of these susceptibilities as a function of the dimensionless product $(\omega_o - \omega)T_2$.

3.2.2.2. Microscopic Theory

In an assembly of identical spins of spin number S, the excess population in the lower of the two adjacent magnetic levels $|M_s\rangle$ and $|M_{s-1}\rangle$ is found from equation (3.24.) to be

$$n = \frac{N_o h\nu_o}{(2S + 1) kT_s}$$

where $h\nu_o$ is the energy separation between these two levels. The net power absorbed by transitions between these two levels is

$$\frac{N_o h^2 \nu_o \nu}{(2S + 1) kT_s} P_{M_s \leftrightarrow M_{s-1}} \quad \ldots\ldots \quad (3.29.)$$

where the transition probability $P_{M_s \leftrightarrow M_{s-1}}$ is given by

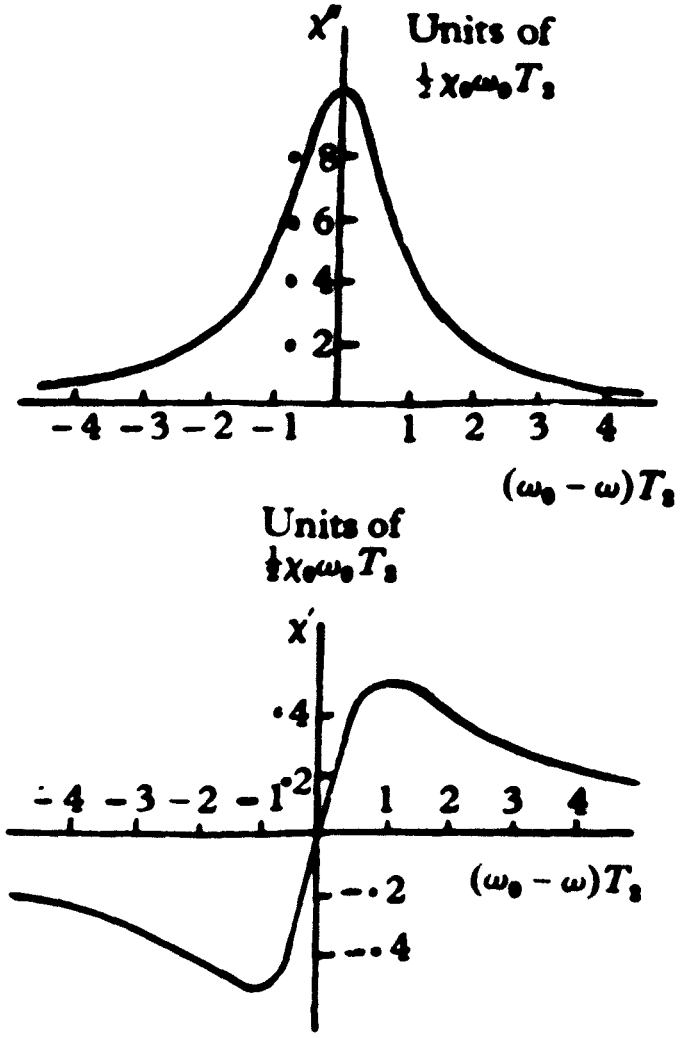

FIG. 3.1. THE BLOCH SUSCEPTIBILITIES.

$$P_{M_s \longleftrightarrow M_{s-1}} = \frac{1}{4}\gamma^2 H_1^2 (S + M_s)(S - M_s + 1)\, g(\nu) \ldots\ldots \quad (3.30.)$$

where $g(\nu)$ is the normalised line shape function

$$\text{i.e. } \int_0^\infty g(\nu)\, d\nu = 1 \quad \ldots\ldots \quad (3.31.)$$

The factor $g(\nu)$ takes account of the processes which destroy the phase coherence between the inducing radiation and the interacting spin.

The total power absorbed per c.c. is obtained by substituting from equation (3.30.) into equation (3.29.) and summing over all levels. This gives

$$P = \left[\frac{N_0 g^2 \beta^2 S(S+1)}{3KT_s}\right] 2\pi^2 \nu\, \nu_0 H_1^2 g(\nu) \ldots\ldots \quad (3.32.)$$

Comparing this with equation (3.27.), one gets

$$\chi'' = \frac{\pi}{2}\left[\frac{N_0 g^2 \beta^2 S(S+1)}{3KT_s}\right] \nu_0\, g(\nu)$$

$$= \frac{\pi}{2}\chi_0(T_s)\, \nu_0\, g(\nu) \quad \ldots\ldots \quad (3.33.)$$

$\chi_0(T_s)$, here, is the d.c. susceptibility corresponding to the spin temperature T_s. If there is saturation so that there is no thermal equilibrium between the lattice and the spin system, then $\chi_0(T_s) = Z\chi_0$, where χ_0 is the d.c. susceptibility at the lattice temperature $T(= T_s Z)$ in the absence of saturation. The high-frequency out-of-phase susceptibility then becomes

$$\chi'' = \frac{\pi}{2}\chi_0 Z\, \nu_0 g(\nu) \quad \ldots\ldots \quad (3.34.)$$

The in-phase susceptibility can be found with the aid of

Kronig-Kramers relations

$$\chi'(\nu) = \frac{2}{\pi} \int_0^\infty \frac{\nu' \chi''(\nu') d\nu'}{\nu'^2 - \nu^2}$$

$$\chi''(\nu) = -\frac{2\nu}{\pi} \int_0^\infty \frac{\chi'(\nu') d\nu'}{\nu'^2 - \nu^2} \quad \ldots\ldots \quad (3.35.)$$

If the oscillating magnetic field is small, so that $\gamma^2 H_1^2 T_1 T_2 \ll 1$, there is no saturation and

$$\chi'' = \frac{\pi}{2} \chi_0 \nu_0 \, g(\nu) \quad \ldots\ldots \quad (3.36.)$$

whereas from Bloch equations (3.28.),

$$\chi'' = \pi \chi_0 \nu_0 \left[\frac{T_2}{1 + T_2^2 \, 4\pi^2 (\nu_0 - \nu)^2} \right] \quad \ldots\ldots \quad (3.37.)$$

Comparing equations (3.36.) and (3.37.), the line shape function is given by

$$g(\nu) = \frac{2T_2}{1 + T_2^2 \, 4\pi^2 (\nu_0 - \nu)^2} \quad \ldots\ldots \quad (3.38.)$$

which is a Lorentzian function. The peak value is given by

$$[g(\nu)]_{max} = 2T_2$$

so that

$$T_2 = \tfrac{1}{2}[g(\nu)]_{max} \quad \ldots\ldots \quad (3.39.)$$

This equation is in fact taken as the general definition of T_2. This definition is consistent with its usage in Bloch equations when the latter apply.

3.3. Line Widths

3.3.1. Definitions

Line widths are usually expressed as the frequency separation between half-power points. Since very often it is the

derivative of the curve that is experimentally traced, it is much easier to measure the frequency separation of the maximum-slope points of the absorption curve and sometimes this is quoted as the line width.

Line width can be defined in another way by making use of the normalisation of the line shape function; it is then defined as $\Delta\nu = \frac{1}{[g(\nu)]_{max}}$

Line shapes are much more difficult to calculate theoretically. Generally, different moments are calculated for comparison with experiment. The nth moment is defined as

$$\langle(\Delta\nu)^n\rangle = \int_{-\infty}^{+\infty} g(\nu) (\nu - \nu_0)^n d(\nu - \nu_0) \qquad (3.40.)$$

3.3.2. Mechanisms of Line Broadening

3.3.2.1. Natural Width

This arises from Heisenberg's uncertainty principle. The spins in all levels except the lowest one have a finite 'life time' because of the probability of spontaneous emission. Thus all such levels have a finite energy spread, which gives rise to the finite widths of the corresponding transitions. Classically, the natural line width may be thought of as due to radiation damping. The natural line shape is found to be Lorentzian, but as this line width varies as the cube of resonant frequency, it is very small in electron resonance experiments and is masked by other types of broadening.

3.3.2.2. Spin-Lattice and spin-Exchange Interactions

Both of these have the effect of increasing the line width through the uncertainty principle by reducing the life-time of the states involved. But whereas the broadening due to spin-lattice interaction is temperature dependent and can be reduced by working at low temperatures, the line-width due to spin-exchange process is temperature-independent.

It may be noted that for most free radicals at low temperatures, the direct contribution of spin-lattice relaxation to line widths is negligible due to very small values of λ and large values of Δ in the equations (3.15.). However, the spin-lattice relaxation may affect the line widths in free radicals in another way. If the spin-lattice interaction is too weak, saturation sets in and leads to a broadening of the line (Sec. 3.3.4.).

3.3.2.3. Dipolar Interaction

Dipolar spin-spin interaction can take place (a) between the unpaired electron and the spins of unpaired electrons of other radicals, (b) between unpaired electron and the nuclear spins in the same radical, and (c) the unpaired electron and the nuclear spins in the neighbouring radicals. The splittings of energy levels due to the factors (a) and (b) are often of the same order of magnitude whereas the interaction (c) is much weaker and is not considered here. Also it is sufficient to confine attention to the nearest neighbours only.

The anisotropic dipolar hyperfine splitting is proportional to $(3\ Cos^2\theta-1)$ where θ is the angle between a molecular axis of symmetry and the external magnetic field H. In specimens other than single crystals, θ would have a random distribution and there would be a spread in the energy of the unpaired electron.

The dipolar interaction between the electron spins will also show a similar $(3\ Cos^2\theta-1)$ variation where θ is now the angle between the line joining the two radicals and the external magnetic field. Hence, in a non-crystalline specimen, dipolar interaction between electron spins will also produce a similar broadening as the dipolar hyperfine interaction.

3.3.2.4. Motional Narrowing.

The above arguments about dipolar broadening apply when the radicals are held rigidly in position or at least when their motion is slow relative to the precession of the dipole. However, if the molecular motion and diffusion are rapid so that the local field changes many times during a single rotation of the dipole in its precession, the local field would be averaged out and the lines narrowed down. This process is known as 'motional narrowing' and has been described in detail by McConnell (1956). In case of internal rotation of groups, such as CH_3, the hyperfine broadening due to the protons of the rotating group would be averaged out whereas other protons would contribute their full broadening. This mechanism probably

accounts for the reduction of line widths from 25 to 10 gauss for most radicals trapped in low temperature hydrocarbon glasses (Fujimoto and Ingram, 1958).

3.3.2.5. Exchange Narrowing

The isotropic exchange interaction is represented by the term

$$\frac{1}{4} J_{12} (1 + 4\vec{S}_1 . \vec{S}_2)$$

where the exchange integral, J_{12}, has an integrand depending on the extent to which the wave-functions of the two electrons overlap in space. Since the orbital wave functions are not spherically symmetric in crystals, the spin-orbit interaction gives rise to an anisotropic exchange interaction as well which can be reduced to the form of a dipolar interaction. However, since spin-orbit interaction in free radicals is very small, anisotropic exchange can be neglected from the present considerations.

A number of complicated effects arise from exchange interaction under different conditions. Only one of these, which is relevant to the free radical studies is mentioned here. Van Vleck (1948) has shown that if the spins are all identical (i.e. have the same g-value and prcess about the same axis) and $S' = \frac{1}{2}$, the isotropic exchange interaction contributes to the fourth moment but not to the second moment. Since the total area of the line is constant, the effect is that the

centre part of the line is narrowed and the tails broadened. This peaking of the line shape is called exchange narrowing. In almost all other cases exchange does contribute to the second moment and thus cause a broadening. It may be noted that exchange-narrowed lines have Lorentzian shape.

3.3.2.6. Delocalisation Narrowing

This is the motational narrowing due to the delocalisation of the unpaired electron in a molecular orbital (Walter et al., 1956). The motion of the unpaired electron in the delocalised orbital may average the dipolar interaction and produce a line narrowing.

3.3.3. Homogeneous and Inhomogeneous Broadening

At this stage, it is useful to discuss this classification due to Portis (1953). A homogeneously broadened line implies that energy absorbed from the microwave field is distributed to all the spins and thermal equilibrium of the spin system is maintained through resonance.

In inhomogeneous broadening, the energy is transferred only to those spins whose local fields satisfy the resonance condition.. It is useful in this case to think of spin packets having little or no interaction with each other and of width given by local fields. Then the overall response of the spin system will be a superposition of the individual responses of the spin packets.

The examples of the two mechanisms falling into the two categories are

(i) homogeneous broadening:

Interaction with the radiation field, spin-lattice interaction, spin-exchange process, exchange interaction, molecular motion and electron delocalisation, etc.

(ii) inhomogeneous broadening:

Mangetic field inhomogeneity, dipolar interaction between spins with different resonant frequencies, hyperfine interaction, g-value anisotropy, etc.

3.3.4. Experimental Sources of Broadening

3.3.4.1. Power Saturation Broadening

For systems like free radicals that have long spin-lattice relaxation times, spins, when excited, may not return to the ground level sufficiently quickly for thermal equilibrium to be maintained. This happens when the incident power is high. Since saturation is maximum at the peak of the resonance curve and falls off on both sides, the lines will be broadened on saturation.

However, this is true of homogeneously broadened lines only. In the case of inhomogeneously broadened lines, each spin packet will saturate individually and their peak heights would reduce by the same fraction. Hence the overall resonance curve which is the envelope. of individual resonances would decrease in height, but retain the same shape.

3.3.4.2. Inhomogeneous Field

Since each of the spin packets will have different resonant frequencies, the overall line shape will be broadened.

3.3.4.3. Modulation Broadening

Karplus (1948) showed that the modulation of the source or the sample are equivalent, and if either is modulated at a frequency, ν, then 'side bands' appear on both sides of the 'true' resonance and separated from it by the modulation frequency . Classically, a high frequency modulation of the magnetic field may be thought of as a modulation of the Larmor precessional frequency which would thus produce side-bands. These would be resolved or contribute to the line width, only if ν is of the order of or greater than the line width, and their magnitude is sufficient to produce a noticeable effect.

CHAPTER IV

EXPERIMENTAL TECHNIQUES

4.1. General Discussion

4.1.1. Principle of Detection

It was seen in Chapter III that the high-frequency susceptibility has an in-phase component χ' and a quadrature component χ''. The total susceptibility can thus be written as

$$\chi = \chi' - j\chi'' \qquad \ldots\ldots \qquad (4.1.)$$

The power absorbed per unit volume of the paramagnetic specimen is given by

$$P_{\text{unit vol.}} = \tfrac{1}{2}\omega H_1^2 \chi'' \qquad \ldots\ldots \qquad (4.2.)$$

where ω is the angular frequency and H_1 the amplitude of the r.f. field. Since the sample volume is limited by the region of homogeneity in the pole-gap of the magnet, a sufficiently large amount of power can be absorbed only if the sample is placed in a region of concentrated microwave power. This necessitates the use of a cavity.

The working of a cavity spectrometer can be best explained in terms of its low frequency analogue where the cavity is replaced by a series tuned circuit consisting of an inductance, a capacitance and a resistance. The impedance of a coil containing the paramagnetic specimen can be written as

$$Z_M = R_E + j\omega L + j\omega L_s \qquad \ldots\ldots \qquad (4.3.)$$

where L is the inductance of the empty coil and L_s is the

contribution of the specimen to the net inductance of the coil when filled. The subscript E in R_E stands for electric loss and signifies that the dielectric losses have been included in R_E. The ratio of L_s to L can be written as

$$\frac{L_s}{L} = \frac{4\pi\chi\int_s H_1^2\, dV}{\int_c H_1^2 dV} = 4\pi\chi\eta \quad \ldots\ldots \qquad (4.4.)$$

where the filling factor $\eta = \int_s H_1^2 dV / \int_c H_1^2 dV$, the integrals being taken over the sample volume and the inside volume of the coil respectively. Thus defined, the filling factor is a ratio of the energy stored in the empty space of the same volume and position as the specimen to the energy stored in the whole of the empty coil. The impedance Z_M then becomes

$$Z_M = R_E + j\omega L + j\omega(4\pi\chi'\eta L - j\, 4\pi\chi''\eta L)$$

$$= R_E + j\omega L + j\omega\, 4\pi\chi'\eta L + \omega\, 4\pi\chi''\eta L$$

The impedance of the coil far off magnetic resonance is

$$Z_E = R_E + j\omega L$$

as the susceptibilities are vanishingly small under this condition. Therefore, the change of impedance due to magnetic resonance in the specimen is

$$\Delta Z = Z_M - Z_E = \omega\, 4\pi\chi''\eta L + j\omega L\, 4\pi\chi'\eta \qquad (4.5.)$$

The phenomenon of magnetic resonance can, thus, be described in terms of the passive elements

$$\Delta R = 4\pi\omega\chi''\eta L \quad \ldots\ldots \qquad (4.6.a.)$$

$$\Delta L = 4\pi\chi'\eta L \quad \ldots\ldots \qquad (4.6.b.)$$

To observe the resonance phenomenon, both χ' and χ'' can, thus, be measured as a change of the impedance of the cavity. This impedance itself can be determined by observing either the wave reflected from the cavity or the wave transmitted through it.

A reflection-cavity spectrometer incorporates the use of a microwave bridge whereby the resistive and the reactive components of the impedance looking at the cavity can be separated from each other. In a transmission-cavity spectrometer, on the other hand, only the resistive component can be measured, and so the microwave bridge is dispensed with. This makes it easier to operate a transmission-type spectrometer, especially when the conditions of experiment, like the variation of the cavity temperature, require frequent and quick tuning of the spectrometer. Moreover, the problem of avoiding a superposition of absorption and dispersion signals does not arise, Hence transmission-type spectrometers were used for the work reported in this thesis and only these will be discussed.

It may however, be noted that it is possible to observe both absorption and dispersion in a transmission cavity spectrometer by feeding an additional signal, taken from the same source, to the detector without allowing it to pass through the cavity. By suitably choosing the amplitude and phase of the additional signal, any combination of χ' and χ'' can be obtained. This technique is known as 'microwave bucking'.

4.1.2. Elementary Analysis of a Transmission-Type Spectrometer

A low frequency analogue of the transmission-cavity spectrometer is shown in Fig. (4.1.), where the generator is represented by a voltage source with open circuit voltage V_G in series with an internal resistance R_G, the load across which the signal is measured is represented by a resistance R_L and the cavity is represented by the series tuned circuit, LCR_E.

The voltage transmission coefficient for this circuit, far removed from magnetic resonance, is given by

$$TE = \frac{V_L}{V_G} = \frac{R_L}{R_L + R_G + R_E + j(\omega L - \frac{1}{\omega C})} \qquad (4.7.)$$

whereas, near resonance, it is

$$T_M = \frac{R_L}{R_L + R_G + R_E + \Delta R + j[\omega(L + \Delta L) - 1/\omega C]} \qquad (4.8.)$$

Writing $R_L + R_G + R_E$ as R and $(\omega L - 1/\omega C)$ as X, it is seen that the change in V_L at magnetic resonance is

$$\Delta V_L = \left(\frac{\partial V_L}{\partial R}\right)_X \Delta R + \left(\frac{\partial V_L}{\partial X}\right)_R \Delta X$$

$$= (\Delta V_L)_X + (\Delta V_L)_R$$

where $$(\Delta V_L)_X = \left(\frac{\partial V_L}{\partial R}\right)_X \Delta R = -\frac{R_L}{(R + jX)^2} \Delta R \qquad (4.9.a.)$$

and $$(\Delta V_L)_R = \left(\frac{\partial V_L}{\partial R}\right)_X \Delta X = -\frac{R_L}{(R + jX)^2} j\Delta X \qquad (4.9.b.)$$

It is seen from equations (4.9.) that the sensitivity is

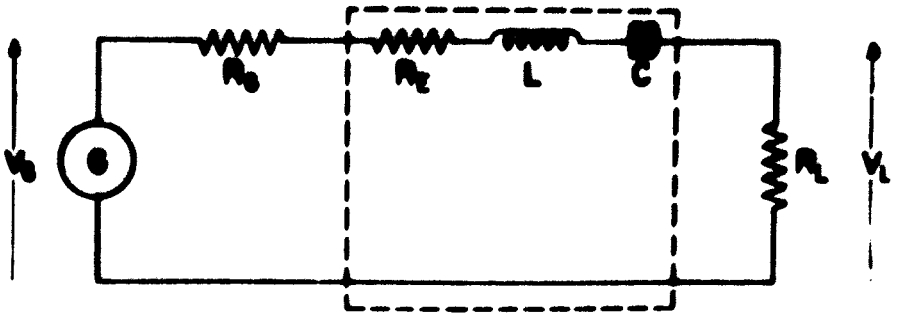

FIG. 4.1. LOW FREQUENCY ANALOGUE OF A TRANSMISSION - CAVITY SPECTROMETER.

maximum when the generator is tuned to the resonant cavity. Under this condition, equations (4.9.) become, using equations (4.6.),

$$(\Delta V_L)_X = -\frac{R_L}{R^2}\Delta R = -\frac{R_L}{R^2}4\pi\omega\chi''\eta L \qquad (4.10.a.)$$

and

$$(\Delta V_L)_R = -\frac{R_L}{R^2}j\Delta X = -\frac{R_L}{R^2}j4\pi\omega\chi'\eta L \qquad (4.10.b.)$$

It is seen that $(\Delta V_L)_X$ is in phase with V_L, whereas $(\Delta V_L)_R$ is in quadrature to it. The increase in the modulus of V_L due to χ'' would, therefore, be of the first order, whereas that due to χ' would be of the second order. Therefore, to a first order, a transmission-cavity spectrometer will not respond to the dispersion provided that the generator is tuned to the cavity.

To carry the analysis further, the circuit losses may be described in terms of the Q factor. For the circuit of Fig. (4.1.), the following Q's may be defined:

the unloaded or isolated circuit Q, $Q_{UE} = \dfrac{\omega_{OE} L}{R_E}$

the external Q due to the generator, $Q_{RG} = \dfrac{\omega_{OE} L}{R_G}$

the external Q due to the load, $Q_{RL} = \dfrac{\omega_{OE} L}{R_L}$

The subscript E in ω_{OE} signifies that the shift in resonant frequency due to the dielectric constant of the specimen has been taken into account.

The total loss of the circuit when connected to the generator

and the load is represented by the loaded Q, Q_{LE}, given by

$$\frac{1}{Q_{LE}} = \frac{R_G + R_L + R_E}{\omega_{OE} L} = \frac{1}{Q_{RL}} + \frac{1}{Q_{RG}} + \frac{1}{Q_{UE}} \quad \ldots\ldots \quad (4.11.)$$

In terms of Q_{LE}, equation (4.7.) becomes

$$T_E = T_{OE} \frac{1}{1 + i\, Q_{LE} \left(\frac{\nu}{\nu_{OE}} - \frac{\nu_{OE}}{\nu} \right)} \quad \ldots\ldots \quad (4.12.)$$

where T_{OE} is the voltage transmission coefficient at circuit resonance, $\nu = \nu_{OE} = \frac{1}{2\pi\sqrt{LC}}$. Similarly, equation (4.8.) becomes

$$T_M = T_{OE} \frac{1}{1 + \frac{Q_{LE}}{Q_M} + i\, Q_{LE} \left(\frac{\nu}{\nu_{OM}} - \frac{\nu_{OM}}{\nu} \right)} \quad \ldots\ldots \quad (4.13.)$$

where the new resonant frequency is given by

$$\nu_{OM} = \nu_{OE} \sqrt{1 + \frac{\Delta L}{L}} = \nu_{OE} \frac{1}{\sqrt{1 + 4\pi\eta\chi''}} \simeq \nu_{OE} (1 - 2\pi\eta\chi'') \quad (4.14.)$$

and the magnetic Q, Q_M, is defined as $Q_M = \frac{\omega L}{\Delta R}$. Substituting for ΔR from equation (4.6.a.), one gets

$$Q_M \simeq 4\pi\chi''\eta \quad \ldots\ldots \quad (4.15.)$$

Fig. (4.2.) shows a plot of both T_E and T_M for a particular value of the external magnetic field.

Finally, one gets, from equation (4.13.),

$$\chi'' = \frac{1}{4\pi\eta Q_{LE}} \left[\frac{T_{OE} - T_{OM}}{T_{OM}} \right] \quad \ldots\ldots \quad (4.16.)$$

Equation (4.16.) shows how χ'' may be measured at different magnetic fields to give the entire spectrum.

In actual practice, the cavity has to be coupled to the

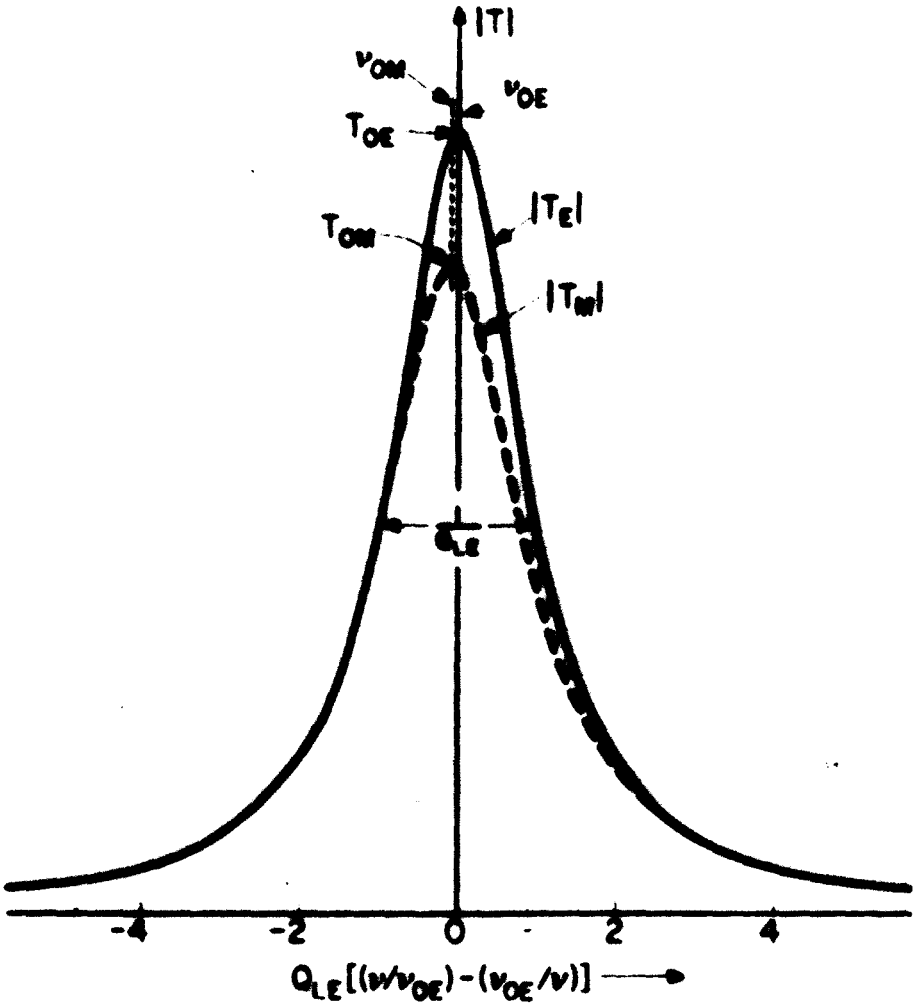

FIG. 4.2. PLOT OF T_E AND T_M.

waveguide run through iris holes. The iris holes may be represented by low-frequency inductive coupling. It can be seen that the equivalent circuit of the spectrometer, when referred to the detector terminals, has the same form as the circuit in Fig. (4.1.). Thus the analysis given here applies to an actual spectrometer in its broad aspects.

4.1.3. The Detection and Display Systems

Generally, either a bolometer or a crystal rectifier is used as the detector of the microwaves. Bolometers have high conversion loss at low powers and, hence, are unsuitable for free-radical work; because the free-radicals have long relaxation times and tend to saturate easily if too much microwave power is employed. Therefore, for free-radical and other studies where saturation is likely to occur, the crystal detector is almost always used.

Several methods can be employed for the detection and display of the resonance absorption in a transmission cavity spectrometer and those commonly used are described below.

(a) D.C. Detection.

This method was used in earlier investigations, where the magnetic field was changed manually and the crystal output measured, point by point, with the help of a sensitive galvanometer. However, this method involves detection of small changes of power at a large power level and is unsuitable for small concentrations of paramagnetic centres. The sensitivity can

be improved by using a null-method incorporating the use of a d.c. bridge and a d.c. amplifier. However, drifts become an important problem with d.c. systems and an a.c. method is to be preferred.

(b) Crystal-Video Detection.

In this type of detection, a cyclic variation of the magnetic field over a range large enough to cover the whole width of the line is used. The x-plates of an oscilloscope are fed, through a phase-shifter, from the source which provides the field modulation and the amplified signal from the detector is applied to the Y-plates. Thus resonance absorption is directly displayed on an oscilloscope. There would be two traces on the oscilloscope, one corresponding to the excursion of the modulation from a low to high magnetic field and the other to the excursion in the reverse direction. These two traces can be made to superimpose by adjusting the phase between the field-modulation voltage and the oscilloscope time base voltage.

For a faithful reproduction of the line-shape, the amplifier should be a wide-band one so as to allow all the important Fourier components of the signal to pass through. A bandwidth of about 10 to 20 times the modulation frequency is a reasonable choice. However, the large bandwidth adversely affects the signal-to-noise ratio and a narrow band system is to be preferred.

(c) Small Amplitude Field Modulation.

A narrow band system can be used if the amplitude of field modulation is considerably less than the line width. The

principle of small amplitude field modulation is as follows. Since the power output is proportional to the line-shape function, $g(H)$, expressed in terms of the magnetic field, the output at any instant of time when the constant magnetic field is H_o and a modulation $H_m \text{Cos}\, \omega_m t$ is applied can be calculated from a Taylor series expansion of $g(H)$ about the value H_o:

$$g(H) = g(H_o + H_m \text{Cos}\omega_m t) = g(H_o) + g'(H_o) H_m \text{Cos}\omega_m t + \tfrac{1}{2} g''(H_o) H_m^2 \text{Cos}^2 \omega_m t + \ldots\ldots \quad \ldots\ldots \quad (4.17.)$$

It is seen that if the modulation amplitude is small enough, the a.c. part of the output is of frequency $\frac{\omega_m}{2\pi}$ and of amplitude proportional to the derivative of the line-shape function at the magnet field H_o. Thus the derivative of the entire spectrum can be traced out by measuring the amplitude of the time-varying output as a function of the external magnetic field. A narrow-band amplifier tuned to the modulation frequency $\frac{\omega_m}{2\pi}$ is used in order to filter out components of noise at frequencies outside a small range about $\frac{\omega_m}{2\pi}$. The circuit used to detect the amplitude of the time-varying output is generally a phase-sensitive one in which case not only the amplitude but the sign of the derivative is also recorded. The phase-sensitive detector is generally followed by a circuit with adjustable time-constant to reduce the bandwidth further and the output is fed through a d.c. amplifier on to a pen recorder. In fact, the bandwidth of the detection system in this case is determined by that of the time-constant circuit (Feher, 1957) and the bandwidth of the narrow band

amplifier is irrelevant as long as the noise voltages are not so large as to saturate it.

It is seen from equation (4.17.) that for high sensitivity, H_m should be large. But this is precisely the condition for the other terms in the Taylor expansion to become important. Hence a large value of H_m would distort the line-shape. However, since the exact reproduction of the line-shape is often not important, a compromise value of modulation amplitude equal to half the line-width is generally chosen.

4.2.4. Sensitivity Considerations

The general method of analysis for the consideration of sensitivity is to consider a low frequency analogue circuit referred to the detector terminals and to find the conditions for the maximum signal-to-noise ratio at the output of the display system. A detailed theory on the sensitivity of paramagnetic absorption techniques has been worked out by Feher (1957). Though some of the details of his observations have to be changed in the light of the recent developments, especially in regard to the detecting crystals and the klystrons, his basic theory is quite comprehensive and valid and the present discussion is based on his paper.

The first step is to maximise the detector output with respect to the coupling of the resonant cavity to the waveguide run. It is found that for maximum detector output, the input and output coupling should be equal and given by the relation

$$n^2 = r/R_o \qquad \ldots\ldots \qquad (4.18.a.)$$

for square-law detection and

$$n^2 = r/2R_o \qquad \ldots\ldots \qquad (4.18.b.)$$

for linear detection. Here R_o is the characteristic impedance of the waveguide, and r represents the resistive losses in the cavity and includes dielectric losses. The corresponding fractional changes in the detector output are, respectively,

$$\frac{\Delta P}{P_o} = -\frac{8}{27} 4\pi \chi'' \eta Q_o \qquad \ldots\ldots \qquad (4.19.a.)$$

and

$$\frac{\Delta V}{V_o} = -\frac{1}{8} 4\pi \chi'' \eta Q_o \qquad \ldots\ldots \qquad (4.19.b.)$$

where Q_o is the unloaded Q of the cavity.

However, the optimum coupling optimises the detector output whereas it is the signal-to-noise ratio that needs to be improved. The conditions for this are now considered.

If the detector is assumed to be an ideal resistor matched to the characteristic impedance R_o of the waveguide, then the noise voltage across it is

$$V_{RMS} = \sqrt{2R_o kT\Delta\nu} \qquad \ldots\ldots \qquad (4.20.)$$

because both the waveguide system and the matching resistor contribute to the noise. Assuming linear detection, for illustration, and equating the expression for V_{RMS} from equation (4.20.) to that for the voltage change ΔV in equation (4.19.b.), the absolute minimum detectable susceptibility is found to be

$$\chi''_{min.abs.} = \frac{2}{\pi \eta Q_o} \left(\frac{kT\Delta\nu}{P_o}\right)^{\frac{1}{2}} \qquad \ldots\ldots \qquad (4.21.)$$

In the actual case of a crystal detector followed by an amplification and display system, the output noise power is increased by a factor of

$$Ni/L + F_A + t_D - 1$$

where N_i = the noise figure at the input of the crystal,

L = the conversion loss of the crystal defined as 1/G where the conversion gain, G, is defined in the usual way,

F_A = the noise figure of the amplifier,

and t_D = the noise temperature ratio of the crystal detector. Also, the signal will be reduced by a factor of 1/L due to the conversion loss in the crystal. The expression for the minimum detectable susceptibility then becomes

$$\chi''_{min.actual} = \frac{2}{\pi \eta Q_o} \left[\frac{(Ni/L + F_A + t_D - 1) L k T \Delta\nu}{P_o} \right]^{\frac{1}{2}} \qquad (4.22.)$$

The factor

$$\frac{\chi''_{min.actual}}{\chi''_{min.abs.}} = \left[(Ni/L + F_A + t_D - 1) L \right]^{\frac{1}{2}} \quad ..... \qquad (4.23.)$$

is defined as the 'sensitivity loss factor' and measures the loss of senstivity due to the detecting system.

It is thus seen that the sensitivity of the spectrometer depends on the product ηQ_o, the temperature T, the bandwidth $\Delta\nu$, the microwave power P_o and the sensitivity loss factor. The product ηQ_o and the temperature T are largely determined by the requirements, and the limitations, of the experiment. The

bandwidth is reduced by using phase-sensitive detection and is controlled by the time constant circuit. The limit to this is set by the rapidity with which the spectra are to be observed, and the stability of the equipment. The microwave power has to be considered along with the sensitivity loss factor as it affects the noise temperature ratio and the conversion loss of the crystal.

The sensitivity loss factor is now to be considered. Equation (4.22.) shows that three distinct parts of the spectrometer, i.e. the microwave run, the crystal detector, and the amplification and display system, contribute to the total noise and, hence, to the sensitivity loss factor. Any noise arising from the frequency instability of the cavity caused by thermal fluctuations or electromechanical vibrations affects χ'' only to a second order, and to that extent need not be considered in a transmission-cavity spectrometer. Further, at the low power levels generally required for free radical studies, the klystron noise becomes much less than the crystal noise and is not of much importance.

The excess crystal noise decreases inversely with the frequency of detection. The amplifier noise, on the other hand, is negligible up to about 10Mc/s but starts increasing with frequency above it. The optimum region for detection frequency for a particular crystal may be from about 10 Mc/s to 100 Mc/s. However, there is another factor which limits the choice of such

high modulation frequencies. It has been seen in Chapter III, that a high frequency field modulation produces modulation broadening of the resonance lines. The modulation broadening, in frequency units, is of the same order as the modulation frequency. Hence the upper limit to the modulation frequency is set by the homogeneity of the static magnetic field and the expected line widths of the substance to be investigated.

The microwave power level also affects the crystal noise. The excess crystal noise increases with increasing microwave power but the conversion loss decreases, and the crystal has to be operated near the minimum of the resultant curve. This, however, prevents the independent adjustment of power level according to the requirements of the sample. This difficulty may be overcome in a transmission-type spectrometer by 'bucking' microwave power from the klystron into the crystal through two directional couplers without allowing it to pass through the cavity. However, this makes the spectrometer sensitive both to absorption and dispersion and introduces complexities to that extent.

4.2. Description of the Apparatus

In the free radical work of the type reported in this thesis, the specimen is available in large quantities and it has to be contained in silica tubes. Under these conditions, an X-band spectrometer is preferable to a K or Q-band one inspite of the greater inherent sensitivity of the latter. This is because the silica tube would cause a significant dielectric loss

in the small-sized K- or Q- band cavity, and it is impossible to reduce the wall thickness of the silica tube too much for reasons of mechanical strength. On the other hand, the availability of large quantities of the specimen makes it possible to fill the large-sized X- band cavity effectively. The work described here was, therefore, carried out on an X- band spectrometer, though some spectra were checked at K-band as well. The X-band spectrometer will, therefore, be described in greater detail followed by a brief description of the K-band spectrometer.

4.2.1. The X-band Spectrometer.

The low voltage 723 A/B klystron is used as the source of microwave radiation. It has a power output of about 20 mW at about 9370 Mc/s and is tunable mechanically over a range of about 1000 Mc/s (8700 to 9600 Mc/s) and electronically by about 40 Mc/s between the half power points of a given mode. The valve operates with a cathode to resonator potential of 300 volts and with a resonator current of about 15 mA. The reflector-to-cathode potential is variable from 10 to 150 volts and the diode (6 X 5) in the reflector circuit prevents the reflector from becoming positive with respect to the cathode.

The voltages applied to the klystron are stabilised by means of the regulator tube 12E1 in conjunction with the tube 6SJ7 as the amplifier (Fig. 4.3.). There is an arrangement for providing a 50 c/s sweep to the reflector voltage for purposes of tuning (Figs. 4.3. and 4.4.). The klystron heater supply is

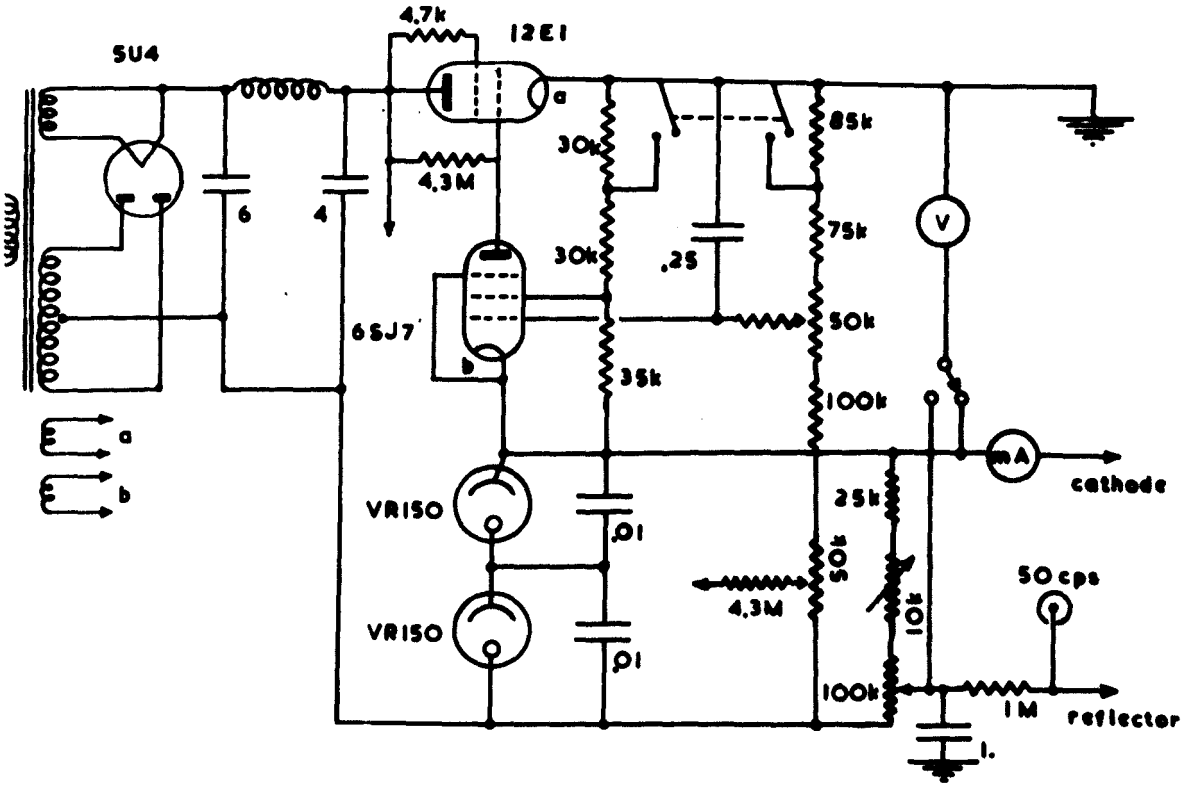

FIG. 4.3. KLYSTRON POWER SUPPLY.

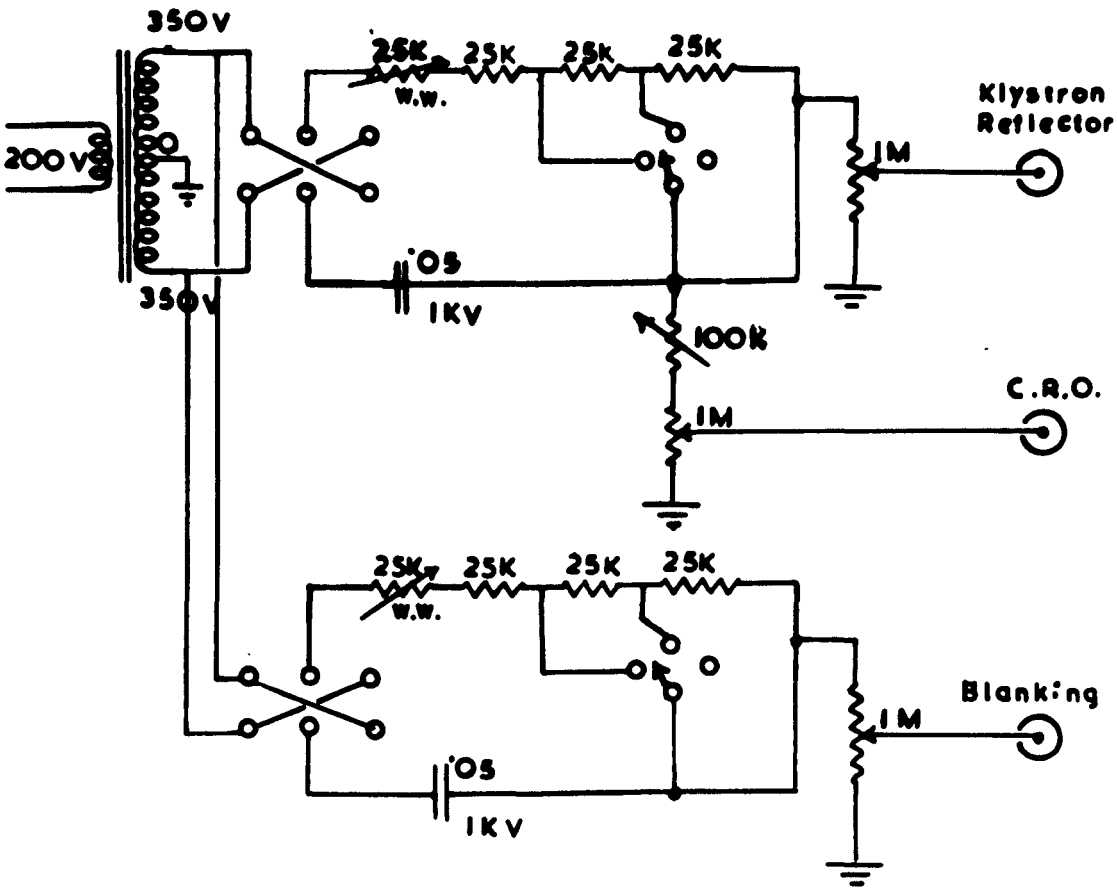

FIG. 4.4. 50c/s. PHASE -SHIFTER AND BLANKING CIRCUIT.

from a 6-volt lead accumulator to eliminate any possible mains pick-up. No precautions have been taken for the stabilisation of frequency and power. However, an automatic frequency control, locking the klystron to the cavity would be a definite advantage.

The klystron is coupled electrically to the waveguide through a probe inserted in the centre of the broadside of the waveguide at a distance of $\lambda g/4$ from the shorted end. The coupling probe, which is connected to the cavity of the klystron, is electrically insulated from the waveguide so that the waveguide could be earthed irrespective of the earthing point in the klystron power supply.

The klystron frequency is very sensitive to fluctuations of valve temperature and the change of frequency is about 0.25 Mc/s per degree centigrade. The temperature of the valve is stabilised by immersing the whole assembly in high voltage transformer oil. An 'O-ring' rubber seal was placed between the probe and the waveguide to prevent oil leaking into the waveguide run. Cold water can be circulated through a spiral of copper tubing immersed in the oil to keep the temperature of the bath down, though it has been noted that even without flowing water, the klystron settles down after some time and works satisfactorily.

(b) <u>The waveguide run</u>.

To prevent coupling between the reflected waves from the waveguide bends and discontinuities and the klystron, a ferrite

isolator is included immediately after the klystron. The isolator has a forward attenuation of less than 1 db and backward attenuation of about 30 db at the centre of its band; it has a bandwidth of 800 Mc/s centred on 9350 Mc/s and can handle 10 W in the forward direction with ordinary air convection cooling.

The isolator is followed by a parallel-strip type attenuator and a three-hole directional coupler. The directional coupler is used for monitoring purposes, but once the spectrometer has been aligned, it can be dispensed with, unless a frequency measurement of the microwave radiation is desired.

American size brass waveguide of rectangular cross-section (0.900 x 0.400 in. internal diameter) is used throughout. Where two sections of the waveguide are coupled together, a Contar screwed ring coupler (with a choked and a plain flange together) is employed. When this is not possible, the coupling is made through rectangular flat flanges which are firmly bolted together. The microwave run is generally broken at one of these flat flanges by using a thin mica sheet in between the two coupling flanges and placing insulating sleeves on the bolts. This serves to prevent the formation of any hum loops through the waveguide run. A block diagram of the waveguide run, and the other parts of the spectrometer is shown in Fig. (4.5.).

(c) The Absorption Cavity.

The absorption cavity is made out of British size brass waveguide of cross-section (1.000 x 0.500 in. inside dimensions).

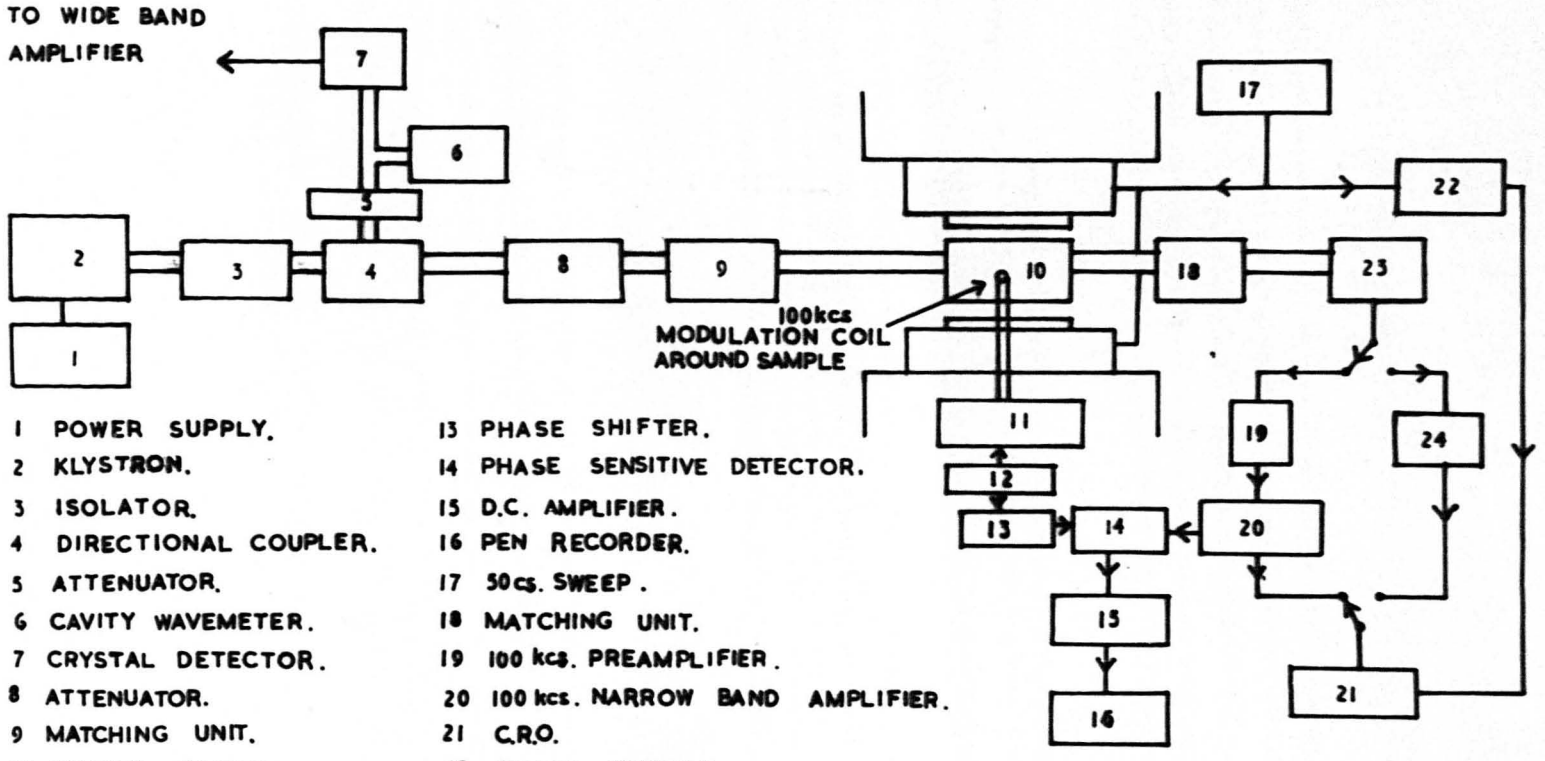

FIG. 4.5 X — BAND SPECTROMETER.

FIG. 4.6. X - BAND SPECTROMETER.

It is rectangular and operates in the H_{014} mode. The choice of this mode is a compromise between two factors, (i) high Q and (ii) large filling factor. The Q of the cavity is approximately given by

$$Q \simeq \frac{\text{volume of the cavity}}{\delta \times \text{surface area of the cavity}} \quad \ldots\ldots \quad (4.24.)$$

where δ is the skin depth. Hence, a high Q would correspond to large ratios of volume to surface area i.e. to large number of loops in the cavity, whereas this would adversely affect the filling factor. The H_{014} mode is found to be a reasonable compromise. The cavity is made slightly longer than the calculated value and is ground down till the transmitted power is a maximum for the best tuning region of the klystron.

The cavity lies horizontally in the field gap with its broad side vertical. It has a central hole in the top narrow side. A brass tube about 2" long and of internal diameter slightly greater than that of the central hole is soldered vertically to the narrow face of the cavity concentric with the hole (Fig. 4.7.a.). A brass plunger of nearly the same length fits inside the brass tube. There are three vertical groves on the outside of the plunger through two of which the high-frequency field modulation coils can be inserted in the cavity and through the third a thin g-marker tube can be inserted. The specimen tube, made of silica and of about 5 mm. external diameter and 0.5 mm. wall thickness, is inserted into the cavity

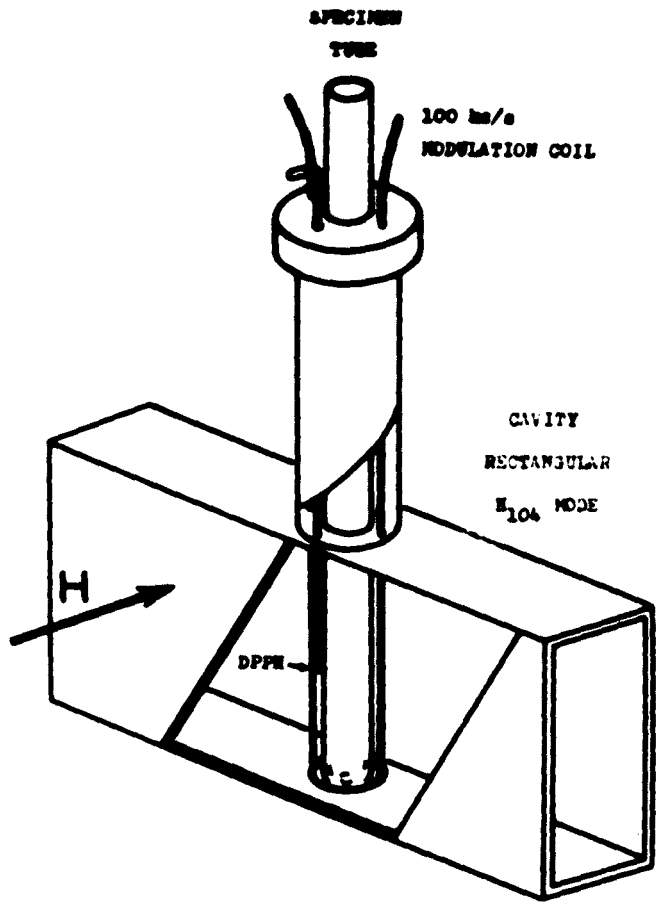

FIG. 4.7(a). SAMPLE CAVITY.

through a central hole in the plunger. Thus the specimen tube goes into the region of maximum magnetic field and minimum electric field of the microwave radiation.

Two pieces of brass foil, 0.003 in. thick, are put across the cavity waveguide to form the end walls of the cavity. The cavity is coupled to the waveguide run on either side through centrally placed iris holes, one in each piece of the brass foil. The size of the holes is empirically adjusted so as to maximise the size of a signal on the oscilloscope. The plain flanges of the cavity and the waveguide, with the brass foil in between, are firmly bolted together. There are right angle upward bends in the waveguide, one on either side of the cavity, so that the cavity can be immersed in a low temperature bath if necessary. The bends are followed by two 'heat breaks' one on either side of the cavity again. These are thinned-down sections of waveguide, with a wall thickness of 0.010 in. and fitted into a close fitting block of paxolin. The 'heat breaks' reduce the heat conduction from the low temperature bath down the waveguide. The whole assembly is shown in Figs. (4.7.a. and 4.7.b.).

(d) The Detector.

A metal-germanium crystal diode is used as the detector as these crystals have much better noise characteristics than the metal silicon ones. The crystal is held in a side arm of the waveguide and a pick-up stub is used to couple to the E-vector

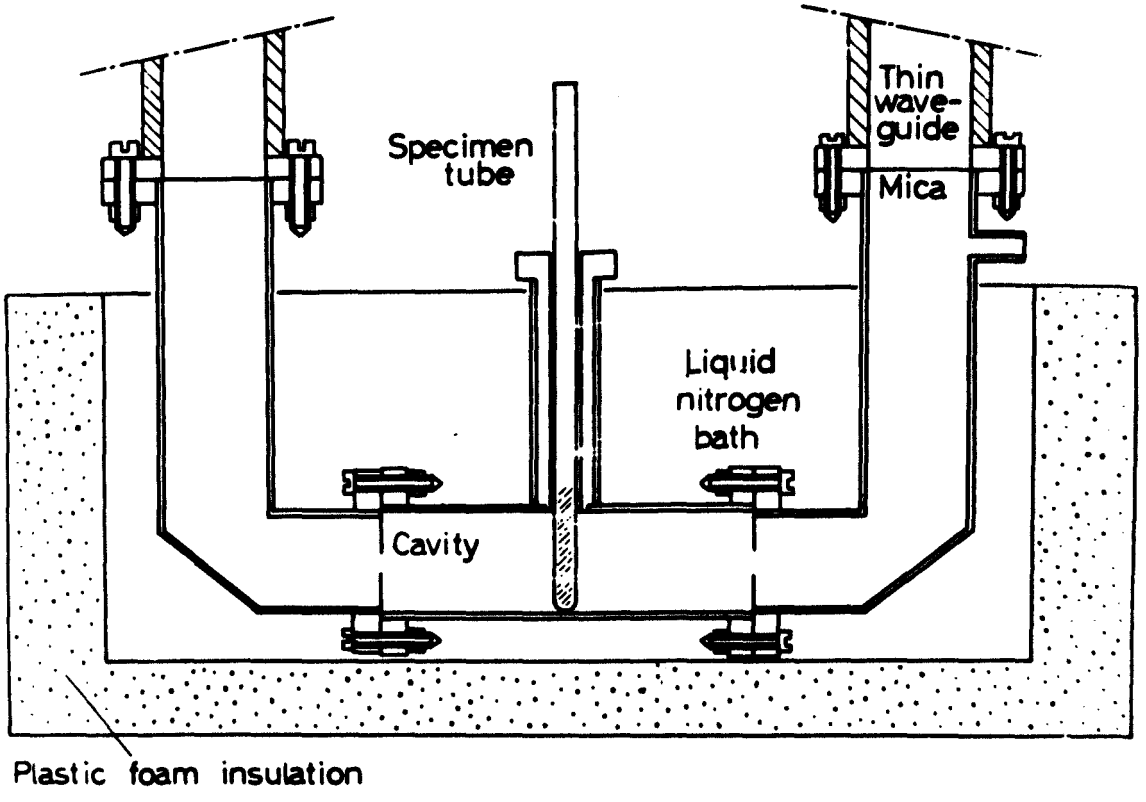

FIG. 4.7(b). LOW TEMPERATURE CAVITY.

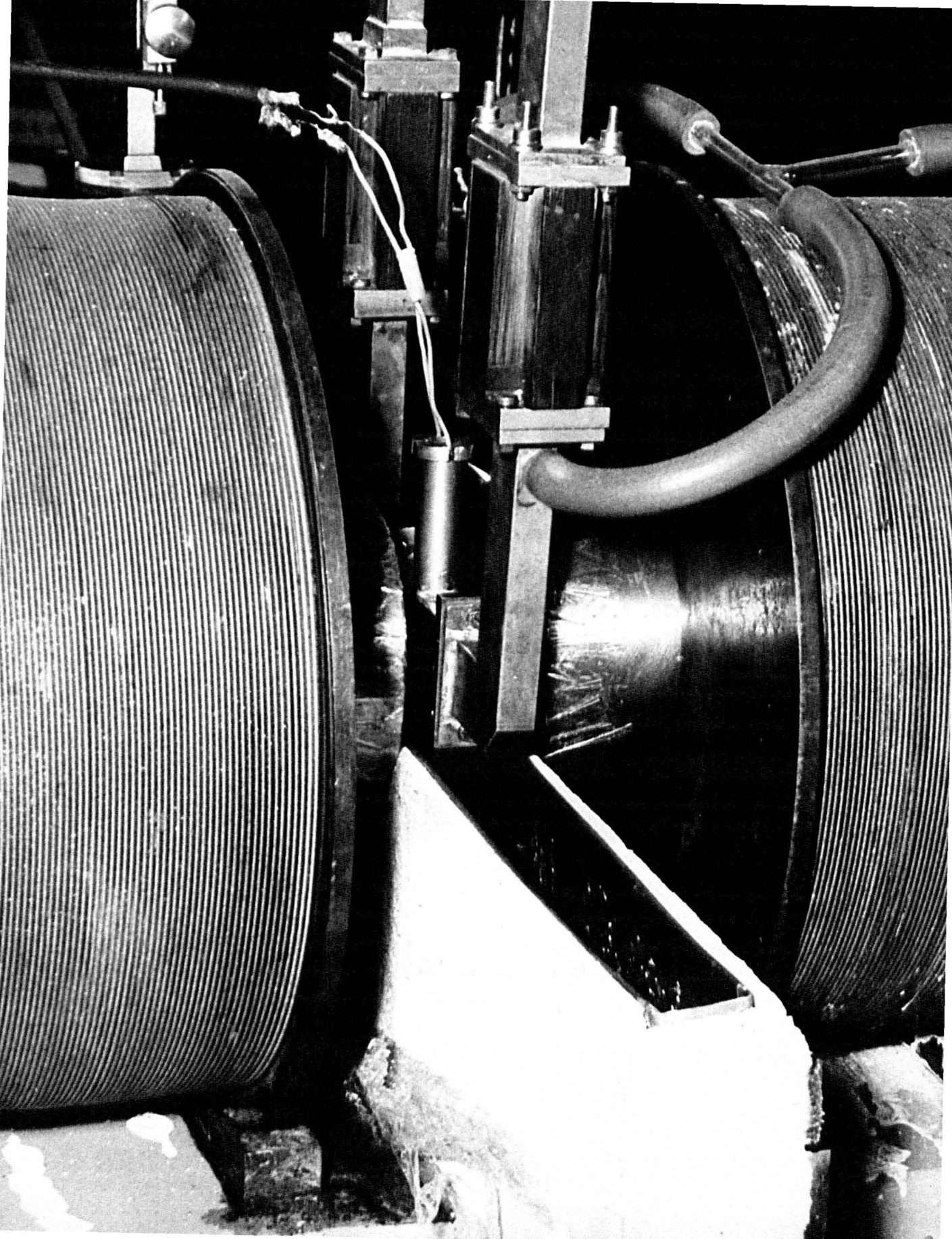

FIG. 4.8.(a). X - BAND CAVITY REGION.

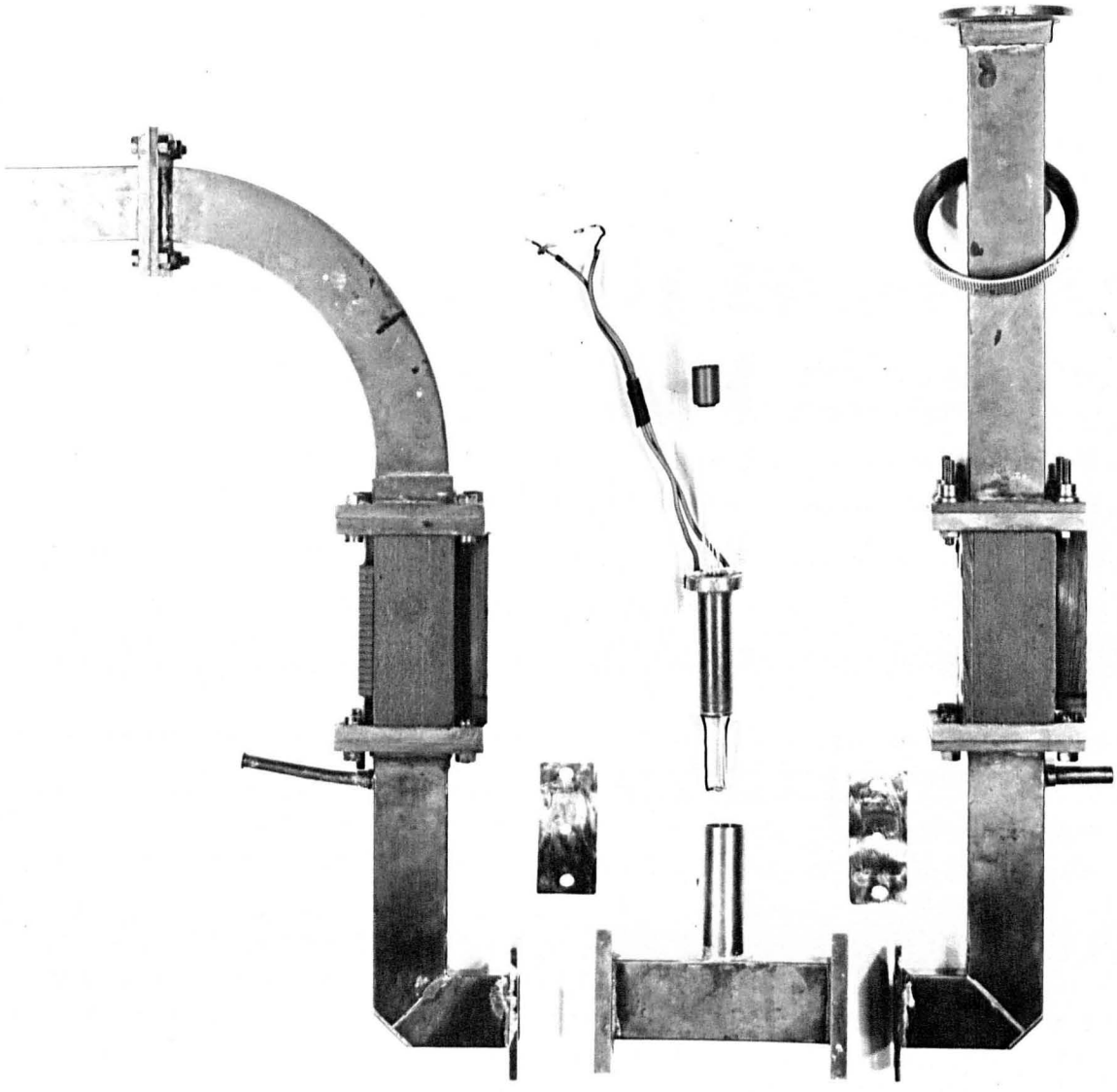

FIG. 4.8(b). X - BAND CAVITY.

of the wave. Power is matched into the coupling stub by the use of a shorting plunger approximately $\lambda g/4$ away. The detected output is taken out through a waveguide-coaxial line transition.

(e) The Display System.

The output from the crystal detector is fed into a 100 Kc/s pre-amplifier, which is the low-noise first stage of the 100 Kc/s narrow band amplifier. The input circuit is designed to match the impedance of the crystal (400 ohms) and is followed by a double triode in cascode (Fig. 4.9.). The gain of the pre-amplifier is about 1200.

There is an arrangement for switching the crystal output on to a wide-band amplifier (Fig. 4.10.). This arrangement is necessary for the initial tuning up of the spectrometer and for crystal video detection. A meter in the input circuit of the wide-band amplifier allows the d.c. crystal currentto be monitored. There is a separate input provided for the proton resonance meter. The output from the wide-band amplifier is fed directly on to the Y plates of the oscilloscope.

For phase-sensitive detection, the output from the pre-amplifier is fed into a three-stage narrow band amplifier (Fig. 4.11.) having a bandwidth of about 1 Kc/s and a gain of about 10^6.

This is followed by a phase-sensitive detector (Fig. 4.12.), which is a modification of Schuster's circuit (Schuster, 1951). The mixer value 6SN7 acts as a gate alternately opening and

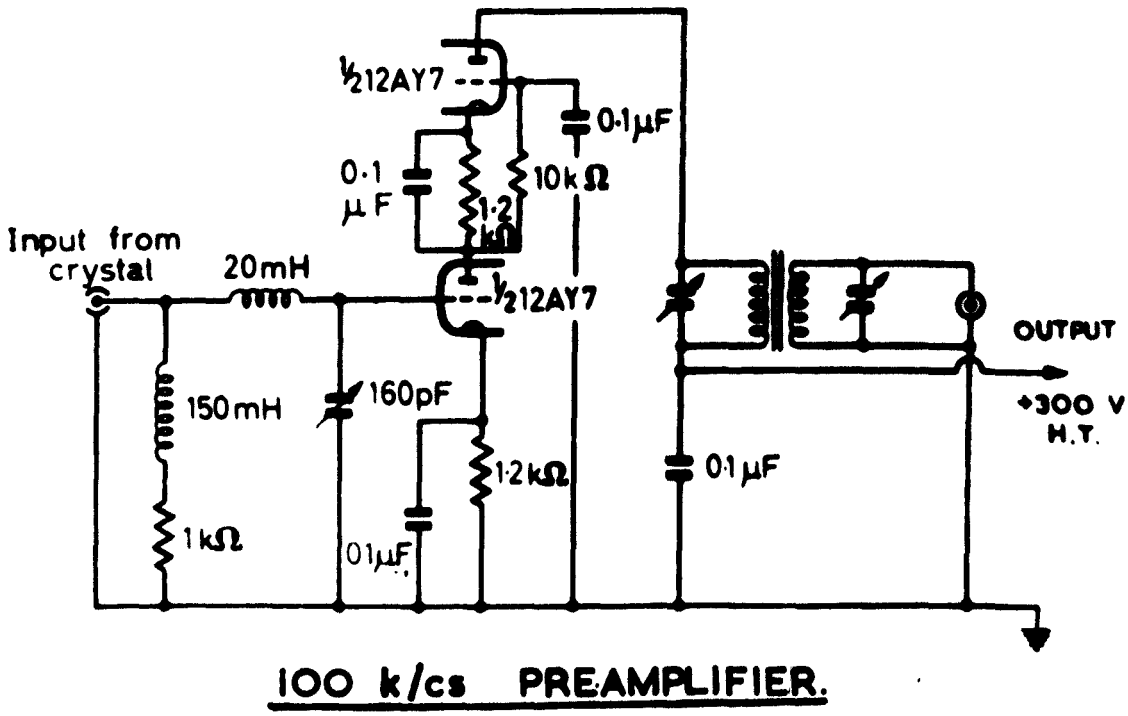

100 k/cs PREAMPLIFIER.

FIG. 4.9.

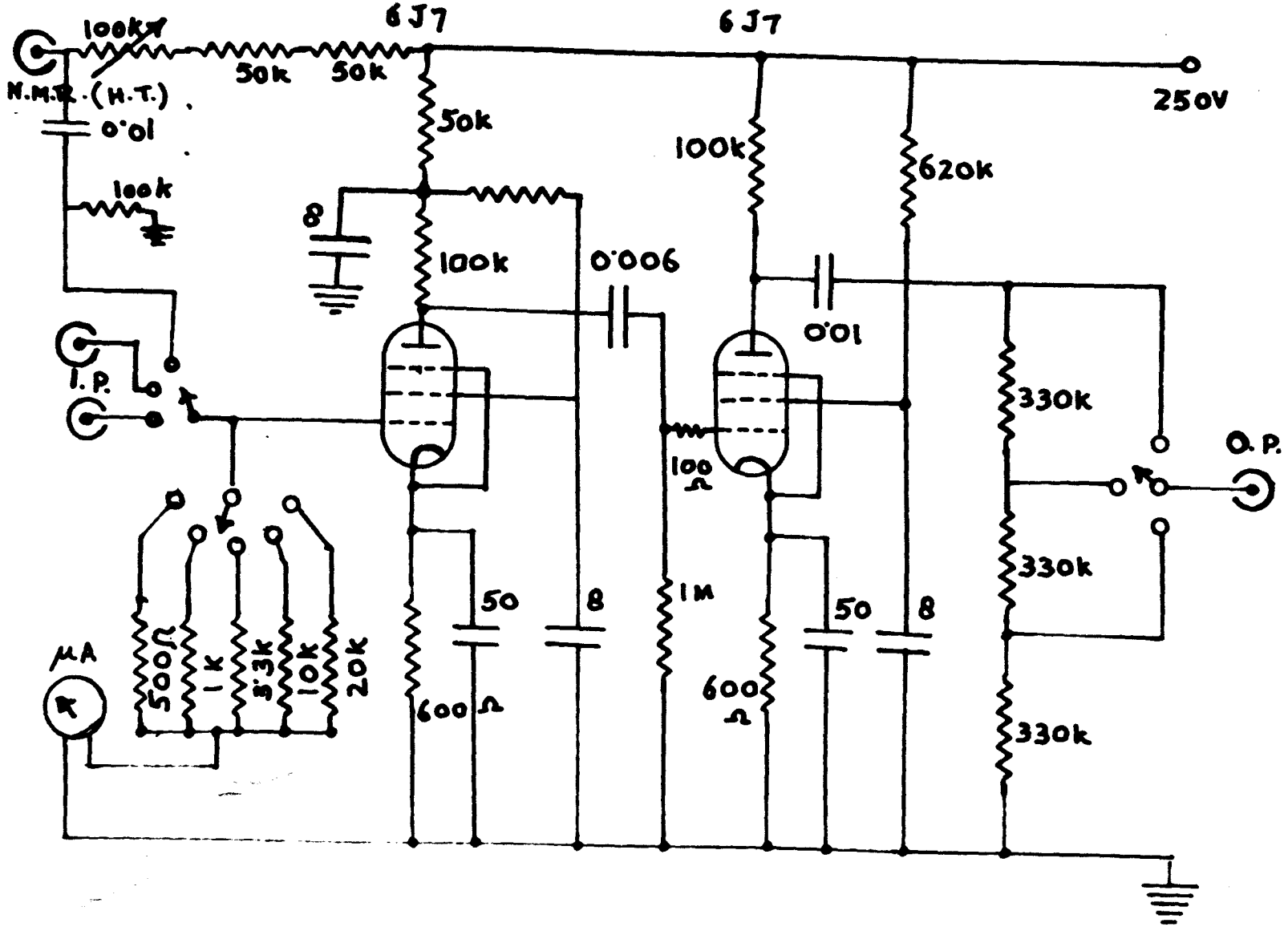

Fig. 4.10. WIDE - BAND AMPLIFIER.

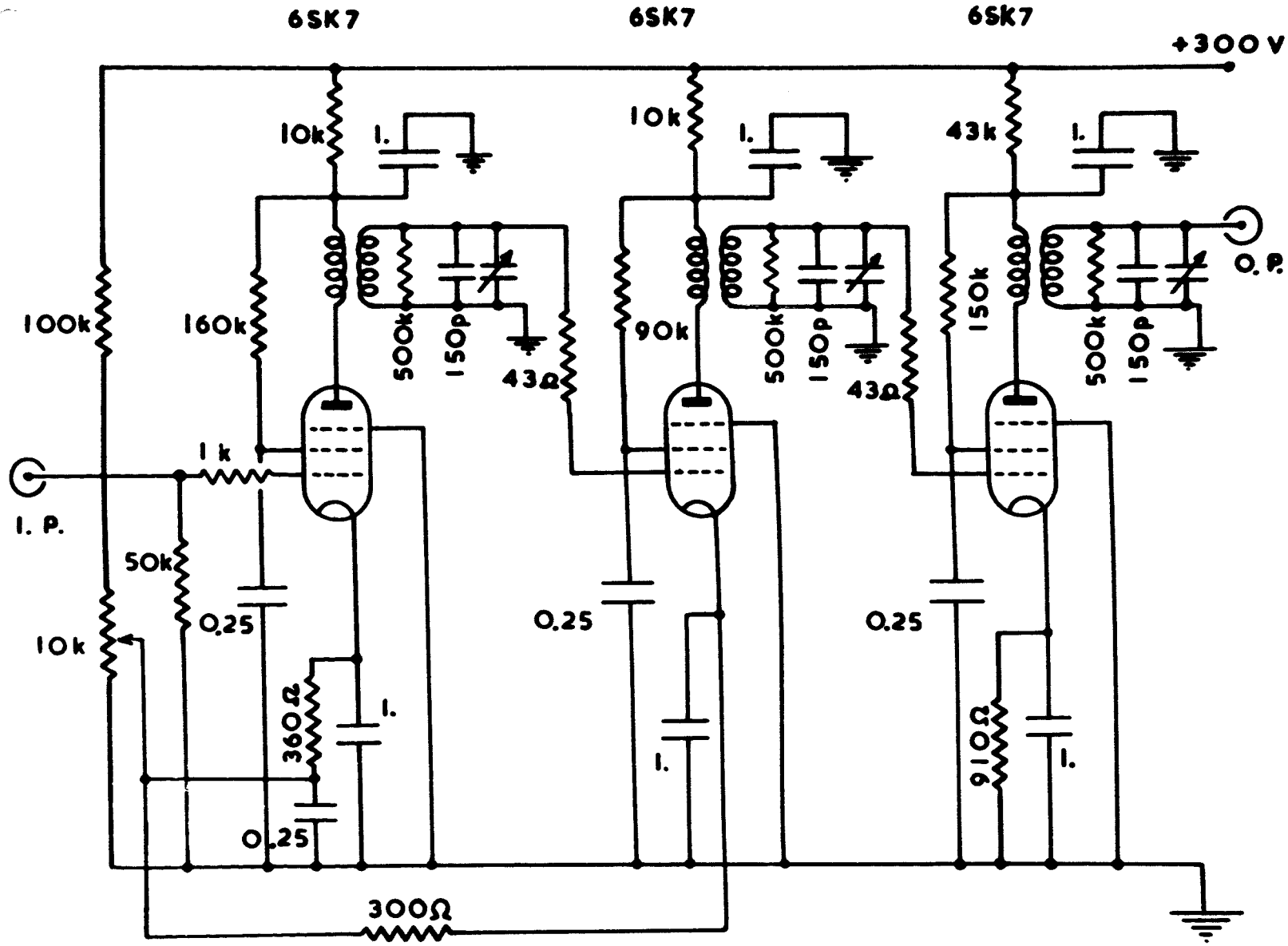

Fig. 4.11. 100 Kc/s NARROW - BAND AMPLIFIER.

shutting the two triodes. The gating action is controlled by the reference voltage which is of the same frequency as the signal. The signal thus causes a smoothed-out voltage drop across the anode loads of 6SN7, positive on one of them during one-half of the cycle and negative on the other during the next half. Thus the points A and B in Fig. (4.12.) have a d.c. potential difference varying slowly according to the signal amplitude. The d.c. potential difference also depends on the phase of the signal with respect to the reference and is a maximum when the two are either in phase or 180 degrees out of phase.

The output from the phase-sensitive detector is fed through a time-constant network into a difference type d.c. amplifier and a cathode follower, Fig. (4.13.) and is then passed on to a milliammeter and a pen-recorder connected in series. Thus the out-of-balance signal from the phase-sensitive detector, which is proportional to the derivative of the absorption, appears as a change in current through the automatic recording meter.

(f) Magnetic Field.

The d.c. magnetic field is produced by a Newport Type A electromagnet with a soft iron yoke and 4" diameter mild steel pole pieces. The pole-gap is adjustable and is kept as narrow as possible for good homogeneity but wide enough to allow the use of a low temperature bath around the cavity. Each magnetising

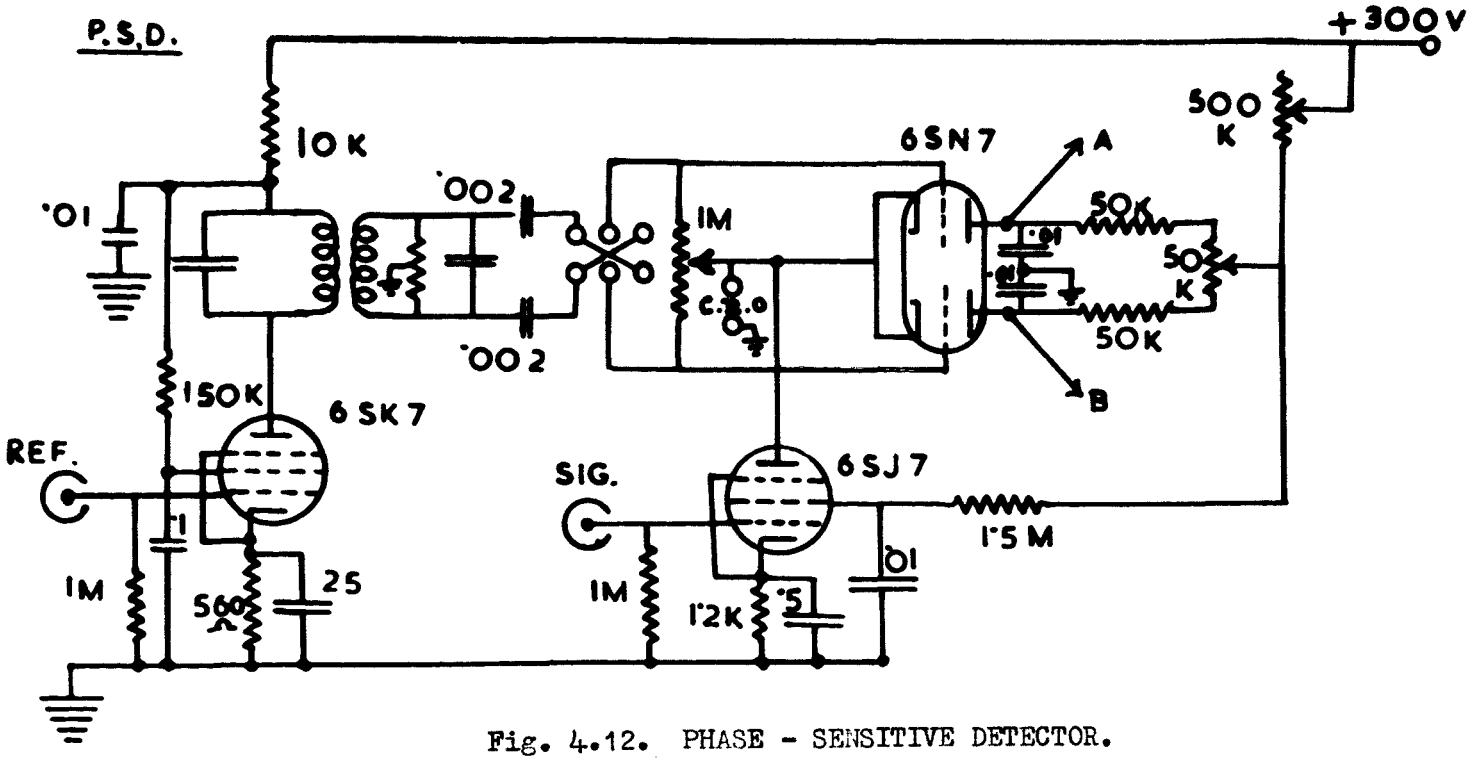

Fig. 4.12. PHASE - SENSITIVE DETECTOR.

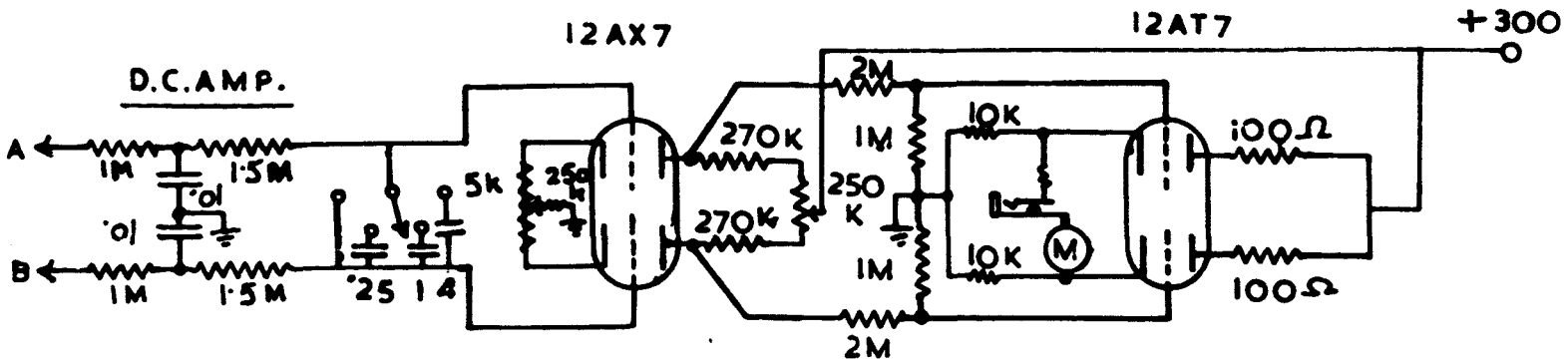

Fig. 4.13. D.C. AMPLIFIER.

coil has a resistance of 17.5 ohms and contains about 3550 turns of double glass covered copper wire. The coils are connected in parallel and are fed from a Newport stabilised Power Unit (Type B4). With a pole gap of 1.75 in. and a field of about 3000 gauss, the field inhomogeneity over the sample volume is less than 2 gauss. The power supply has a short term stability of about 1 in 10^4. The slow sweep of the main magnetic field is applied by changing the main magnetising current. This is effected by feeding the sweep terminals of the power supply from a motor driven 10 K potentiometer fed from an H.T. battery. A voltage sweep of about 20 volts is necessary to change the current by one ampere.

For low-frequency high-amplitude field modulation as required for crystal-video detection, high impedance auxiliary coils are mounted on the pole-pieces. They are wound with special heat and moisture resistance 'Pignam' covered copper wire (30 s.w.g.) so as to have the maximum number of turns possible in the space available around the pole pieces. The auxiliary coils are fed from a Variac autotransformer and produce a field modulation depth of about 800 gauss at the main field of about 3000 gauss.

The high-frequency low-amplitude field modulation for derivative recording is supplied by a single loop of wire placed inside the cavity (Fig. 4.7.a.) and fed from a crystal controlled 100 kc/s oscillator through a power amplifier with a step-down

matched and tuned output transformer (Fig. 4.14.). The high-frequency field is parallel to the static field and its amplitude can be estimated by means of a search coil. The same oscillator unit also provides the reference voltage through an attenuator and a phase shifter for the phase-sensitive detector.

(g) Low Temperature Set Up.

The absorption cavity and the waveguide run designed for low temperature work have already been described. For actual working at low temperatures, the cavity is immersed directly in a bath of liquid oxygen or liquid nitrogen. The coolant is contained in a rectangular brass box thermally insulated with polystrene foam on the outside. All the joints in the waveguide run are liberally coated with glycerol (to which some 'teepol' has been added) before being lowered down in the coolant. This provides a good low temperature seal and prevents the coolant leaking into the cavity. The rectangular trough is filled regularly with the help of a non-magnetic metal funnel. To prevent moisture condensing inside the cavity, moisture-free nitrogen gas is passed through it during the experimental run. If liquid nitrogen is used as the coolant, the flow of nitrogen gas through the cavity also prevents the condensation of oxygen in the cavity. The nitrogen gas is dried by bubling it through concentrated sulphuric acid and is precooled to the temperature of the coolant before being fed into the cavity. It enters into the waveguide run through two holes just below the

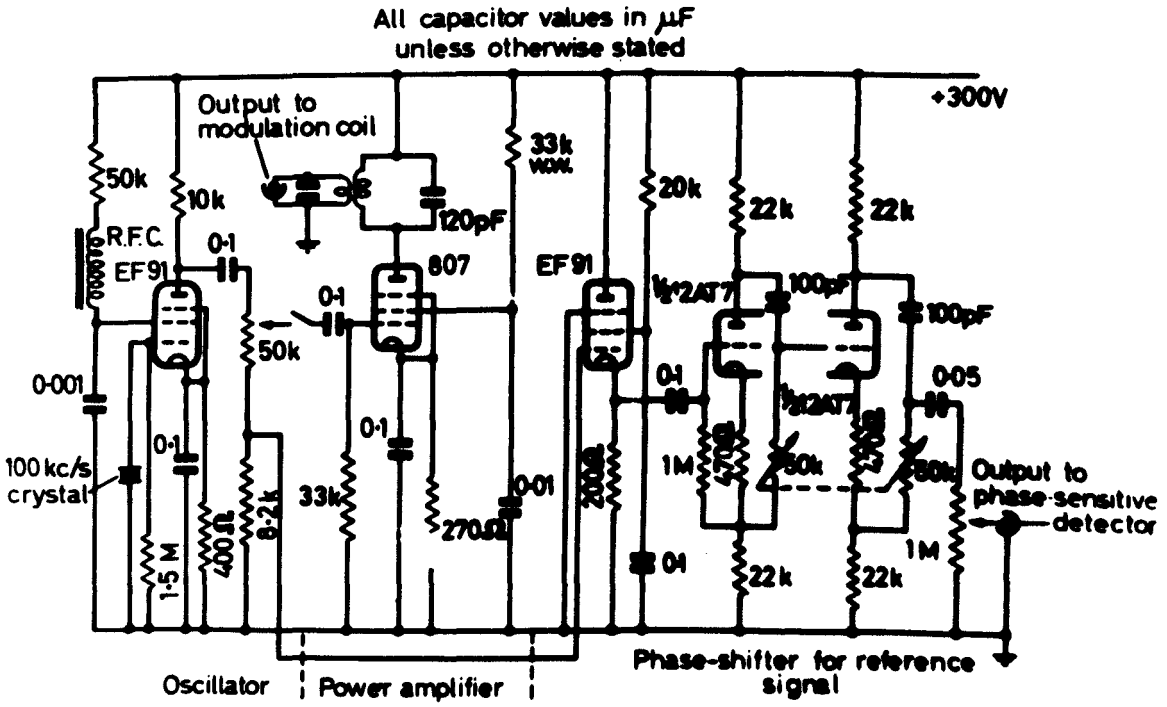

FIG. 4.14. 100kc/s POWER OSCILLATOR AND PHASE - SHIFTER.

heat breaks and comes out through the central hole in the cavity designed for the insertion of the sample tube. Thin mica windows are placed at the lower flange of the heat breaks to prevent nitrogen gas flowing out into the rest of the waveguide run.

Only two temperatures (i.e. liquid oxygen and liquid nitrogen temperatures) are available with this particular design of cavity, however, and it was thought desirable to develop a variable low-temperature cavity so that temperature variation of spectra could be studied. It was decided that the temperature of the cavity should be varied rather than that of the sample alone for reasons of thermal stability. Many different systems were tried utilising different ways of cooling the cavity and varying the different parameters of the cooling arrangements. The most satisfactory arrangement was found to be a cavity around which a spiral of narrow-bore copper tubing was soldered. A stream of nitrogen gas cooled by passing it through a very long and narrow coiled copper tubing immersed in liquid oxygen is passed through the tube around the cavity. The cavity is well insulated with polystrene foam as thick as possible consistent with the pole-gap. The temperature of the sample can be varied from room temperature to 140°K with this set-up without taking any special precautions regarding the mechanical strength of the pressure line.

However, most free radicals that were studied decay to a

negligible concentration at temperatures below 130°K and a very simple arrangement was found to be much better and quite satisfactory for temperature variations in this region. The usual cavity is, in this case, immersed in liquid oxygen or liquid nitrogen and the sample is warmed up above this temperature by passing warm nitrogen gas through the cavity. An arrangement for passing nitrogen gas through the cavity already exists but the flow line had to be modified to suit the different requirements. First of all, sulphuric acid cannot be used as a drying agent for the flow speeds involved and this is replaced by some other drying arrangement. In fact, removal of moisture and carbon dioxide has been of great concern as the narrow tubes are very liable to be blocked with the formation of ice or solid CO_2 at these low temperatures. A drying arrangement that has been found satisfactory consists of a tube of silica gel followed by a soda-lime tube and a low temperature trap. The latter consists of a number of wide-bore copper U-tubes filled with metal turnings and immersed in liquid oxygen or liquid nitrogen. Any residual moisture or carbon dioxide is trapped on the large surface area provided by the metal turnings and the copper tube. A flowmeter is also included in the circuit and is used for relative indications of the flow rates. It consists of a variable constriction in a rubber tube on both sides of which there are side tubes connected to the two ends of a silicon-oil manometer. The copper spiral tube which was used to precool the gas has been left

in the circuit. This enables the gas to be precooled if necessary, or otherwise acts as a heat exchanger for the cold gas coming out of the low temperature trap. It can also be used, if necessary, to pre-warm the gas above room temperature before letting it into the cavity.

It is possible by this method to raise the temperature of the sample conveniently by about 50°C i.e. up to about 130°K if liquid nitrogen is used and 145°K if liquid oxygen is used. In fact, it has been observed that even if the gas is precooled, the temperature of the sample depends very much on the rate of gas flow and this should be borne in mind while making observations at fixed liquid oxygen and nitrogen temperatures. The temperature variation due to short term fluctuation of the gas flow is less than 0.5°C. It had been noted that in the old cavity assembly, the level of liquid nitrogen fell considerably in the trough thus causing a frequency drift of the cavity and a temperature drift at the sample during a run. Also any filling of liquid nitrogen in the trough during a run caused much disturbance in the working of the spectrometer. The level changes and the corresponding temperature drifts are avoided in the present design by using a larger and better insulated trough, and a funnel held at a lower level and away from the cavity allows the coolant to be poured into the trough without much disturbance to the spectrometer. The temperature fluctuations due to the fall of level in the trough is about 0.5°K for low rates

of gas flow and about $2^{\circ}K$ for quite high flow rates.

The temperature of the sample is measured with the help of a thermocouple, one junction of which is embedded in the sample, the other junction being immersed in liquid nitrogen. The thermocouple is introduced into the sample before freezing it for irradiation and its position in the sample tube is adjusted so as to be at the centre of the cavity. It has been checked that the thermocouple itself does not give any signals and the spectra of samples with and without the thermocouple have been compared to ensure this. Being almost at the elctric node, the thermocouple is not found to cause any appreciable damping. The thermocouple potentiometer (Croydon) is calibrated in 10 μV scale divisions, which correspond to about $0.5^{\circ}C$ in this region. The accuracy of absolute temperature determination depends on the temperature of the reference bath, because the temperature of liquid nitrogen depends on the quantity of impurities (oxygen etc.) dissolved in it and may vary by 3 or $4^{\circ}C$.

This method of changing the sample temperature is in many ways more convenient than that of putting the sample tube in a dewar inside the cavity and cooling it by gas flow. The dewar assembly is very fragile specially because of the narrow inlet and outlet tubes. It introduces a large quantity of dielectric into the cavity in regions where the electric field is no longer very small. Also unless an external high-frequency field modulation is used with the help of specially designed cavities, the modulation

coils would be further away from the electric node and would thus cause much more damping of the microwave power. Unless special care is taken to stabilise the flow rate well, small fluctuations would cause relatively large changes of temperature of the sample because of its small heat capacity. A smaller sample tube and hence smaller quantities of the sample would have to be used and the narrow inlet and outlet tubes would be prone to blockage due to ice formation unless special care is taken to make the gas sufficiently moisture-free.

The straight forward system of passing warm nitrogen gas through the cavity does not have these disadvantages. The sample is fairly well locked to the cavity and hence is stable against temperature fluctuations. Since only small changes of temperature are required, low rates of flow may be used; in fact, it has been observed that the rate of gas consumption in this method of temperature variation is considerably less than in most other methods. Finally if the gas flow stops accidently due to blockage or otherwise, the temperature would be lowered down and the free radicals would stabilise rather than decay. Thus from the point of simplicity and practical convenience, this method is preferable to the alternative design. However, its range is limited and it is very desirable to have a variable temperature system covering a wide range. Cold nitrogen boiled off from a large liquid nitrogen dewar by electric heating and passed through copper tubing wound around the cavity might achieve this.

4.2.2. The K-Band Spectrometer

The K-band spectrometer is also of transmission type (Fig. 4.16.). The microwave radiation is generated by the reflex klystron type 2K33. It has a maximum power output of about 40 mW, and a mechanical frequency tuning range of about 10% and an electronic tuning range of a few tens of Mc/s, and operates at 9 mA plate current. The cathode-to-anode potential is 2000 V and is supplied by a conventional series-stabilised power supply which also supplies variable voltages for the reflector and the grid (down to 600 V and 200 V respectively below the cathode). A diode in the reflector circuit prevents the reflector from becoming positive with respect to the cathode. There is also provision for a 50 c/s sweep to be applied to the reflector voltage for tuning. The heater current is supplied by a 6V lead accumulator, and the anode of the klystron is earthed. The klystron is cooled by air-flow from a small fan mounted close to it.

The klystron is coupled directly into the waveguide and is matched into it by a tunable shorting plunger mounted diametrically opposite to the output guide. It is locked to a transmission type cavity wavemeter by 33 Kc/s modulation of the reflector voltage. The cavity wavemeter operates in H_{01p} mode as this mode has a higher Q than that due to the dominant mode H_{11p}. A clearance between the cylindrical walls of the cavity and the tunable plunger prevents surface currents flowing from the curved to the flat surface of the cavity and thus suppresses the degenerate

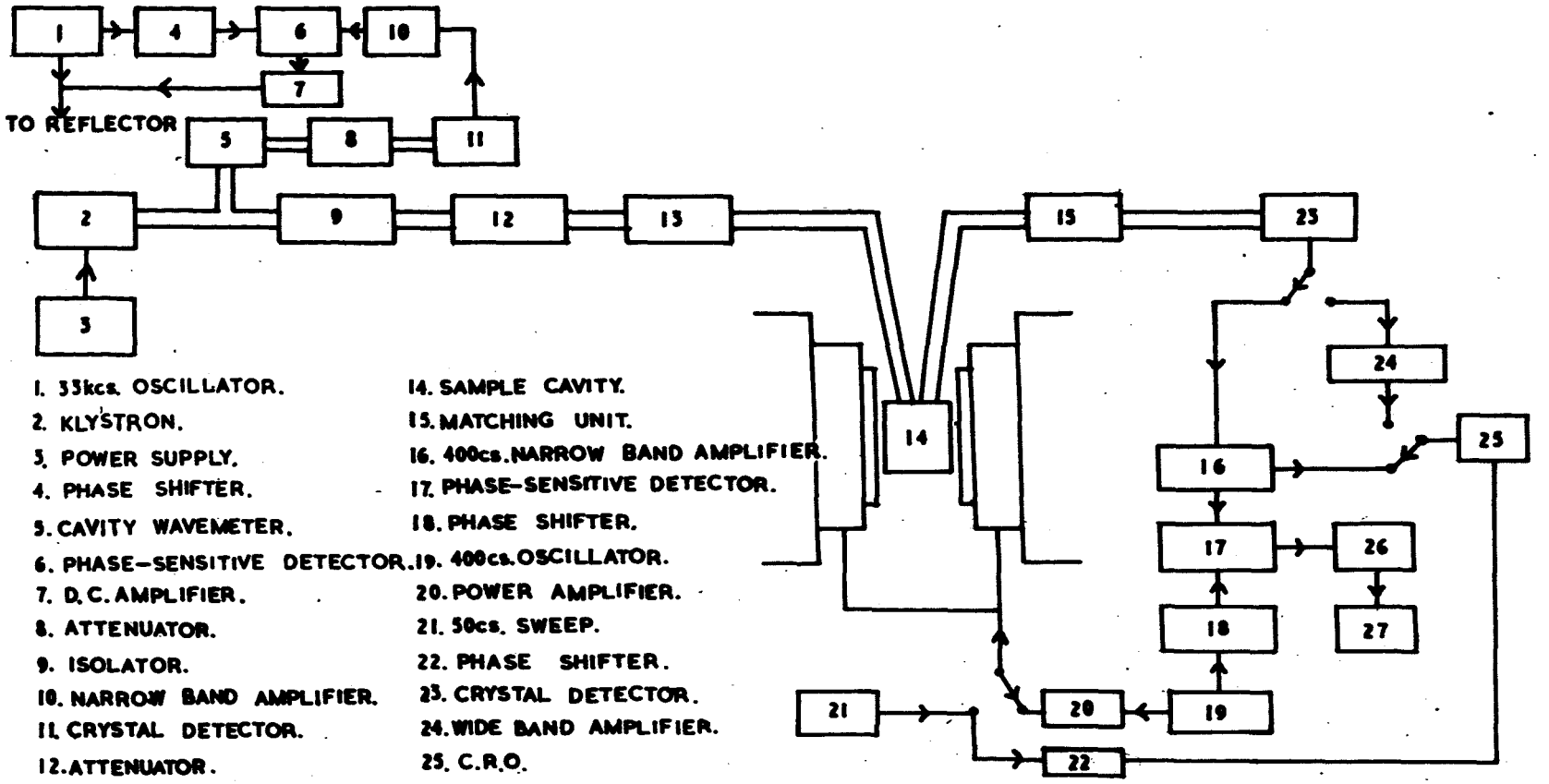

1. 33kcs. OSCILLATOR.
2. KLYSTRON.
3. POWER SUPPLY.
4. PHASE SHIFTER.
5. CAVITY WAVEMETER.
6. PHASE-SENSITIVE DETECTOR.
7. D.C. AMPLIFIER.
8. ATTENUATOR.
9. ISOLATOR.
10. NARROW BAND AMPLIFIER.
11. CRYSTAL DETECTOR.
12. ATTENUATOR.
13. MATCHING UNIT.
14. SAMPLE CAVITY.
15. MATCHING UNIT.
16. 400cs. NARROW BAND AMPLIFIER.
17. PHASE-SENSITIVE DETECTOR.
18. PHASE SHIFTER.
19. 400cs. OSCILLATOR.
20. POWER AMPLIFIER.
21. 50cs. SWEEP.
22. PHASE SHIFTER.
23. CRYSTAL DETECTOR.
24. WIDE BAND AMPLIFIER.
25. C.R.O.
26. D.C. AMPLIFIER.
27. PEN RECORDER.

FIG. 4-16 K-BAND SPECTROMETER.

E_{11p} mode. The cavity is coupled to the waveguide run through two iris holes, λ_g apart, along the central line on its narrow side and placed symmetrically about the axis of the cylinder. Such a feed suppresses the odd modes. The output coupling is through a single hole in the curved surface of the cavity and lying in a plane parallel to the axis of the cylinder and making an angle of 45^0 to the central line of the main waveguide at a distance of $\lambda g/4$ from the end face of the cavity. The H_{11p} mode which has a node at this point will, thus, not couple power into the detecting arm. The free space wavelength is calculated from the observed values of λ_g by the relation

$$\frac{1}{\lambda^2} = \frac{1}{\lambda_g^2} + \frac{1}{\lambda_c^2} \qquad \ldots\ldots \qquad (4.25.)$$

where the critical wavelength is

$$\lambda_c = 1.64r \qquad \ldots\ldots \qquad (4.26.)$$

for the H_{01p} mode in a cavity of radius r.

The wavemeter is followed by an attenuator and a three-slot directional coupler for montoring purposes. After this is a squeeze-section phase-shifter (with a slot 10" long and 1/16" wide along the centre of the broad side) followed by the absorption cavity and another similar phase-shifter.

The design of the cavity is radically different from that used in the X-band spectrometer and requires special mention. It is a cylindrical cavity with diameter as small as possible

and long feeds so that it can be lowered directly into a tailed silvered dewar, Fig. (4.18.). It operates in H_{011} mode so that the maximum of the microwave magnetic field lies along the axis. A tunable plunger forms the bottom surface of the cavity. The design of a cylindrical cavity for operation in the H_{01p} has already been discussed in connection with the cavity wavemeter. Thus a choke joint is not used between the plunger and the cavity wall; rather a clearance is left there. There is a central hole at the top to which a brass tube is soldered so that the sample tube can be lowered through it into the cavity. The cavity is excited through two iris holes on the top, one on each side of the central hole. The size of the coupling holes is adjusted empirically. The input and the output waveguides are almost vertical and have their narrow sides adjacent to each other. They are made of german silver so as to act as 'heat breaks'. Because of the small diameter of the cavity, and the central hole at the top, the waveguide dimensions have to be smaller than those normally used at K-band. This necessitates the use of taper sections to minimise the reflections produced at the transition, and also the smaller waveguides are filled in with tapered push-fit distrene rods of rectangular cross-section so as to keep the critical wavelength larger than 1.25 cm. Thin sheets of mica are inserted across the waveguides at the transition and sealed with Vaseline. When working at temperatures below 90^{o}K, the cavity is pumped

FIG. 4.18. K - BAND CAVITY.

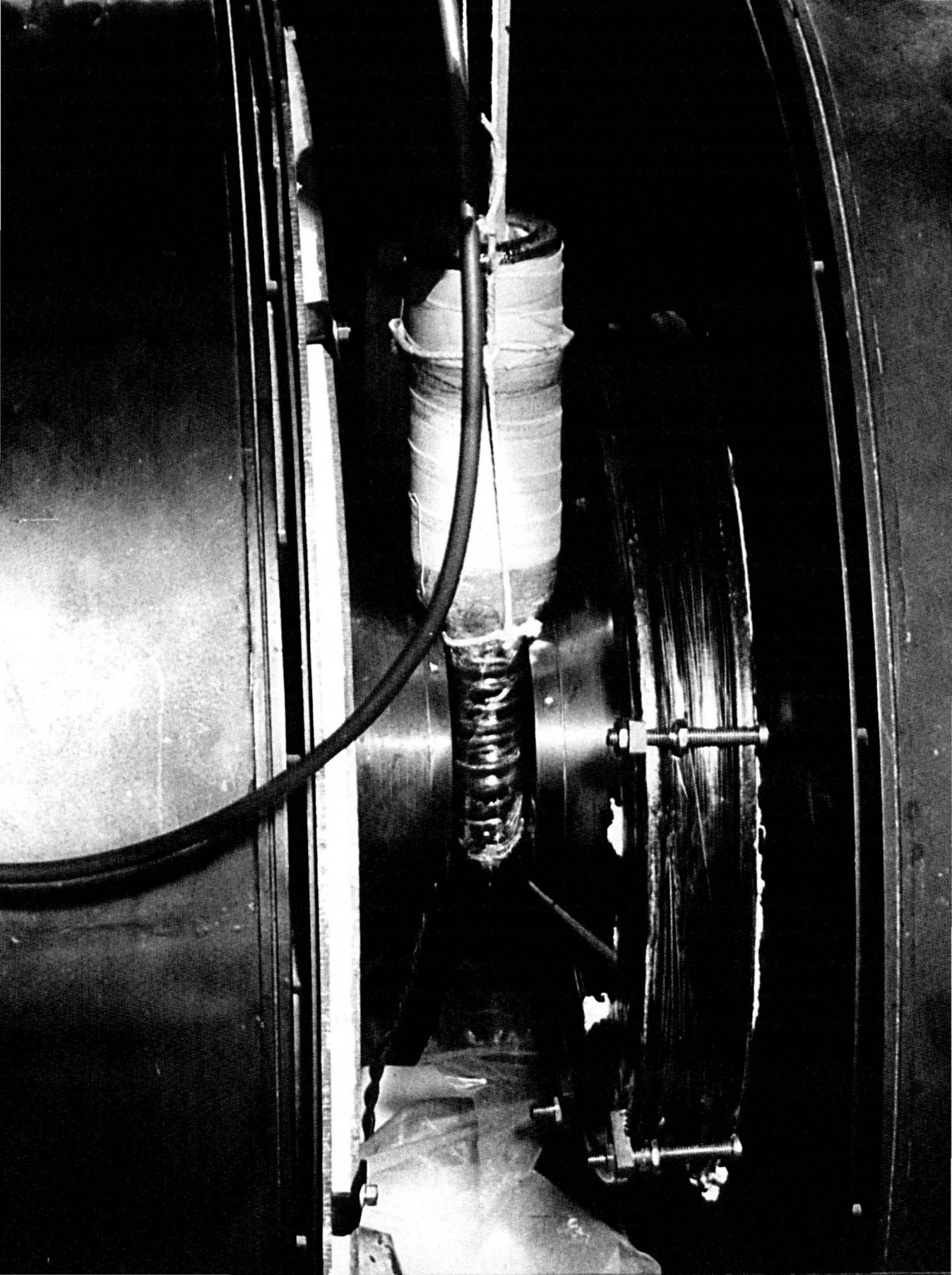

FIG. 4.17. K - BAND CAVITY REGION.

out by a backing pump through an inlet tube in the middle of the broad side of one of the waveguides just below the mica windows. This prevents oxygen condensing inside the cavity.

To work at low temperatures, the cavity is first tuned at room temperature and then detuned such that it will come in tune again on contraction at low temperatures. A tight-fitting cup is placed over the lower end of the cavity and liberally smeared with glycerol-teepol mixture so as to form a good low temperature seal.

The crystal holder is at the end of the run and has a stub coupling for the crystal and a waveguide-coaxial line transition for the detector output. A 1N26 silicon tungsten crystal is used as the detector and a shorting plunger at the end of the waveguide matches power into the coupling stub. The waveguide run is broken at one point to prevent any formation of pick-up loops. A 400 c/s phase-sensitive detection system is used, and there is an arrangement for crystal-video display as well.

The Newport Type D magnet with adjustable pole gaps is used with this spectrometer. The magnet is designed for single crystal work and is mounted on a turn table. However, the orientation of the magnetic field does not affect the intensity of the resonance lines as the axial microwave magnetic field in a vertically placed H_{01p} cavity is always perpendicular to the horizontal d.c. magnetic field. The low frequency field

modulation (both 50 c/s used for crystal-video and 400 c/s for phase-sensitive detection) are applied externally through modulation coils mounted on the yoke. The magnet has a field homogeneity of at least 1 in 10^5 over 1 cm^3 and is fed from a B4 Newport current-stabilised Power Unit.

4.3. Experimental Procedure

4.3.1. Measurement of the Magnetic Field

The main magnetic field is measured with the help of a proton resonance magnetometer. A crystal-video display of the proton resonance signal from water, clycerol, or paraffin wax on the oscilloscope is used to determine the magnetic field, from the measurement of the frequency of the proton resonance. The proton resonance frequency is related to the magnetic field by the relation

$$H = 234.87 \times \nu \qquad \ldots\ldots \qquad (4.27.)$$

where H is in gauss and ν is in Mc/s.

The proton resonance meter actually used has a circuit due to Robinson, (Fig. 4.19.), and its frequency is measured with a heterodyne frequency meter (model LM-14, U.S. Navy), which has crystal controlled check points and is accurate to 0.01% over a wide temperature range. Ordinary water is found to give a satisfactory signal, though some paramagnetic impurity may be mixed with water to decrease the relaxation time, if necessary.

A calibration curve of the magnetic field against the

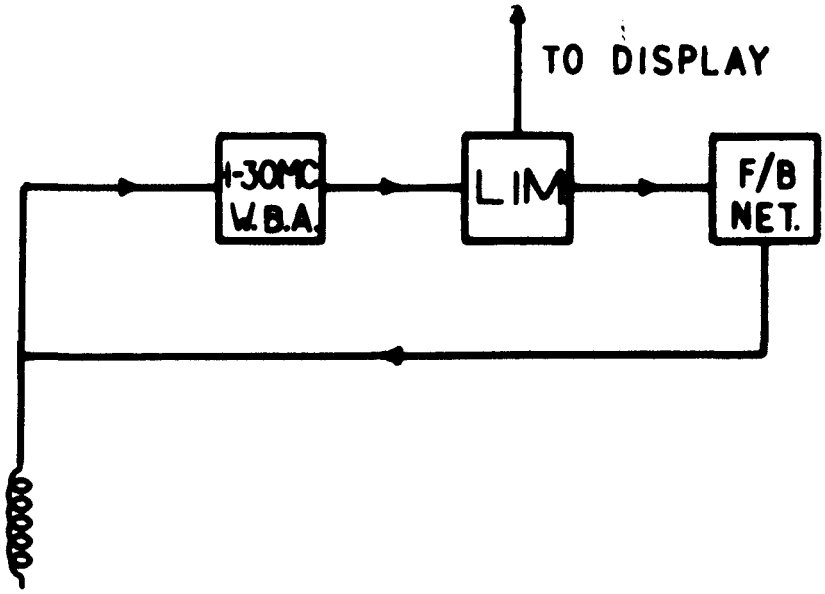

BLOCK DIAGRAM OF THE NUCLEAR MAGNETIC RESONANCE SPECTROMETER (AFTER ROBINSON)

FIG. 4.19.

magnetising current is drawn and used unless an accurate determination is required. The magnetic field is taken through the complete cycle before each setting to avoid the hysterlsis effects and the magnetic field is set only from one direction i.e. either when the current is increasing or decreasing.

4.3.2. Determination of Hyperfine Splittings and Line-Widths

Determination of hyperfine splittings and line-widths involves the calibration of the field sweep. This can be effected by displaying the proton resonance signal on both sides of the electron resonance signal and measuring the proton resonance frequencies corresponding to both these settings. The proton resonance head is held outside the cavity but as close as possible to the sample under investigation.

However, because of the inhomogeneity of the magnetic field and lack of space in the pole-gap, a simultaneous proton resonance measurement cannot always be made. A better method is to make use of the known hyperfine splittings of some standard substance. Peroxylamine disulphonate ions in benzene solution give three equally spaced lines of equal intensity (due to h.f. interaction with the nitrogen nucleus) with an over-all splitting of 26 gauss (Pake et al., 1952) and are very suitable for this purpose, specially because the hyperfine splittings in many frozen free radicals are of the same order. Unfortunately, these ions are not very stable and, so, difficult to use for any length of time.

There is a third and simpler, though less accurate, method for calibrating the field sweep. This utilises the difference in g-values of free radical signals from diphenylpicrylhydrazyl (DPPH) and ultramarine. The field separation between the two signals is given by

$$\Delta H_o = \frac{h\nu_o}{\beta}\left(\frac{1}{g_1} - \frac{1}{g_2}\right) \qquad \ldots\ldots \qquad (4.28.)$$

and is found to be 43 gauss at about 9,400 Mc/s. A variation of 100 Mc/s in the klystron frequency corresponds to a change of about 0.4 guass in ΔH. Since the frequency of the non-tunable cavity would not change by 100 Mc/s even on cooling, a value of 43 guass may be assumed for ΔH if the klystron frequency is close to 9,400 Mc/s. The accuracy of this method may however be increased by calibrating ΔH with a proton resonance meter at a known klystron frequency under favourable conditions and correcting the subsequent measurements for change of the klystron frequency according to the relation

$$\frac{\Delta H}{\nu} = \frac{\Delta H}{\nu_o} \qquad \ldots\ldots \qquad (4.29.)$$

The klystron frequency can, of course, be measured with the help of a wavemeter fed through the monitoring directional coupler.

4.3.3. Determination of g-Values

Most of the free radicals have their g-factor close to the free-spin value. The following procedure is the one most

convenient for accurate determination of the g-value in such a case. A standard sample of known g-value (usually DPPH) is inserted into the cavity along a grove in the plunger which carries the 100 Kc/s modulation coils (Fig. 4.5.a.). If the field sweep is calibrated and the klystron frequency is measured the g-value separation can be determined from the relation

$$\frac{\Delta g}{g} = \frac{\Delta H}{H - \Delta H} = \frac{\Delta H}{h\nu/g\beta - \Delta H}$$

$$\simeq \frac{g\beta\Delta H}{h\nu} \qquad \ldots\ldots \qquad (4.30.)$$

where g and H refer to the corresponding quantities for the g-marker (i.e. DPPH) and ν is the klystron frequency. If the signal from the experimental sample overlaps that from DPPH, ultramarine may be used as a g-marker instead. However, the ultramarine signal is very wide and may overlap part of the signal under investigation. Also an accurate determination of the peak of the absorption curve would be difficult for a broad signal and, to that extent, the use of ultramarine as a g-marker will limit the accuracy of the results.

4.3.4. Determination of Free-Radical Concentration

The absolute magnitudes of free radical concentrations may be required for the study of the mechanism of free radical production (e.g. in quantum yield determinations). The usual method is to compare the intensity of absorption of the sample under investigation with that of a standard sample. The usual standard substance is DPPH because it is quite stable in

crystalline form and has one unpaired spin per molecule. However this is not suitable for use for low concentration measurements, because of the difficulty of diluting it sufficiently. Also the DPPH radicals decay when diluted either in a liquid or a powder.

The standards used in practice depend on the special conditions of experiment. Voevodsky (1958) has used a single crystal of $CuCl_2.2H_2O$ weighing about 1 mg as a standard. If properly oriented, its spectrum will not overlap with that of the unknown sample and the spectra of both the samples could be traced simultaneously. The alternative to this is to place the standard free radical sample at a different maximum of the microwave magnetic field in the same cavity and to alter the static field at the standard sample with the help of local coils or mild steel discs (Köhnlein and Müller, 1960). Wurster's blue gives a very nearly Lorentzian line and can be used if the absorption from the unknown is also Lorentzian.

Hoskins and Pastor (1960) have found dextrose charred at 560°C to be much superior to DPPH as a standard in many ways under a wide variety of conditions. The charred dextrose shows no variation in line width, g-value, spin-density, thermal relaxation time and stability over a wide range of temperature and has a line width of 0.6 gauss.

However, for ordinarly purposes, carbon formed at 500°C is quite satisfactory. It is calibrated against DPPH and diluted

by various amounts with calcium carbonate powder, which has been previously checked for the presence of any paramagnetic impurities. The samples having different free radical concentrations are cross-checked against each other to obtain quantitative agreement.

For the actual determination of concentration, the integrated intensities of absorption from the unknown and the standard samples have to be compared. The area under the absorption curve is proportional to the product of the height of the absorption derivative curve and the square of the width at maximum height, and the constant of proportionality depends upon the line-shape. Hence if the lines to be compared are of identical shape, the ratio of (height x width^2) would give the relative concentration. If one of the lines has a Gaussian and the other a Lorentzian shape, and if both of them have identical areas, then it is found that

$$\frac{(hW^2)_G}{(hW^2)_L} = 3.49 \qquad \ldots\ldots \qquad (4.31.)$$

This relation may be used if either the unknown or the standard sample has a Gaussian shape and the other a Lorentzian. Finally, it may be noted that for accurate measurements, corrections have to be applied for the differences in the size, shape, position and dielectric properties of the two samples.

CHAPTER V

DESCRIPTION OF EXPERIMENTS AND EXPERIMENTAL RESULTS

5.1. Production and Trapping of Free Radicals

The experimental techniques generally used for the production of frozen free radicals fall into two classes, (a) decomposition of the parent molecules in the gas phase in a flow system followed by rapid freezing, and (b) 'in situ' decomposition of the frozen parent molecules. The decomposition of the parent molecules can be carried out by photolysis, radiolysis (γ or X-rays), particle bombardment (electrons, neutrons, ions or atoms), electrical discharge (low frequency, r.f., or microwave), and pyrolysis. Electrical discharge and pyrolysis are generally used for production of free radicals in the gaseous phase whereas for 'in situ' production, radiolysis and photolysis are more common. In the gas phase production, however, undesired reactions may occur before condensation. In the case of 'in situ' production, high energy quanta, X-rays. and γ-rays, operate through secondary processes involving extremely high energies with a wide spread of values. Particle bombardment and electrical discharge also suffer from the same disadvantage. Thus many different kinds of species may be produced by these methods, making an analysis of the e.s.r. spectrum very difficult. Of all the methods, photolysis in situ provides the most suitable means of producing free radicals in low temperature solids. The available energy

is known and can be varied according to the requirements of the experiment. Fewer types of species are produced due to the low energies involved and the energy of the quanta can, in principle, be varied to give only one type of species provided secondary reactions do not take place. Knowledge of the photochemistry of the substance in the gaseous or the liquid state can be invoked to facilitate the interpretation of the low temperature e.s.r. spectra and the mode of excitation can be postulated with some certainty. Moreover, the photoproduction of free radicals at low temperatures is not a very complicated experimental procedure, the technique being quite straight forward.

However, there are limitations to the photolytic production as well. Not all substances can be decomposed photolytically. The quantum yield is generally small. Even in the substances that are known to decompose photolytically in the gaseous or the liquid state, the 'in situ' production of free radicals might be inhibited either due to de-excitation by the matrix or due to Franck-Rabinowitsch effect. That this effect may be very important is shown by the experiments of Sowden and Davidson (1956), where the quantum yield dropped radically when the photolysis was carried out at 77^{o}K instead of at room temperature. The low quantum yield at the lower temperature was due to the high recombination probability of the dissociation products in the solid state. Unless the fragments produced by the primary decomposition have sufficient energy to diffuse away from the centre of production, they may be constrained to remain in

proximity by the solid environment. If so, the probability of recombination becomes very high.

Inspite of these limitations, photolysis is, in general, the most satisfactory way of producing free radicals in low temperature glasses. For all the work reported in this thesis, ultra-violet irradiation was used to produce the photolysis. Two wavelengths were employed, λ2537 and λ3655. The source of λ3655 is a 250 W medium pressure mercury arc lamp, with an arc gap of 1 cm. and enclosed in a fused quartz envelope. More than 90% of the emission from the lamp is confined in the region of the transitions $6s6d$, $^3D_{1,2,3} - 6s6p, ^3P_2$ (λ3662.88, λ3654.83, λ3650.15). The lamp is operated from the mains in series with a choke to prevent the system becoming unstable due to the arc operating in the region of negative resistance. The source of 2537 is a 600 W low pressure mercury discharge lamp operated from a transformer with a secondary voltage of 5000 V. About 98% of the emission is confined to the transition $6s6p, ^3P_1 - 6^2s, ^1S_0$($\lambda$2536.52). Since it is the resonance radiation, it can be very easily self-reversed and the lamp has to be in the form of a thin and long tube along which a low pressure discharge is passed. In the lamp employed the discharge tube is in the fom of a spiral, wound so as to produce a luminous concave surface. This surface faces an aluminised concave mirror placed coaxially with respect to the lamp.

The sample is contained in a silica tube with an internal diameter of about 5mm and a wall thickness of about 0.5 mm. While irradiating it is kept immersed in liquid nitrogen held in an unsilvered fused silica dewar. When cooled down to liquid nitrogen temperature, most substances formed transparent, but heavily cracked, glasses. However, the cracking, if not too dense, is an advantage, because it produces many internal reflections, thus increasing the interaction of light with the sample. The cracks also provide numerous sites for the free radicals. Some substances were opaque and white when cooled down to low temperatures. However, opacity to visible light does not necessarily imply opacity to the ultraviolet radiation and these substances also frequently showed e.s.r. spectra. While irradiating, the sample was rotated frequently about a vertical axis, to ensure sufficient irradiation from all sides.

5.2. Choice of Matrix

The physical and chemical properties of the solid material in which the radicals are trapped are of prime importance. Physically the solid should have sufficient rigidity, correct volatility and good thermal conductivity, and chemically it should be inert. For photoproduction of free radicals, the matrix should also be transparent to the photolysing radiation at the temperature chosen.

The rigidity of the matrix is very important. If the

medium is too soft, recombination through diffusion would severely limit the life-time of the radicals. If, on the other hand, it is too strong, the fragments would be prevented from flying apart and this would again lead to large recombination probabilities and low quantum efficiency. The probability of Franck-Rabinowitsch recombination will, of course, also depend strongly on the energy of the incident quanta. The thermal properties of the medium are also of great importance for the stabilisation of free radicals. If the thermal conductivity is poor, any energy that is degraded into heat will lead to local heating and will liberate the free radicals, thereby increasing the recombination probability.

The suitability of a matrix depends largely on the reactivity of the species to be stabilised. For instance, hydrocarbon glasses such as ether - isopentane - alcohol (EPA) form good matrices for optical spectroscopic studies of aromatic radicals, but are not suitable for the storage of aliphatic radicals which can abstract hydrogen from these media. For the same reasons, the EPA glass cannot be used for the production of secondary radicals through the primary photolysis of highly photosensitive substances like hydrogen peroxide.

Chemical reactivity has been the overriding consideration in choosing the media in the present work. To minimise the production of unwanted species, the parent molecules themselves are chosen to form the host lattice in all but a few cases.

The technique of production, is thus reduced to the simple procedure of directly photo-irradiating the substance to be investigated in a silica tube. All the substances investigated form satisfactory glasses near liquid nitrogen temperatures.

5.3. Plan of the Work

The present work arose out of the experiments performed by Fujimoto and Ingram (1958), on the secondary radicals produced in aliphatic alcohols by the primary photolysis of H_2O_2. The spectra from these substances were studied at three readily available temperatures and some changesin spectra were observed. In particular the difference in spectra of isopropanol at 77°K and at 110°K could be explained on the assumption of the quenching of internal rotation of the methyl groups. However, a controlled change of temperature of the sample was not possible in this work and the radicals had to be freshly prepared each time for observation at the three different temperatures. As an extension to this work, the following steps were planned:

(a) to check if the primary photolysis of the alcohols also contributed to the production of free radicals; if so, to use only the primary photolysis for free radical production in order to minimise the numner of the different species produced;

(b) to incorporate a variable temperature cavity, so that a controlled variation of the temperature of observation could be possible;

(c) to investigate the change of spectra of saturated and unsaturated aliphatic alcohols with temperature over as wide a range of temperature as possible, with particular regard to the reversibility, or otherwise, of spectra with respect to change of temperature;

(d) to study other substances likely to give simple radicals with two or three methyl groups with a view to seeing if any change in the rotation of the methyl groups could be observed;

(e) to investigate if the line broadening is reduced by diluting the substance under investigation in a non-proton diamagnetic matrix; this is important in view of the fact that some spectra seemed to show some unresolved structure.

(f) to see if free radicals can be produced in single crystals of simple molecules by u.v. irradiation; this would reduce the h.f. dipolar broadening and would also enable an analysis of the anisotropic h.f. interactions to be made. The work performed along these lines is reported below. The low temperature cavity has already been described in Chapter IV under the discussion of the experimental techniques.

5.4. Primary Photolysis

It was found that a satisfactory quantum yield of alcohol radicals was obtainable by primary photolysis alone, both at λ2537 and at λ3655, though the irradiation times were relatively longer than those when hydrogen peroxide was added. Hence all the work on alcohols reported here was carried out without

adding any photo-sensitive substance like hydrogen peroxide to the sample under investigation. It was, however, noticed that the spectra obtained by primary photolysis were, in almost all cases, basically similar to those obtained with hydrogen peroxide.

5.5. Change of Spectra with Temperature

The substances investigated for change in spectra with temperature can be grouped into the following classes:

(a) Substances likely to give simple free radicals with two or three methyl groups. The substances investigated in this group were dimethylamine, $(CH_3)_2$ NH, and tert.-butyl chloride, $(CH_3)_3$ CCl.

(b) Saturated aliphatic alcohols. Only the lower members of the series were investigated. These were methanol, CH_3OH, ethanol, $CH_3.CH_2OH$, n-propanol, $CH_3.CH_2.CH_2OH$, iso-propanol, $(CH_3)_2.CHOH$, and n-butanol, $CH_3.(CH_2)_2.CHOH$.

(c) Unsaturated aliphatic alcohol. The only unsaturated alcohol investigated was allyl alcohol, $CH_2:CH.CH_2OH$.

(d) Substituted hydrocarbons. Chloroform, $CHCl_3$, and carbon tetrachloride, CCl_4, were the two substances investigated under this category.

It was found that, on warming, all the saturated alcohols gave a highly unsymmetrical signal before they completely decayed. The allyl alcohol, and, chloroform and tetrachloride, were investigated to check if the unsymmetrical signal was

associated with the functional group, OH, or was due to the alkyl radical itself.

To study the change in spectra with temperature, the samples were u.v. irradiated at liquid nitrogen temperature for a few hours so as to allow a reasonable concentration of free radicals to build up. All the substances mentioned above were irradiated with λ2537 and most of them were also irradiated with λ3655. Spectra of the same irradiated samples were recorded at different temperatures, the latter being measured both before and after each run with the help of a thermocouple as described in Chapter IV. The samples were re-cooled to the lowest available temperature at the various stages of warming-up so as to find whether the change of spectra with temperature was reversible or not.

5.6. The Diamagnetic Dilution of the Matrix

Two techniques for the diamagnetic dilution of the matrix were investigated, (a) dilution with a non-proton chemical solvent, and (b) condensation of a mixture of the substance under investigation and some chemically inert gas with zero or small nuclear magnetism.

Carbon tetrachloride was chosen as the non-proton solvent. Chloroform, $CH\,Cl_3$, and iso-propylamine, $(CH_3)_2CH.NH_2$, were soluble in carbon tetrachloride and the solution as such was used for irradiation. Iso-propanol and solution of ammonia in water did not mix with carbon tetra chloride and the mixture was

shaken well before freezing at liquid nitrogen temperature for irradiation. About 10^{-4} moles of hydrogen peroxide were mixed with the sample, wherever necessary for the production of free radicals. Different dilutions between 1:4 and 1:10 were tried.

For the inert gas matrix technique, krypton was chosen as it has a higher melting point (116°K) compared with that of argon (84°K). This was important because liquid nitrogen which was used as the coolant for the condensation has a temperature of 77°K. Xenon which has a still higher melting point (161°K) is much more expensive. The isotopes of krypton having any nuclear magnetism (~1 nuclear magneton) have together a relative amundance of only 12%. Ammonia was used as the parent substance for the production of free radicals. A stream of ammonia gas from a dewar of liquid ammonia was allowed to mix with krypton from a 1-litre 1-atmospheric pressure flask. The quantities of the two gases in the mixture were read with the help of a mercury-manometer attached to the mixing chamber. A dilution of 1:4 was used. The total pressure of the mixture was one atmosphere. After the mixture was allowed to stand for some time, it was condensed in the sample tube by immersing the lower end of the sample tube in liquid nitrogen.

It was found that even after a long time, the condensation was very meagre though sufficient condensation took place if only ammonia was condensed. The condensed sample did not show any spectra on irradiation, because of the insufficient deposition

of the mixture.

Carbon dioxide was also used as the diluting substance, as it has a sublimation point (193°K) close to the melting point of ammonia (199°K). However, ammonia reacted with carbon dioxide and a white opaque solid was deposited along the walls of the mixing chamber and the sample tube. It could be ammonium carbonate, $(NH_4)_2\ CO_3$, or ammonium carbamate, $NH_4CO_2NH_2$, both the reactions being possible in the presence of moisture. The small deposit in the sample tube again did not show any spectra on irradiation. The λ2537 mercury line was used for all the irradiation reported in this section.

5.7. Single Crystal Irradiation

Single crystals of ammonium magnesium sulphate, $(NH_4)_2SO_4.MgSO_4.GH_2O$, were grown, and irradiated with λ2537 both at room temperature and at 77°K for about three hours each. For room temperature work, the crystal was mounted on a plastic rod with the help of vaseline or 'durofix'. The cement was, however, not satisfactory for low temperature work and the crystal was tied to the rod with the help of a fine thread. The irradiated crystal, however, showed no signals at either temperature. A single crystal of glycine was also irradiated with λ2537. No signal was obtained after 24 hours of u.v. irradiation, though 18 hours of irradiation with 40 kV X-rays gave a large signal.

5.8. Purity of the Chemicals

The chemicals used in these experiments were of the 'analar' grade if available from the British Drug House Limited. The absolute ethyl alcohol was of spectroscopic grade and was supplied by James Burrough Limited. No attempts were made for further purification of the chemicals.

5.9. Recorded Spectra

The spectra obtained from the various irradiated substances at different temperatures are given in Figs. (5.1.) - (5. 9.). In all cases except that of allyl alcohol, the spectra did not recover the low temperature structure when cooled down from higher temperatures; rather they retained the structure corresponding to the temperature to which they had been warmed up. Thus the change of spectra with temperature was found to be irreversible in all these cases. Hence the spectra obtained when the samples were cooled down after warming have not been reproduced here. However the allyl alcohol showed some interesting features when cooled down at different stages of warming up and these spectra have therefore been included.

Some spectra from substances diluted with carbon tetrachloride have been given along with the ones from undiluted specimens (Figs. 5.10-5.13.). In general, when no signals were observed, the recordings have not been reproduced.

Table 1

Details of Experiments on the Change of Spectra with Temperature

Fig.No.	Substance investigated	Chemical Formula	Wavelength of U.V. radiation (Å)	Time of irradiation (hours)	Gain Setting of the amplifier
5.1.	Dimethylamine	$(CH_3)_2.NH$	2537	$9\frac{1}{2}$	40
5.2.	tert. Butyl Chloride	$(CH_3)_3.CCl$	2537	$7\frac{1}{2}$	70
5.3.(a)	Methanol	$CH_3.OH$	2537	$5\frac{1}{2}$	45
5.3.(b)	Methanol	$CH_3.OH$	3655	$5\frac{1}{2}$	70
5.4.(a)	Ethanol	$CH_3.CH_2.OH$	2537	5	20
5.4.(b)	Ethanol	$CH_3.CH_2.OH$	3655	4	70
5.5.(a)	n-Propanol	$CH_3.CH_2.CH_2.OH$	2537	3	40
5.5.(b)	n-Propanol	$CH_3.CH_2.CH_2.OH$	3655	4	60
5.6.	n-Butanol	$CH_3.(CH_2)_3.OH$	2537	$6\frac{1}{2}$	30
5.7.(a)	iso-Propanol	$(CH_3)_2.CH.OH$	2537	$5\frac{1}{2}$	55
5.7.(b)	iso-Propanol	$(CH_3)_2.CH.OH$	3655	$5\frac{1}{2}$	70
5.7.(c)	iso-Propanol	$(CH_3)_2.CH.OH$	3655	4	55
5.8.(a)	Allyl alcohol	$CH_2:CH.CH_2.OH$	2537	$7\frac{1}{2}$	70
5.8.(b)	Allyl alcohol	$CH_2:CH.CH_2.OH$	2537	7	70
5.8.(c)	Allyl alcohol	$CH_2:CH.CH_2.OH$	2537	8	70
5.9.	Chloroform	$CHCl_3$	2537	$8\frac{1}{2}$	70

All substances were irradiated without H_2O_2 at liquid nitrogen temperature.

Table 2

Details of Experiments on the Dilution of the Matrix

Fig. No.	Sample Irradiated	Dilution = ratio of volumes	Time of irradiation (hours)	Gain setting of the amplifier
5.10.(a)	$(CH_3)_2.CH.NH_2$	-	2	40
5.10.(b)	$(CH_3)_2.CH.NH_2 + CCl_4$	1:4	2	20
5.10.(c)	$(CH_3)_2.CH.NH_2 + CCl_4$	1:8	2	10
5.11.(a)	NH_3 (in water)	-	3	60
5.11.(b)	NH_3 (in water) + CCl_4	1:6	3	60
5.12.(a)	$(CH_3)_2.CH.OH$	-	3	75
5.12.(b)	$(CH_3)_2.CH.OH + CCl_4$	1:10	3	75
5.13.(a)	$CHCl_3$	-	2	70
5.13.(b)	$CHCl_3 + CCl_4$	1:10	2	70

All the substances were irradiated with 2537 at 77°K. About 10^{-4} moles of H_2O_2 were added in the case of isopropylamine, ammonia and isopropanol. Carbon tetrachloride by itself did not give a signal.

Table 3

Gain setting and relative gain of the narrow band amplifier.

Gain Setting	Relative Gain
10	1
20	4
30	10
40	20
50	40
60	76
70	108

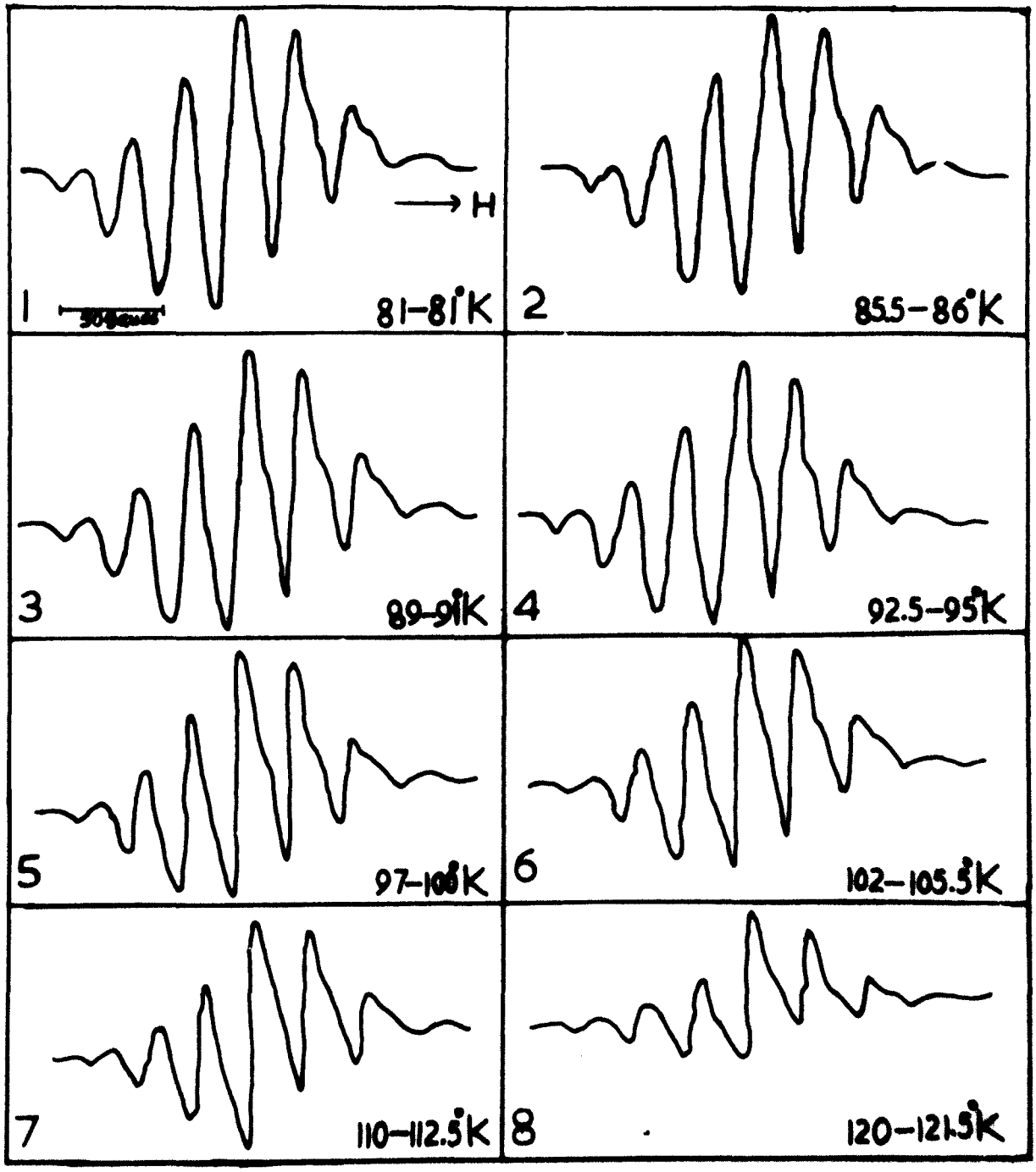

FIG. 5.1. DIMETHYLAMINE. Wavelength 2537.

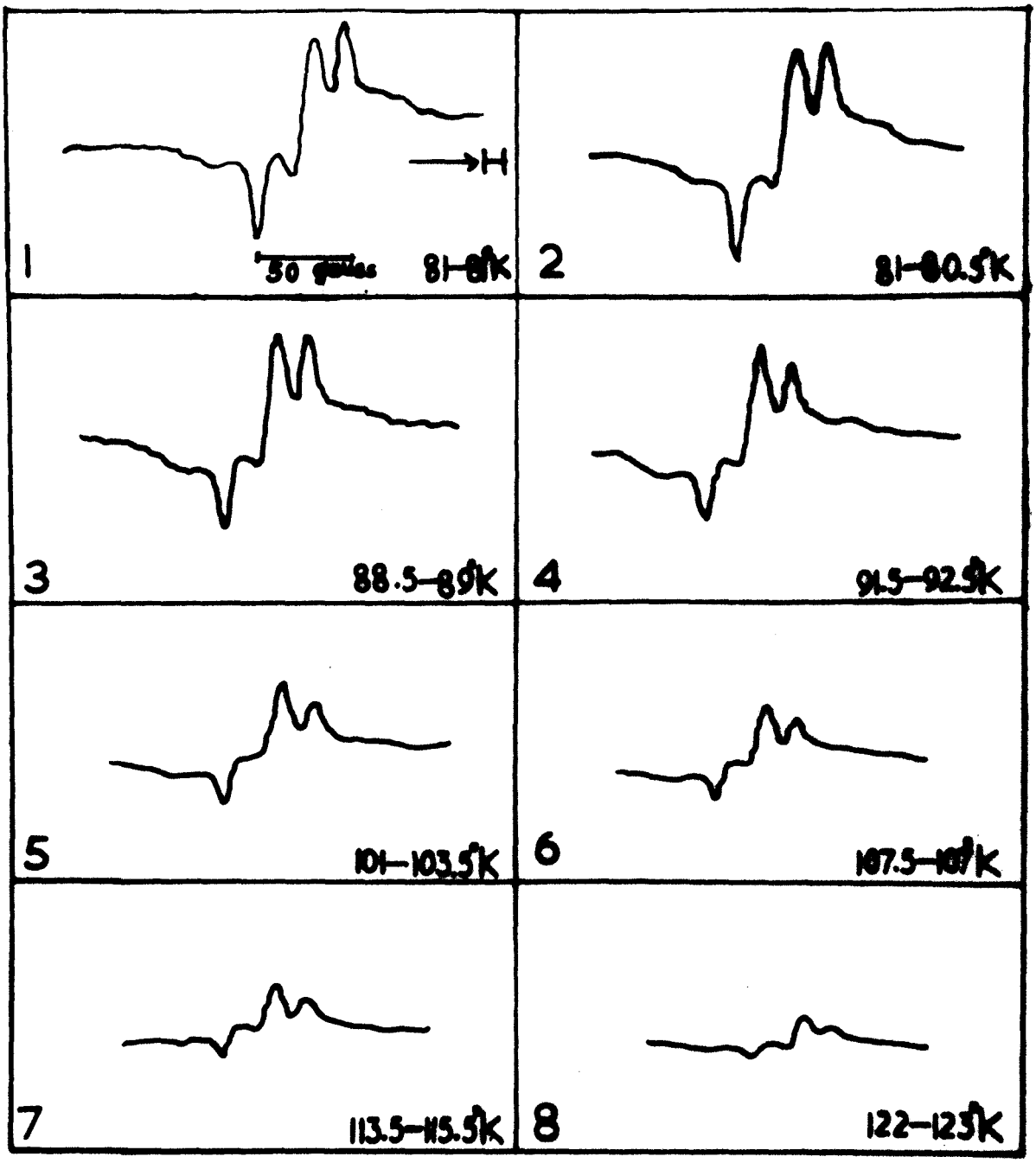

FIG. 5.2. tert. - BUTYL CHLORIDE. Wavelength 2537.

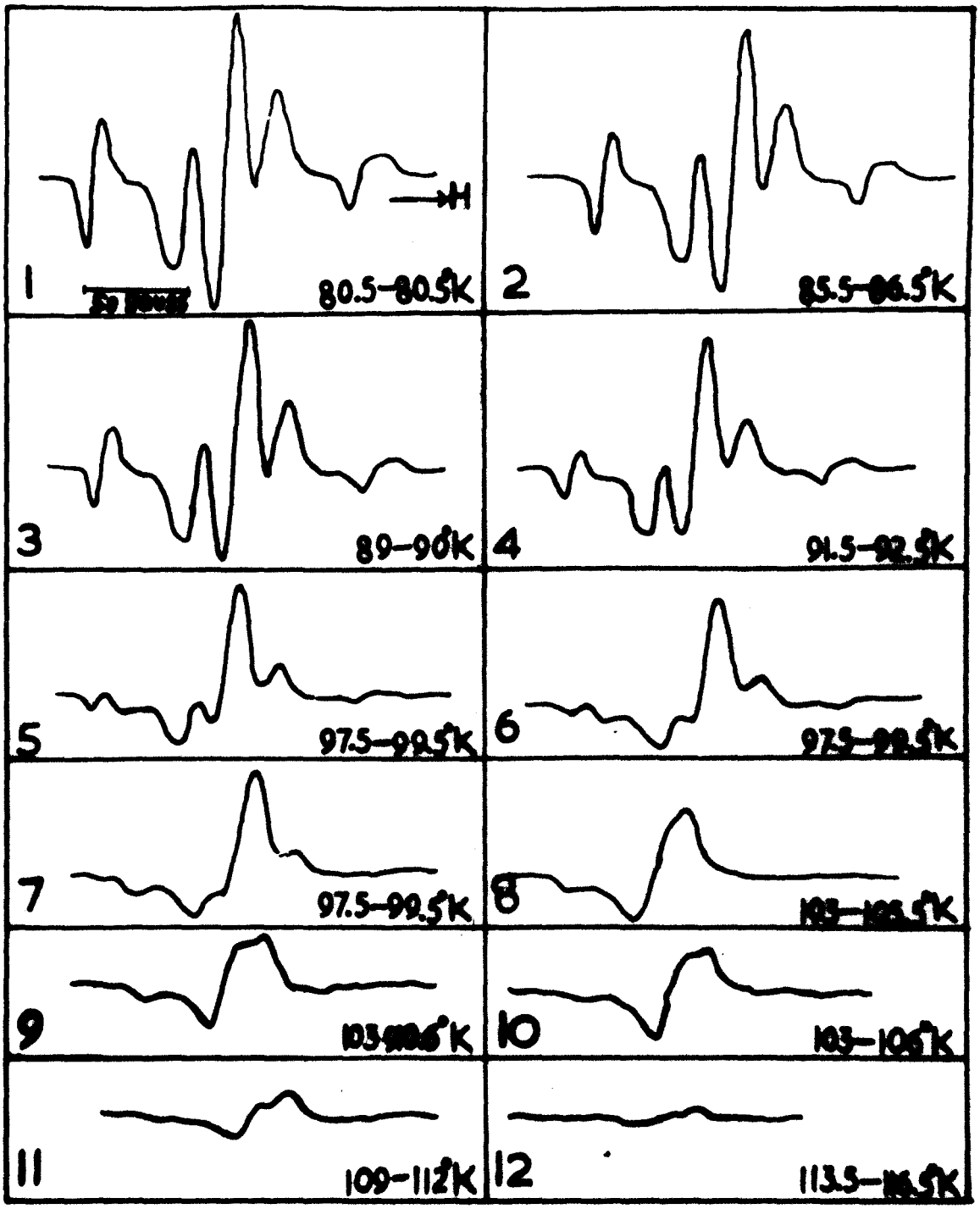

FIG. 5.3(a). METHANOL. Wavelength 2537.

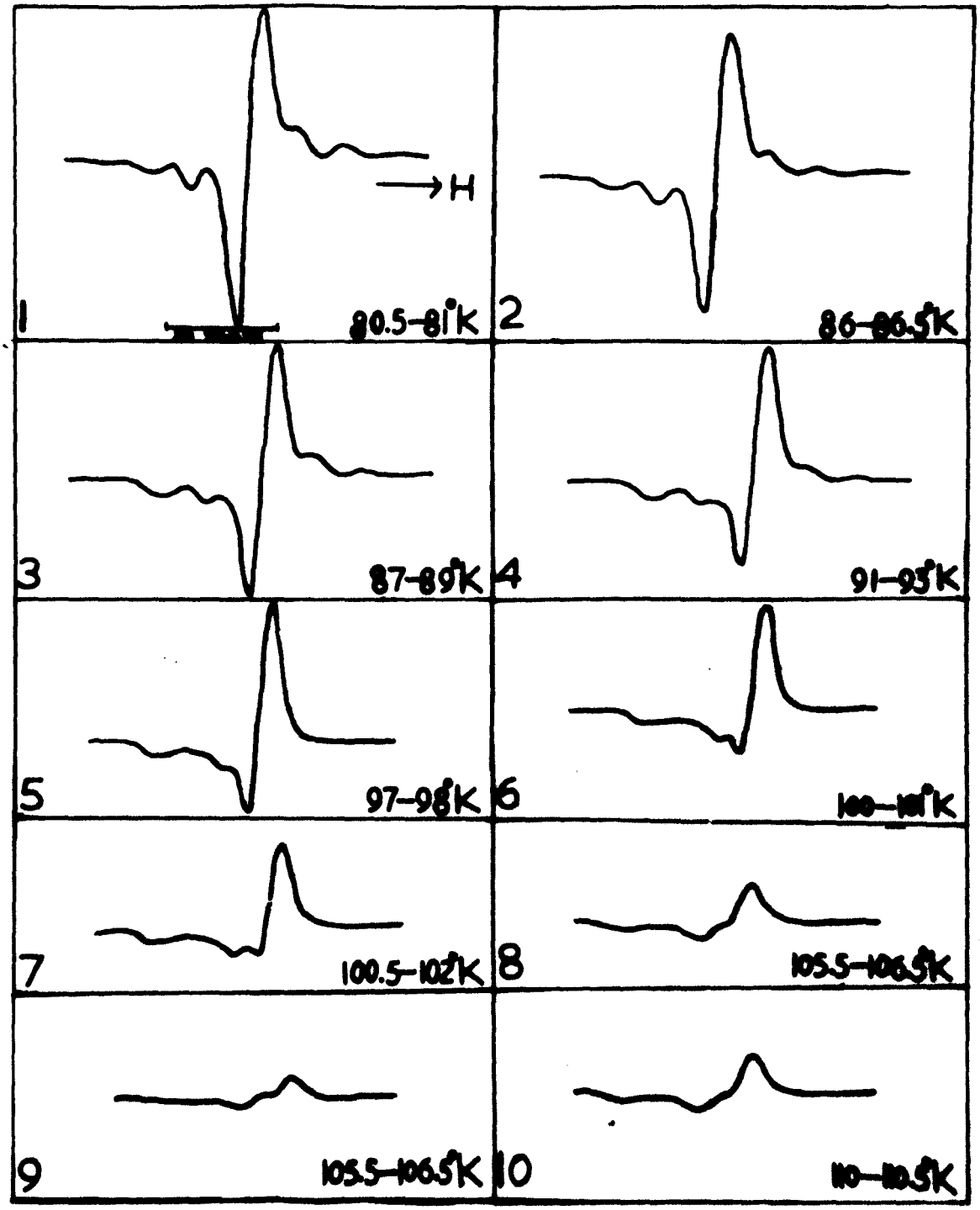

FIG. 5.4(a). ETHANOL. Wavelength 2537.

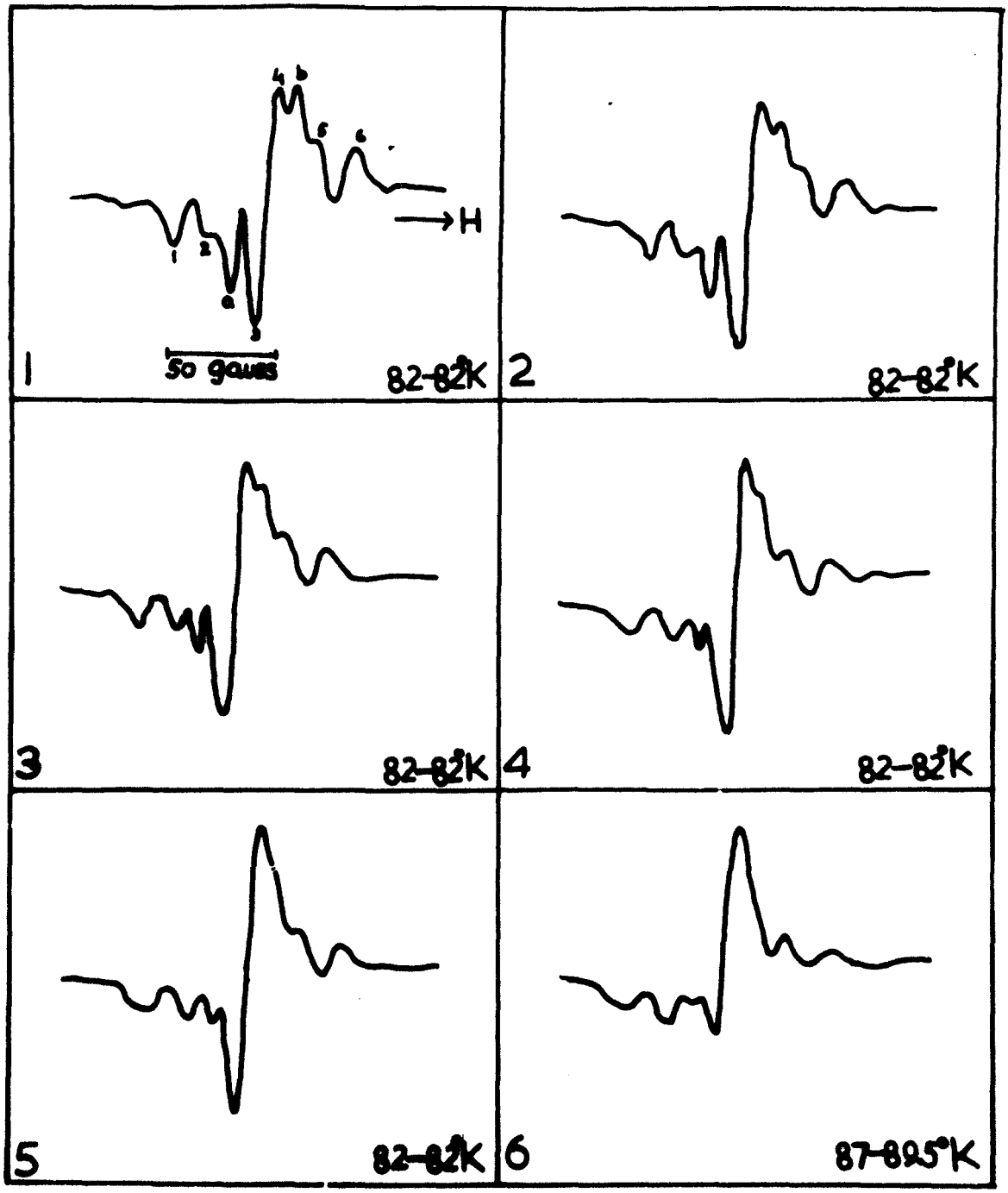

FIG. 5.4(b). ETHANOL. Wavelength 3655.

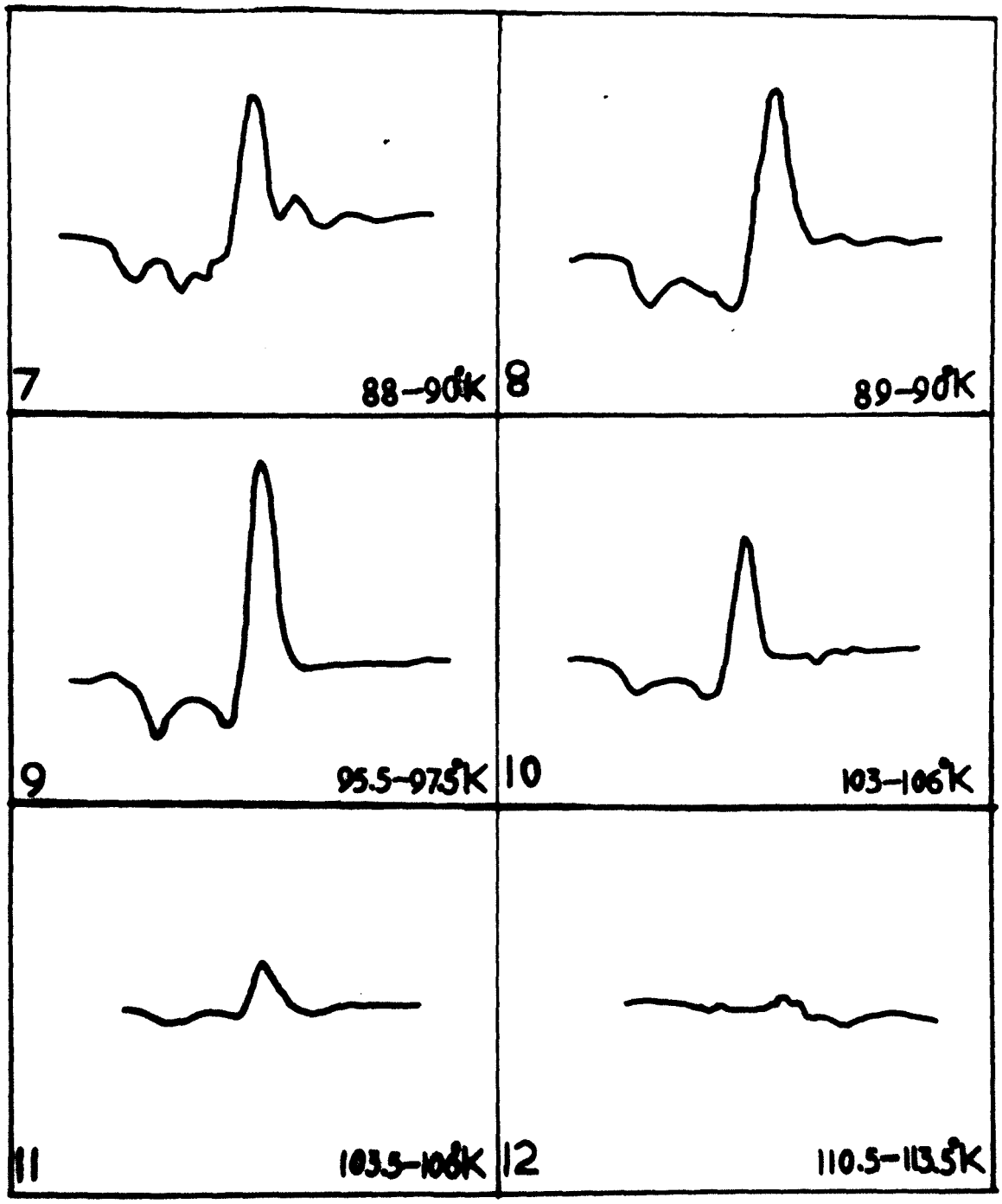

FIG. 5.4(b). ETHANOL. Wavelength 3655.

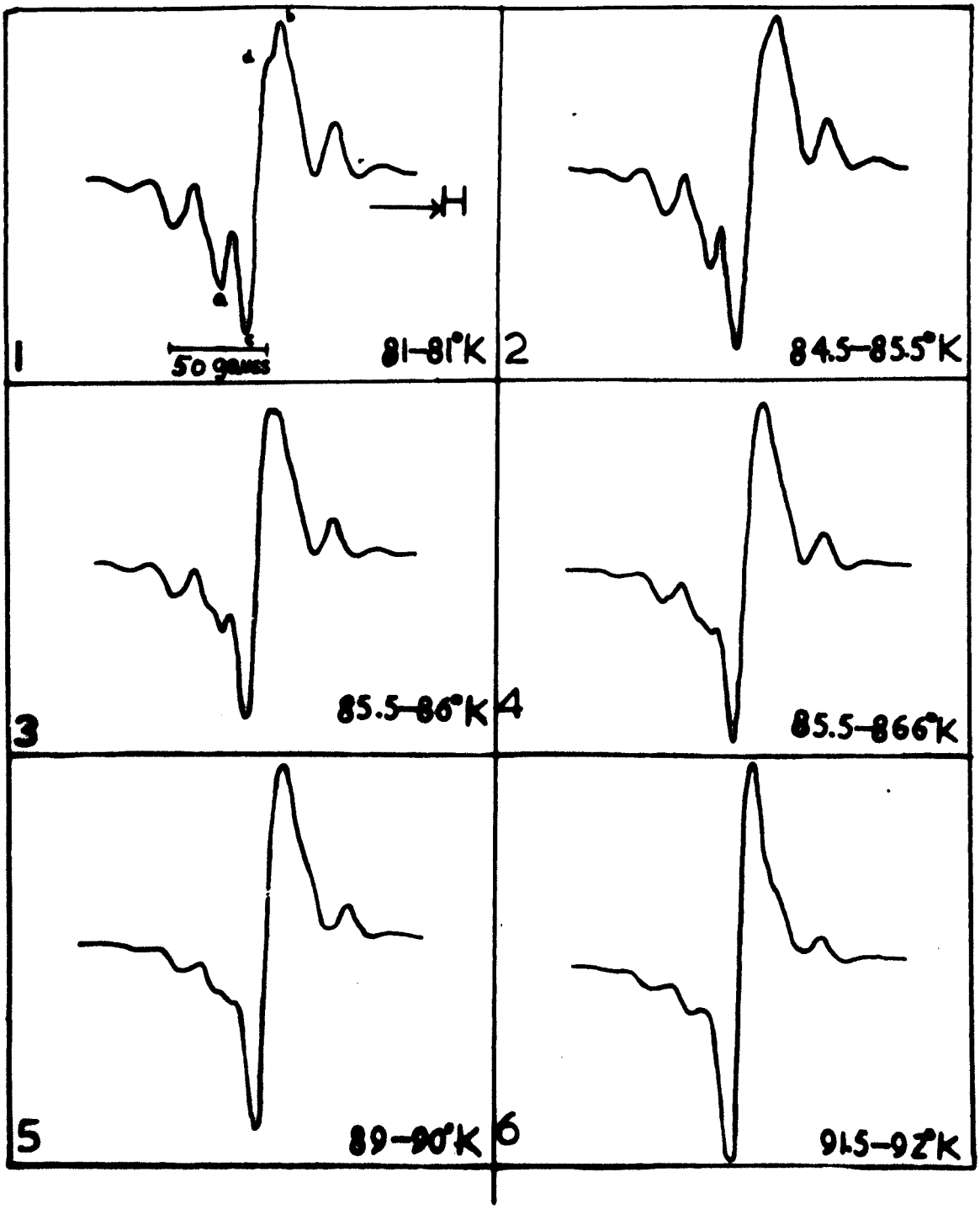

FIG. 5.5(a). n - PROPANOL. Wavelength 2537.

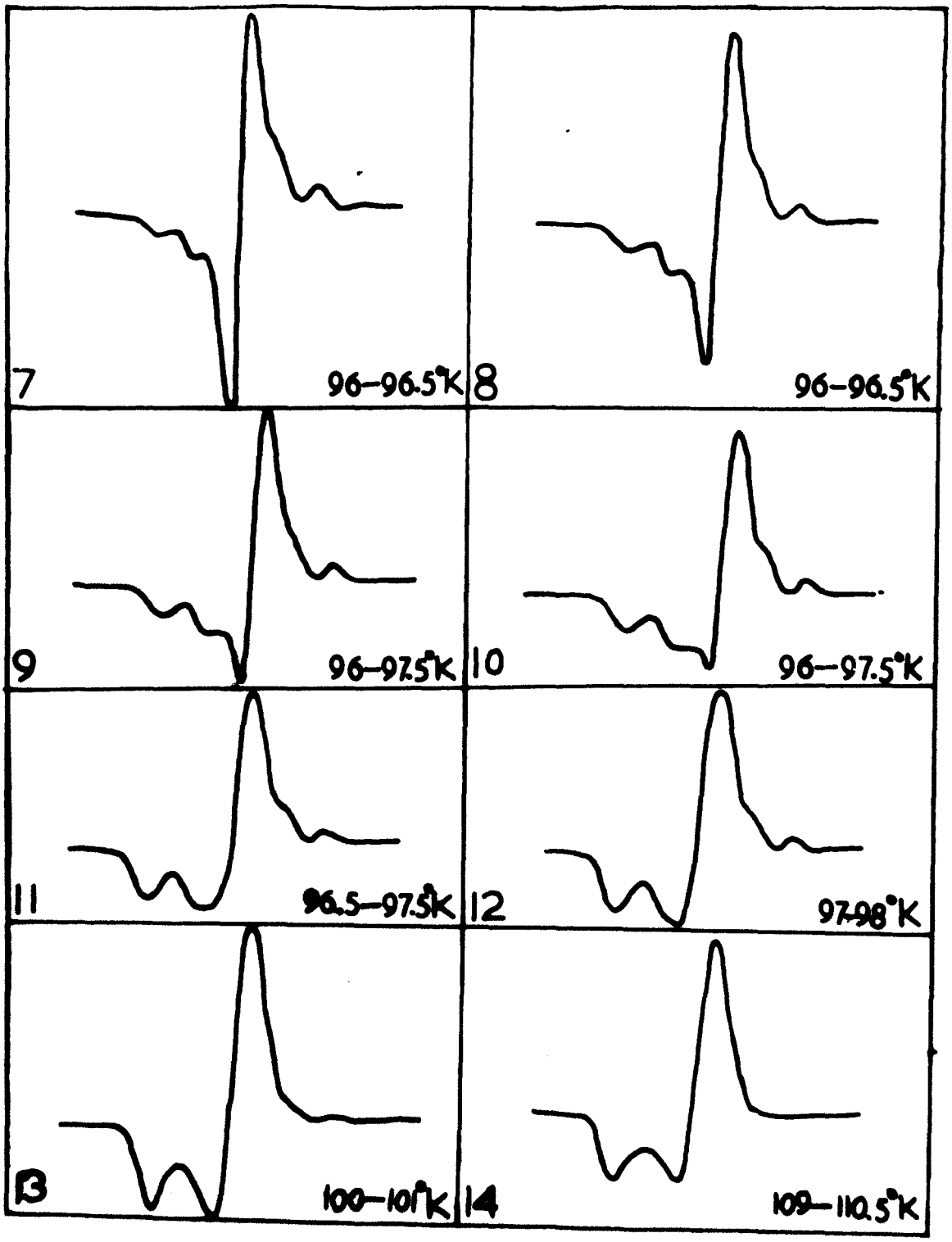

FIG. 5.5(a). n - PROPANOL. Wavelength 2537.

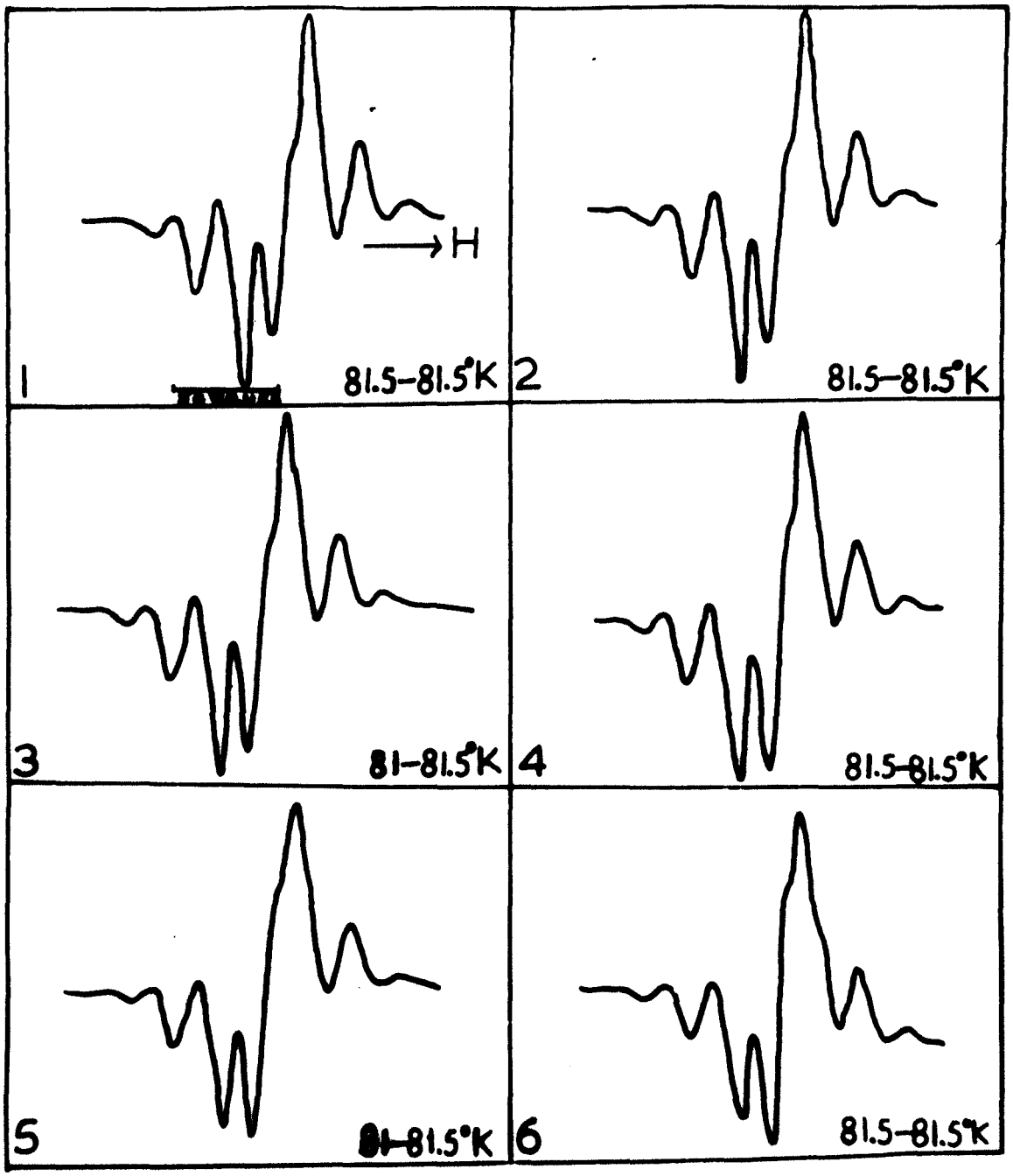

FIG. 5.5(b). n - PROPANOL. Wavelength 3655.

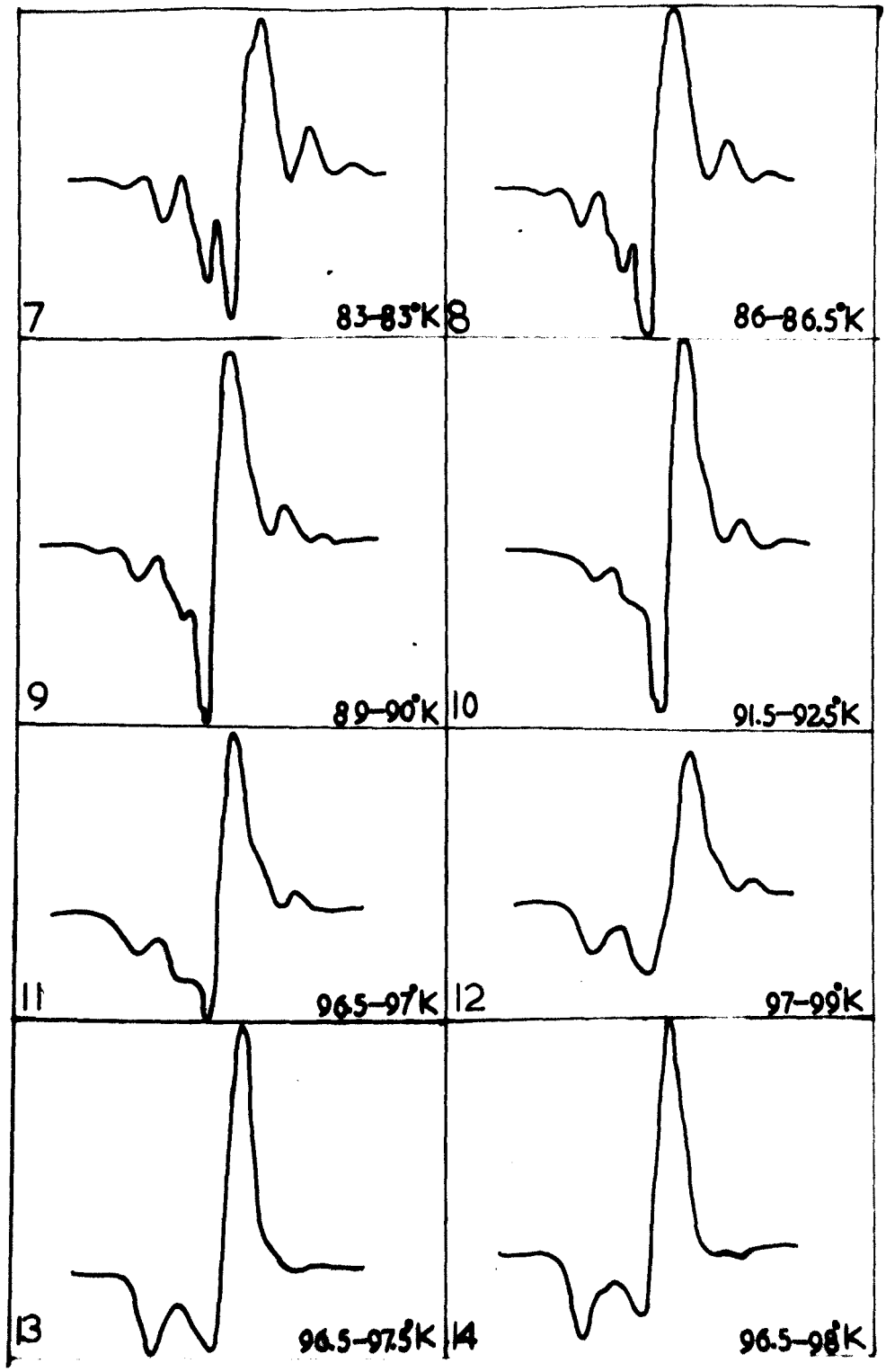

FIG. 5.5(b). n - PROPANOL. Wavelength 3655.

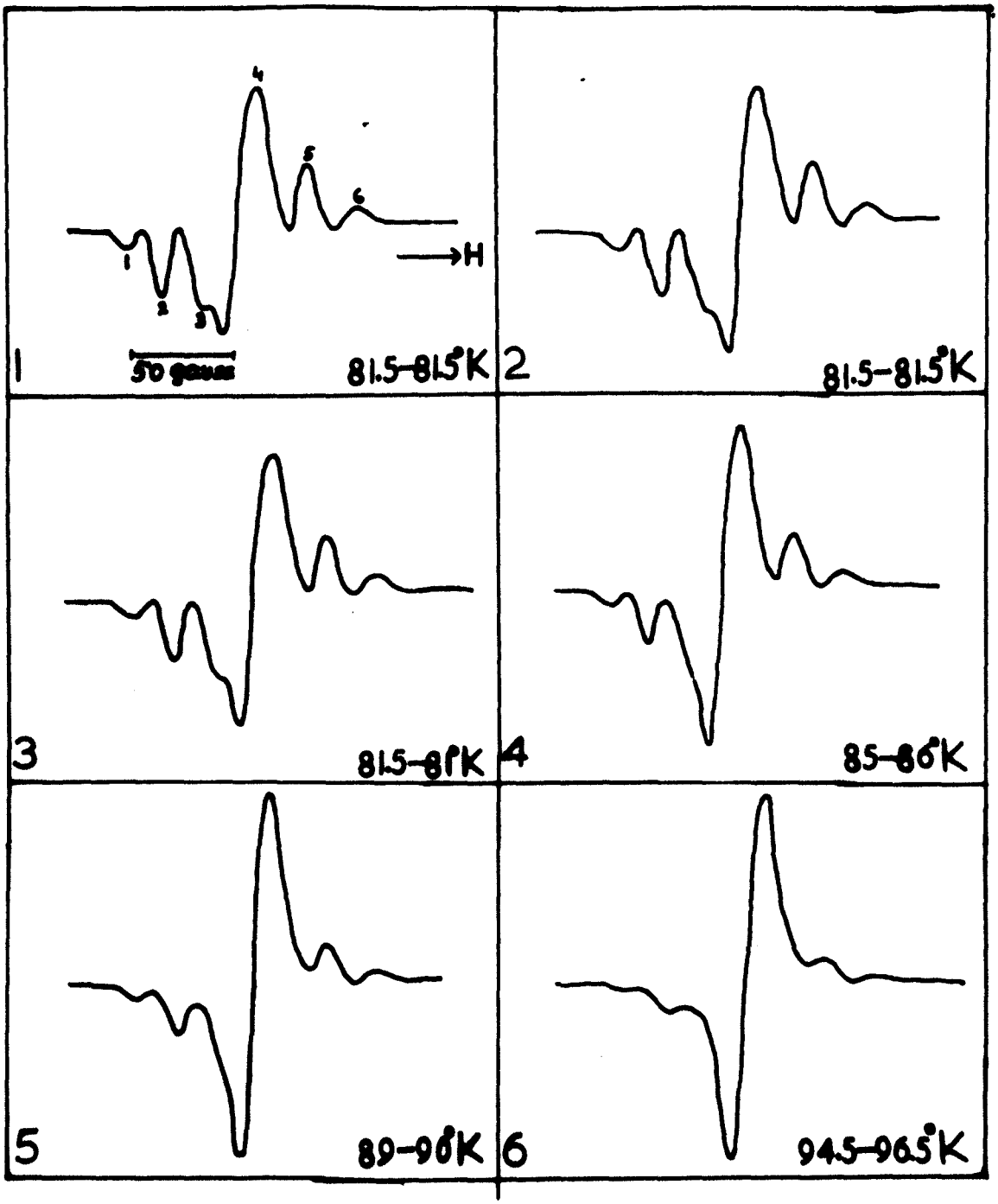

FIG. 5.6. n - BUTANOL. Wavelength 2537.

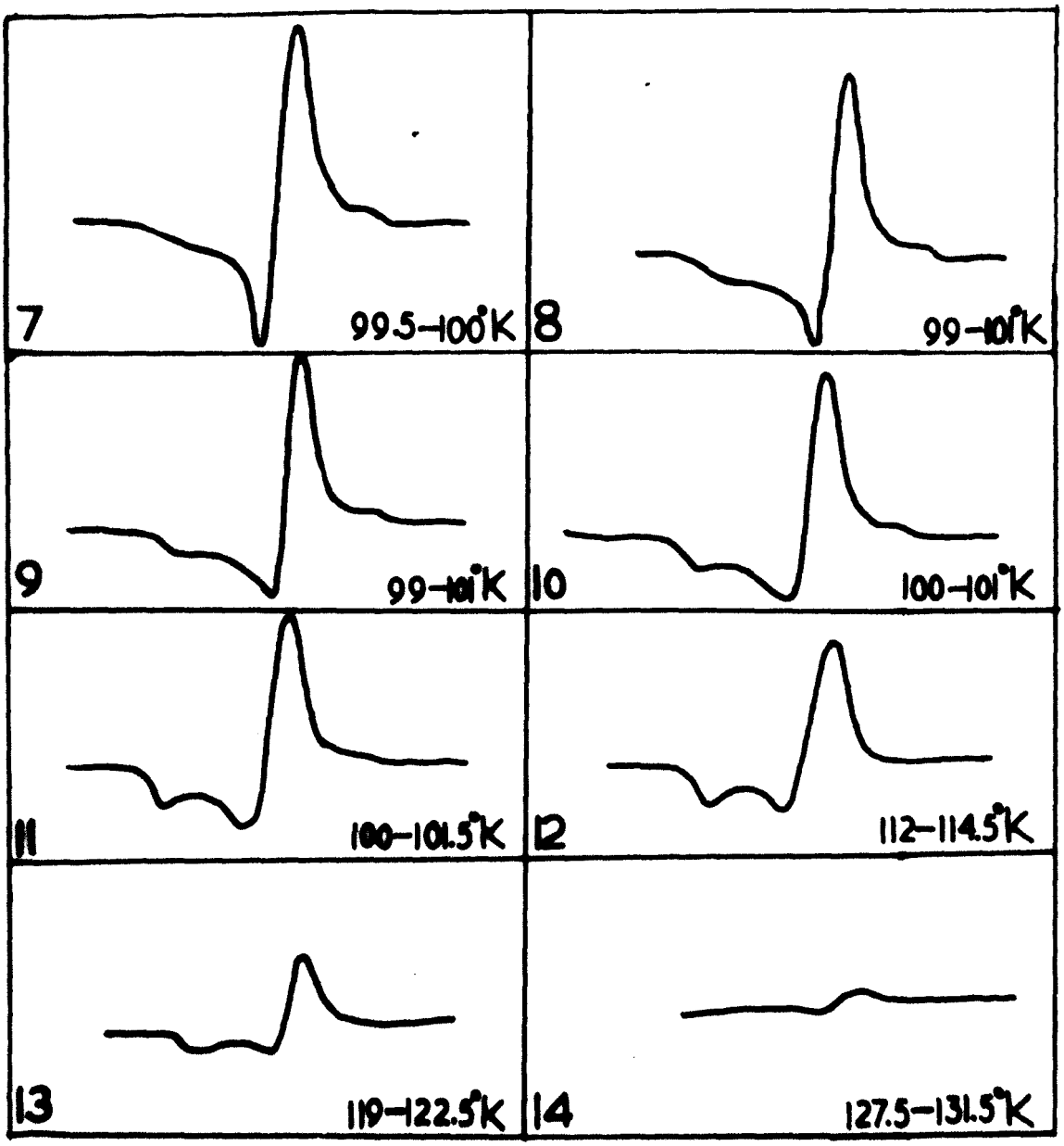

FIG. 5.6. n - BUTANOL. Wavelength 2537.

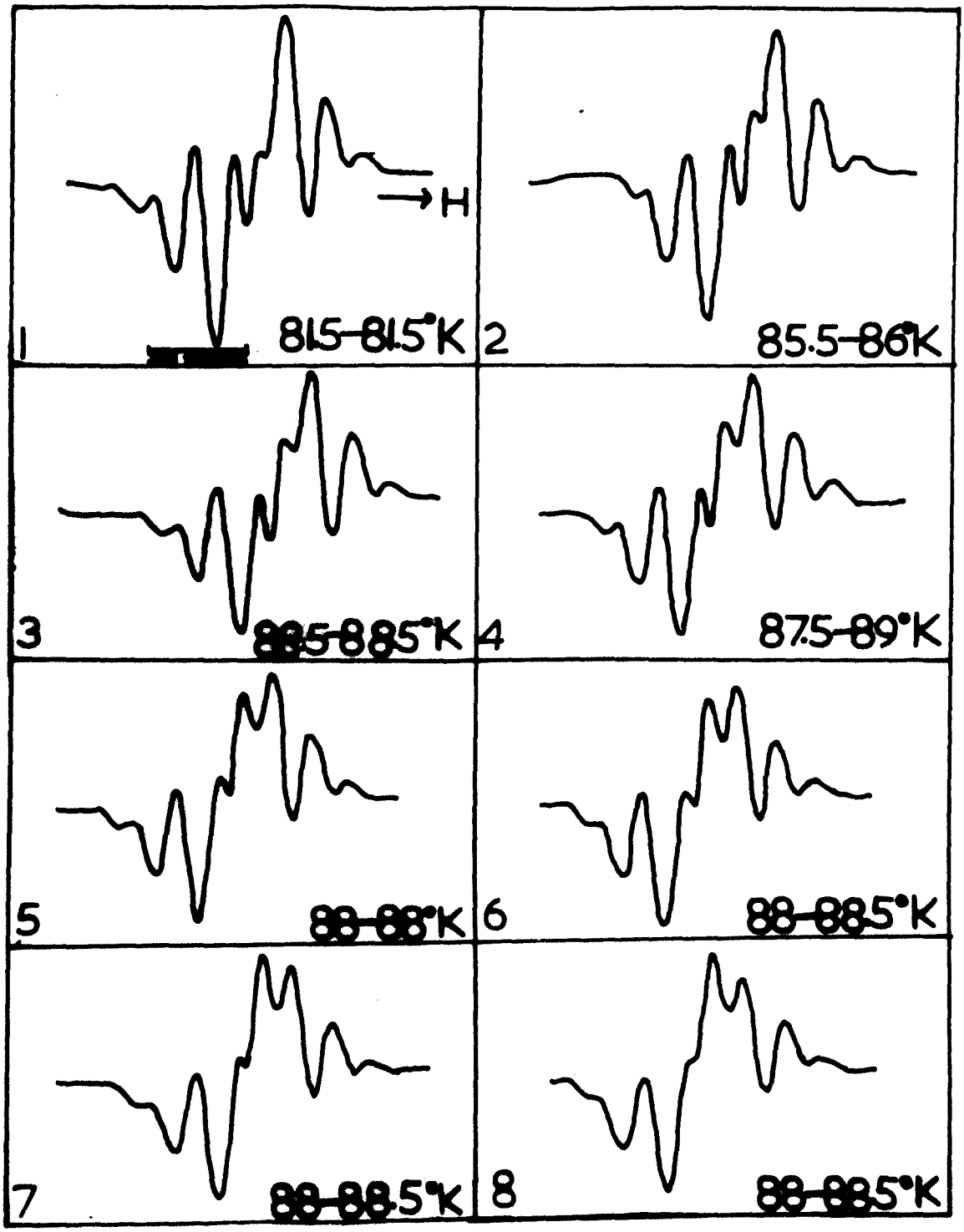

FIG. 5.7(a). iso - PROPANOL. Wavelength 2537.

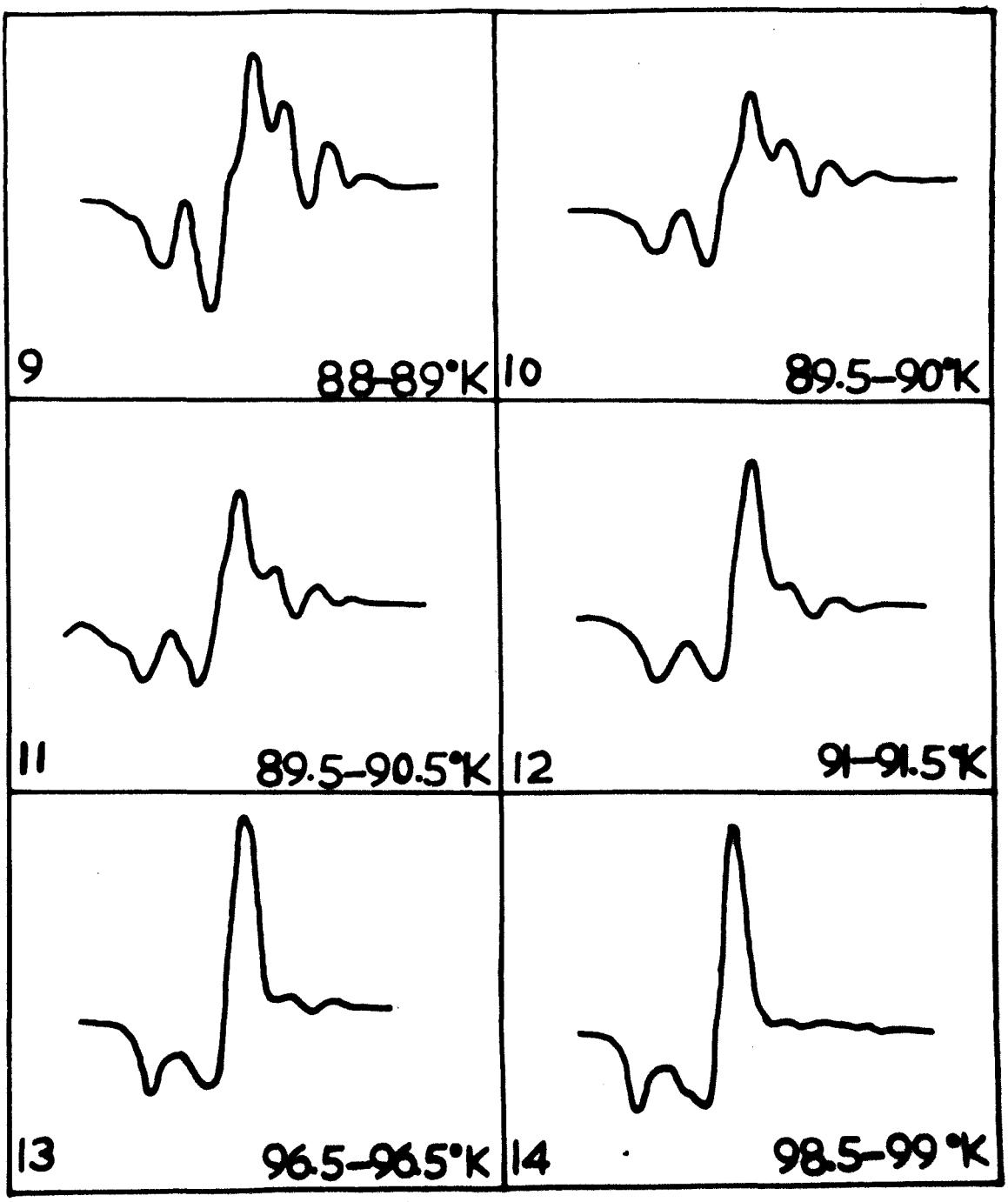

Fig. 5.7(a). iso - PROPANOL. Wavelength 2537.

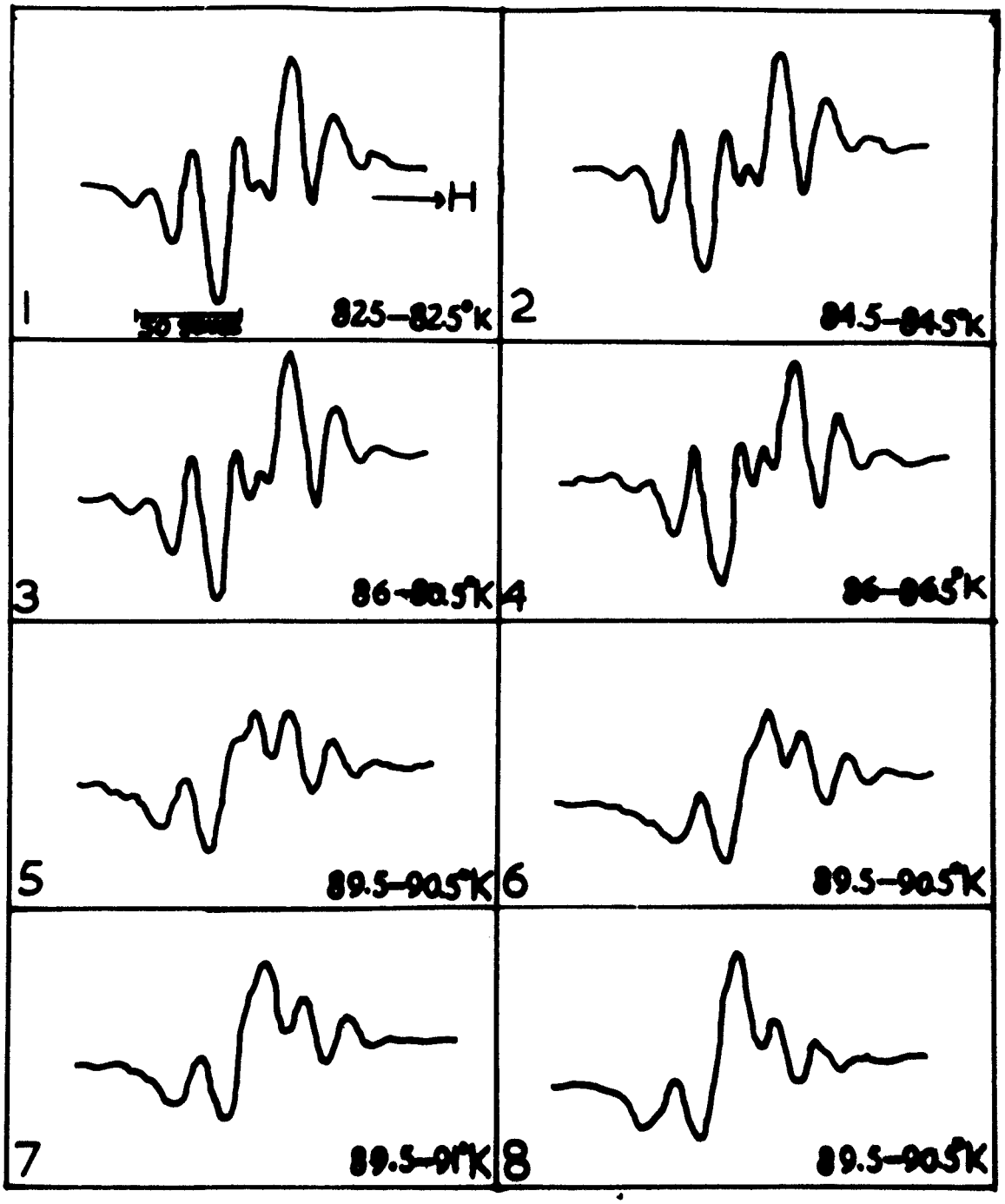

FIG. 5.7(b). iso - PROPANOL. Wavelength 3655.

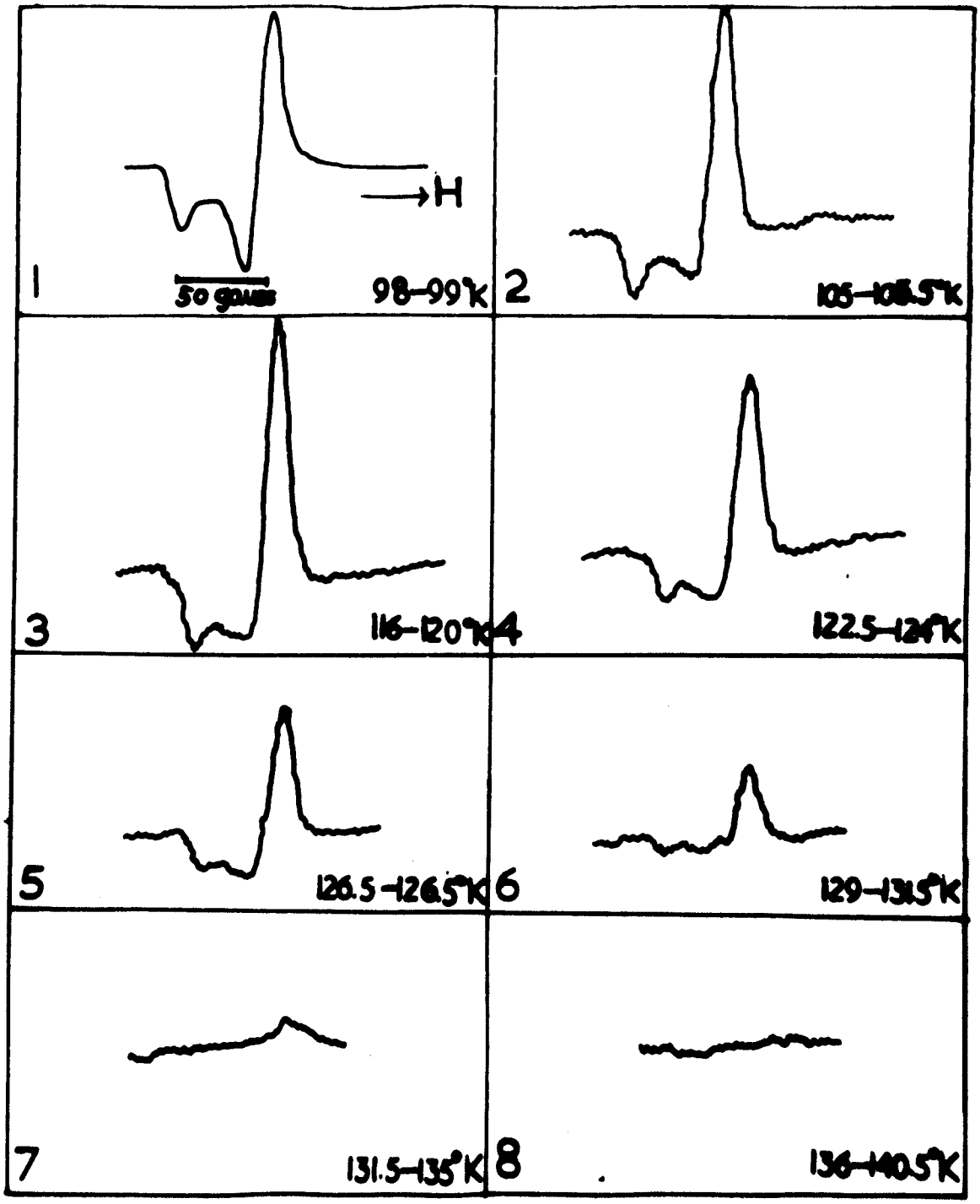

FIG. 5.7(c). iso - PROPANOL. Wavelength. 3655.

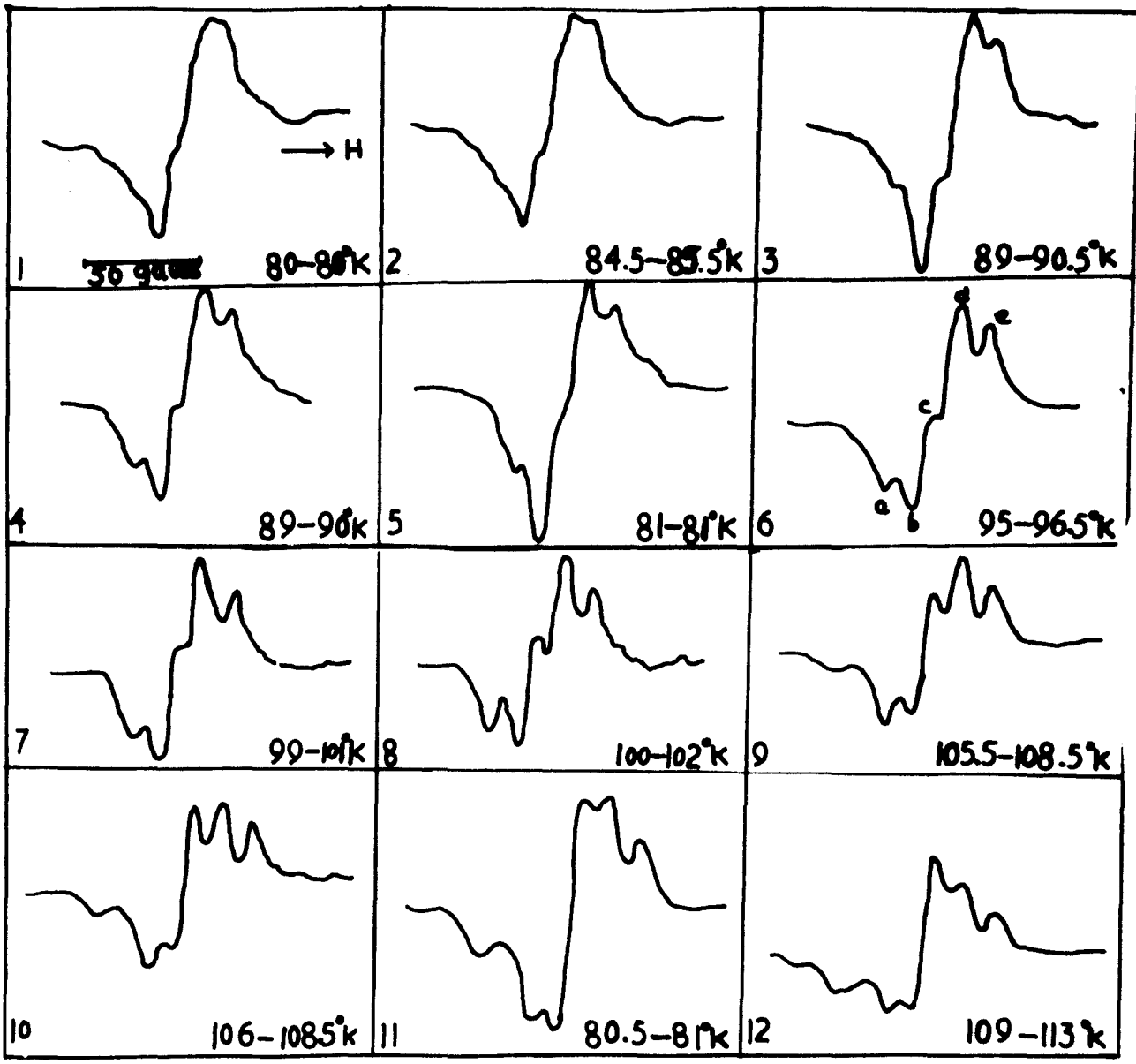

FIG. 5.8(a). ALLYL ALCOHOL. Wavelength 2537.

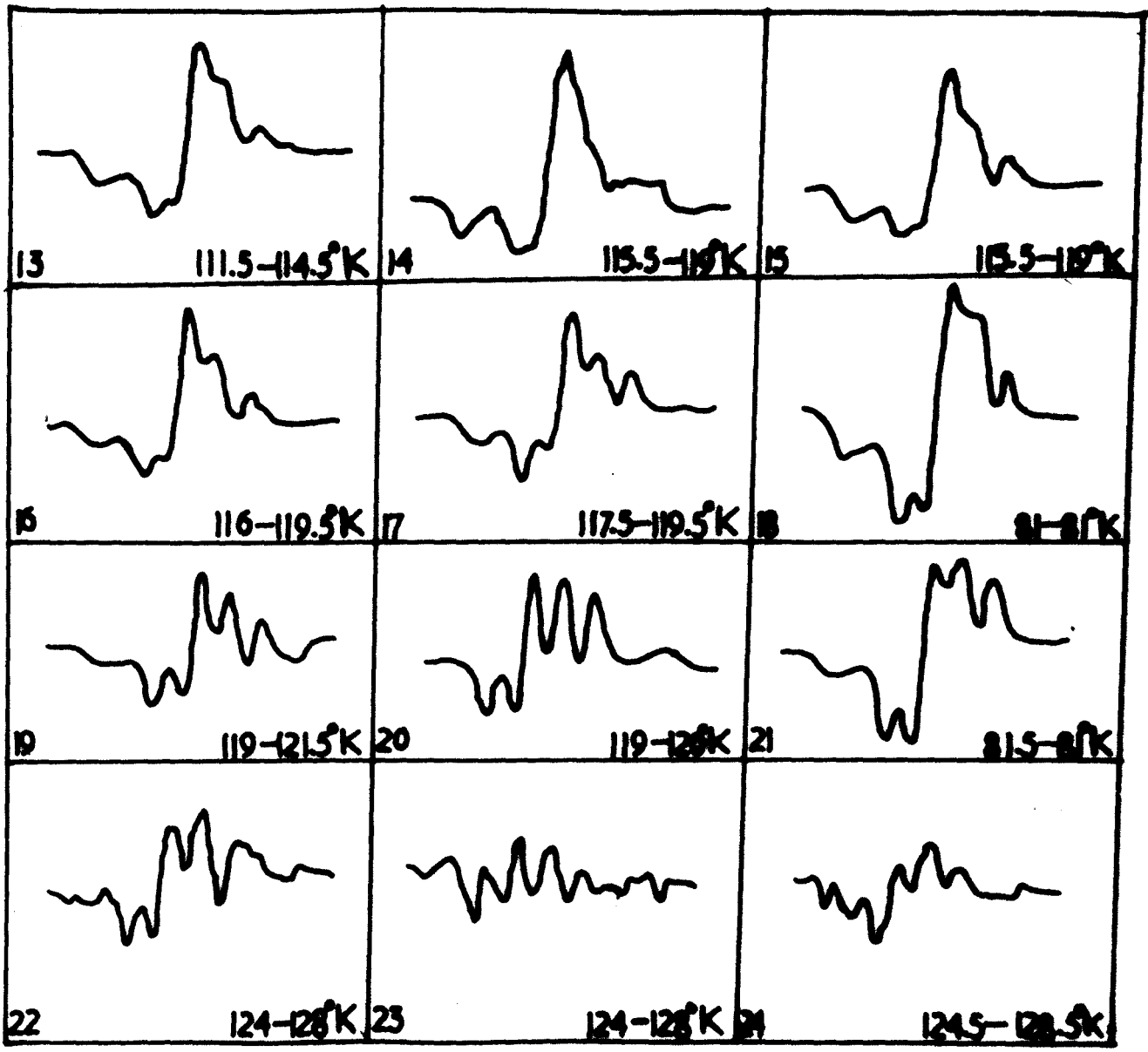

FIG. 5.8(a). ALLYL ALCOHOL. Wavelength 2537.

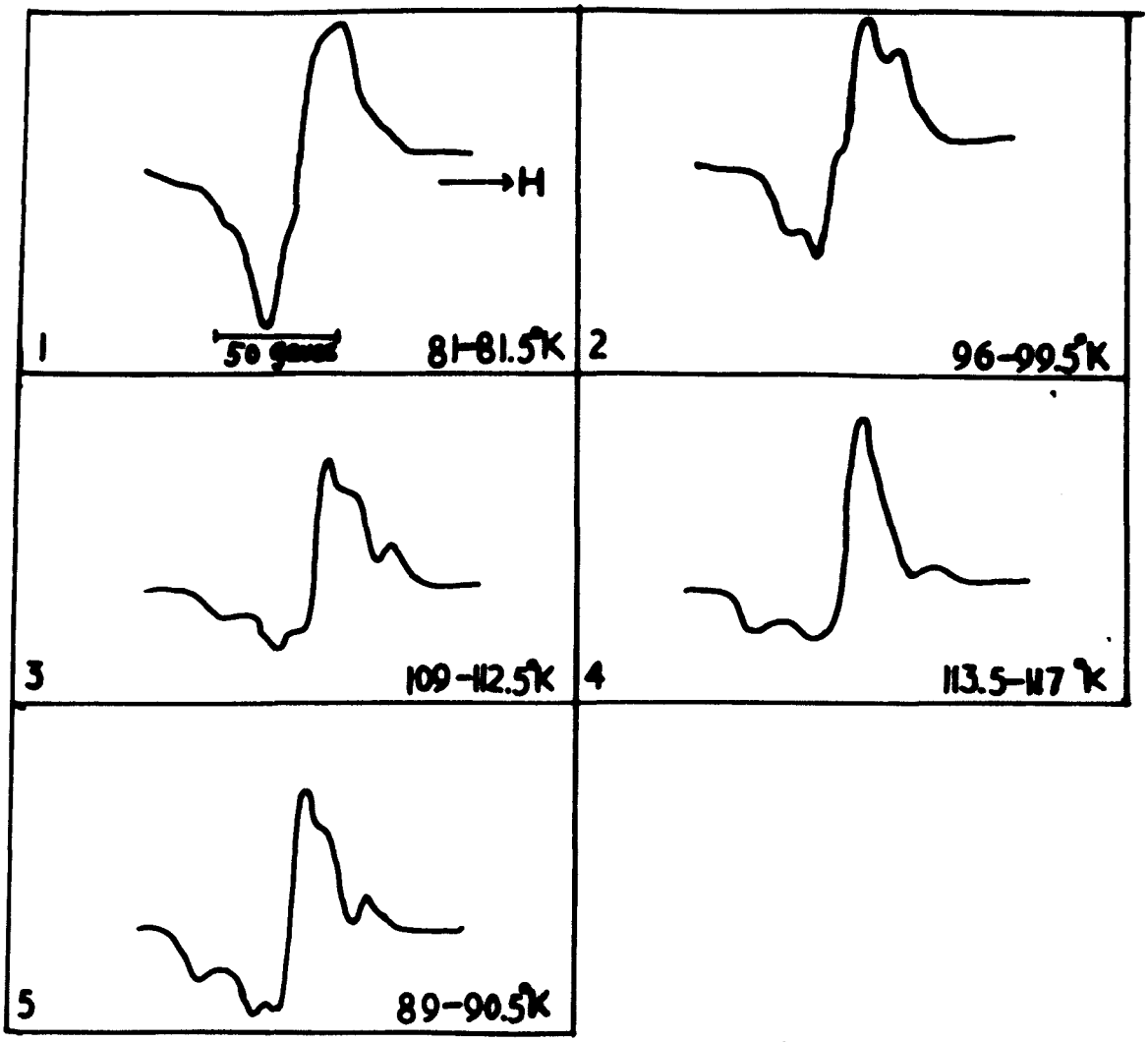

FIG. 5.8(b). ALLYL ALCOHOL. Wavelength 2537.

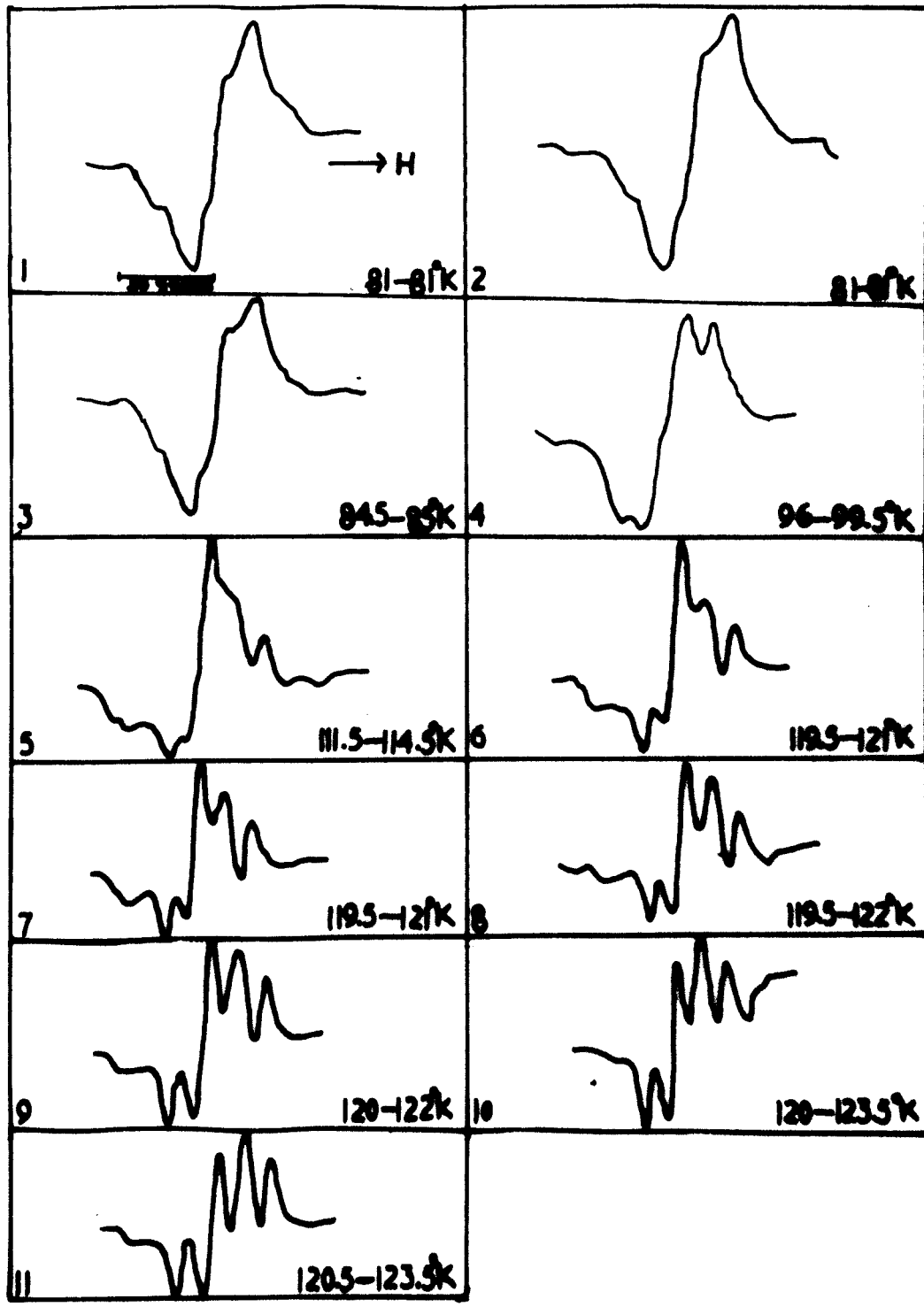

FIG. 5.8(c). ALLYL ALCOHOL. Wavelength 2537.

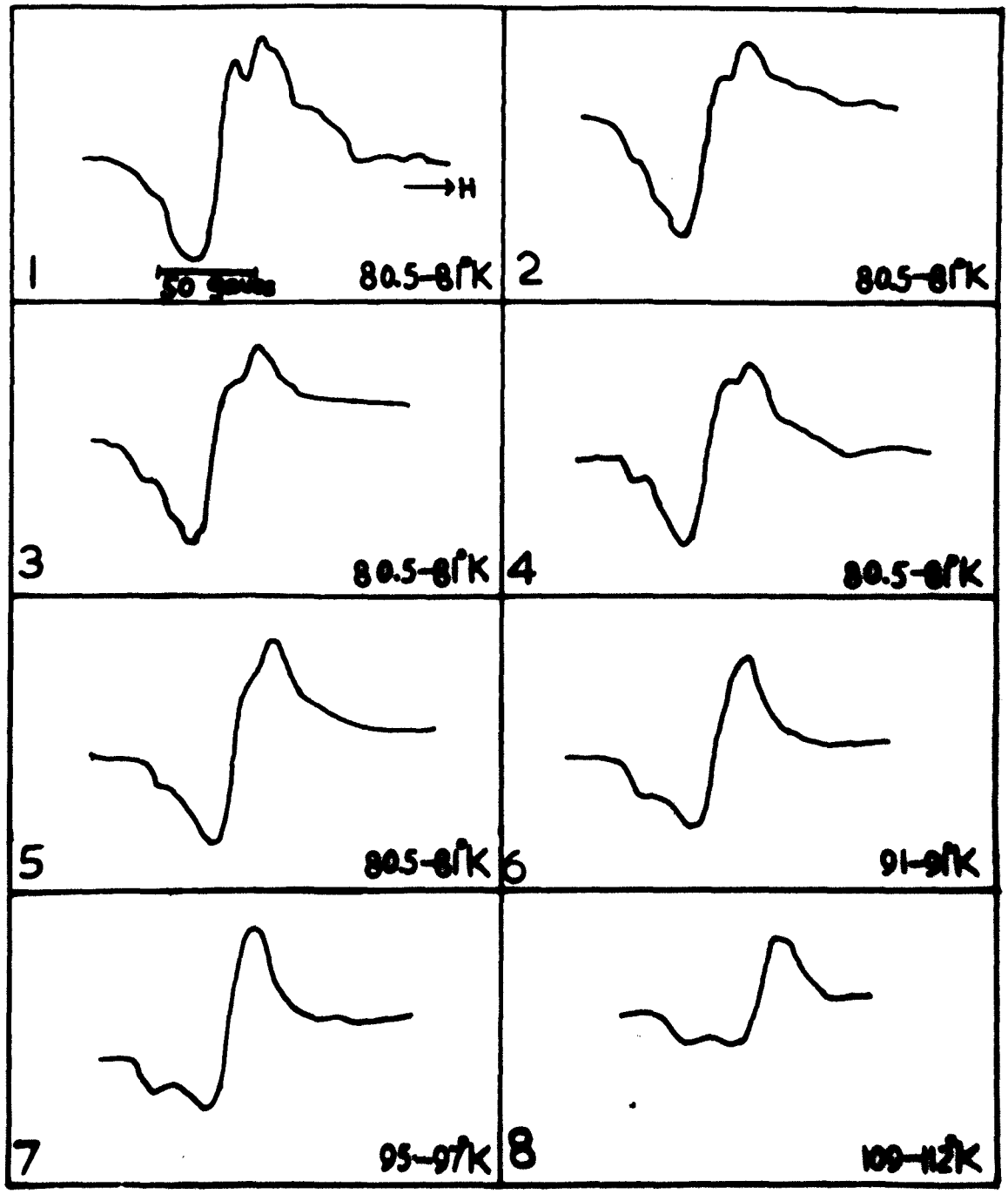

FIG. 5.9. CHLOROFORM. Wavelength 2537.

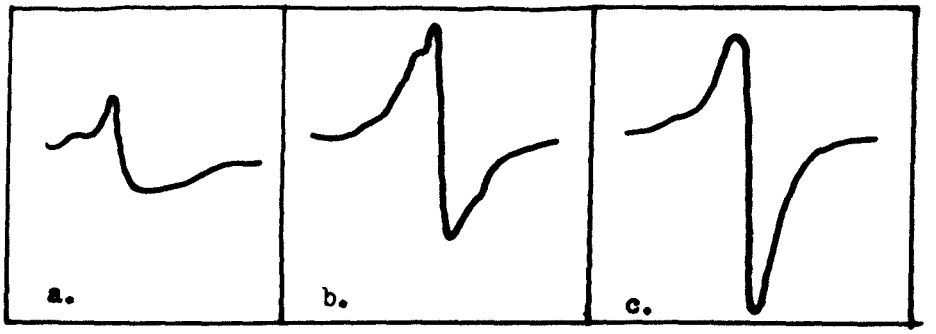

FIG. 10.

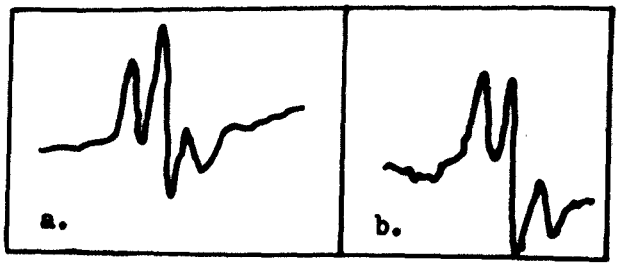

FIG. 11.

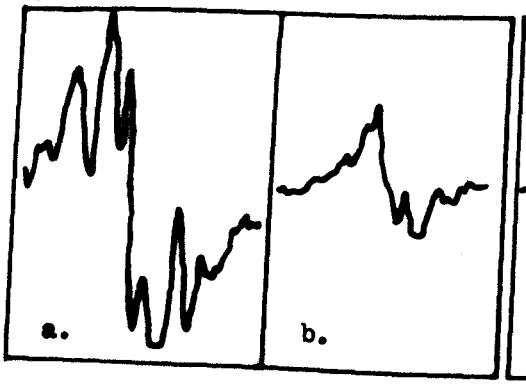

FIG. 12.

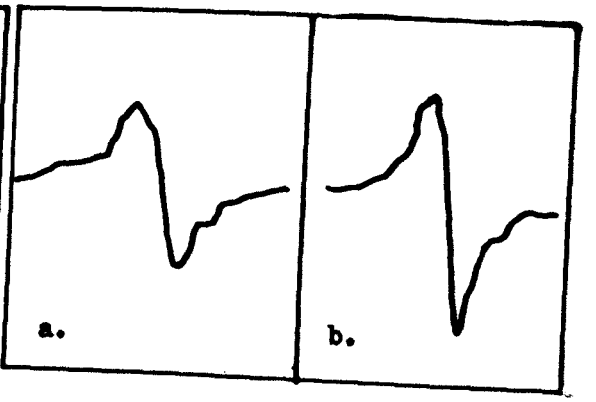

FIG. 13.

CHAPTER VI

DISCUSSION

6.1. Production of Free Radicals in Alcohols

For the photodissociation of any molecule, two conditions must be met:

(1) the energy of the quanta must be equal to or greater than the dissociation energy of the bond which is ruptured, and

(2) the light used for irradiation must be absorbed by the substance.

The dissociation may take place through any of the following processes:

(a) the molecule is excited to a repulsive state (for the two fragments),

(b) in the excited electronic state, the vibrational level to which excitation takes place lies above the dissociation limit, so that the molecule dissociates on its outward vibrational excursion.

(c) the excited electronic state crosses another state of the type (a) or (b), so that at the point of crossing the molecule passes from one state to the other.

Direct excitation into the vibrational continuum of the ground electronic state is not possible because of the selection rules.

Now it is known that alcohols do not absorb in the regions of λ2537 and λ3655 (Waters, 1948). However, as seen in Chapter V, large concentrations (10^{15} -10^{18} per gm.) of free radicals

were observed in the low temperature photolysed alcohol glasses. The mechanisms which could be responsible for this are,

(i) primary photolysis of alcohol molecules due to modifications of selection rules in the solid state due to the crystal fields of the matrix,

(ii) secondary reactions due to the primary photolysis of impurities, and

(iii) photo-sensitisation due to absorbed oxygen or the walls of the sample tube.

For primary photolysis, the quantum of energy absorbed must be equal to or greater than the bond dissociation energy. Table 1 gives an idea of the magnitudes of the bond dissociation energies involved vis-a-vis the energy of the quanta.

Table 1

(Cottrell, 1958)

Bond	Bond dissociation energy (Kcal/mole)	Wavelength	energy (Kcal/mole)
CH_2 - H	88	λ2537	112.6
CH_3 - H	101	λ3655	78.1
CH_3 - CH_3	83		
CH_3 - OH	$\sim$90		
$CH_3.CH_2$ - OH	$\sim$90		
O - H	101		

It is thus seen that the energy of λ3655 per quantum is in all

probability less than any of the bond dissociation energies involved. The dissociation energy of the weakest bond, C - C, comes quite close to the quantal energy of λ3655. However, methanol which is photolysed by λ3655 does not have any C - C bonds. Moreover, in other alcohols, the present work and other evidences also indicate breakage of other than C - C bonds. In the light of these considerations, primary photolysis does not seem to be the main mechanism for free radical production.

The secondary radical production by the primary photolysis of impurities, particularly aldehydes and ketones ($\sim$0.05%), could give spin concentrations of about 10^{18} per gm. However, spectroscopic grade ethyl alcohol also gave free radical concentrations of the same order as obtained from other alcohols. This suggests that the photolysis of impurities is again not the main contributory factor for the free radical production in alcohol glasses. Water which is present as an impurity in ethyl and other alcohols would not undergo primary photolysis, as water does not absorb in this region (Goodeve and Stein, 1931).

The most likely mechanism for the production of free radicals in these glasses seems to be photosensitisation due to absorbed oxygen. Liquid oxygen shows absorption bands in both the regions (λ 2537 and λ3655). The energy of the oxygen molecules can then be transfered to the alcohol molecules by collisions of the second kind. This process can lead to a large free radical concentration even if a small amount of oxygen were absorbed. Photosensitisation

due to the walls of the sample tube seems to be another possibility. However, in the solid state at low temperatures, this mechanism would be confined to the surface of the sample, Making a liberal assumption that the molecules within 100 A^o from the wall would be able to exchange energy with it, the number of free radicals produced comes out to be about 10^{16} spins per gm., a value less than the observed ones in many cases. However, the effective range of 100 A^o has been rather arbitrarily chosen and the excitation might propagate to longer distances.

6.2. Change of Spectra with Temperature.

The e.s.r of a free radical at low temperatures may change with temperature either due to a physical or a chemical change, or both, taking place inside the sample. An assembly of frozen free radicals in a matrix is, of necessity, in an unstable state, though the passage to the stable state is very slow. A rise of temperature helps in, and hastens, this process. The passage to the stable state may involve two types of chemical changes, (a) the decay of free radicals by recombination, and (b) conversion of one species into another prior to decay. In the first case, if different species of free-radicals are initially produced and if their decay rates are different and are affected to different extents by changes of temperature, then the overall spectrum will show a change in structure as it is warmed up. In the second case, the relative proportion of the two species will again be different at different

temperatures and hence the overall spectrum would change as the specimen is warmed up. Because of the unidirectional nature of the passage from the unstable to the stable state, these chemical changes would be irreversible with respect to change of temperature. Physical changes (e.g. quenching of internal rotation) would, on the other hand, be reversible in this respect. If both physical and chemical changes occur, then if the specimen is warmed up and cooled down again, the spectra obtained on recooling would resemble neither the initial spectrum nor the spectrum corresponding to the higher temperature.

In all the substances investigated, except allyl alcohol, the changes in spectra were found to be irreversible with respect to changes of temperature. In dimethylamine, no first order change in the structure of the spectrum was observed. However, on recooling, the initial size of the spectrum was not restored, thereby showing that radicals had decayed on warm-up. Absence of any change in the structure of the spectrum indicates that only one species of free radicals is primarily responsible for the spectrum.

In all other cases, a change in the structure of the spectrum was noted on warming. In all the saturated alcohols except methanol, some components of the spectra seemed to grow whereas the other components decayed. This suggests that interconversion of the species is taking place. The chemical nature of the changes in the spectrum is further confirmed by the fact that in

almost all cases, at some temperatures, the spectra changed with the passage of time even though the specimen was held at the same temperature. This is particularly noticeable in Figs. (5.4.a.), (5.5.a.), (5.5.b.), (5.6.), (5.7.a.) and (5.7.b.). The fact that the change in spectra with the passage of time is more pronounced at certain temperatures shows that the properties of the glass change discontinuously.

The spectra from allyl alcohol show interesting changes with temperature; these will be described when discussing spectra from individual substances.

6.3. Mechanisms of h.f. Interactions in Free Radicals

The products of the photolysis of low temperature glasses can, in principle, be identified by the hyperfine structure in their electron resonance spectra. In glasses, however, the anisotropic hyperfine interaction only produces a broadening of the line and it is only the isotropic part that gives rise to a hyperfine structure. For the isotropic hyperfine interaction to take place, it is essential that the unpaired electron should have a finite probability density at the magnetic nuclei. The majorities of the radicals supposed to be responsible for the observed spectra in the present case have, in their conventional structures, vanishing probability densities at the protons (the only magnetic nuclei in the case of alcohols), but they still show hyperfine structure. Before taking up the discussion of the individual spectra, therefore, it is worthwhile discussing the mechanisms

responsible for these 'anomalous' hyperfine structures in the free radical e.s.r. spectra. The mechanisms were first investigated both, theoretically and experimentally, for aromatic free radicals. For simplicity, they will be considered here for the case of hypothetical fragments abstracted from the aromatic radicals. The mechanisms are basically the same for both aromatic and aliphatic radicals, and, with slight modifications, the theory can be applied to the latter.

The contact hyperfine Hamiltonian can be written as

$$\mathcal{H}_N = \frac{8\pi}{3} g_e g_I \beta^2 \sum_k \delta(\vec{r}_{KN}) \vec{s}_k . \vec{I}_N \qquad \ldots\ldots \quad (6.1.)$$

where k refers to the electrons and N to the nucleus. Only one magnetic nucleus has been considered here for convenience.

In a strong magnetic field, where the coupling between the electron spins and nuclear spins are much weaker than the coupling of these with the external magnetic field, the expression for the contact hyperfine Hamiltonian can be written in terms of only the z-components of spin, as

$$\mathcal{H}_N = 8\pi g_e g_I \beta^2 \sum_k \delta(r_{kN}) \, s_{kz} . I_{Nz} \qquad \ldots\ldots \quad (6.2.)$$

This is because the expressions $S_x I_x + S_y I_y (= \frac{1}{2}(S_+ I_- + S_- I_+))$ give rise to non-diagnol terms only in the z-representation.

The Hamiltonian $_N$ can also be written in terms of the coupling constant a_n as

$$\mathcal{H}_N = h a_N \, S_z . I_{Nz} \qquad \ldots\ldots \quad (6.3.)$$

where S_z is the total z-component of the electron spin angular

momentum. The coupling constant a_N can be expressed in terms of the quantities occuring in the equation (6.2.) by taking the expectation values of both the expressions (1) and (2) in the electronic ground state. This gives

$$a_N = \frac{8\pi g_e g_I \beta^2}{3h} \frac{\langle \psi_1 | \sum_k \delta(\vec{r}_{kN}) s_{kz} | \psi_1 \rangle}{\langle \psi_1 | s_z | \psi_1 \rangle} \quad \ldots\ldots \quad (6.4.)$$

This expression thus predicts a non-vanishing h.f. interaction only when the electron orbital has a finite value at the nucleus in question. However, the aromatic free-radicals, which have the unpaired electron in the π-orbitals in the Huckel approximation show isotropic hyperfine interactions with the 'in-plane' protons. Hyperfine interaction with methyl-group protons of the aromatic free radicals have also been observed. This anomalous behaviour is explained in the first case by invoking configuration interaction and in the second case by hyperconjugation. These two mechanisms are described below.

6.3.1. 'In-Plane' Protons

Venkataraman and Fraenkel (1956) pointed out that the isotropic hyperfine interaction of the unpaired electron with the ring protons in p-benzosemiquinone ion was due to π-σ transmission of spin polarisation arising from configuration interaction. For an illustration of this mechanism, a hypothetical fragment CH, abstracted from an aromatic radical, is considered here. It is assumed that, in the zeroth order, the single unpaired electron is in a pure $2p_z$ orbital on the carbon atom and the two paired

electrons are in the σ- bonding orbital. The occurrence of unpaired spin density at the proton can be explained in terms of three approximate descriptions of molecular electronic structure. These are (i) valence bond, (ii) molecular orbital, and (iii) unrestricted Hartree-Foek approximations. All the three methods have been considered in detail by McConnell and Chestnut (1958) and would only briefly be described here.

6.3.1.1. Valence-Bond Approximation

In valence bond approximation, the π- σ transmission of spin-polarisation takes place through exchange coupling between different atomic orbitals. This would mix the ground state wave-function with the excited state wave-functions. The zero-order valence bond wave-functions that are mixed due to exchange interactions must be eizenfunctions for $S_z = + \frac{1}{2}$ (or $-\frac{1}{2}$) and $S^2 = 3/4$. The following three spin-orbital configurations have $S_z = +\frac{1}{2}$:

$$\Phi_1 = \text{Aphs}\alpha\alpha\beta$$
$$\Phi_2 = \text{Aphs}\alpha\beta\alpha \qquad \ldots\ldots \qquad (6.5.)$$
$$\Phi_3 = \text{Aphs}\beta\alpha\alpha$$

Here p denotes the p_z orbital on the carbon atom, h the sp^2 trigonal planar hybrid orbital centered on the carbon atom and directed towards the proton and s the s-orbital on the proton. The expression phs$\alpha\alpha\beta$ stands for $p(1)h(2)s(3)\ \alpha(1)\alpha(2)\alpha(3)$, etc. A is the antisymmetrisation and renormalisation operator and is given by

$$A = \frac{1}{(K!)^{\frac{1}{2}}} \sum_{p} (-1)^{\gamma} p \qquad \ldots\ldots (6.6.)$$

where K is the total number of electrons in the wavefunction to be antisymmetrised and γ is even or odd according as the permutation P is even or odd.

The linear combinations of the functions (6.5.) that are eigenfunctions of S^2 corresponding to the eigenvalue 3/4 are

$$\psi_1^{\circ} = \frac{1}{\sqrt{2}} (\phi_1 - \phi_2) = \frac{1}{\sqrt{2}} \text{ Aphs}(\alpha\alpha\beta - \alpha\beta\alpha)$$

and $$\psi_2^{\circ} = \frac{1}{\sqrt{6}} (\phi_1 + \phi_2 - 2\phi_3) = \frac{1A}{\sqrt{2}} \text{ phs}(\alpha\alpha\beta + \alpha\beta\alpha - 2\beta\alpha\alpha)$$

$\ldots\ldots$ (6.7.)

The wavefunction ψ_1° corresponds to the ground-state electronic configuration of the CH fragment whereas ψ_2° represents an excited electron configuration. The ground-state wavefunction ψ_1° gives no contact hyperfine coupling with the proton. This coupling can arise through a mixture of ψ_1° and ψ_2° which comes about through an atomic exchange coupling mechanism. The first-order perturbation theory gives the following for the 'mixed' ground-state wavefunction, ψ_1',

$$\psi_1' = \psi_1^{\circ} + \lambda\psi_2^{\circ} \qquad \ldots\ldots (6.8.)$$

where $\lambda = \frac{-\mathcal{H}_{21}}{\Delta W}$; $\mathcal{H}'_{21} = \langle \psi_2^{\circ} | \mathcal{H}' | \psi_1^{\circ} \rangle$; $\Delta W = W_2 - W_1$ (6.9.)

Here $\mathcal{H}'$ is the electron repulsion term in the Hamiltonian and W_2 and W_1 are the energy eigen-values for the states ψ_2° and ψ_1° respectively. Here it has been assumed that $|\lambda|^2 << 1$. Explicit

calculation shows that

$$\mathcal{H}'_{21} = -\frac{\sqrt{3}}{2}(J_{ph} - J_{ps})$$

where $$J_{ph} = \langle p(1)\ h(2) \left| \frac{e^2}{r_{12}} \right| h(1)\ p(2) \rangle \qquad (6.10.)$$

and $$J_{ps} = \langle p(1)\ s(2) \left| \frac{e^2}{r_{12}} \right| s(1)\ p(2) \rangle$$

Equations (6.4.) and (6.12.), therefore, together give

$$a_{CH} = (-1)\ \frac{(J_{ph} - J_{ps})}{\Delta W}\ a_H \ \ldots\ . \qquad (6.11.)$$

where

$$a_H = \frac{8\pi\ g_e g_I \beta^2}{3h} \left| s(0) \right|^2$$

Here the overlap integral $S_o = \langle h | s \rangle$ has been neglected. If this is not done, the expression for a_{CH} is modified by a factor $(1 - S_o^4)$ in the denominator.

6.3.1.2. Molecular Orbital Theory

In a molecular orbital description of the CH fragment, the σ-bonding orbital is a linear combination of the atomic and hybrid orbitals, s and h:

$$\sigma = \frac{1}{[2(1 + S_o)]^{\frac{1}{2}}}\ (s + h) \qquad (6.12.)$$

Equal proportions of s and h in equation (6.12.) imply neglect of ionic character of the CH bond. This has been assumed for simplicity.

The lowest energy configuration is given by

$$\psi_1^o = A\,\sigma\sigma\,p\,\alpha\beta\alpha \qquad \ldots\ldots \qquad (6.13.)$$

This configuration, however, does not give any contact hyperfine splitting due to the proton, but the admixture of higher configurations does. The excited configuration that admixes with the ground-state configuration must have the same symmetry as ψ_1^o and it must be an eigenfunction of S_z and S^2 with eigen-values $+\frac{1}{2}$ (or $-\frac{1}{2}$) and 3/4 respectively. Further, it should not be much separated in energy from ψ_1^o. There are two such configurations:

$$\psi_2^o = \frac{1}{\sqrt{6}} A\,\sigma\sigma^*\,p(2\alpha\alpha\beta - \alpha\beta\alpha - \beta\alpha\alpha) \ldots\ldots \qquad (6.14.)$$

and $$\psi_3^o = \frac{1}{\sqrt{2}} A\,\sigma\sigma^*\,p(\alpha\beta\alpha - \beta\alpha\alpha) \qquad \ldots\ldots \qquad (6.15.)$$

where σ^* is the normalised antibonding orbital orthagonal to and given by

$$\sigma^* = \frac{1}{[2(1 - S_0)]^{\frac{1}{2}}} (s - h) \qquad \ldots\ldots \qquad (6.16.)$$

Of the wavefunctions ψ_2^o and ψ_3^o, the latter corresponds to a combination of the singlet $\sigma\sigma^*$ with the doublet p and would lead to no hyperfine interaction. Hence only the admixture of ψ_2^o need be considered. The 'mixed' ground-state wavefunction would therefore be

$$\psi_1 = \psi_1^o + \lambda\psi_2^o \qquad \ldots\ldots \qquad (6.17.)$$

λ is evaluated by a variational calculation. If the variational parameter λ is assumed to be small, i.e. if

$|\lambda|^2 << 1$, one gets

$$\lambda = -\frac{\mathcal{H}_{21}}{\Delta W} \qquad \ldots\ldots \qquad (6.18.)$$

Equations (6.4.) and (6.17.), then, give

$$a_{CH} = \frac{32\pi}{3\sqrt{6}} \lambda g_e g_I \beta^2 \sigma(0)\, \sigma^*(0) \qquad (6.19.)$$

Also from equations (6.12.) and (6.16.), one gets

$$\sigma(0)\,\sigma^*(0) = \tfrac{1}{2} \frac{1}{(1 - S_0^2)^{\frac{1}{2}}} \left[|s(0)|^2 - |h(0)|^2 \right] \qquad (6.20.)$$

so that equation (6.19.) becomes

$$a_{CH} = \frac{16\pi}{3\sqrt{6}} \lambda g_e g_I \beta^2 \frac{1}{(1 - S_0^2)^{\frac{1}{2}}} \left[|s(0)|^2 - |h(0)|^2 \right] \qquad (6.21.)$$

Finally, λ is found, by explicit calculation, to be given by

$$\lambda = \frac{3}{2\sqrt{6}} \frac{1}{(1 - S_0^2)^{\frac{1}{2}}} \frac{J_{ps} - J_{ph}}{\Delta W} \ldots\ldots \qquad (6.22.)$$

so that $$a_{CH} = -\tfrac{1}{2} \frac{1}{(1 - S_0^2)} \frac{J_{ph} - J_{ps}}{\Delta W} a_H$$

assuming $$|h(0)|^2 \approx 0$$

6.3.1.3. Unrestricted Hartree-Fock Method

In a Hartree-Fock self-consistent field method, the energy of the CH fragment is minimised using an antisymmetrised variational function

$$\phi = A\sigma\sigma' p\, \alpha\beta\alpha \qquad \ldots\ldots \qquad (6.23.)$$

Here, σ and σ' are two CH bonding orbitals which are varied

independently of one another to minimise the ground-state energy. The functions σ and σ' have been taken to be different in order to take the correlation of the σ electrons with the unpaired electron into account; the $\sigma\alpha$ electron has spin parallel to the unpaired electron spin and the $\sigma'\beta$ electron has spin antiparallel to it. To this extent, σ and σ' will be identical if the σ-π interaction is neglected.

The function, ϕ, however, is not an eigenfunction of S^2. Two doublet eigenfunctions can be generated from ϕ:

$$\psi_1 = \frac{1}{\sqrt{2(1+S^2)}} A\sigma\sigma'p(\alpha\beta\alpha - \beta\alpha\alpha) \quad \ldots\ldots \quad (6.24.)$$

$$\psi_2 = \frac{1}{\sqrt{6(1-S^2)}} A\sigma\sigma'p(2\alpha\alpha\beta - \alpha\beta\alpha - \beta\alpha\alpha) \quad (6.25.)$$

where the overlap integral S is

$$S = \langle \sigma | \sigma' \rangle \quad \ldots\ldots \quad (6.26.)$$

Now if σ-π interaction is neglected, $\sigma = \sigma'$, so that ψ_1 becomes identical with ϕ and ψ_2 does not exist. When σ-π interaction is a significant perturbation, $\sigma \neq \sigma'$ and ψ_2 mixes in with ψ_1. The 'mixed' ground-state wave function is

$$\psi = \psi_1 + \lambda\psi_2 \quad \ldots\ldots \quad (6.27.)$$

When $|\lambda|^2 << 1$, one gets

$$a_{CH} = \frac{8\pi}{3} g_e g_I \beta^2 \frac{2\lambda}{\sqrt{3(1-S^4)}} \left(|\sigma'(0)|^2 - |\sigma(0)|^2 \right) \quad (6.28.)$$

As a first approximation, σ and σ' could be regarded as

different linear combinations of s and h, so that $|\sigma'(0)|^2 - |\sigma(0)|^2$ would again be proportional to $|s(0)|^2$.

Thus it is seen that the unrestricted Hartree-Foek method of describing the indirect hyperfine splittings involves essentially the same qualitative ideas as those of the valence bond and molecular orbital methods.

6.3.1.4. Unpaired Electron Distribution and Hyperfine Splittings

So far it has been assumed that in the zeroth order approximation the unpaired electron is confined to the p_z orbital on the carbon atom. However, if the delocalisation of the unpaired p_z electron takes place as in an aromatic radical, the unpaired electron distribution has to be considered. The operator, ρ, representing the spin density in the atomic orbital χ on the nucleus N is defined by the operator equation

$$\rho \sum_{kz} s_{kz} = \sum_{k} \Delta_{N\chi}(k)\, s_{kz} \qquad \ldots\ldots \quad (6.29.)$$

where $\Delta_{N\chi}(k)$ is a three dimensional step-function such that $\Delta_{N\chi}(k) = 1$ when the electron k is in an atomic orbital χ on the nucleus N and $\Delta_{N\chi}(k) = 0$ elsewhere.

In an aromatic radical in the zeroth order, the unpaired electron is contained in the π-orbital. Hence orbital χ, in this case, stands for the p_z orbital on the carbon nuclei. The hyperfine splitting constant is then given by

$$a_N = Q\rho_N \qquad \ldots\ldots \quad (6.30.)$$

where ρ_N is the spin density in the p_z orbital on the carbon

nucleus N and Q is the hyperfine coupling constant (equivalent of a_{CH} of sections (6.3.1. (1,2,3.)).

It may be noted that ρ_N may have negative values as well, subject to the restriction that for a monoradical

$$\sum_N \rho_N = 1 \qquad \ldots\ldots \quad (6.31.)$$

(McConnell and Chestnut, 1958). Since the hyperfine splitting of an electron resonance line is independent of the sign of the coupling constant a_N, the total spread of the hyperfine spectrum will be

$$\sum_N |a_N| = Q \sum_N |\rho_N| \qquad \ldots\ldots \quad (6.32.)$$

This is greater than the value of Q obtained on neglecting the spin unpairing as represented by the negative spin density.

6.3.2. Methyl Group Protons

The contact hyperfine interaction of the unpaired electron of methyl substituted aromatic radicals with the methyl group protons is finite because of hyperconjugation. The effect of hyperconjugation in producing an odd electron density at the methyl group protons can be discussed either by valence bond (McLachlan, 1958), or by molecular orbital (Bersohn, 1956; Chestnut, 1958) theory. As a simple model for illustrating the effect of hyperconjugation, a hypothetical radical consisting of a methyl group attached to a trigonal planar carbon atom is considered here. The conventional structure in which the unpaired electron is in a $2p\pi$ atomic orbital is assumed.

6.3.2.1. Valence-Bond Theory

Fig. (6.1.) shows the atomic orbitals of a radical in which the odd electron occupies the 2_z orbital of a trigonal carbon atom with three coplanar sp^2 bonds to one of which a methyl group is joined. All the filled atomic orbitals not shown in the diagram are disregarded. The 'normal' structure would be represented by

$$\psi_0 = (t_1h_1)(t_2h_2)(t_3h_3)(t_4c_1)p \quad ..... \quad (6.33.)$$

where the electrons in the atomic orbitals within a parenthesis are paired together. This description neglects all exchange integrals except those belonging to the four main bonds. However, the orbital p will have some exchange integrals with the orbitals t_1, t_2, t_3 and c_1. This will mix ψ_0 with the structures

$$\begin{aligned}
\psi_c &= (t_1h_1)(t_2h_2)(t_3h_3)(c_1p)t_4 \\
\psi_1 &= (t_1p)(t_2h_2)(t_3h_3)(t_4c_1)h_1 \\
\psi_2 &= (t_1h_1)(t_2p)(t_3h_3)(t_4c_1)h_2 \quad ..... \quad (6.34.) \\
\psi_3 &= (t_1h_1)(t_2h_2)(t_3p)(t_4c_1)h_3
\end{aligned}$$

Exchange interactions not included in equation (6.34.) have negligible spatial overlap between the corresponding orbitals. The structures corresponding to equation (6.34.) are shown in Fig. (6.2.).

The correct zeroth-order eigenfunctions will be orthogonal combinations of $\psi_0, \psi_1, \psi_2, \psi_3$ and ψ_c and are obtained by the

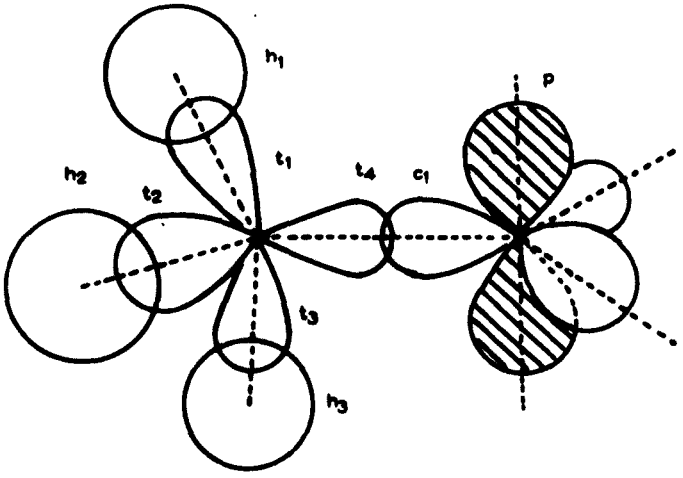

FIG. 6.1. ORBITALS FOR VALENCE BOND CALCULATION.

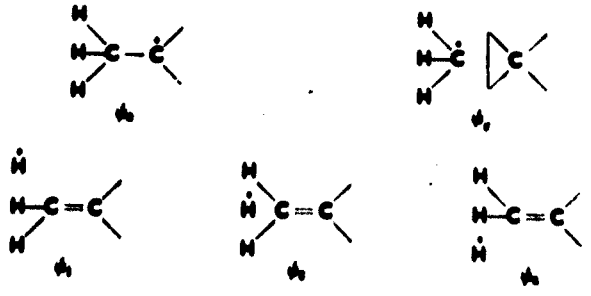

FIG. 6.2. BASIC RESONANT STRUCTURES.

diagnolisation of the matrix $[\mathcal{H}_{ij} - WS_{ij}]$. This leads to the following zeroth-order wave functions:

$$\begin{aligned}
\Phi_0 &= \Psi_0 \\
\Phi_1 &= \frac{1}{\sqrt{3}} (\Psi_0 - 2\Psi_c) \\
\Phi_2 &= \Psi_0 - 2/3 (\Psi_1 + \Psi_2 + \Psi_3) \\
\Phi_3 &= \frac{1}{\sqrt{3}} (\Psi_1 + \omega\Psi_2 + \omega^2\Psi_3) \\
\Phi_4 &= \frac{1}{\sqrt{3}} (\Psi_1 + \omega^2\Psi_2 + \omega\Psi_3)
\end{aligned} \qquad \ldots\ldots \qquad (6.35.)$$

where $\omega = \exp(2\pi i/3)$

The true wavefunction for the ground state can, then, be written as

$$\Phi = \Phi_0 + \lambda_1 \Phi_1 + \lambda_2 \Phi_2 + \lambda_3 \Phi_3 + \lambda_4 \Phi_4 \qquad (6.36.)$$

A perturbation calculation gives (McLachlan, 1958)

$$\Phi = \Psi_0 + \frac{J(c_1 p)}{2J(c_1 t_4)} [\Psi_c - \tfrac{1}{2}\Psi_0] + \sum_{r=1,2,3} \frac{J(t_r p)}{2J(t_r h)} [\Psi_r - \tfrac{1}{2}\Psi_0] \qquad (6.37.)$$

as the true wavefunction. Here J's are the exchange integrals.

Finally, the function Φ leads to the spin densities

$$\pm \frac{J(t_1 p)}{2J(t_1 h_1)} \qquad \ldots\ldots \qquad (6.38.)$$

in the orbitals h_1 and t_1 of the C-H bond and

$$\pm \frac{J(c_1 p)}{2J(c_1 t_4)} \qquad \ldots\ldots \qquad (6.39.)$$

in the orbitals t_4 and c_1 of the C-C bond. The total spin density in each bond is zero.

So far the odd electron in the orbital p has been assumed always to have spin α. If, however, the part of the molecule containing the trigonally hybridised carbon atom resonates between various structures with different spins in the orbital p, then the spin polarisation induced on the methyl proton is found to be proportional to the unperturbed spin density in p. The expression for the spin density at each proton thus becomes

$$\rho_H = \frac{J(t_1 p)}{2J(t_1 h)} \rho_p \qquad \ldots\ldots \qquad (6.40.)$$

where ρ_p is the spin density in orbital p. The hyperfine splitting constant a_H for a methyl proton is thus given by the relation

$$a_H = Q \rho_p \qquad \ldots\ldots \qquad (6.41.)$$

It is thus seen that the hyperfine structure due to methyl protons arises in the same way as that due to protons directly attached to the trigonally hybridised carbon atom: exchange coupling between non-bonded atomic orbitals modifies the conventional pairing scheme for the electrons in the bonds and allows the unpaired spin to move on to a proton.

If the methyl group rotates rapidly about the C-C bond, the three protons become equivalent and the spin density at the proton is proportional to the average value of the exchange

integral $J(t_1p)$. This is $\frac{1}{2}(J_o + J_1)$ where J_o and J_1 are the values of this exchange integral when the CH_1 bond is respectively perpendicular and parallel to the nodal plane of p. Neglecting J_1 which will be very small, the spin density on each proton becomes

$$\rho_H = \frac{J_o}{4J(t_1h_1)}\ \rho_p \qquad \ldots\ldots \qquad (6.42.)$$

6.3.2.2. Molecular Orbital Theory

To elucidate the hyperconjugative contact hyperfine interaction according to molecular orbital theory a hypothetical $\dot{C}$-CH_3 radical, extracted from a methylated aromatic radical is again considered.

If the z-axis is taken along the C-C bond and the x and y axes are chosen with respect to the three H-atoms as shown in Fig. (6.3.), then the 1s orbitals of the H-atoms can be combined to give the orbitals

$$\sigma_z = \frac{1}{\sqrt{3}}\ (a + b + c)$$

$$\pi_x = \frac{1}{\sqrt{6}}\ (2a - b - c) \qquad \ldots\ldots \qquad (6.43.)$$

$$\pi_y = \frac{1}{\sqrt{2}}\ (b - c)$$

where a,b,c are the 1s orbitals on the H-atoms 1,2,3. The first of these has a σ-type symmetry about the z-axis and the other two have π-type symmetry about the yz and zx planes respectively. The methyl group carbon can now be [redacted] diagonall

hybridised. One of the two hybrids (σ_1) is directed towards the ring and the other (σ_2) is directed towards the centre of the equilateral triangle formed by the methyl hydrogens. The orbitals formed by a combination of σ_z and σ_2 would then represent a localised σ bond between C and H_3. Similarly p_x and p_y of the methyl group carbon combine with π_x and π_y of H_3 respectively to give π-type bonds between C and H_3. The CH_3 group can, thus, be treated as a triple bond conjugated with the aromatic hydrocarbon.

The ring carbon is assumed to be trigonally hybridised. The C-C bond is again taken as the z-axis and the plane of the trigonal bonds is taken as the y' z-plane. The axes x' and y' have been assumed to be rotated by an angle θ relative to the x,y axes (Fig. 6.4.) of the CH_3 group for the sake of generality. The unpaired electron will predominantly occupy the $p_{x'}$ orbital on this ring carbon.

The π-type H_3 group orbital which will match the symmetry of the $p_{x'}$ orbital of the unpaired electron will be

$$\pi_x \cos\theta + \pi_y \sin\theta \qquad \ldots\ldots \qquad (6.44.)$$

and the corresponding orbital for the methyl carbon will be

$$p_x \cos\theta + p_y \sin\theta \qquad \ldots\ldots \qquad (6.45.)$$

The complete π-type orbital occupied by the unpaired electron, would, therefore, be given by

$$P'_x = p_{x'} + k_1(\pi_x \cos\theta + \pi_y \sin\theta) + k_2(p_x \cos\theta + p_y \sin\theta) \qquad \ldots\ldots \qquad (6.46.)$$

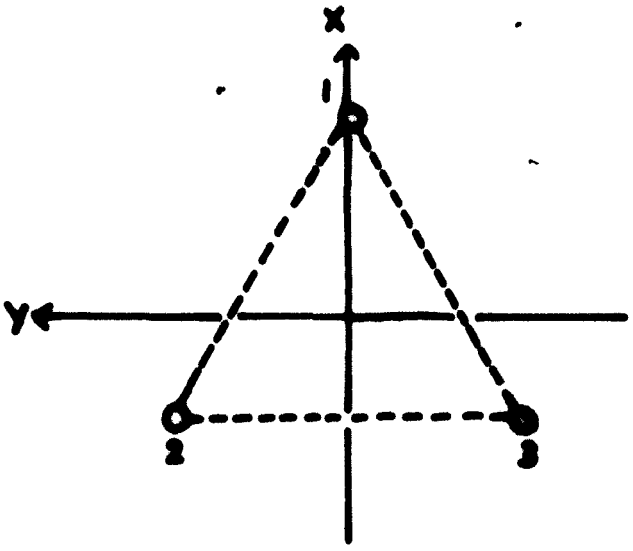

FIG. 6.3.

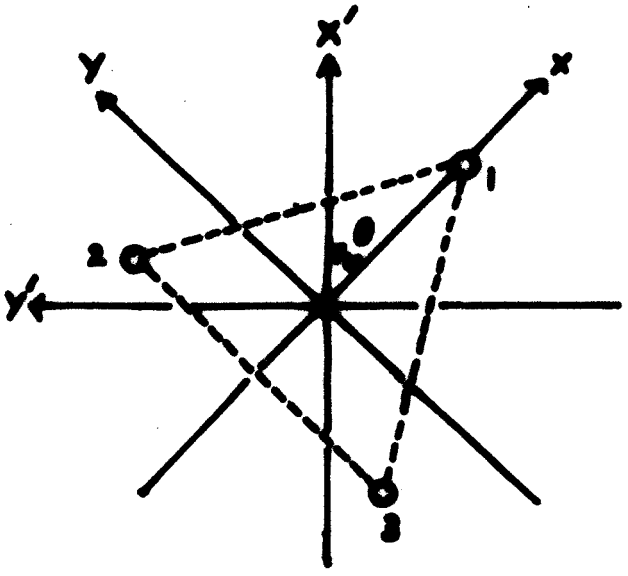

FIG. 6.4.

ROTATION OF THE METHYL GROUP.

The wavefunction P_x' may now be used to determine the expectation value of the hyperfine Hamiltonian,

$$\frac{8\pi}{3} g_e g_I \beta^2 \sum_n \vec{S}.\vec{I}_n \, \delta(\vec{r} - \vec{r}_n) \qquad \ldots\ldots \qquad (6.47.)$$

Only expectation value of $\delta(\vec{r} - \vec{r}_n)$ need be calculated. Considering only the first order terms, one gets, from equation (6.46.),

$$(P_x' \,|\, \delta(\vec{r} - \vec{r}_n) \,|\, P_x') = k_1^2 (\pi_x \,|\, \delta(\vec{r} - \vec{r}_n) \,|\, \pi_x) \mathrm{Cos}^2\theta + k_1^2 (\pi_y \,|\, \delta(\vec{r} - \vec{r}_n) \,|\, \pi_y) \mathrm{Sin}^2\theta \qquad (6.48.)$$

so that the hyperfine coupling constant for the nth proton becomes

$$a_n = \frac{8\pi}{3} g_e g_I \beta^2 k_1^2 \, (\pi_x \,|\, \delta(\vec{r} - \vec{r}_n) \,|\, \pi_x \mathrm{Cos}^2\theta + (\pi_y \,|\, \delta(\vec{r} - \vec{r}_n) \,|\, \pi_y) \mathrm{Sin}^2\theta \qquad \ldots\ldots \qquad (6.49.)$$

The matrix elements of the delta-function occurring in equation (6.49.) can be calculated with the help of the equations (6.43.).

Finally, if the methyl group is rotating rapidly, all the protons become equivalent and the average values of $\mathrm{Sin}^2\theta$ and $\mathrm{Cos}^2\theta$, $(\frac{1}{2})$, have to be substituted in equation (6.49.).

6.4. Spectra from Individual Substances

A study of the change of spectra of/the different substances with temperature shows that, in the majority of the cases, the observed spectra are due to more than one free radical species that, in general, decay at different rates. There is also evidence of interconversion among these species. This, together with the

lack of sufficient resolution in the spectra of these glasses, makes an analysis of the chemical processes involved extremely difficult. Any inference about the nature of all the species taking part in these chemical processes can, therefore, be only speculative rather than conclusive. However, the species mainly responsible for the observed spectrum near liquid nitrogen temperature can, quite often, be more definitely identified. Sometimes, when the central part of the spectrum from the main species has been too much modified due to the overlap of spectra from other species, the number of h.f. components has been determined by a measurement of the total spread of the h.f. spectrum and the separation of the adjacent components in the outer wings. This, of course, implies equal coupling with the interacting protons.

As even a small error in the derivative tracing due to the non-linearity of the field sweep or a drift of the base line produces a large effect in the integrated absorption curve, the parameters of the derivative spectra have been directly used, wherever possible, to determine the parameters of the e.s.r spectrum. The hyperfine component lines have been assumed to be Gaussian in shape for the analysis. The component lines in the spectrum of the main species have all been assumed to have the same linewidth. Whenever the spectra are well-resolved, this assumption is seen to be justified on measurement. The spectra from the individual substances are described below.

6.4.1. Dimethylamine $(CH_3)_2$ NH

A 25/30% ω/v solution of dimethylamine in water was irradiated with λ2537. The spectrum is seen to consist of seven hyperfine components. The ratio of the peak-to-peak heights in the derivative curve is given below along with the theoretically calculated intensity ratios for equal coupling with six protons:

Experimental ratio: 1.5:6.5 : 14.8:20: 15.2: 6.5: 0.65

Theoretical ratio: 1 : 6 : 15:20: 15: 6: 1

It is thus seen that the unpaired electron is interacting with six nearly equivalent protons. As the response of the pen-recorder to small signals is not very reliable, the intensities of the central components rather than those of the extremities have been compared with the theoretical values. A comparison of the theoretical intensity ratio with that of the peak-to-peak height of the derivative curve is justified if the widths of the component lines are equal and are sufficiently less than their separation. Both these conditions are found to be satisfied in the present case.

The observed separation between the adjacent components is 29 gauss. The field separation between the maximum-slope points of a hyperfine component is 10 gauss, and, assuming the line shape to be Gaussian, this gives a value of $10 \times 2 \ln 2 \simeq 14$ gauss for the line width (between half-power points) of the hyperfine components.

No first order change in the hyperfine structure of the spectrum is observed on raising the temperature of the sample. This indicates that only one type of species is primarily responsible for the spectrum. That the reduction in the size of the signal on warming is not only due to the Boltzmann factor is shown by the fact that, on recooling the sample to the lowest attainable temperature, the original size of the signal is not restored. Thus the spectra obtained from dimethylamine at different temperatures provide a good example of the simple decay of a single species on warming.

The seven line spectrum with the intensity ratios very nearly equal to those predicted theoretically for six equivalent protons suggests that it is due to the $(CH_3)_2N$ radical. Assuming a trigonal planar hybridisation of the nitrogen atom with the lone pair in one of the σ orbitals, the unpaired electron in the p_z orbital and the two CH_3 groups attached to the two remaining σ orbitals, equal hyperconjugative overlap of the unpaired electron with the six protons implies that free rotation of the two methyl groups is taking place over the whole range of temperature. The much weaker hyperfine coupling due to the nitrogen nucleus is not resolved.

The production of the $(CH_3)_2N$ radical on the photolysis of dimethylamine has also been postulated by Bamford (1937). The products of the photolysis of dimethylamine are mainly hydrogen and a polymer. Bamford has suggested the following mechanism

$$(CH_3)_2NH + h\nu \rightarrow (CH_3)_2N + H$$

$$H + (CH_3)_2NH \rightarrow (CH_3)N + H_2$$

$$2(CH_3)_2N \longrightarrow (CH_3)_2NH + CH_3NCH_2$$

followed by the polymerisation of the radical CH_3NCH_2.

A study of the observed e.s.r. spectrum and the supporting chemical evidence suggest that the seven-line spectrum is due to the $(CH_3)_2N$ radical. The slight asymmetry observed in the e.s.r. spectra may be due to the presence of CH_3NCH_2 radical.

6.4.2. tert. Butyl Chloride $(CH_3)_3CCl$

Since the dissociation energy for the C-Cl bond (about 80 Kcal/mole) is much less than that for the C-H bond (about 100 Kcal/mole), the photolysis of $(CH_3)_3.CCl$ might be expected to give $(CH_3)_3C$ radicals. However, on irradiation with λ2537, tert. Butyl Chloride gives an asymmetrical three line spectrum, with a separation of about 16 guass between the adjacent components. Thus the odd electron is seen to interact with only two protons. It is evident that the radical

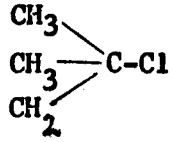

is being formed. The interaction of the odd electron with the protons on the same carbon atom takes place through configuration interaction. Since no first-order interaction can take place between the unpaired electron and the other

protons, this radical will give rise to a three line spectrum.

No major changes in the spectra with temperature were observed, though some change in the relative heights of the peaks in the derivative curve was noticed. This change in the relative heights was irreversible with respect to the changes of temperature. The asymmetry of the spectrum may be due to the presence of a species giving a single line slightly displaced from the centre of the three line spectrum. The change in the relative heights of the peaks may be due to the growth of this single line spectrum on warming. Two bumps are also observed, one on either side of the three line spectrum. These may be due to the presence of other radical species or due to very weak coupling with the remaining protons in the other methyl groups.

The formation of the

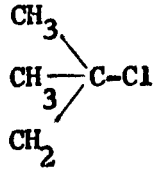

rather than the $(CH_3)_3C$ radical on photolysis in low temperature glasses may be explained to be due to the cage effect. The heavy chlorine atom may not be able to escape the Franck-Rabinowitsch cage. If so, the recombination probability will be high and the quantum yield low. On the other hand the hydrogen atom, being much lighter, will easily escape recombination

6.4.3. Methanol CH_3OH

When irradiated with λ 2537, methanol shows an inner triplet and an outer doublet in its spectrum.

The hyperfine components in the inner triplet have a line width of about 17 gauss and the adjacent components have a separation of about 20 gauss. The signal is slightly asymmetric and the asymmetry increases as the temperature is raised. That this is a chemical change is shown by its irreversibility with respect to change of temperature. As the temperature is raised, a single line spectrum seems to grow near the centre of the overall spectrum. In fact, this growth of the central single line on warming is a recurrent feature in the spectra of most of the substances that were investigated.

The triplet has also been observed by Luck and Gordy (1956), Matheson and Smaller (1958), and Zeldes and Livingston (1959) on high energy irradiation of methanol. Luck and Gordy observed a hyperfine splitting of 15 gauss, whereas Matheson and Smaller found it to be 18 gauss.

The outer doublet has a splitting of about 140 gauss. The two components of the doublet are not symmetrical and the narrow one has a line width of 14 gauss. A large splitting of 140 gauss implies that the unpaired electron is interacting with only one proton and that there is a very large spin-density in the s-orbital of this proton.

This unsymmetrical doublet has also been observed by the EPR staff of Varian Associates (1960), but their inner spectrum was a quartet (assigned to be due to the CH_3 radical) rather than

a triplet. A splitting in excess of 120 gauss was observed. The splitting did not change when CH_3OD was irradiated. This shows that the outer doublet is not due to the OH radical.

Patat investigated the photolysis of methyl alcohol at ordinary temperatures in the region from 1800 - 2000 A^o (Steacie, 1954a). Formaldehyde was found to be one of the products of the photolysis. The following primary processes were proposed by him:

$$CH_3\ OH + h\nu \longrightarrow CH_2OH + H$$
$$\longrightarrow CH_3O + H$$
$$\longrightarrow CH_3 + OH$$

However, no H-atoms are detectable in the photolysis of ethanol (Noyes and Leighton, 1941; Steacie, 1954b), and the process is probably a dissociation into an ethyl and a hydroxyl radical:

$$C_2H_5\ OH + h\nu \longrightarrow C_2H_5 + OH$$

By analogy the reaction

$$CH_3OH + h\nu \longrightarrow CH_3 + OH$$

seems to be the most likely mechanism in the photolysis of methanol.

It is, therefore, postulated that the primary reaction in the photolysis at low temperatures is also

$$CH_3OH + h\nu \longrightarrow CH_3 + OH$$

The OH radical abstracts H from CH_3OH:

$$OH + CH_3OH \longrightarrow H_2O + CH_2OH$$

The inner triplet is postulated to be due to the CH_2OH radical. Since the OH radical is sufficiently mobile, there will be a relatively quick build up of the CH_2OH radical.

The CH_3 radical would initiate the following reactions:

$$CH_3 + CH_3OH \longrightarrow CH_4 + CH_3O$$
$$CH_3 + CH_3O \longrightarrow CH_4 + HCHO \qquad \text{(Steacie, 1954,c)}$$

This explains the formation of formaldehyde as a reaction product.

The outer doublet is due to a small radical having one proton such that the unpaired electron is largely localised on it so as to give a splitting of 140 gauss. Since the experiments of the EPR staff of Varian Associates indicate that this radical is not OH, the other small one-proton radical likely to occur is CHO. This radical may be produced by the photolysis of HCHO:

$$HCHO + h\nu = H + CHO$$
$$H + HCHO = H_2 + CHO \qquad \text{(Steacie, 1954,d)}$$

It may be noted that the outer doublet was not observed by Fujimoto and Ingram (1958). Since the production of CH_2OH radical in their experiments was due to the proton extraction by the OH radical (obtained by the primary photolysis of H_2O_2), not enough CH_3 radicals would have been present in their sample to give formaldehyde and the CHO radical.

It is seen that as the temperature is raised a central single

line seems to grow while the overall signal decays. This single line may be due to the CH_3O radical. Presence of the CH_3 radicals is another possibility which could lead to the asymmetrical shape of the spectrum at the higher temperatures.

The change of the spectrum with temperature when λ3655 is employed for photo-irradiation is similar, in the broad aspects, to that when λ 2537 is employed, though the quantum yield is much smaller in the former case as expected. It is noticed that the spectrum at about 92°K obtained on irradiation with λ2537 corresponds to the spectrum at about 82°K obtained on λ3655 irradiation. This is due to the fact that λ2537 can maintain a predominant concentration of CH_2OH radicals during irradiation, whereas the small quantum yield at λ3655 allows appreciable proportions of the other radicals to be built up as well during irradiation.

6.4.4. Ethanol C_2H_5OH

The spectrum obtained from ethanol irradiated at λ2537 shows a quintet with a very strong singlet in the centre. The separation of the adjacent hyperfine components in the quintet is 20 gauss and the overall spread is about 85 gauss. The latter agrees fairly well with 89 gauss and 93 gauss spread of the quintet observed by Matheson and Smaller (1958), and Luck and Gordy (1956), respectively on high energy irradiation of ethanol.

The overall spectrum obtained on irradiation of ethanol

with λ3655 seems to be a superposition of a quintet, a central singlet, and another component spectrum (indicated by the peaks a,b in Fig. 5.4.(b).1). The last one will henceforth be referred to as the (a,b) spectrum.

With the passage of time, but with the sample held at the initial temperature (82°K), the (a,b) spectrum decays and the central singlet grows stronger until the spectrum starts resembling that obtained on irradiation with λ2537. However, the resemblance is never quite complete and the final decay of the free-radicals is seen to be somewhat different in the two cases.

The photolysis of ethanol at liquid nitrogen temperature was also investigated by Voedvodsky et al (1954). They used CH_3I,HI and CH_3CHO to produce the primary radicals and the e.s.r spectra was investigated both during irradiation and upon light extinction. They observed a quartet during irradiation and an additional central peak upon light extinction. The two spectra were reversible in this respect. The following mechanism was postulated to explain these observations:

$$HI + h\nu \longrightarrow H + I$$

$$I + CH_3\,CH_2OH \longrightarrow HI + CH_3CH_2O$$

$$CH_3\,CH_2O + h\nu \rightleftharpoons CH_3 + HCHO$$

The presence of the additional line on light extinction was explained to be due to the ethoxy radical (CH_3CH_2O) which is thermodynamically more stable than the methyl radical. The

incomplete disappearance of the quartet on light extinction was assumed to be due to the reverse reaction being hindered by the lattice defect sites where the free radicals are trapped.

However, in the present work, the spectra definitely show a quintet at least on irradiation with $\lambda 2537$. Since no H-atoms are detected in the photolysis of ethanol at 2000 A^{o} (Nayes and Leighton, 1941; Steacie, 1954 b) at ordinary temperatures, it is reasonable to postulate the following mechanism for the photolysis in the present case:

$$CH_3CH_2OH + h\nu \rightarrow CH_3CH_2 + OH$$

$$CH_3CH_2OH + OH \rightarrow CH_3CHOH + H_2O$$

The radical CH_3 CH_2OH gives rise to the quintet.

The ethoxy radical may be produced by the reaction

$$CH_3CH_2 + CH_3\ CH_2OH \rightarrow C_2H_6 + CH_3CH_2O$$

Since the spin density at the carbon atom would be strongly attenuated due to the oxygen atom, and the h.f. coupling to the protons on the / α-carbon will be an order of magnitude smaller (about 2 or 3 gauss), and there would be practically no h.f. interaction with the proton on the / the β-carbon. The small splitting of 2 or 3 gauss will, however, not be resolved, and the ethoxy radical can thus give rise to a singlet spectrum. Alternatively, the singlet spectrum could be due to a peroxide radical. In this case the spin-density at the α-carbon would be almost completely quenched. The peroxide radical may be formed in the presence of absorbed oxygen by the following mechanism:

(a) $CH_3\ CH_2OH + h\nu \rightarrow CH_3CH_2 + OH$

$CH_3\ CH_2OH + OH \rightarrow CH_3CHOH + H_2O$

(b) Presence of aldehydes among the products of photolysis of ethanol suggests the step

$CH_3CH_2 + CH_3CHOH \rightarrow C_2H_6 + CH_3CHO$

(c) Aldehyde and oxygen give, in the presence of alcohol:

$CH_3\ CHO + h\nu \longrightarrow CH_3 + CHO$

$CH_3\ CHO + CH_3 \longrightarrow CH_4 + CH_3CO$ (Bower, 1949)

$CH_3CO + O_2 \longrightarrow CH_3CO.O_2$

$CH_3CO.O_2 + CH_3CH_2OH \longrightarrow 2CH_3.COOH + H$

(d) Finally, the photolysis of $CH_3.COOH$ gives

$CH_3.COOH \longrightarrow CH_3COO + H$

The central singlet line is seen to be more intense relative to the quintet when λ2537 is employed for irradiation, than it is when λ3655 is employed. This suggests that the central singlet line is the result of a second photolysis, like the one assumed above to explain the presence of the peroxy radical. However, there is no definite evidence for the central singlet to be either due to the ethoxy or the peroxy radicals and the mechanism proposed above is only a suggestion.

6.4.5. n-Propanol $CH_3(CH_2)_2OH$

The spectra from n-Propanol on irradiation with λ2537 and λ3655 are both similar to the one obtained with ethanol on long wavelength irradiation. At low temperatures, the overall spectrum seems to be a superposition of a five or six line spectrum, a central single line, and the (a,b) spectrum.

A measurement of the overall spread of the five or six line spectrum and the separation between the adjacent component lines in its wings indicates that it is actually a six-line spectrum. The separation between the adjacent lines is about 20 gauss. It is postulated that this spectrum is due to the radical $CH_3.CH.CH_2OH$ where the unpaired electron primarily interacts with the protons on the adjacent carbons only. The hyperfine interaction of the unpaired electron with these protons is hyperconjugative whereas that with the proton on the same carbon is through configuration interaction. This explains the unequal coupling in the two cases.

The spectrum obtained on irradiation with λ3655 is similar to that obtained when λ2537 is employed, except that the (a,b) spectrum is much stronger in the case of long wavelength irradiation. Further, the (a,b) spectrum is seen to decay considerably with the passage of time while the sample is maintained at the lowest available temperature. In the spectra of the sample obtained on irradiation with either wavelength, the

(a,b) spectrum decays and the central singlet grows with rising temperature and the spectra from both these samples at the higher temperaturesare almost identical.

6.4.6. n-Butanol $CH_3(CH_2)_3OH$

The spectra from n-Butanol on irradiation with λ2537 is seen to be similar to that from n-Propanol except that the (a,b) spectrum does not seem to be present. Measurements of the overall spread and the separation of the adjacent components in the wings indicate that a six line spectrum is present. This is attributed to the radical, $CH_3.CH.CH_2.CH_2OH$, where the coupling is primarily to the protons on the adjacent carbons only, there being no mechanism for the first-order interaction of the unpaired electron with protons on the α-carbon. The separation between the adjacent component lines in the wings is found to be 20 gauss.

6.4.7. iso-Propanol $(CH_3)_2CHOH$

When irradiated with λ2537, iso-Propanol shows a seven-line spectrum where the central component is masked by another single line spectrum. This single line spectrum is much weaker than that observed in the spectra of ethanol, n-propanol and n-butanol. The single line spectrum is again seen to grow with temperature and in this process, it considerably modifies the appearance of the overall spectrum in the central region, sometimes making it look like a six-line and sometimes a seven line spectrum. The spectra obtained at different temperatures on

irradiation with λ3655 also show fairly similar features. That these changes of spectra are chemical in nature is shown by their irreversibility with respect to changes of temperature. The observed separation of the hyperfine components is 18 gauss and the overall spread 110 gauss. The seven-line spectrum can be explained to arise from the hyperconjugative coupling of the unpaired electron with the protons of the methyl groups in the radical $(CH_3)_2.COH$, if the methyl groups are assumed to rotate freely. The species giving rise to the central spectrum is, however, difficult to identify.

6.4.8. Allyl Alcohol $CH_2:CH.CH_2OH$

The spectra of allyl alcohol obtained on irradiation with λ2537 shows interesting features. When the sample is recooled to the lowest attainable temperature at various stages of warming, the spectra obtained correspond neither to the initial low temperature spectrum, nor to the temperature to which the sample has been warmed, but to intermediate temperatures. This shows that both the chemical and the physical changes are responsible for the observed change of spectra with temperature. As seen in Figs. 5.8. (a,b, and c), the spectrum near 80°K corresponds to two species one of which decays rapidly on warming and is not restored on recooling. The spectra No. 6 in Fig. 5.8.(a), obtained at about 96°K, is the most symmetrical of all and resembles that observed by Fujimoto and Ingram (1958) on irradiation with λ3655 in presence of H_2O_2. The spin densities

on the three carbon atoms in the radical CH_2:CH.CH OH are theoretically found to be 0.622,-0.231, and 0.622 respectively (Lefkovits et al., 1955). The smaller splitting due to the proton on the central carbon atom is not resolved in the present case, and only the quartet due to the protons on the end carbon atoms is observed.

When the temperature is raised still further, the peak c (Fig. 5.8.a) is seen to develop. A comparison with the similar growth of a central spectrum in other alcohols indicates the growth of a new species but the equal splittings between the peaks c and b, and d and e, suggest that the growth of the peak c is due to a physical process resulting in the change of coupling constants due to the proton on the central carbon atom. On raising the temperature still further the spectrum gradually takes on a highly asymmetrical shape 'Figs. (5.8.a.) and (5.8.b.) like other alcohol, but at a temperature of about 120°K the resolution improves considerably showing well resolved spectra Figs. (5.8.a.) and (5.8.b.). This improvement in the resolution is associated with the onset of some form of motional narrowing at this temperature. In general recooling results in some loss in resolution as expected.

6.4.9. Chloroform $CHCl_3$

The spectrum from chloroform obtained on irradiation with λ2537 shows a very poor resolution, though there are indications of a triplet being present. The spectrum is also

seen to change considerably with temperature and becomes highly asymmetric at the higher temperatures. The poorly resolved spectrum together with its change with temperature suggest that a number of species are present.

The reaction

$$CHCl_3 + h\nu \longrightarrow CHC_2 + Cl$$

does not seem likely to occur, inspite of the low dissociation energies of the C-Cl bonds. The Cl radical being a heavy one is not likely to escape the Franck-Rabinowitsch cage and the two fragments would have a large probability of recombination if this reaction takes place. This is also supported by the fact that CCl_4 did not show any e.s.r. signal on photolysis at low temperatures.

The following mechanism is, therefore, proposed:

$$CHCl_3 + h\nu \longrightarrow CCl_3 + H$$

followed by the secondary reactions

$$\begin{aligned} H + CHCl_3 &\longrightarrow HCl + CHCl_2 \\ H + CHCl_2 &\longrightarrow CH_2Cl_2 \\ H + CH_2Cl_2 &\longrightarrow CH_2Cl + H \\ H + CH_2Cl &\longrightarrow CH_3Cl \end{aligned} \qquad \text{(Steacie, 1954, e)}$$

The radicals present in this sequence may be responsible for the poorly resolved overall spectrum.

6.5. Dilution of the Matrix and Single Crystal Irradiation

The spectra in Fig. (10) - (13), show that, on dilution with

CCl_4, the signals are, in some cases, larger, and, in the other cases, smaller than those obtained without of CCl_4. The increase in the size of the signals may be due to the fact that the matrix becomes less rigid on dilution with CCl_4 so as to provide a weaker 'cage'. The decrease in the signal strength may be either due to the reduction in the number of parent molecules per c.c. or because the matrix becomes so soft as to allow a larger number of the photolysis products to recombine. The resolution is not seen to improve, in any case, due to dilution with CCl_4. ;In fact, it is seen to worsen in some cases. This may be due to the fact that CCl_4 itself reacts if H atoms are present in the glass as a result of the photolysis of the actual substance investigated. The superposition of spectra from these radicals would adversely affect the resolution to some extent.

In the case of the dilution with a rare gas by condensation of the mixture, it is noted that the technique used is not powerful enough to condense enough krypton which has a boiling point rather close to liquid nitrogen. It is thought that condensation under high pressures would be helpful. Another difficulty is the unequal condensation of the two substances. Condensation directly from slow and narrow streams of the two substances would give a more uniform mixture.

The fact that no spectra are observed from the single crystals on irradiation with ultraviolet light, together with the fact that X-ray irradiation gives large signals, indicate that

u.v. irradiation is not strong enough to eject the free radical fragments out of the cage.

Conclusions

The work described in this thesis is mainly concerned with the investigation of the change of spectra of aliphatic alcohols and some other substances with temperature, with particular regard to the possibility of a change in the rotation of the methyl groups in these radicals. The variable low temperature cavity developed for this purpose has been described in Chapter III. In all the substances except allyl alcohol, the changes in the spectra have been found to be irreversible with respect to the changes of temperature. The changes that have been observed are thus shown to be chemical in nature. The observed spectra and their change indicate that more than one free radical species are taking part. These species have different rates of decay and there is also evidence of inter-conversion among them. Under these conditions, a definite analysis of the nature of the species responsible for the observed changes of spectra is not possible. Almost all the substances including chloroform show a highly asymmetric spectrum on warming. This unsymmetrical spectrum is found in the case of allyl alcohol as well, though on further warming it changes into a well-resolved spectrum. It has not been possible to identify the species responsible for this asymmetric line. However, it seems to be due to the slow rotation of a

molecule containing an oxygen atom. The axis of rotation could then become the axis for g-value variation and the asymmetrical line could be obtained with a peak at the $g_{\perp}$ position and a shoulder at the $g_{\parallel}$ position. Alternatively the asymmetrical line could arise from the overlap of two species with slightly different g-values or due to anisotropic hyperfine interaction. A comparison of the observed 'splitting' in the asymmetrical line at different microwave frequencies will be helpful in deciding whether the asymmetry is due to g-value variation or anisotropic hyperfine interaction.

Some experiments were also performed on the dilution of the matrix with substances having zero or very small nuclear magnetism. The experiments indicate that chemicals like CCl_4 and CO_2 are not suitable because of the possibility of these reacting chemically. Experiments on the condensation of the mixture of the specimen and some inert gas were not conclusive. Single crystal studies indicated that u.v. irradiation of single crystals was not likely to produce reasonable concentrations of free radicals.

The results obtained from these experiments suggest that the following points need further investigation:

(a) The mechanism of the photolytic decomposition of alcohols at the wavelengths employed. Degassing the sample before irradiation would indicate whether the production of free radicals is due to photosensitisation by absorbed oxygen.

Floating the sample in liquid nitrogen during irradiation and observation would decide if this is due to surface effects, whereas a measurement of the maximum available concentration of free radicals on prolonged irradiation would tell whether the photolysis is due to the primary decomposition of impurities.

(b) The nature of the free radical species present and the chemical processes taking place during and after photolysis. Some spectra change with time even at the lowest available temperature. This indicates that these reactions start taking place as soon as the irradiation is switched off. The development of a variable temperature cavity with provision for 'in situ' irradiation will be helpful in the study of the growth of radicals with irradiation time at different temperatures and their decay on light extinction.

(c) The origin of the asymmetrical line obtained from most samples on warming up. A comparison of the splittings observed at X- and K- or Q- bands would be helpful.

(d) Further development of the rare gas dilution technique. Condensation from slow and narrow streams of the substances required to be mixed may lead to a more efficient mixing.

REFERENCES

Abragam, A. and Pryce, M.H.L., (1951) Proc. Roy. Soc. A.205, 135.

Bamford, C.H., J.Chem.Soc., (1939), 17.

Bass, A.M., and Broida, H.P., Eds. (1960), 'Formation and Trapping of Free Radicals', Academic Press.

Bersohn, R., 1956, J.C. p. 24,1066.

Bleaney, B., and Stevens, K.W.H., (1953) Repts.Progs. in Physics 16, 108.

Bloch, F., and Siegert, A., (1940), Phys.Rev., 57, 522.

Bowen, E.J., (1949), 'The Chemical Aspects of Light', Clarendon Press, Oxford, p. 219.

Chestnut, D.B., (1958), J.C.P., 29, 43.

Cottrell, T.L., (1958), 'The Strength of Chemical Bonds', Butterworth Scientific Publications, London.

Dirac, P.A.M., (1947), 'The Principles of Quantum Mechanics', Clarendon Press, Ch.XI.

Fraenkel, G., (1960) Technique of Organic Chemistry, vol. I, Physical Methods Part IV, (Ed. Weissberger) Interscience.

Feher, G., (1957), Bell System Technical Journal, 36, 449.

Frosch, R.A., and Foley, H.M., (1952), Phys.Rev. 73, 718.

Fromherz, H., and Schneller, H., (1933), Z.Physik.Chem. B20, 158.

Fujimoto, M., and Ingram, D.J.E., (1958), Trans. Faraday Soc. 54, 1304.

Goodeve, and Stein (1931) Trans. Farday,Soc. 27, 393.

Griffiths, J.H.E., (1960), 'The Theory of Transition Metal Ions', p. 323-324.

Hoskins, and Pastor, (1960) J.Appl.Phys. 31, 1506.

Ingram, D.J.E., (1958) 'Free Radicals as Studied by Electron Spin Resonance', Butterworths.

Karplus, R., (1948), Phys.Rev. 73, 1027.

Kohnlein, W., and Muller, A., (1961), 'Free Radicals in Biological Systems', (Editors, Blois et al), Academic Press, New York and London, p.113.

Kotani, M., (1960), Progr.Theor.Phys.Supp. No.14 p.1.

Kronig, R. de L., (1939), Physica, 6, 33.

Landau, L.D., and Lifshitz, E.M., (1958) 'Quantum Mechanics', Pergamon Press, p. 486.

Lefkovits, H.C., Fain, J., and Matsen, F.A., (1955) J.C.P., 23, 1690.

Low, W., (1960), Suppl. 2, Solid State Physics, Academic Press, p. 54.

Luck, C.F., and Gordy (1956), W.J. Amer.Chem.Soc., 78, 3240.

McConnell, H.M., (1956), J.Chem.Phys., 25, 709; (1958) J.Chem.Phys. 29, 1422.

McConnell, H.M., and Chestnut, D.B., (1958), J.Chem.Phys. 28, 107.

McLachlan, A.D., (1958), Molecular Physics, 1, 235.

Nafe, J.E., and Nelson, E.B., (1948), Phys.Rev., 73, 718.

Noyes, W.A., Jr., and Leighton, P.A., 'The Photochemistry of Gases' Reinhold Publishing Corporation, New York, 1941, p. 422.

N.M.R. EPR Staff of Varian Associates, (1960), N.M.R. and EPR Spectroscopy Pergamon Press, New York, p. 250.

Pake, G.E., (1956) in 'Solid State Physics', Vol. 2, Academic Press, (Eds. Seitz, F., and Turnball, D.).

Pake, G.E., Townsend, J., and Weissman, S.I., (1952), Phys.Rev. 85, 682.

Pearse, R.W.B., and Gaydon, A.G., (1950), 'Identification of Molecular Spectra', Chapman and Hall, p. 195-196.

Portis, A.M., (1953), Phys.Rev. 91, 1071.

Pryce, M.H.L., (1949), Nature, London, 164, 116.

Pryce, M.H.L., (1950) Proc.Phys.Soc. A 63, 25.

Rabi, I.I., (1937), Phys.Rev., 51, 652.

Schuster, N.A., (1951), Rev.Sci.Instrum., 22, 254.

Smaller, B., and Matheson, M.S., (1958), J.C.P., 28, 1169.

Sowden, R.G., and Davidson, N., (1956), J.Amer.Chem.Soc., 78, 1291.

Steacie, E.W.R., 'Atomic and Free Radical Reactions', (1954) Vol. 1 and 2, American Chemical Society Monograph Series Reinhold Publishing Corporation, New York, Pages (a) 616, (b) 616, (c) 617, (d) 283, (e) 658.

Van Vleck, J.H., (1932), 'The Theory of Electric and Magnetic Susceptibilities, Clarendon Press Oxford, p.273.

Van Vleck, J.H., (1935), J.Chem.Phys., 73, 807.

Van Vleck, J.H., (1948), Phys.Rev., 74, 1168.

Venkataraman, B., and Fraenkel, G., (1956), J.Chem.Phys., 24, 737.

Voedodsky, V.V., (1959), Symposium on Free Radical Stabilization, BVI., (Trapped Radicals at Low Temperatures, Aug. 31, Sept. 2, (1959), Sponsored by the National Bureau of Standards, Washington.

Walter, R.I., (1956), J.Chem.Phys. 25, 319.

Waters, W.A. Chemistry of Free Radicals, (1948), p.123, Oxford.

Weisskopf, V.F., (1949), Rev.Mod.Phys., 21, 305.

Zeldes, H. and Livingston, R., (1959), J.Chem.Phys., 30, 40.